



NAVAL POSTGRADUATE SCHOOL

MONTEREY, CALIFORNIA

DISSERTATION

**RADIO FREQUENCY SIGNAL RECEPTION VIA
DISTRIBUTED WIRELESSLY NETWORKED SENSORS
UNDER RANDOM MOTION**

by

William A. Lintz

September 2009

Dissertation Supervisors:

John McEachen
Murali Tummala

Approved for public release; distribution is unlimited

REPORT DOCUMENTATION PAGE			<i>Form Approved OMB No. 0704-0188</i>	
Public reporting burden for this collection of information is estimated to average 1 hour per response, including the time for reviewing instruction, searching existing data sources, gathering and maintaining the data needed, and completing and reviewing the collection of information. Send comments regarding this burden estimate or any other aspect of this collection of information, including suggestions for reducing this burden, to Washington headquarters Services, Directorate for Information Operations and Reports, 1215 Jefferson Davis Highway, Suite 1204, Arlington, VA 22202-4302, and to the Office of Management and Budget, Paperwork Reduction Project (0704-0188) Washington DC 20503.				
1. AGENCY USE ONLY (Leave blank)		2. REPORT DATE September 2009	3. REPORT TYPE AND DATES COVERED Dissertation	
4. TITLE AND SUBTITLE: Radio Frequency Signal Reception via Distributed Wirelessly Networked Sensors Under Random Motion			5. FUNDING NUMBERS	
6. AUTHOR(S) William A. Lintz			8. PERFORMING ORGANIZATION REPORT NUMBER	
7. PERFORMING ORGANIZATION NAME(S) AND ADDRESS(ES) Naval Postgraduate School Monterey, CA 93943-5000			10. SPONSORING / MONITORING AGENCY REPORT NUMBER	
9. SPONSORING / MONITORING AGENCY NAME(S) AND ADDRESS(ES) N/A				
11. SUPPLEMENTARY NOTES The views expressed in this thesis are those of the author and do not reflect the official policy or position of the Department of Defense or the U.S. Government.				
12a. DISTRIBUTION / AVAILABILITY STATEMENT Approved for public release; distribution is unlimited			12b. DISTRIBUTION CODE	
13. ABSTRACT (maximum 200 words) <p>This research investigates the reception of radio frequency signals using wirelessly networked autonomous sensor nodes under random motion. Emphasis is placed on investigating effects of random motion on sensor array beamforming. Novel techniques to conduct array operations in spite of the node motion are offered. Conflicting priorities of energy consumption and array operational requirements are addressed to demonstrate performance of the proposed solutions.</p> <p>The issues of node management in a beamforming application, degradation of beamforming performance due to element motion, the need for a weight reset time determination method, and the effect of unsteady element orientation in network communications are explored for system implementation. Examination of Doppler shift due to node motion demonstrated that its impact is negligible on beamforming performance. The management system proposed for the wireless sensor network enabled sensor operation while preserving node energy. Analysis of independent node motion on beamforming performance produced a relationship between motion and gain percent change on aim point. A novel methodology was offered to determine weight reset times with elements in motion. Investigation of unsteady antenna orientation produced an innovative method to mitigate communications degradation. Each proposal proved superior to alternate approaches in terms of performance and energy conservation.</p>				
14. SUBJECT TERMS Sensor Networks, Beamforming, Random Motion, Orientation			15. NUMBER OF PAGES 293	
			16. PRICE CODE	
17. SECURITY CLASSIFICATION OF REPORT Unclassified	18. SECURITY CLASSIFICATION OF THIS PAGE Unclassified	19. SECURITY CLASSIFICATION OF ABSTRACT Unclassified	20. LIMITATION OF ABSTRACT UU	

THIS PAGE INTENTIONALLY LEFT BLANK

Approved for public release; distribution is unlimited

**RADIO FREQUENCY SIGNAL RECEPTION VIA DISTRIBUTED
WIRELESSLY NETWORKED SENSORS UNDER RANDOM MOTION**

William A. Lintz
Commander, United States Navy
B.E.E., Villanova University, 1992
M.S. Electrical Engineering, Naval Postgraduate School, 1997

Submitted in partial fulfillment of the requirements for the degree of

DOCTOR OF PHILOSOPHY IN ELECTRICAL ENGINEERING

from the

**NAVAL POSTGRADUATE SCHOOL
September 2009**

Author:

William A. Lintz

Approved by:

John McEachen
Professor of Electrical and
Computer Engineering
Dissertation Committee Chair
and Dissertation Co-Advisor

Murali Tummala
Professor of Electrical and
Computer Engineering
Dissertation Co-Advisor

Roberto Cristi
Professor of Electrical and
Computer Engineering

David Jenn
Professor of Electrical and
Computer Engineering

Christopher Frenzen
Professor of Mathematics

Approved by:

Jeffrey Knorr, Chair, Department of Electrical and Computer
Engineering

Approved by:

Douglas Moses, Vice Provost of Academic Affairs

THIS PAGE INTENTIONALLY LEFT BLANK

ABSTRACT

This research investigates the reception of radio frequency signals using wirelessly networked autonomous sensor nodes under random motion. Emphasis is placed on investigating effects of random motion on sensor array beamforming. Novel techniques to conduct array operations in spite of the node motion are offered. Conflicting priorities of energy consumption and array operational requirements are addressed to demonstrate performance of the proposed solutions.

The issues of node management in a beamforming application, degradation of beamforming performance due to element motion, the need for a weight reset time determination method, and the effect of unsteady element orientation in network communications are explored for system implementation. Examination of Doppler shift due to node motion demonstrated that its impact is negligible on beamforming performance. The management system proposed for the wireless sensor network enabled sensor operation while preserving node energy. Analysis of independent node motion on beamforming performance produced a relationship between motion and gain percent change on aim point. A novel methodology was offered to determine weight reset times with elements in motion. Investigation of unsteady antenna orientation produced an innovative method to mitigate communications degradation. Each proposal proved superior to alternate approaches in terms of performance and energy conservation.

THIS PAGE INTENTIONALLY LEFT BLANK

TABLE OF CONTENTS

I.	INTRODUCTION.....	1
A.	BACKGROUND AND MOTIVATION	1
B.	OBJECTIVE	11
C.	ORGANIZATION	14
II.	BACKGROUND	17
A.	STOCHASTIC MODELS.....	17
1.	Gaussian Random Variable	21
2.	Uniform Random Variable	22
3.	Beta Random Variable	23
4.	Rician Random Variable.....	25
5.	General Random Motion.....	25
B.	ELECTROMAGNETICS AND COMMUNICATIONS.....	31
1.	Antennas	35
2.	Free-space Communications.....	39
3.	Array Beamforming.....	46
a.	<i>Adaptive Beamforming</i>	54
b.	<i>Grating Lobes</i>	55
c.	<i>Mutual Coupling</i>	60
d.	<i>Beam Squint</i>	61
4.	Time Difference of Arrival.....	63
C.	WIRELESS SENSOR NETWORKS	65
III.	BEAMFORMING USING WIRELESS NETWORK CONNECTIVITY	69
A.	ARRAY PERFORMANCE WITH RANDOM NODE DISTRIBUTION AND IMPRECISE LOCATION INFORMATION.....	70
B.	ARRAY PERFORMANCE WITH NODES IN STOCHASTIC MOTION	81
1.	Analysis of Simple Motion in a Two-element Array.....	83
2.	Analysis of Doppler Effect on Array Factor Due to Independent Motion.....	92
C.	ARRAY PERFORMANCE WITH INTERMITTENT NODE PARTICIPATION	100
IV.	RADIO FREQUENCY WIRELESS SENSOR NETWORK WITH INDEPENDENTLY MOBILE NODES.....	111
A.	MANAGEMENT METHODOLOGY EMPHASIZING SIGNAL DETECTION IN RADIO FREQUENCY SENSOR NETWORK NODES.....	112
B.	BEAMFORMING WITH DISTRIBUTED MOBILE ELEMENTS IN A WIRELESS SENSOR NETWORK	129
C.	DETERMINING WEIGHT RESET TIMING IN A WIRELESS SENSOR NETWORK WITH INDEPENDENTLY MOBILE ELEMENTS	148

D.	PAIR-WISE WIRELESS COMMUNICATIONS PERFORMANCE WITH UNSTEADY NODE ORIENTATION IN A SENSOR NETWORK	157
V.	CAPSTONE SIMULATION USING THE PROPOSED TECHNIQUES	177
A.	MODEL SETUP.....	178
B.	APPLICATION OF TECHNIQUES	182
VI.	CONCLUSION	191
A.	CONTRIBUTIONS.....	192
B.	AREAS OF FUTURE RESEARCH.....	194
	LIST OF REFERENCES	197
APPENDIX A.	BETA DISTRIBUTION	205
APPENDIX B.	ANTENNA EFFICIENCY.....	207
APPENDIX C.	SIMPLE PATTERNS	209
APPENDIX D.	NON-COHERENT	211
APPENDIX E.	ITERATIVE COMPARISON	215
APPENDIX F.	DOPPLER SHIFT	221
APPENDIX G.	DOPPLER SMEAR.....	223
APPENDIX H.	ARRAY FACTOR PATTERN	227
APPENDIX I.	OFFSET POSITIONS	231
APPENDIX J.	ONE DIMENSION PERTURB	237
APPENDIX K.	MOTION SMEAR.....	241
APPENDIX L.	AIM POINT GAIN CHANGE.....	245
APPENDIX M.	CHANGE PERCENTAGE FACTOR	249
APPENDIX N.	RESET ENERGY	251
APPENDIX O.	CHANGE PERCENTAGE EXPECTED VALUE	253
APPENDIX P.	PATTERN PROJECTION AND POLARIZATION	257
APPENDIX Q.	POTENTIAL ORIENTATION	259
APPENDIX R.	ORIENTATION / POLARIZATION FACTOR	261
APPENDIX S.	TRANSMISSION STRENGTH CORRECTION.....	267
	INITIAL DISTRIBUTION LIST	269

LIST OF FIGURES

Figure 1.	Traditional tactical radio frequency signal intercept scenario featuring a single operator supporting unit operations. Opposition units, in red, are shown positioned behind obstructions.....	4
Figure 2.	A tactical radio frequency signal intercept scenario featuring two intercept operators supporting unit operations.....	6
Figure 3.	A tactical radio frequency signal intercept scenario featuring multiple intercept operators supporting unit operations.....	7
Figure 4.	A tactical radio frequency signal intercept scenario featuring multiple intercept nodes attached to unit members as platforms. Radio frequency signal intercept data is networked to a local processing operator.....	9
Figure 5.	A tactical radio frequency signal intercept scenario featuring a beamformed array with radio frequency signal intercept data sent to a local processor.	10
Figure 6.	A tactical radio frequency signal intercept scenario featuring a beamformed array with multiple main beams formed by simultaneous processing of intercept data.	11
Figure 7.	Probability density function for a Gaussian random variable distribution with mean and standard deviation shown.	22
Figure 8.	Probability density function for a uniform random variable distribution.	23
Figure 9.	Probability density function for a beta random variable distribution. Various values of shape parameters α and β are shown.	24
Figure 10.	A one-dimensional, single step random walk aligned to the x -axis.....	27
Figure 11.	A one-dimensional random walk with single steps (forward or backward) aligned to the x -axis.	28
Figure 12.	A two-dimensional random walk with single steps in the x - y plane and forced time-step movement.....	29
Figure 13.	A two-dimensional random walk with multiple steps in the x - y plane.....	29
Figure 14.	A spherical coordinate system with respect to standard Cartesian coordinates.	34
Figure 15.	Antenna element in closed surface with observation point at r	36
Figure 16.	The gain pattern for a dipole antenna. The gain pattern for an isotropic element is included for comparison.	38
Figure 17.	The probability space for signal detection. Note that although probabilities appear Gaussian, any probability distribution is possible.....	45
Figure 18.	A two-element array with a target emitter in two dimensional space.....	47
Figure 19.	A system diagram of a two-element array.	48
Figure 20.	A two-element coherent array pattern in two dimensions.	50
Figure 21.	A generalized array structure with I elements.	51
Figure 22.	A multi-node array with random distribution in a two-dimensional space.	51
Figure 23.	A five-element array with elements randomly distributed in two dimensions.	54
Figure 24.	Gain pattern from the five-element, two-dimensional array in Figure 23.	54

Figure 25.	A four-element array with symmetrically placed nodes. Nodes have a distance $d = 0.2$ to nearest adjacent node.	56
Figure 26.	Azimuth of normalized pattern associated with the array in Figure 25 and a scan angle of $\phi_o = 90^\circ$	57
Figure 27.	A four-element array with symmetrically placed nodes. Nodes have a distance $d = 1.2$ to nearest adjacent node.....	58
Figure 28.	Azimuth normalized pattern associated with the array in Figure 27 and a scan angle of $\phi_o = 90^\circ$	58
Figure 29.	A four-element array with symmetrically placed nodes. Nodes have a distance $d = 3$ to nearest adjacent node.....	59
Figure 30.	Azimuth of normalized pattern associated with the array in Figure 29 and a scan angle of $\phi_o = 90^\circ$	59
Figure 31.	A six-element array with randomly spaced nodes. Spacing shown is in meters.....	62
Figure 32.	The array factor pattern for the array in Figure 31 at various frequencies.	63
Figure 33.	The basic setup for application of the time difference of arrival technique. ...	64
Figure 34.	The two-sided hyperboloid formed by the TDOA solution from two elements.	65
Figure 35.	The relative angles in a Doppler effect problem.....	68
Figure 36.	A uniformly random distribution of nodes in two dimensions.	70
Figure 37.	A moderately arranged set of nodes.....	71
Figure 38.	A three-node array (Distance in wavelengths).....	72
Figure 39.	A nine-node array (Distance in wavelengths).....	73
Figure 40.	Normalized array factor pattern for array in Figure 38 with $\phi_o = 60^\circ$ and $\theta_o = 90^\circ$	73
Figure 41.	Normalized array factor pattern for array in Figure 39 with $\phi_o = 60^\circ$ and $\theta_o = 90^\circ$	74
Figure 42.	Normalized array factor azimuth pattern associated with Figure 40.	75
Figure 43.	Normalized array factor azimuth pattern associated with Figure 41.	75
Figure 44.	Array from Figure 38 with a 0.1 wavelength positioning error in the negative y-axis direction applied to the red node.....	79
Figure 45.	Array from Figure 39 with a 0.1 wavelength positioning error in the negative y-axis direction applied to the red node.....	80
Figure 46.	Cross-section comparison of normalized array factor patterns for the array in Figure 38 versus array with node offset shown in Figure 44.....	80
Figure 47.	Cross-section comparison of normalized array factor patterns for the array in Figure 39 versus array with node offset shown in Figure 45.....	81
Figure 48.	A two-element array with element spacing, d	84
Figure 49.	Array pattern in x - y plane for two-element array in Figure 48 with $\alpha = 0^\circ$	86
Figure 50.	Array pattern in x - y plane for the two-element array in Figure 48 with $\alpha = 250^\circ$	87
Figure 51.	The two-element array from Figure 48 modified by positive x -axis motion of node two.	88

Figure 52.	Array pattern in x - y plane of the modified two-element array in Figure 51.	89
Figure 53.	The two-element array from Figure 48 modified by positive y -axis motion of node two.	90
Figure 54.	Array pattern in x - y plane of modified two-element array.	92
Figure 55.	General reception array geometry with respect to a target transmitter.	94
Figure 56.	Geometry of reception array with transmitter in motion.	95
Figure 57.	An array with elements and target transmitter in two-dimensional random motion.	96
Figure 58.	A ten-element array with Uniform random distribution (Distance in wavelengths).	97
Figure 59.	Cross-section along the x - y plane of the normalized array pattern from the array in Figure 58.	98
Figure 60.	Cross-section along the x - y plane of the normalized array pattern from the array in Figure 58 with Doppler smear compared with the pattern from static elements.	99
Figure 61.	Absolute difference between the normalized array pattern in the x - y plane for the array with static elements and with Doppler smear.	99
Figure 62.	Vulnerable Nodes.	101
Figure 63.	The array from Figure 38 modified to show one node intermittent (Distance in wavelengths).	102
Figure 64.	Cross-section along the x - y plane of the normalized array pattern from the array in Figure 63 where one node is intermittent compared with the pattern from the full array in Figure 38.	105
Figure 65.	The array from Figure 39 modified to show one interior node intermittent (Distance in wavelengths).	106
Figure 66.	Cross-section along the x - y plane of the normalized array pattern from the array in Figure 65 where one interior node is intermittent compared with the pattern from the full array in Figure 39.	107
Figure 67.	The array from Figure 39 modified to show one exterior node intermittent.	108
Figure 68.	Cross-section along the x - y plane of the normalized array pattern from the array in Figure 67 where one exterior node is intermittent compared with the pattern from the full array in Figure 39.	108
Figure 69.	Probability of detection versus receive antenna gain under differing levels false alarm constraint.	118
Figure 70.	The structure of parameters in the system methodology.	120
Figure 71.	Flow chart depicting post-detection processing for the wireless sensor network array.	122
Figure 72.	Energy cost versus number of nodes in an iteration where cost is constrained with respect to the additional nodes.	126
Figure 73.	The difference in energy cost between the proposed method and the method in [10] versus the number of nodes involved in TDOA.	127
Figure 74.	A comparison of array gain for a randomly distributed 10-element array versus the same array after random motion is applied to the elements.	132
Figure 75.	A comparison of motion at different node speeds in terms of the percentage of wavelength per sample versus frequency of interest.	133

Figure 76.	Percentage of gain lost in the target direction over time where $N = 2$ in the case of random element motion. Each line represents a separate instance of 100 iterations.	135
Figure 77.	Percentage of gain lost in the target direction over time where $N = 5$ in the case of random element motion. Each line represents a separate instance of 100 iterations.	136
Figure 78.	Percentage of gain lost in the target direction over time where $N = 10$ in the case of random element motion. Each line represents a separate instance of 100 iterations.	136
Figure 79.	Percentage of gain lost in the target direction over time where $N = 40$ in the case of random element motion. Each line represents a separate instance of 100 iterations.	137
Figure 80.	Histogram of modified change percentage, \mathbb{C} , for wirelessly connected arrays with element nodes in independent random motion for $N = 2$ and Rician ratio distribution line.	140
Figure 81.	Histogram of modified change percentage, \mathbb{C} , for wirelessly connected arrays with element nodes in independent random motion for $N = 5$ and Rician ratio distribution line.	140
Figure 82.	Histogram of modified change percentage, \mathbb{C} , for wirelessly connected arrays with element nodes in independent random motion for $N = 10$ and Rician ratio distribution line.	141
Figure 83.	Histogram of modified change percentage, \mathbb{C} , for wirelessly connected arrays with element nodes in independent random motion for $N = 40$ and Rician ratio distribution line.	141
Figure 84.	A comparison of transmission energy between a method using the proposed metric and a method with continuous updates over a single cycle, \mathbb{N} . The energy per transmission is normalized, so unit size in arbitrary.....	147
Figure 85.	Energy difference (arbitrarily scaled based on application) between the proposed method and the first alternate method at various settings for \mathbb{N}_{A_1} . For analysis, settings of $\delta = 1$, $\chi = 0.1$, and $N = 8$ were applied.	154
Figure 86.	Arrangement of a pair of nodes (Nodes B and C) in communication plus a check node (Node A), which exhibits desired orientation.....	161
Figure 87.	Check Node A and Node B with Node B rotated to the x-axis. Note: Axes y' and z' are parallel to the y and z axes and are shown for convenience.....	163
Figure 88.	Arc-length element rotation compared to approximation using angle projection.	164
Figure 89.	Magnitude of efficiency factors for gain pattern and polarization versus function angles ψ and \aleph , respectively.....	165
Figure 90.	Example of potential function angles for pattern and polarization in a communications pair with a variety of drops from ideal.	165
Figure 91.	Transmission Factor over 50,000 runs for $w_B = 5^0$ and $w_C = 5^0$	167
Figure 92.	Transmission Factor over 50,000 runs for $w_B = 8^0$ and $w_C = 10^0$	168

Figure 93.	Transmission Factor over 50,000 runs for $w_B = 15^0$ and $w_C = 15^0$168
Figure 94.	Transmission Factor over 50,000 runs for $w_B = 15^0$ and $w_C = 20^0$169
Figure 95.	Histogram of transmission factor, \mathbb{F} , compared with a beta distribution, where $w_B = 5^0$ and $w_C = 5^0$170
Figure 96.	Histogram of transmission factor, \mathbb{F} , compared with a beta distribution, where $w_B = 8^0$ and $w_C = 10^0$170
Figure 97.	Histogram of transmission factor, \mathbb{F} , compared with a beta distribution, where $w_B = 15^0$ and $w_C = 15^0$171
Figure 98.	Histogram of transmission factor, \mathbb{F} , compared with a beta distribution, where $w_B = 15^0$ and $w_C = 20^0$171
Figure 99.	Histogram of normalized signal magnitude distribution in a signal hop with the model based correction factor, Φ . Target received power is arbitrary power units based on application.174
Figure 100.	Agent position in Pythagoras modeling in first phase level showing individual unit member interaction where each dot is an individual agent, the yellow background indicates terrain, and the brown notes terrain changes (in this case, “road” conditions).181
Figure 101.	Detail position in Pythagoras modeling in second phase showing detail group interaction where each blue dot is a unit with multiple agents, the yellow background indicates terrain, and the brown notes terrain changes (in this case, “road” conditions).. The blue dot on the lower left represents the way-point motion goal.181
Figure 102.	Agent positions translated to meters with a single reference point.184
Figure 103.	Sub-area agent positions with reference point shifted to the center of the sub-area. Agents depicted in red are selected for the initial iteration.185
Figure 104.	A three-dimensional depiction of the coherent array beamforming result from the first iteration.186
Figure 105.	The normalized array pattern in the x - y plane from the first iteration.186
Figure 106.	The two-dimensional cross-section of the array factor result at the time step indicated for change versus the initial configuration of the first iteration.188
Figure 107.	The normalized two-dimensional cross-section of the array factor result at the time step indicated for change versus the initial configuration of the second iteration.189
Figure 108.	The normalized two-dimensional cross-section of the array factor result at the time step indicated for change versus the initial configuration of the third iteration.189

THIS PAGE INTENTIONALLY LEFT BLANK

LIST OF TABLES

Table 1.	Array pattern differences due to Doppler smear over various velocities.....	100
Table 2.	Mean, standard deviation and Kolmogorov-Smirnov goodness-of-fit data for the arrays in Figure 80, Figure 81, Figure 82, and Figure 83.....	145
Table 3.	Mean percent change $(\mathbb{C}(\theta, \phi, t))$	155
Table 4.	An abbreviated listing of agent position versus time step.	182
Table 5.	Estimated reset time values and associated change percentage from Pythagoras agent motion.....	188
Table 6.	Beta distribution factors arising from assigned wobble factors for agent to agent and agent to base station links.....	190

THIS PAGE INTENTIONALLY LEFT BLANK

EXECUTIVE SUMMARY

An antenna array consists of a set of physically separate antenna elements operating as a single entity for signal transmission or reception. Information from each element is intelligently combined to optimize signal reception or transmission. This process, known as “beamforming,” improves performance over a single element antenna because the combination produces an increase of gain with respect to a specific spatial target direction and correspondingly deemphasizes gain from alternative directions. The effect of array beamforming is attractive in applications because of increased performance and the ability to implement using unsophisticated antenna elements. An alternative of a single “specially tuned” antenna structure may be impractical in implementation or cost.

Antenna arrays are attractive for military applications because of their ability to train towards an intended target signal, mitigate effects of potential interfering or jamming signals, and operate with simple and rugged elements. Conventional array design includes physical connections between elements and the processing sink. Additionally, traditional design assumes element positions are known and static. Such design has been used to great success in the military for unit communications as well as interception of adversary communications. However, the static and wired nature of array design has also influenced military operations, as communications in specific bands require radio signal sites be stationary. Alternatively, when mobility is necessary, complex, delicate, or inefficient elements are used.

The advent of wireless networking, and specifically wireless sensor networks, has made the possibility of separated and autonomous applications feeding a centralized process realizable. Implementation of an antenna array through a wirelessly connected network of radio frequency signal sensors is a natural extension of the wireless sensor network concept. Connection of individual elements via a wireless network certainly offers ease of implementation constrained only by bit error loss of wireless links compared to the previous wired connection. However, with the elements wirelessly networked, new engineering issues arise. Autonomous sensor nodes provide the benefit

of independent operation but also must be properly managed to preserve limited battery life. Array elements, no longer tied to a specific location through wired connections, bring the concept of individual mobility to fore. This is a significant design and realization issue because knowledge of spatial positioning is instrumental in traditional beamforming. A further effect of motion, element stability, also requires study regarding system performance.

This dissertation investigates some fundamental issues that hinder the implementation of reception of radio frequency signals using wirelessly connected sensor nodes under individual random motion as an antenna array. Although a number of problems exist for specific realizations, an analytical study has been applied to the foremost issues and novel techniques are proposed to mitigate problems where necessary.

The initial problem in creating a coherent array using elements connected by wireless sensor network is in the management of network assets. Although it is obvious that elements must be available and provide data to a central data sink for combination, the paradigm that in a wireless sensor network each node is autonomous crosses into operating parameters. A novel management technique directly focused on supporting sensor operation while preserving network energy is thus proposed. This methodology focuses the sensor system on detection of signal presence, and it compares favorably to alternative methods in terms of system response and energy conservation.

In considering element motion in the array, the question of perturbation due to Doppler shift is present. The work demonstrates that Doppler shift due to physical motion of array elements provides negligible perturbation of the beamforming solution. This conclusion, based on simulation, showed negligible change in beam pattern in the specific application in which phase center is held constant. This result assisted in simplifying the solution methods developed to address other issues caused by nodes in random motion.

Continuing the analysis, this research considered the ability to operate a coherent beamforming array while array elements are independently mobile. Although efficient management of individual sensor nodes allows such an array to exist, overhead from meta-data and constant array weight recalculation make operation untenable. The work

on beamforming algorithms and their operation under non-ideal conditions enabled the proposed novel method of using a probability based scheme to manage this issue. The research demonstrated its contribution in that although the nodes exhibit independent motion, when combined with the beamforming structure a predictable pattern emerges based on a Rician ratio distribution. Knowledge of this distribution allows for delay in resetting array weights for coherent combination. This revealed the potential to conserve energy in meta-data transfer as a further contribution, preserving energy in the network while continuing to provide array factor gain at the required level.

With the knowledge of a proposed management structure to operate a radio frequency signal sensor network and the distribution associated with an array with nodes in independent motion, consideration of the entire problem of a signal sensor array with mobile nodes was undertaken. A technique for implementation of these methods in order to determine an appropriate time to update array weights was thus required. A novel algorithm was proposed based upon an eight-step procedure. This method enables the previously proposed management method and the defined beamforming percent change distribution algorithm to work together in determining the time for weight reset and demonstrates specific energy savings and/or performance improvement compared to alternative methods.

Proper function of a data intensive wireless sensor network requires solid communications links. In order to assist in improving data exchange when nodes are mobile, node orientation was considered. Antenna polarization and tilt may have a specifically deleterious effect on communications links, but they are often considered in a static sense. The proposed method combines physical motion and element attributes in a free-space link in order to assess the most-likely loss of power due to these factors. With this knowledge, a mitigation strategy was developed, which successfully improved transmission performance. This method provided energy savings compared to alternative techniques while keeping required bit error rate at a desired level.

This dissertation provides innovative solutions to major issues in the implementation of a wirelessly networked beamforming array. Each of the novel methods proposed performs better than the alternative methods available in literature, and the research significantly contributes to implementation.

THIS PAGE INTENTIONALLY LEFT BLANK

ACKNOWLEDGMENTS

Thanks are due to my parents for their love and devotion in raising me to strive for knowledge and achievement. My adorable daughter also deserves thanks for her patience with a busy father, unconditional affection, and boundless joy. Most of all, appreciation is deserved for my angelic wife, for she was the source of my motivation through this long process, my solace when necessary, and my pride always.

THIS PAGE INTENTIONALLY LEFT BLANK

I. INTRODUCTION

A study is presented regarding the use of a wireless sensor network with independently mobile nodes as a signal reception system. Well-established concepts including array beamforming and wireless networking are challenged by the sensor network limitations and autonomous movement, degrading traditionally expected results for sensor performance and network data exchange. Novel concepts are offered in regards to management of sensor node resources, mitigation of motion effects on sensor data synchronization, optimization of sensor solution timing in the combination process, and improvement of wireless network data exchange. Each of these schemes is defined and compared to conventional processes in terms reflected in system performance.

A. BACKGROUND AND MOTIVATION

From strategic to tactical levels in military operations, the roles and requirements associated with collection of information have become paramount. Joint Vision 2020 directly states the key requirement for forces to gain and maintain Information Superiority in order to achieve domination across the full collection of potential operations [1]. Specifically, it states “Information superiority is fundamental to the transformation of the operational capabilities of the joint force.” Defined in Joint Publication 1-02, Information Superiority is the “operational advantage derived from the ability to collect, process, and disseminate an uninterrupted flow of information while exploiting or denying an adversary’s ability to do the same [2].” Proliferation of sensors to accomplish Information Superiority is a natural progression, which is matched with the trends of technology increasing the abilities of sensors, associated distribution networks and processing. Indeed, the maturation process of sensor networks has shown a dramatic growth from the initial visions of limited capability structures to multimedia capable systems considered for deployment in greater varieties of applications and aboard diverse platforms [3].

A specific application of sensor networks for reception of radio frequency signals is a piece of the Information Superiority puzzle, and it is in this context of military

operations towards and achievement of Information Superiority that the analysis of radio frequency signal reception using a wireless sensor network with independently mobile nodes will be presented. Although the applications of such a sensor network and proposed techniques for implementation may apply outside of this defining context, the direct application of this research to military operations demonstrates obvious utility.

Radio frequency signal reception across the spatially separated nodes of a sensor network implies the employment of techniques for either antenna array beamforming or spatial diversity in reception. This effort will consider the nodes operating as a beamforming array. To elucidate, an antenna array consists of a set of physically separate antenna elements operating as a single entity for signal transmission or reception. Signal information from each element is intelligently combined to optimize signal reception or transmission. This process, known as “beamforming,” improves performance versus a single element because the combination of signal information produces an increase in gain corresponding to a specific spatial angle from the array and correspondingly deemphasizes gain from alternative directions [4]. The effect of array beamforming is attractive in applications because of increased performance and the ability to implement using uncomplicated antenna elements. Antenna arrays are attractive for military applications because of their ability to train towards an intended target signal, mitigate effects of potential interfering or jamming signals, and operate in non-ideal environments with simple and rugged elements. Conventional array design includes physical connections between elements and the data processing sink. Further, traditional design assumes element positions are known and static. Such design has been used to great success in the military for unit communications as well as intercept of adversary communications. However, the static and wired nature of array design has also influenced military operations, as communications in specific bands require that radio signal sites be stationary. Alternatively, when mobility is necessary, complex, delicate, or inefficient elements are used.

The advent of wireless networking, and specifically wireless sensor networks, has made the possibility of separated and autonomous applications feeding a central processor realizable. Connection of individual antenna elements via a wireless network

to form an array certainly offers ease of implementation constrained only by bit error loss of wireless links compared to the previous wired connection. However, with the elements no longer tied to a specific location through wired connections, the concept of individual element mobility comes to fore. Element sensors packaged as man-portable equipment appear to offer the ability to carry an array forward in a battlefield environment, offering the benefits of array operation without the restriction of static positioning, but significant design and realization issues also come to light, since the knowledge of array spatial positioning is instrumental in traditional design. Further, both the ability to manage the network and provide assurance of data availability are impacted.

Within the context of Information Superiority under military operations, the scenario of a ground-based signal sensor field operated in a forward area is offered as a single illustration of how such a radio frequency receiving wireless sensor network may be envisioned and why an array system is preferable to current operational methods. A signal sensor field may be defined as a group of sensors deployed with the intent to detect signal presence, receive/demodulate, and find/fix electronic communications from an uncooperative target. As depicted in Figure 1, traditionally a single military tactical signal intercept operator has sole responsibility for intercepting opposition force radio communications. The operator moves with his unit to maintain the ability to support maneuvers in the operating area. To accomplish his task, the operator is outfitted with signal collection equipment that is man-portable, where the limitations of man-portability include weight, robustness, and independent operability. Additionally, the equipment must be broadly applicable across a set of target signals in order to provide the greatest value against uncertain conditions. Therefore, an individual operator will need to physically carry sensor equipment in hostile environments while prosecuting communications that vary in even the most basic of signal parameters such as center frequency and bandwidth. Tradeoffs between signal intercept capability and equipment physical parameters are therefore necessary and obvious.

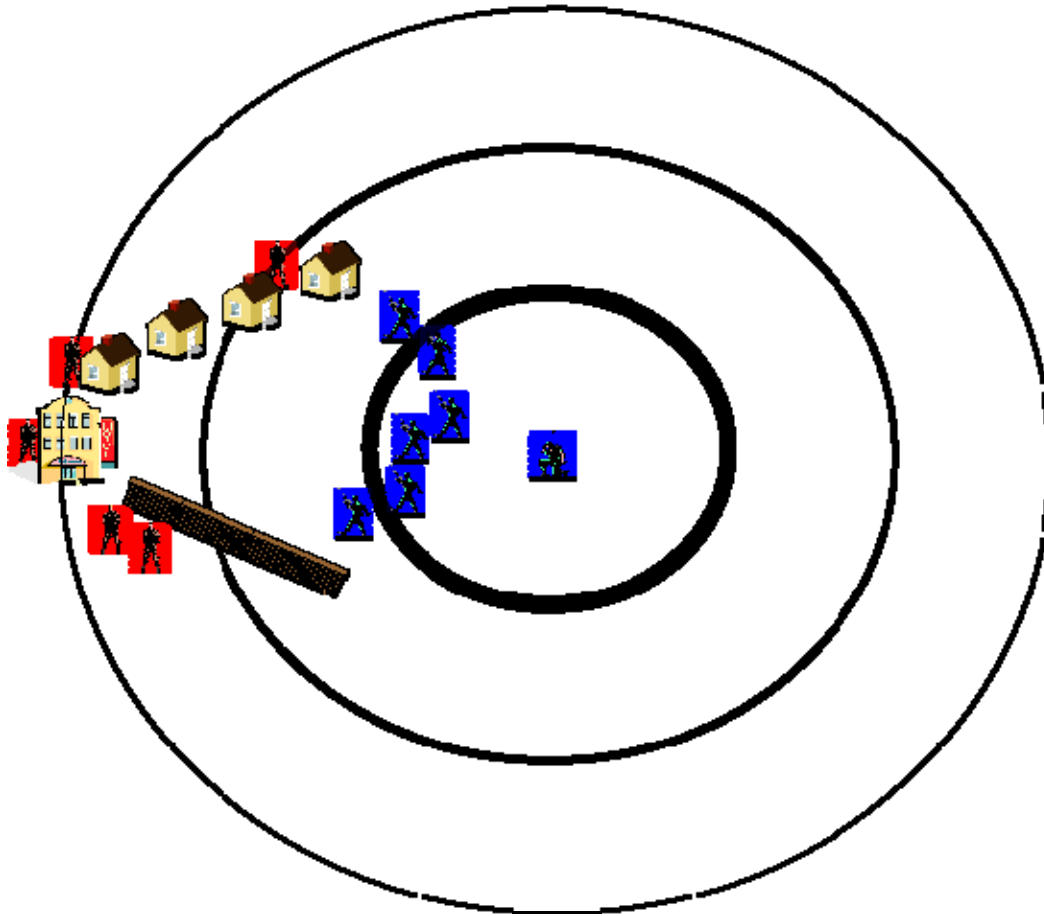


Figure 1. Traditional tactical radio frequency signal intercept scenario featuring a single operator supporting unit operations. Opposition units, in red, are shown positioned behind obstructions.

In order to meet the challenges and tradeoffs described, military research has produced a variety of solutions in terms of signal processing, operator controls, and energy conserving solutions. However, the specific limitation of a signal spatially located element remains at issue. Generic range rings are included in Figure 1 surrounding the intercept operator. Although the range rings do not properly account for all signal propagation issues with respect to terrain and reflection / refraction from obstacles among other issues, they are depicted to demonstrate that radio frequency signal reception from a single omni-directional element does not have the benefit of emphasizing reception toward a known direction of interest, such as towards a threat vector, or minimizing reception from azimuths of lesser interest or directions with

potential interferers. Further, target signal geo-location or even general direction, is unavailable to the operator without external assistance. While it should be noted that specialized antenna assemblies exist to assist with directionality and / or direction finding, the trade-off for specialized solutions is generally a limitation of applicability across the set of the target signal spectrum or reduction in man-portability factors. Therefore, alternate solutions must be considered to increase signal intercept capability while maintaining the ability to operate in the field.

A scenario of multiple (two in this case) radio frequency signal intercept operators is shown in Figure 2. Again using traditional guidelines, the intercept operations function independently but are coordinated for information exchange. Such an exchange normally involves a voice link, distribution of target responsibilities, and sharing of a limited set of meta-data. While this scheme certainly represents an increase in ability to prosecute a target signal set and support unit operations, the drawbacks associated with the single element with respect to signal reception at each operator's position continues to be present. Operators, and their respective collection equipment, fundamentally access the radio frequency environment separately. Therefore, spatial emphasis (or de-emphasis) is not available to the operator.

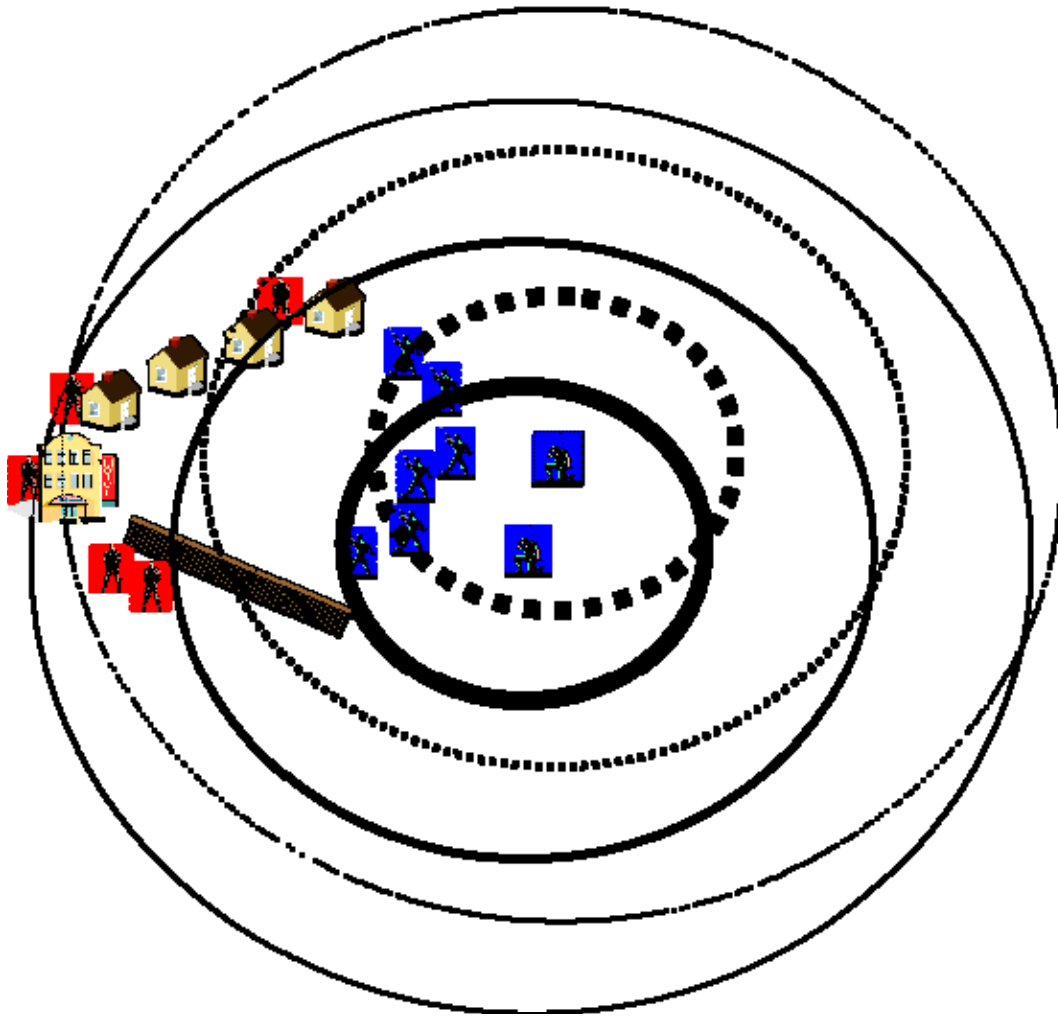


Figure 2. A tactical radio frequency signal intercept scenario featuring two intercept operators supporting unit operations.

Obviously, this concept is furthered by the addition of multiple radio frequency signal intercept operators, as shown in Figure 3. Coordination of operations as described in the two operator scenario continues to improve the ability of intercept operations to respond to diverse threats, even with the operation of individual antennas failing to improve spatial emphasis (or de-emphasis). However, this scenario also demonstrates that manpower increases to support improvements in radio frequency signal intercept may become unwieldy, overwhelming other unit operational needs. Alternate solutions are then necessary to maximize the range and quality of radio frequency signal intercept operations while minimizing the “cost” to provide this capacity.

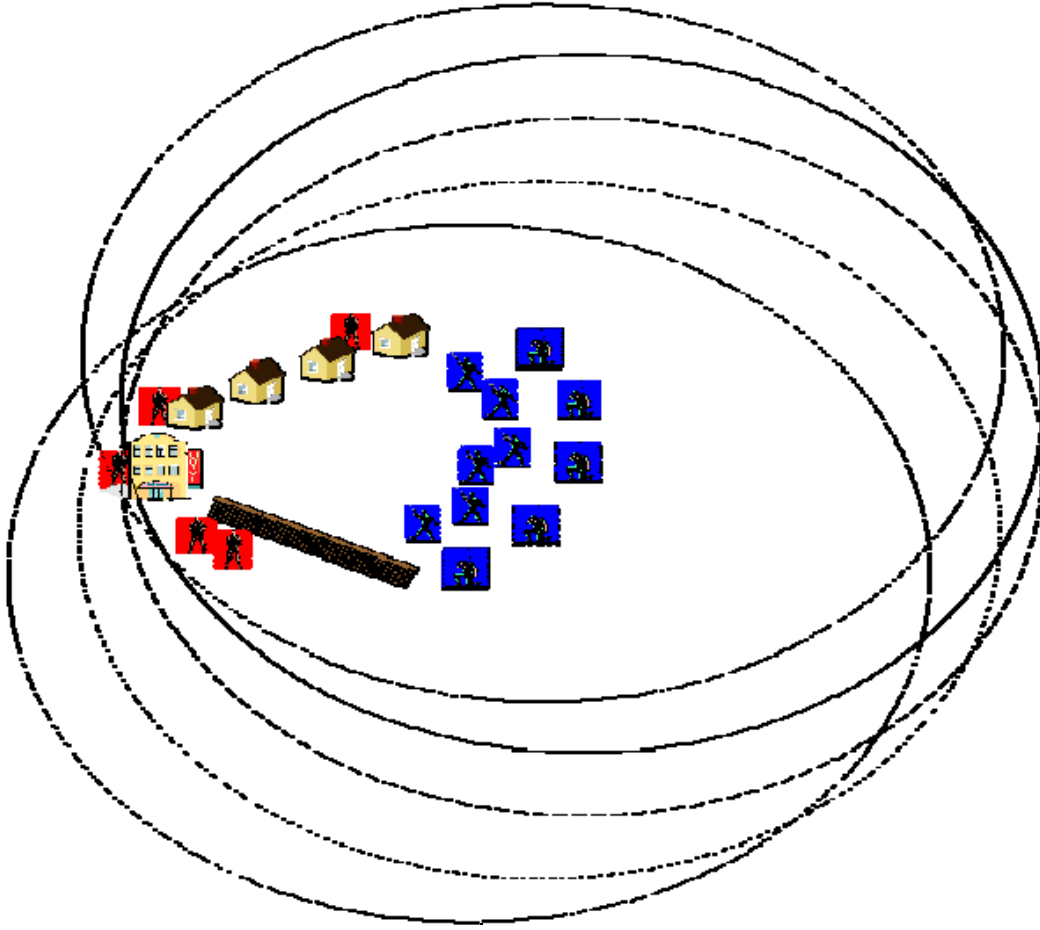


Figure 3. A tactical radio frequency signal intercept scenario featuring multiple intercept operators supporting unit operations.

The tactical radio frequency signal intercept operator scenarios described almost innately advertise themselves as an application for a sensor network. Indeed, an alternate description of the operators as individual sensor nodes distributed across a target environment is fitting. In their traditional state connected by voice communications, the processed intercept data is shared. However, if instead the raw signal data is distributed to a central processing site, not only can the individual processing take place, but intelligent combination of the intercept may be performed in order to achieve beamforming as described. The advent and advances of network communications makes this kind of data exchange in a robust fashion possible. Previous research, such as that in [5], [6], [7], and [8], investigated usefulness and implementation of arrays of wireless sensor network nodes in transmission for the purpose of exfiltrating data. Due to the

nature of wireless sensor nodes as envisioned, these studies provide particular insight with regards to mitigation strategies for imperfect position knowledge, degradation due to phase offsets, and implementing methodologies for randomly deployed stationary nodes. In each instance, the concept of forming a transmission array using nodes in their random spatial arrangement was demonstrated as valid. The concept of implementing the wireless sensor nodes to form a reception array, vice a transmission array, was covered by [9] and [10], which are summarized in [11]. These studies cover a methodology to implement a radio frequency signal intercept array using stationary randomly deployed sensor nodes and a specific technique to increase array processing gain while conserving network energy.

The application of a wireless sensor network in the defined scenario is therefore sound. Under the scenario defined in [10], autonomous sensor nodes would be deployed into a threat environment. These sensor nodes are activated by a central controller with the responsibility to detect signals of interest, wake nodes required for signal intercept, and form the solution. Among the basic concerns with this type of scenario is the inability of the sensor field to move along with the operational units, as described earlier in this section. So, an alternate approach enabling mobility is considered.

Consider each member (or a subset of members) of a military unit as radio frequency signal intercept nodes. This scenario is similar to that described in Figure 3, except that each intercept operator instead simply acts as a platform for a node. In this scenario, individual wireless sensor nodes consist of an omni-directional antenna and receiver as a sensor for target signals, a transceiver and antenna pair for network communications at a frequency outside of the target signal band, an onboard processor, and a battery. Obviously, this package must be small enough not to impact the mobility of the individual acting as the platform. The data collected at each sensor node is then networked for exfiltration to a central processing location, as shown in Figure 4 with three forward sensor nodes and a local intercept and processing operator. Additional data centralization schemes, which may exist, include data passing through a local relay to a remote processing location or data exfiltration through beamforming as discussed in [7].

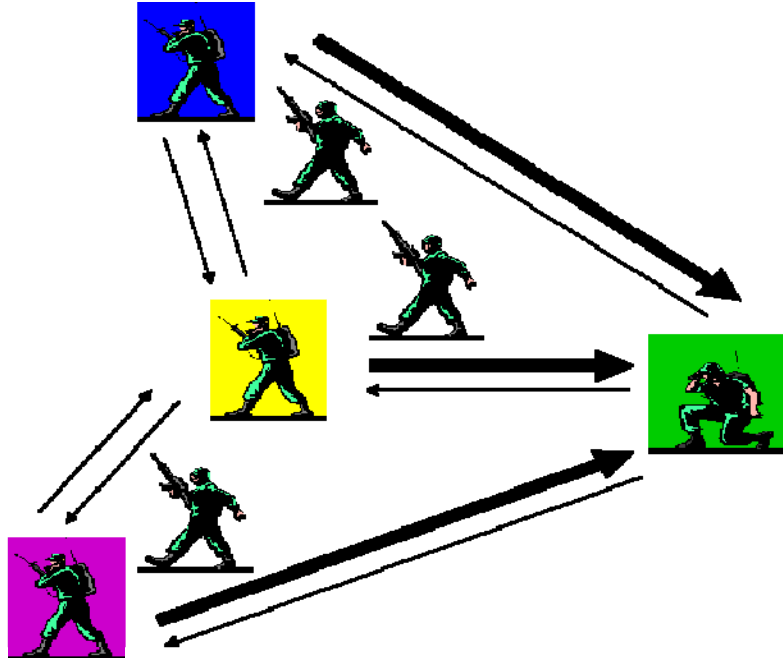


Figure 4. A tactical radio frequency signal intercept scenario featuring multiple intercept nodes attached to unit members as platforms. Radio frequency signal intercept data is networked to a local processing operator.

With the radio frequency signal intercept data from each node available at a central processing location, the coherent combination of input for array beamforming may occur. Such a scenario is depicted in Figure 5. As shown, beamforming enables a measure of spatial emphasis towards a threat vector. Additionally, it enables some capacity to de-emphasize reception from specific vectors, and an assortment of geo-location techniques, such as Time Difference of Arrival (TDOA), become available to assist the operator if knowledge of target emitter position is desired [12].

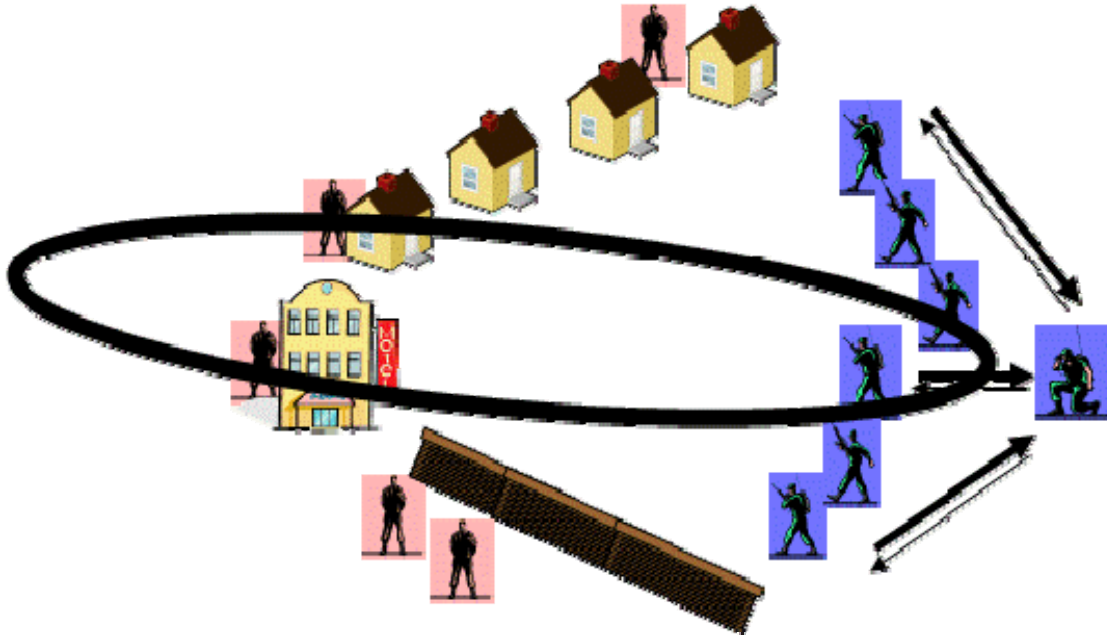


Figure 5. A tactical radio frequency signal intercept scenario featuring a beamformed array with radio frequency signal intercept data sent to a local processor.

With an array beamformed, the question of adjusting the array to achieve desired main beam gain, beamwidth, and azimuth is pre-eminent. Further, the potential for multiple desired main beam azimuths may also be a consideration. In terms of reaching desired gain and beamwidth, it will be seen that those are a function of number of nodes and spatial separation [13] and [14]; therefore, understanding of node deployment and management of sensor resources will be necessary. In conditions where multiple azimuths for the main beam are desired, concurrent processing in the central processing node enables multiple beams simultaneously. A multiple beam / multiple azimuth scenario is demonstrated in Figure 6. In this case, overlapping beams are used to search a broad area with enhanced gain towards the target sector and decreased emphasis in spatial directions, which are not of interest.

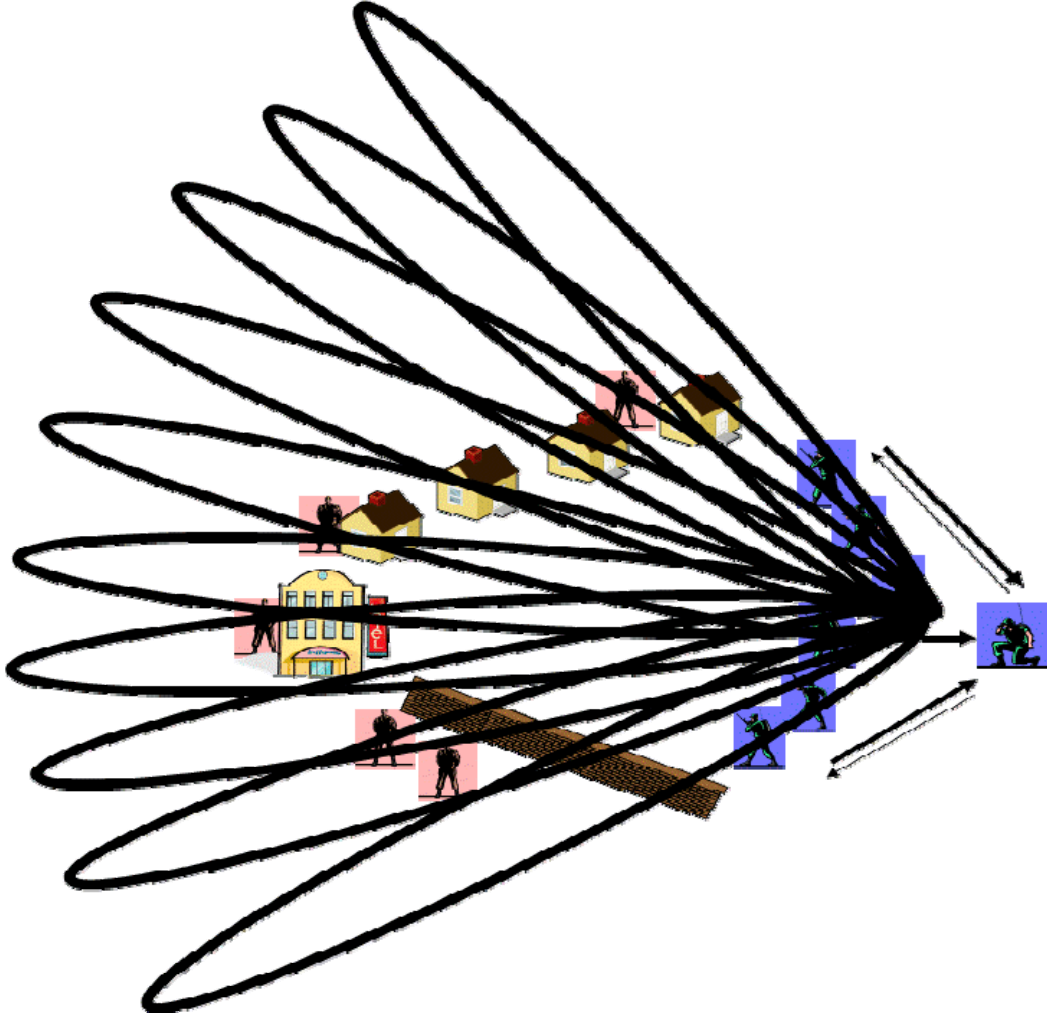


Figure 6. A tactical radio frequency signal intercept scenario featuring a beamformed array with multiple main beams formed by simultaneous processing of intercept data.

B. OBJECTIVE

The scenario of networked nodes attached to military unit members paints a good background scenario to consider implementation challenges. The concepts of antenna arrays and networked communications are well understood, and texts such as [15] and [16], among others, provide solid background on their respective framework. It is with the management of the processes together in a energy conservation environment and the addition of motion in the beamforming and data exchange processes that the application of traditional design and implementation stumble. Analysis of the obstacles encountered

when attempting to conduct radio frequency signal reception using distributed wirelessly networked sensor nodes under random motion as a beamforming array and the proposal of solutions to mitigate the effects of those obstacles is the thrust of this research. The objective is therefore to consider some of the major issues in receiving radio frequency signals in a beamforming solution using elements under independent motion and to propose novel solutions to enable implementation. As will be further described, the major issues considered will be in regard to management of autonomous nodes, beamforming degradation with elements in motion, beamforming weight reset time, and network communications with unstable transceiver elements.

As noted, the management of a deployed sensor network to meet signal intercept operational requirements in a energy constrained environment is a primary issue in system realization. Although it is obvious that elements must be available and provide data to a central core for combination, the paradigm that in a wireless sensor network each node is autonomous crosses into operating parameters. Therefore a novel management technique directly focused on balancing operational and support requirements is necessary and proposed.

In considering the creation of a coherent beamforming array using elements under motion, a series of potential issues immediately emerge. In some of these cases, related work provides insight. The mathematics and established implementation methodologies behind traditional array beamforming generally assume defined antenna placement or, at a minimum, knowledge of relative positioning [4] and [16]. It is from this assumption that these analyses of beam pointing, gain, and beamwidth relations are considered [13] and [14]. Research into other phenomena surrounding array beamforming are also predicated on at least a general knowledge of spatial layout, including grating lobes [17], coupling [4], [18], and [16], and beam squint [19] and [20]. Straying from perfect position knowledge, research on the effects on position errors in [5] and synchronization errors in [21] and [6] implicitly assume an error between actual and assumed position but continue to assess in terms of determining a solution that may then be used to correct the then static error.

This research will instead consider the effects of dynamic random motion on the beamforming solution. It will be clearly demonstrated how the beamformed solution will deteriorate with the loss of positioning precision over time, and a model will be proposed covering the stochastic properties of the array beam as a result of this motion. The stochastic model will demonstrate that the characteristics of the resultant array beam are predictable, even as the positions are altered. Therefore, the opportunity will exist to use the distorted array solution over periods of time, saving energy in the meta-data transfer required to create weights necessary to correct the beam.

Applying the stochastic model, the subsequent concern is determination of an optimal timing for weight resets. Clearly the distorted beam will not be able to meet operational requirements perpetually; however, a process that replenishes weights abruptly does not make adequate use of network node energy. Alternatively, a process that postpones weight updates for too long does not provide beamforming service in keeping with operational requirements. By combining the results of the proposed sensor management algorithm and the proposed stochastic model of the array beam, a methodology is introduced that allows for engineering determination to balance determined beamforming constraints and network energy conservation goals.

Finally, the dilemma of dynamically changing element orientation is considered. It will be demonstrated how this motion can be considered a concern for the beamforming solution; however, the wireless communications connections in the sensor network will be of specific interest. The loss of individual communications links in the network may result in the inability to include all iteration nodes in a beamforming solution. This is shown to greatly affect the expected beamforming solution, which will consider lost communications packets as intermittent element participation. As such, measures must be taken to assure strong physical links exist. However, the general response to meet this challenge, raising transmission power to create a margin over a worst case across the network, does not fully optimize network energy use. A model based on antenna orientation patterns and polarization in a stochastic environment is

proposed as an alternative solution to this issue. With this model, pair-wise connections can be set to deliver a median energy per bit to noise power spectral density ratio as determined for proper operational function.

C. ORGANIZATION

This dissertation is organized as follows. Chapter II provides an overview of stochastic analysis, electromagnetics and communications, and wireless sensor network topics. These subjects are presented without context but are provided to lay a foundation for later analysis and application. Chapter III presents an analysis of coherent beamforming in the presence of motion, including deterioration of solution due to unchecked Doppler effect due to motion, and the result of lost elements in coherent combination.

Chapter IV considers and provides novel solutions to the main issues considered outstanding in Chapter III, and it is broken into four sections. Section A introduces a proposed management methodology for the wireless sensor network tasked with beamforming. This methodology will be introduced in a static system, but it will later be applied to the dynamic motion case. Additionally, this section will present alternate techniques for management in this scenario for the purpose of demonstrating how the proposed technique performs in contrast to other available methods. Section B tackles the concept of beamforming in a random motion environment through the introduction of a stochastic model regarding the beamforming solution. This model will be shown to exhibit predictable characteristics such that a beamforming solution that has been warped by element random motion may continue use without correction for a period of time. The prospect of using this model to save energy in the network will be broached. Section C combines the techniques proposed in Sections A and B to create a method determining optimum timing for weight reset in the beamformed solution to meet both operational and energy constraints. Alternate techniques for determining reset timing will be introduced in this chapter for the purpose of demonstrating how the proposed technique performs in contrast to other available methods. Finally Section D proposes a stochastic model regarding the problem of dynamically random orientation of sensor network nodes in

communications. This model will be applied in a specific scenario and compared against a general link margin increase technique to demonstrate its effectiveness.

Chapter V demonstrates the application of all proposed techniques inside a specific scenario of a unit on foot moving across a field. This chapter illustrates how the proposed methods can be harmonized to target a specified operational problem. Finally, Chapter VI summarizes results and discusses potential future work.

THIS PAGE INTENTIONALLY LEFT BLANK

II. BACKGROUND

This chapter provides an overview of topics necessary for examination of the dissertation research in later chapters. Each topic is presented as an individual unit without connection or context, unless otherwise noted. The intent is to provide an understanding of the subjects, as they will be specifically applied later. While this chapter does not exhaustively cover every subject of interest in the research, the topics reviewed are of significant interest to the problem examined. The topics are presented in three sections covering stochastic models, electromagnetics and communications, and wireless sensor networks.

A. STOCHASTIC MODELS

A process that includes random developments in its composition is referred to as a stochastic process. Such a process is contrary to a deterministic process, which is defined as fully predictable event to event. Within the context of mathematical analysis, stochastic processes are delineated inside the topic of probability theory. In this framework, probability theory defines random events in a stochastic process by defining characteristics of the behavior of random elements. A stochastic model may be formed within probability so that an observed stochastic process may consist of deterministic elements and random elements, where the random elements follow a set of defined behaviors. Definition of the random behaviors is defined through either random variables or random processes [22].

A random variable or a random process is used to define unsystematic events in a system by assigning a probabilistic numerical response to the random behavior. A random variable is defined solely by the random actions of the element, while a random process includes the deterministic aspects of the system and is a function of time. Broadly, an event may be “random” but be defined under some boundaries or rules of selection. A random variable assists in the understanding of the boundaries and rules to the random portion of a process, therefore assisting in the definition of the entire process [22].

The simplest and most illustrative examples for random variables come from games of chance. The rolling of a standard, fair six-sided die clearly produces a random result. However, the result of the roll is guided by specific boundaries and rules that can be described to produce an understanding of the event. The boundaries of the die rolling event are clear in that the result of a single roll is limited to a discrete number between one and six. Further, it is clear that a fair die has an equal probability of landing with any side on top. Therefore, the probability that any individual number is the result of a roll is one in six. Based on this knowledge, the rolling of a standard, fair six-sided die can be represented as a random variable. In this particular instance, a Uniform random variable results, but different phenomena result in different represented distributions.

Generally, random variable distributions are described by a probability density function. In cases where the probability density function is specific to a discrete random variable, it is called a probability mass function [22]. Often the characteristics of the random variable are most important when considering a random variable distribution. The main characteristics of interest are the general distribution shape (as revealed by the probability density function), the mean, and the variance. The mean of a random variable establishes the value where a random variable can expect to reside. For a given continuous random variable, X , the mean can be determined from the expected value of X , defined as $E[X]$, using the probability density function, $f_X(x)$. This is written, from [22], as

$$E[X] = a_X = \int_{-\infty}^{\infty} x f_X(x) dx \quad (1)$$

where a_X is shorthand for the mean of X and the limits of integration are established by the boundaries of integration. For a discrete random variable, integration is replaced by a summation over the probability mass function.

The variance provides an indication of how much the distribution of the random variable is spread away from the mean. Again using the continuous random variable X , the variance can be found, from [22], by

$$E\left[(X - a_X)^2\right] = \sigma_X^2 = \int_{-\infty}^{\infty} (x - a_X)^2 f_X(x) dx \quad (2)$$

where σ_X^2 is established as shorthand for the variance of X . The standard deviation of a distribution is the positive square root of the variance. It is often used instead of variance to define dispersion from the mean as it has the same units as the random variable.

In cases where multiple random variables are used together to form a solution set, the concept of independence becomes important. Multiple random variables combined in a joint event can be described in a joint distribution function. When considering such a scheme, the influence of each variable on the other in the result is significant in analysis. The two functions are considered independent if the joint probability density function is formed by the multiplication of the distribution of the individual events. Considering this for a joint distribution defined by the random variables X and Y , which may be written as $f_{XY}(x, y)$, independence is established by, from [22],

$$f_{XY}(x, y) = f_X(x) f_Y(y) \quad (3)$$

An alternate way to consider the interdependence of random variables is by their correlation and covariance. Correlation describes the strength and direction of the relationship between two random variables. Strictly defined, correlation can be written, from [22], as

$$\begin{aligned} R_{XY} &= E[xy] \\ &= \int_{-\infty}^{\infty} \int_{-\infty}^{\infty} xy f_{XY}(x, y) dx dy \end{aligned} \quad (4)$$

where R_{XY} is established as shorthand for the correlation between the variables of interest. In cases where the random variables X and Y are independent, this can be reduced as

$$R_{XY} = \int_{-\infty}^{\infty} x f_X(x) dx \int_{-\infty}^{\infty} y f_Y(y) dy = a_X a_Y \quad (5)$$

It is important to note that when $R_{XY} = 0$, the two variables are orthogonal. Covariance describes how much variables change together. It can be written, from [22], as

$$\begin{aligned} C_{XY} &= E\left[(x - a_x)(y - a_y)\right] \\ &= \int_{-\infty}^{\infty} \int_{-\infty}^{\infty} (x - a_x)(y - a_y) f_{XY}(x, y) dx dy \end{aligned} \quad (6)$$

where C_{XY} is established as shorthand for the covariance. Through mathematics, it can be shown that

$$C_{XY} = R_{XY} - a_x a_y \quad (7)$$

Therefore, when $C_{XY} = 0$, then X and Y are either independent or uncorrelated, and if they are orthogonal, then $C_{XY} = -a_x a_y$.

Often random variables are combined with deterministic processes, which have a function in time, resulting in a random process. Again using a simple example for illustration, the concept of a random process can be considered through a man walking along a designated path. Assuming a fixed velocity, the position of the man at a given time is easily found in a deterministic sense. However, if the man's position is allowed to vary from the path in a random manner, his specific position at a given time is instead a function of a random process based on the deterministic path and the random additive motion.

Analysis and application of random processes is greatly eased when these processes display simplifying characteristics. Random processes are statistically independent when the joint probability density function governing behavior is a result of the multiplication of the probability density functions of individual random processes for any choice of times. This can be written, from [22], as

$$\begin{aligned} f_{XY}(x_1, \dots, x_N, y_1, \dots, y_N; t_{X_1}, \dots, t_{X_N}, t_{Y_1}, \dots, t_{Y_N}) \\ = f_X(x_1, \dots, x_N; t_{X_1}, \dots, t_{X_N}) f_Y(y_1, \dots, y_N; t_{Y_1}, \dots, t_{Y_N}) \end{aligned} \quad (8)$$

Stationarity describes how much the properties of a random process vary with time. Random processes are stationary if the applicable joint probability function is a

function of the time difference $\tau = t_2 - t_1$ and not of the specific times t_1 and t_2 chosen. Proof of strict sense stationarity through probability density functions is often difficult. However, it is usually acceptable to simply prove that a random process is “wide-sense stationary,” meaning that the mean of a random process is the same for all time and the autocorrelation of a process is only a function of the time difference between any given times. This can be proven for a single random process in comparison with itself, known as auto-correlation, or through comparison of separate random processes, known as cross-correlation. Auto-correlation for a random process $X(t)$ can be written, from [22], as

$$\begin{aligned} R_{XX}(t_1, t_2) &= E(X(t_1)X(t_2)) \\ &= \int_{-\infty}^{\infty} \int_{-\infty}^{\infty} x(t_1)x(t_2)f_{XX}(x_1, x_2; t_1, t_2)dx_1dx_2 \end{aligned} \quad (9)$$

So, in cases with $R_{XX}(t_1, t_2) = R_{XX}(\tau)$ and $E[X(t)] = a_X$ where a_X is constant, the random process $X(t)$ is considered wide-sense stationary.

A variety of random variable distributions exist for use in random processes. There are three principally used in this dissertation. The Gaussian, uniform, beta, and Rician random variables are introduced below for this purpose. Finally, a general discussion regarding random motion modeling is included, as topic will be tied to expected motion in the dissertation scenario.

1. Gaussian Random Variable

A Gaussian random variable distribution, also called a normal distribution, is one of the most applicable distributions in the description of natural events. Generally familiar to most people as a “bell-curve,” a Gaussian distribution is completely defined by knowledge of its mean and variance. This can be seen in its probability density function, given by [22],

$$f_X(x) = \frac{1}{\sqrt{2\pi\sigma_X^2}} e^{-\frac{(x-a_X)^2}{2\sigma_X^2}} \quad (10)$$

This probability density function is illustrated in Figure 7. Additionally in the figure, the mean and standard deviation of the curve are displayed to assist in their context.

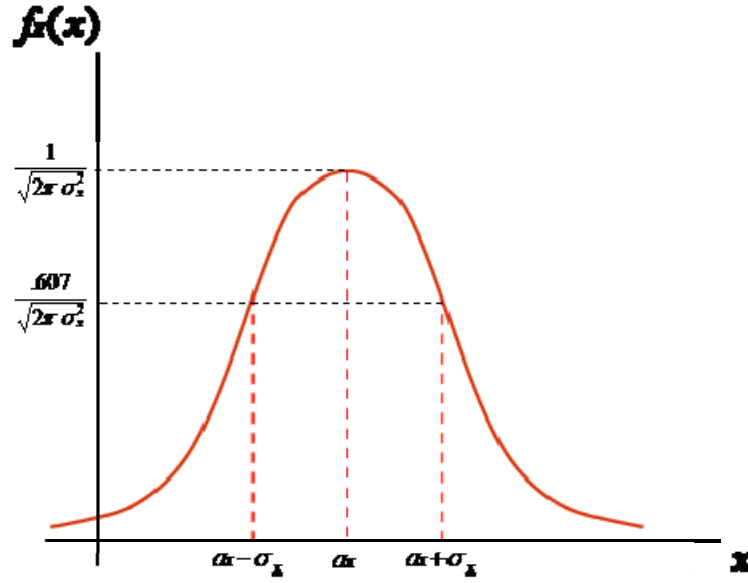


Figure 7. Probability density function for a Gaussian random variable distribution with mean and standard deviation shown.

2. Uniform Random Variable

The uniform random variable distribution has the property that any member of the possible solution set is equally probable. In general, the possible solutions to a uniform distribution are defined between two end points, a and b , which are its minimum and maximum values. The probability density function of a continuous uniform random variable is defined, from [22], as

$$f_x(x) = \begin{cases} \frac{1}{b-a}, & a \leq x \leq b \\ 0, & \text{elsewhere} \end{cases} \quad (11)$$

This distribution can be seen in Figure 8. Applying Equations (1) and (2), the mean and variance for the uniform distribution can be determined as

$$\mu_x = \frac{a+b}{2} \quad (12)$$

$$\sigma_x^2 = \frac{(b-a)^2}{12} \quad (13)$$

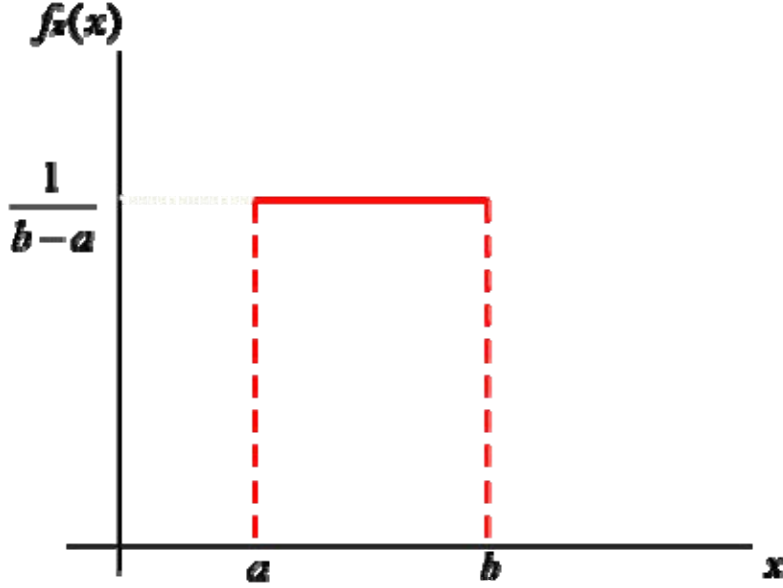


Figure 8. Probability density function for a uniform random variable distribution.

3. Beta Random Variable

The beta random variable is defined within the boundary of zero and one. The distribution accounts for a mean, variance and skew in the distribution, where skew, γ , defines the asymmetry of the data around the mean. Beta random variables are normally defined in the probability density function by two shape parameters, α and β . From [22], the probability density function can be written as

$$f_x(x) = \frac{\Gamma(\alpha + \beta)}{\Gamma(\alpha)\Gamma(\beta)} x^{\alpha-1} (1-x)^{\beta-1} \quad (14)$$

where Γ is defined as the gamma function. The gamma function is defined for complex values, z , as

$$\Gamma(z) = \int_0^{\infty} t^{z-1} e^{-t} dt \quad (15)$$

and for the special case where z is a natural number

$$\Gamma(z) = (z-1)! \quad (16)$$

Examples of the beta function are shown in Figure 9 under various shape parameter choices. The shape parameters are related to the mean, variance and skew of the distribution. The mean of the a beta random variable is written as

$$a_x = \frac{\alpha}{\alpha + \beta} \quad (17)$$

The variance is

$$\sigma_x^2 = \frac{\alpha\beta}{(\alpha + \beta)^2 (\alpha + \beta + 1)} \quad (18)$$

The skew is

$$\gamma_x = \frac{2(\beta - \alpha)\sqrt{\alpha + \beta + 1}}{(\alpha + \beta + 2)\sqrt{\alpha\beta}} \quad (19)$$

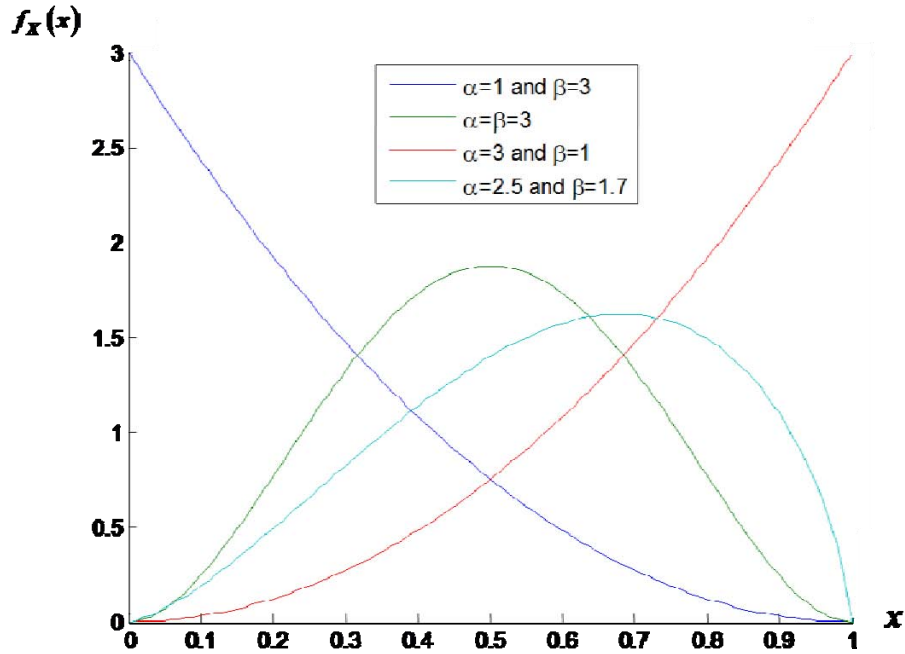


Figure 9. Probability density function for a beta random variable distribution. Various values of shape parameters α and β are shown.

4. Rician Random Variable

The Rician random variable is defined in the interval zero to infinity. This random variable is generally associated with Rician fading in communications theory. Rician fading models signal and interfering signal strength due to multi-path when a single path to the receiver dominates alternate path options. The probability density function, from [22] and [23], is

$$f(x) = \frac{x}{\sigma_x^2} e^{\frac{-(x^2 + a_x^2)}{2\sigma_x^2}} I_0\left(\frac{xa_x}{\sigma_x^2}\right) \quad (20)$$

where I_0 represents the modified Bessel function of the first kind and with order zero, which is written as

$$I_0(\beta) = \frac{1}{2\pi} \int_0^{2\pi} e^{\beta \cos \theta} d\theta \quad (21)$$

For instances when the ratio of the mean to standard deviation is large, the Rician distribution approaches Gaussian in shape, as shown in Figure 7 [23].

5. General Random Motion

Consider again the simple act of walking along a path. Although the path may be followed faithfully, it is not possible for precise positioning along the exact center of the path for the entire journey. A multitude of variables combine in effecting such precision, and these variables may be internal to the walker (e.g., gross and fine motor-skill control and balance) or external (e.g., terrain and weather). The walker's ability to control the troublesome variables may also fluctuate. These effects contribute to variance from the center of the path; however, the general trend of the walker remains along the path. In such a case, the path represents the deterministic element of motion and the varying influences may be introduced as random variables. The act of walking down the path can then be modeled as a random process.

Of course, the number of variables involved in perfectly tracking the motion of an autonomous body is very large, and often factors influencing motion may not be well understood or generally considered. A large body of research exists attempting to

understand motion and describe it, even under the most random of conditions. The most basic of random motion models start with a concept known as “Brownian Motion.” In 1928 Robert Brown, a botany researcher, described the observed microscopic motion of pollen grains in water and solutions. Although he did not specify the cause of the motion nor was he the first to notice the behavior of particles under a microscope, the motion has been named in his honor [24]. The elements that made Brownian motion interesting were that the factors that caused the motion were not evident to the observer and the observed particles moved in a fashion that was considered entirely random. As described by Brown, the particles appeared to jitter and turn over time, but the mean over time appeared to remain constant as the starting position. A set of conventions and observations on Brownian motion lay out its basic points:

- Motion is irregular and is composed of translations and rotations.
- Trajectory appears to have no tangent.
- Particles move independent of one another and are not affected by one another’s presence.
- Smaller particles are more active.
- Medium composition effects motion activity.
- The motion does not cease.
- External energy can excite increased activity.

In Brown’s literal writings, the “medium” is “fluid” and “external energy” is “temperature,” but the general points are used to describe any motion that adheres to these principles [24].

A random walk provides the mathematical and graphical background to describe basic Brownian motion in a discrete sense. In the simplest terms, a random walk determines position by summing a randomly determined position change with the previous position in time. A basic one-dimensional random walk is described, from [25], as

$$x[n] = \sum_{k=-\infty}^n \zeta(k) \quad (22)$$

where $\zeta(k)$ is defined as a function taking on the values of +1 or -1 with respective probabilities P and $1-P$. Such a function is known as a Bernoulli process. Of specific note, the use of the Bernoulli process in defining the random walk means that the value differences of $x[n]$ between any time state n and $n-1$ are independent. If the probability P is equal to 0.5, then the Bernoulli process appears as white noise and the random walk is explicitly defined as a discrete Wiener process. The case of the discrete Wiener process falls under Brownian motion, as it has the statistical properties of zero mean and variance based on the time difference from initial to final observation [25].

The motion defined by the random walk can be assigned dependent on the motion description desired. In doing so, a variety of variations can be assigned to create a very flexible model in terms of dimensionality, speed and probability. The simplest of these is a one-dimensional, single step random walk, as shown in Figure 10. In this implementation, one value of the Bernoulli process indicates no movement, and the other value indicates forward motion along the x -axis by one square.

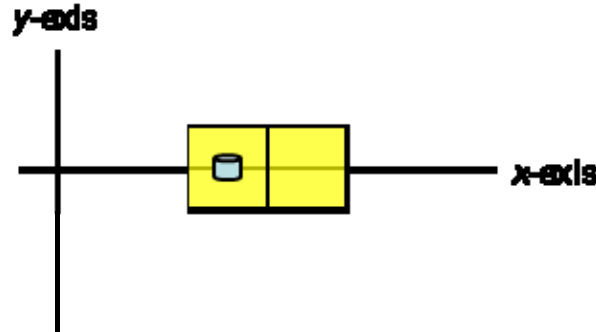


Figure 10. A one-dimensional, single step random walk aligned to the x -axis.

Figure 11 demonstrates the motion associated with a one-dimensional random walk with single steps (forward or backward) along the x -axis. In this case, the position of the node is either incremented or decremented by one step on the axis based the result of the Bernoulli process. When the probabilities associated with the Wiener process are applied and the process is run over several discrete time steps with respect to Equation

(22), it is observed that mean motion away from the starting position is zero, and variance of the process is based on the duration of observation [25].

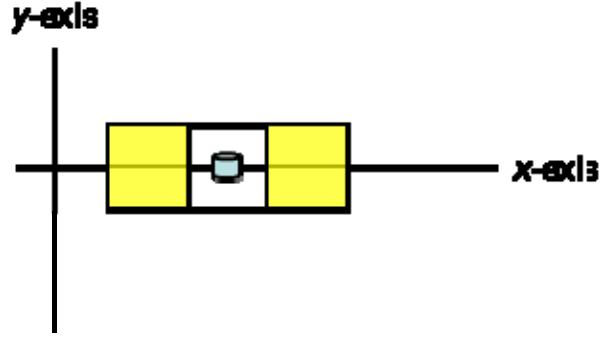


Figure 11. A one-dimensional random walk with single steps (forward or backward) aligned to the x -axis.

Further increasing the complexity of the motion model, Figure 12 shows a simple random walk in two dimensions. Implementing this walk with forced motion at each time step, the position at any given time, $\mathbb{P}[n]$, can be defined as

$$\mathbb{P}[n] = \begin{cases} x[n] = \sum_{k=-\infty}^n \zeta_x(k) \\ y[n] = \sum_{k=-\infty}^n \zeta_y(k) \end{cases} \quad (23)$$

where each dimension has an independent Bernoulli process. When the probabilities are again defined as 0.5 for P_x and P_y , two-dimensional Brownian motion is observed.

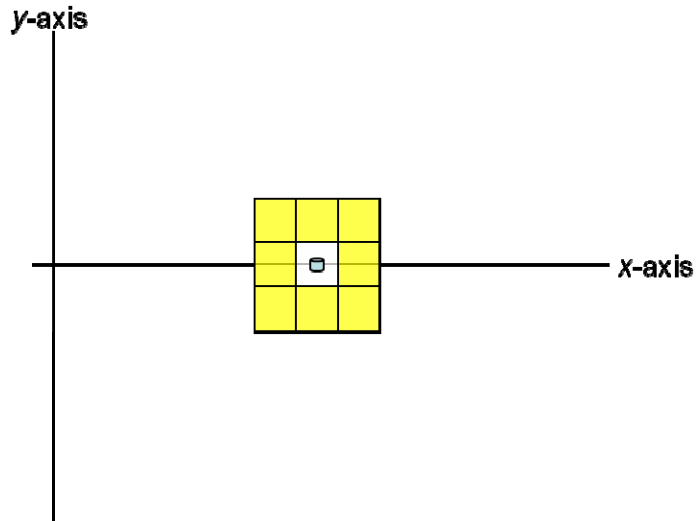


Figure 12. A two-dimensional random walk with single steps in the x - y plane and forced time-step movement.

More complex extensions continue for this model. Figure 13 demonstrates an ability to include two-dimensional motion with variable distances and without forced movement at the time step. The addition of these complexities may then be modeled through simple iteration of the random walk function. Additionally, a variation in the Bernoulli probabilities within individual decision iterations may be applied to further complicate the model.

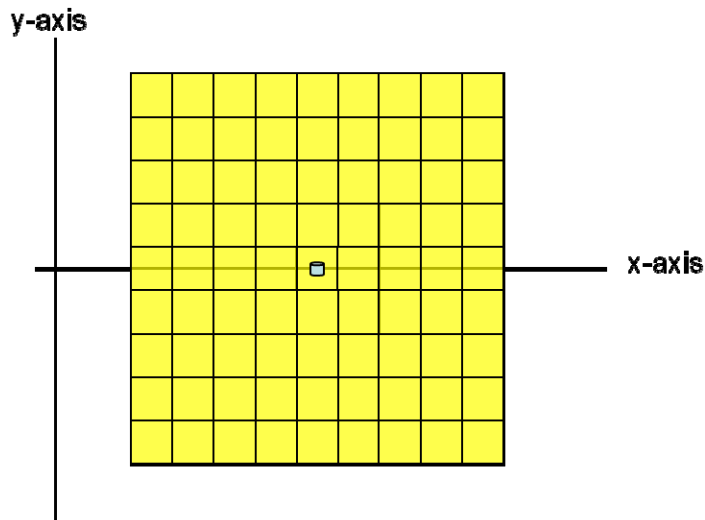


Figure 13. A two-dimensional random walk with multiple steps in the x - y plane.

Using iterations, probabilities and dimensions, a variety of factors covering random motion are thus considered. These include speed, direction, and probability of direction (tied to intended destination and external factors such as terrain). However, the complexity of the Bernoulli probabilities can increase greatly, as they may change with each time-step due to external stimulus and may not be independent of motion of a related body. Accounting for a change of position in a varied but static field is intensive but not difficult to capture in a model. However, correlation of probabilities to other dynamic random motion is not simple to define. Additionally, the influence of past motion on current motion decisions may be of concern. As defined earlier, random walk attributes allow for motion in any direction, potentially with greater probability in some directions and distances. However, it is clear through dynamics that previous position and velocity of motion are critical to determination of next position. As such, the next position becomes conditional on the last. A Markov process is a special case of a conditional random process. In short, a Markov process is conditional only on the previous event in the random process and can be written, per [25], as

$$P[X(t_k) = x_k \mid X(t_{k-1}) = x_{k-1}, \dots, X(t_1) = x_1] = P[X(t_k) = x_k \mid X(t_{k-1}) = x_{k-1}] \quad (24)$$

In general, motion descriptions can be seen as Markov processes, and the dynamics existent at the previous position have the greatest influence on next position probabilities [26].

It is important to note that although simple random walk models may not be adequate to describe the expected motion defined in a scenario, this does not mean that such a model does not offer information of interest. Limiting motion to basic parameters through assumptions may assist in analysis. However, in order to fully apply the variables resident in motion, a different approach is required.

Agent-based modeling is a technique used to determine the action of groups or systems by providing a set of rules to component parts. By focusing on component actions and rules, model creation is simplified in contrast to determination of differential equations meant to describe an entire system. Each component is defined with deterministic and stochastic traits in terms of its own actions and interaction nearby with

other system elements. The reaction of the entire system is then viewed qualitatively through observing the trends of component interaction. As an example, a node may be given the instructions to move with Brownian motion, but the same node may also be told that if it comes within one meter of an adjacent node, to tend in directions away from a potential collision. Such instructions over many closely spaced nodes may not prevent collisions, but a general trend of collision avoidance should be noted. Further, if the space is bounded, a trend for the nodes to spread out over the space should be observed (dependent on the rules provided to the nodes in regards to dealing with the boundaries). Through the application of Monte Carlo modeling techniques, the simulation runs of an agent based model are then used to show motion trends [27].

B. ELECTROMAGNETICS AND COMMUNICATIONS

Electromagnetics is the study of charges and the effect of these charges for the production of currents and fields in static and dynamic conditions. Specific to the topic of communications, electromagnetics is of central importance in defining communications signal propagation from transmitter to receiver and understanding antenna design and performance. As such, a basic examination of electromagnetic field theory and investigations of specific applications are necessary.

Electromagnetic energy traveling through a medium is generally modeled as a set of related fields of electric and magnetic energy that travel as a plane wave. The electric field in an electromagnetic wave, E , is defined in Cartesian coordinates (traveling in the positive z direction), from [4] and [16], as

$$E_x(x, y, z, t) = A_0 \cos(\omega t - \beta z + \phi) \quad (25)$$

where A_0 represents the magnitude of the field, ω is the radial frequency of the wave, β is the phase constant, and ϕ accounts for a phase offset. The electric field shown in Equation (25) is oriented in the x direction. The importance of this orientation will be discussed in Subsection 1 of this section. Physically, temporal frequency and wavelength are more familiar concepts than radial frequency and spatial frequency. Temporal

frequency, f , is defined as the number of event occurrences per unit time, and it is related to radial frequency in a wave, from [4], [28], and [16], as

$$\omega = 2\pi f \quad (26)$$

Wavelength, λ , is defined as the physical distance a wave travels prior to repeating, and it is related to phase constant, from [4], [28], and [16], as

$$\beta = \frac{2\pi}{\lambda} \quad (27)$$

The magnetic field component, H , of the wave is related to the electric field, and this relation is written, from [4], [28], and [16], as

$$H_y(x, y, z, t) = \frac{\hat{z}}{\eta_0} \times E_x(x, y, z, t) \quad (28)$$

where η_0 is the impedance of the medium and \hat{z} indicates wave propagation direction in a unit vector. Before discussing the medium, it should be noted that an orientation in the y direction is associated with the magnetic field. In defining the wave for Equation (25), a direction of propagation and field orientation was assigned as z and x , respectively. The cross function invoked in Equation (28) not only numerically enables multiplication between the vector electric field and scalar of medium resistance, but it also determines the vector direction of the magnetic field by crossing wave direction with electric field direction – in this case $\hat{y} = \hat{z} \times \hat{x}$.

The characteristics of the medium containing the electromagnetic wave effect propagation performance. The medium is primarily described by its permittivity, ϵ , and permeability, μ . These physical factors of the medium directly determine propagation velocity, u_p , and the resistance of the medium through relationships that can be written, from [4] and [16], as

$$u_p = \sqrt{\frac{1}{\mu\epsilon}} \quad (29)$$

$$\eta_0 = \sqrt{\frac{\mu}{\epsilon}} \quad (30)$$

The propagation velocity of an electromagnetic wave in a medium is also linked to the wave's frequency and wavelength. This relationship is written, from [4] and [16], as

$$u_p = \frac{\omega}{\beta} = \lambda f \quad (31)$$

From this linkage, the wavelength and frequency can be directly related to medium permittivity and permeability, from [4] and [16], as

$$\lambda f = \sqrt{\frac{1}{\mu\epsilon}} \quad (32)$$

Finally, the time averaged power density can be represented by the Poynting vector, \bar{P} . The Poynting vector provides the electromagnetic power in the wave based on field strength and is written for the wave defined in Equations (25) and (28), from [4] and [16], as

$$\bar{P} = \frac{1}{2} (E_x \times H_y) \quad (33)$$

Electromagnetic waves are often defined in terms of position from a transmitter; therefore, orientation in terms of a spherical coordinate system is convenient. A figure relating spherical coordinates to the more familiar Cartesian is provided in Figure 14. A solid angle, Ω , is a cone projected from the a point in space. When that point is at the origin of the spherical system, it can be quantified in units of steradians. One steradian is defined as the solid angle, which cuts an area of the surface of the sphere, A , equal to the square of the sphere's radius, r . This is written, from [16], as

$$\Omega = \frac{A}{r^2} \quad (34)$$

The unit of steradians is helpful in defining power density. Additionally helpful is knowledge that the total area of any sphere is 4π steradians.

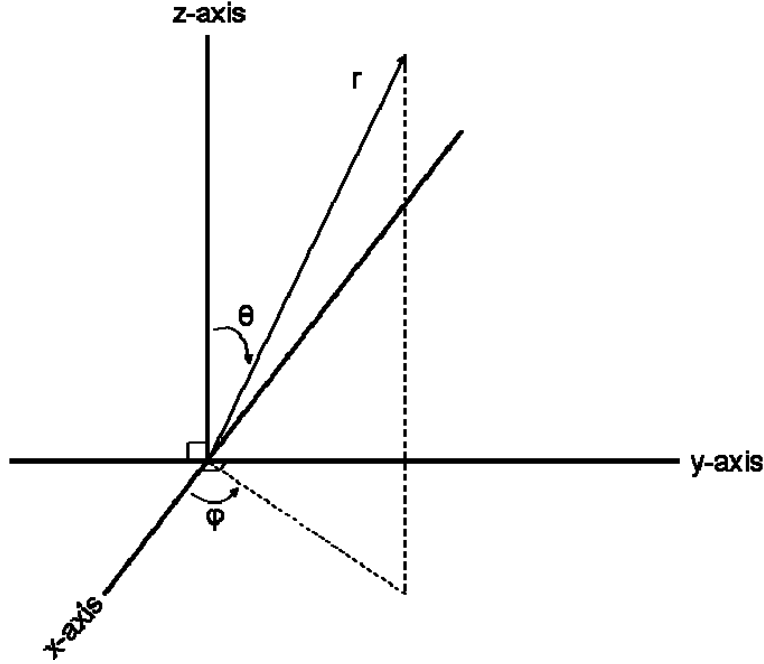


Figure 14. A spherical coordinate system with respect to standard Cartesian coordinates.

In order to consider electromagnetic waves as plane waves, it is generally assumed that the waves are “far” from the transmitting aperture. As a general description, the far field can be defined in terms of a distance, d , from the transmitting aperture as a function of wavelength and/or aperture size, D , from [4], as

$$d \geq \begin{cases} 10\lambda, & D \leq \lambda \\ 10D, & \lambda \leq D \leq 5\lambda \\ \frac{2D^2}{\lambda}, & D \geq 5\lambda \end{cases} \quad (35)$$

In regards to the plane wave estimation, an electromagnetic field departing an unobstructed isotropic element in space obviously would set off from the point in space equally in all directions, resulting in a spherical wave. Complicating that with an irregular antenna shape, the field waves transmit in further irregular patterns. However, an observer is only interested in the portion of the local electromagnetic wave front for

observation. In the same manner that the earth (a large sphere) appears flat to a person standing upon it, a wave will appear as a plane to a receiver in the far field [4].

1. Antennas

An antenna is a transducer, used to convert electromagnetic energy from a wired (or guided) environment into un-guided space, and vice-versa. The result of the transduction of electromagnetic energy is represented in an antenna's radiation pattern.

A far field assumption is used in evaluating an antenna's radiation pattern. Such an assumption not only allows for plane wave representation, but it also isolates the radiative properties of antenna transmission. The physical act of transducing a current in a guided medium into an electromagnetic wave in space creates results aside from the traveling plane wave. Consider a current, J , applied to an antenna of length l . The vector magnetic potential, \bar{A} , can be determined by integrating over the current distribution with respect to field points, from [16], as

$$\bar{A}(r) = \frac{\mu}{4\pi} \iiint \frac{\bar{J}(\bar{r}') e^{-j\beta|\bar{r}-\bar{r}'|}}{|\bar{r}-\bar{r}'|} dv' \quad (36)$$

where $\bar{r} = x\hat{x} + y\hat{y} + z\hat{z}$ represents the observation point in space, and $\bar{r}' = x'\hat{x} + y'\hat{y} + z'\hat{z}$ represents the source point for integration. The magnetic field, \bar{H} , can then be determined by the curl of the vector magnetic potential, from [16], as

$$\bar{H}(r) = \frac{1}{\mu} \nabla \times \bar{A}(r) \quad (37)$$

The electric field is then determined from the magnetic field via Equation (28), and the Poynting vector is available from Equation (33) for a plane wave in the far field (Note: If not in the far-field, Maxwell's equations must be applied). However, the resultant fields appear with electrostatic, inductive, and radiative components. The electrostatic component of the electric field is primarily due to specific charge position. Its strength is inversely proportional to the cube of distance, $1/r^3$; therefore, its effects are primarily felt only near the antenna. The inductive component is due to the velocity of charge

motion. Its strength is inversely proportional to the square of distance from the antenna, $1/r^2$. The radiation component of the antenna, due to charge acceleration, provides the transduction effect of primary interest, as its strength is directly inversely proportional to the distance, $1/r$. Therefore, an assumption of far field is made in order to neglect the electrostatic and inductive terms, [4] and [16].

The radiation pattern describes the spatial distribution of a radiated electromagnetic wave. In the far field, the electrostatic and inductive components can be ignored, so the radiation vector, $\bar{f}_r(\theta, \phi)$, can be determined as part of the vector magnetic potential in Equation (36), from [4] and [16], as

$$\bar{f}_r(\theta, \phi) = \iiint \bar{J}(\bar{r}') e^{j\beta \hat{r} \cdot \bar{r}'} dv' \quad (38)$$

where \hat{r} represents the unit vector towards the observation point and dv' indicates integration over a closed volumetric surface containing the antenna as shown in Figure 15.

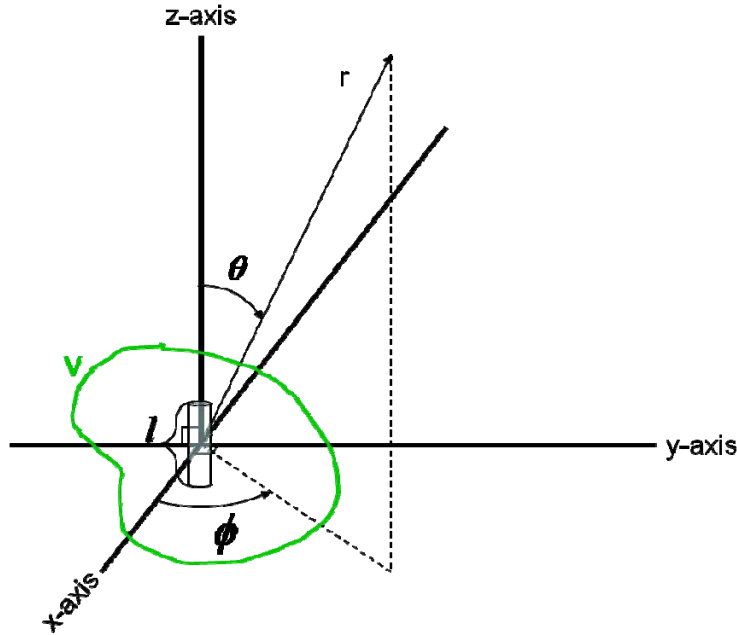


Figure 15. Antenna element in closed surface with observation point at r .

Antenna gain represents the effectiveness for the antenna to transmit in a desired direction relative to an isotropic source. An isotropic antenna is defined as one that uniformly radiates electromagnetic energy equally in all directions. Radiation from such an antenna results in uniform power density at any point in a sphere with radius, r , from the antenna at the origin. This uniform power density, W , from an isotropic element is determined by, from [16],

$$W = \frac{P_t}{4\pi r^2} \quad (39)$$

where P_t indicates transmitted power. Since practical antennas are not capable of acting as perfect isotropic elements, a ratio comparison can be constructed against the isotropic model. Such a comparison demonstrates that power from real-world antennas is received or radiated, in comparison to isotropic models, with increased emphasis in some directions and decreased emphasis in other directions [4] and [16].

Antenna gain, G , can be broken into factors representing maximum gain and spatial variation, from [4] and [16], as

$$G(\theta, \phi) = G_{\max} |f_{\text{norm}}(\theta, \phi)|^2 \quad (40)$$

where G_{\max} is determined, from [4] and [16], by

$$G_{\max} = \frac{4\pi}{\int_0^\pi \int_0^{2\pi} |f_{\text{norm}}(\theta, \phi)|^2 \sin \theta d\theta d\phi} \quad (41)$$

and f_{norm} indicates a normalized quantity.

So, in short, gain pattern is used to define an antenna's ability to radiate electromagnetic energy in a spatial context and is based on a comparison to an isotropic radiator. Figure 16 provides a graphic to demonstrate gain using a dipole antenna with length of half a wavelength. The two-dimensional gain pattern is displayed compared to an isotropic pattern. The antenna is oriented along the $0^\circ - 180^\circ$ axis. It is readily evident that a communications target can be assisted or hindered by gain due to its location relative to the antenna. It should specifically be noted that angles of maximum

and minimum gain do exist. Further, minimum gain may in fact be zero at specific angles, resulting in no ability for an antenna to radiate in that direction.

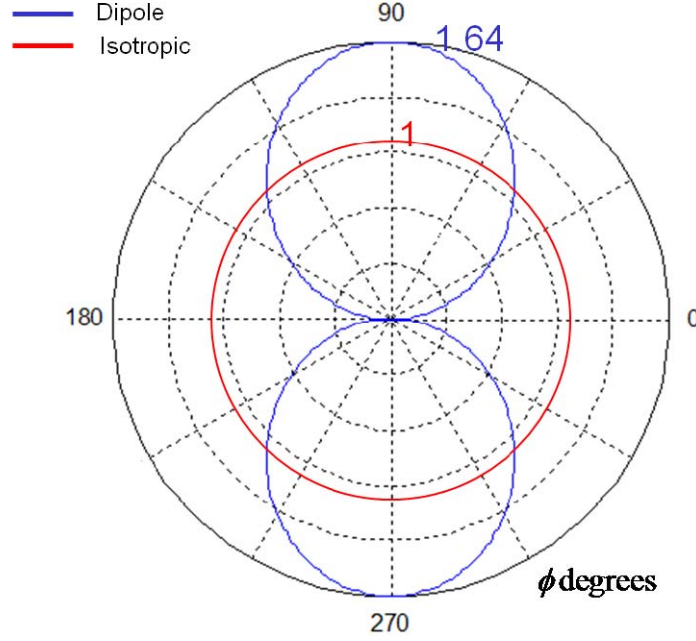


Figure 16. The gain pattern for a dipole antenna. The gain pattern for an isotropic element is included for comparison.

Applying the concept of gain, the power density at a observation point, (r, θ, ϕ) , based on a transmission from an antenna at the origin is determined by, from [4], [28], [18], and [16], is

$$W(\theta, \phi) = \frac{P_t}{4\pi r^2} G(\theta, \phi) \quad (42)$$

In considering reception in an antenna, the principle of reciprocity provides that antennas react in the same manner in terms of gain for both transmission and reception. A reception antenna will have no knowledge of the distance of the transmitter, or if the transmitting antenna was oriented to provide the signal with high or low gain, it will only sense the strength of the incoming power density of the electromagnetic wave. However, similar to the transmitting antenna, the receiving antenna also operates under the physical realities of gain. Therefore, the orientation of the receiving antenna to the incoming electromagnetic wave will help to determine the antenna's responsiveness to the

incoming signal. The specific responsiveness of a reception antenna to an incoming signal is measured by effective area. Effective area, A_e , of an antenna is directly related to gain, from [4], [28], [18], and [16], as

$$A_e = \left(\frac{\lambda^2}{4\pi} \right) G \quad (43)$$

Another factor in antenna performance is polarization. As shown in Equations (25), (28), and (33), plane waves are constructed by electric and magnetic field components that are oriented in given directions. The direction of the electric field component defines a wave's polarization. It is noted that an individual wave may not have field components strictly oriented in a linear direction. Indeed, wave polarizations may be linear (indicating field components are 100% oriented in a given direction, circular (indicating wave components “spin” during transmission), or elliptical (a middle ground between circular and linear polarization). Although all real world wave transmissions are elliptical, linear and circular polarization models are normally used in modeling because they represent the intended transmission polarization [4] and [16].

Both the type of antenna involved in transmission and the orientation of that antenna in reference to the communications system determine the polarization of an electromagnetic wave. In general, linear polarization is used in this dissertation.

2. Free-space Communications

In the most general sense, communications involve the transfer of a message between two parties. In wireless communications, the sender transmits the message into the ether by means of an antenna. This creates an electromagnetic wave that has a power density at the location of the receiver described by Equation (42). The receive antenna in turn senses the generated electromagnetic wave and transduces the energy back into the receiver. The ability of the receive antenna to translate the sensed power density into received power is described by the antenna's effective area as per Equation (43). The receiver power, P_r , is then written, from [28] and [16] as

$$P_r = WA_e \quad (44)$$

This relationship equation can be expanded to demonstrate direct linkages between received power and distance between antennas, transmission power, transmitting antenna gain, and receiving antenna effective area as

$$P_r = \frac{P_t G_t A_e}{4\pi r^2} \quad (45)$$

where the gain of the transmitting antenna is denoted with the subscript t . It should be noted in this expansion that the received power assumes that the electromagnetic wave has been transmitted in free-space. In general, this means that free space properties of permittivity, ϵ , and permeability, μ are applied. This is a reasonable assumption for communications [28]. An additional assumption is that only the direct communications path is relevant. The received power due to electromagnetic effect of multi-path, multiple copies of the same wave reaching the receiver due to reflection, scattering, or other phenomenon, is ignored. The practical effects of multi-path will be reviewed in Section C of this chapter.

The subscript applied to gain in Equation (45) is helpful as the effective area quantity for the receive antenna can be expanded using Equation (43). Therefore, the power reception relationship can be written using gain only to represent the individual antennas as

$$P_r = P_t G_t G_r \left(\frac{\lambda}{4\pi r} \right)^2 \quad (46)$$

A factor, L_o , can be added in the denominator of this equation to account for other losses in signal transmission. Other losses include signal degeneration due to a variety of factors including weather conditions, multi-path interference estimation, and external interference.

As discussed, an antenna operating as a transducer in signal reception simply transforms the power density sensed into a signal in the guided medium necessary for receiver hardware to demodulate and decode. In this function, a receive antenna is unable to discriminate between the intended signal and other electromagnetic activity, which may overlap the frequency band of interest. In addition to the signal of interest,

the electromagnetic spectrum may contain unintentional (or intentional) interfering signals as well as noise. The prediction and “hardening” of wireless communications to interfering signals is outside the scope of this dissertation. However, noise is a universal factor in design and must be addressed.

There are two types of noise that may be considered; colored noise and white noise. Colored noise is caused by spurious electromagnetic disturbances. It is unpredictable in timing and power density. White noise is constructed of continuous noise sources and is defined as having a flat power spectral density over the frequency band of interest. As the existence of white noise is a given, a ratio of signal to white noise power spectral density is generally used to determine the probability of successful communications in a link. The noise power of white noise is defined by the primary source, emissions from atomic particles in motion due to thermal excitation. The relationship between noise power, N , and thermal excitation is written, from [28], as

$$N = kTB \quad (47)$$

where k is Boltzmann’s constant defined as 1.38×10^{-23} W/HzK°, T is the effective temperature of the receiver in Kelvin, and B as receiver bandwidth in Hertz. So, creating a ratio using Equations (46) and (47), the signal-to-noise power ratio, SNR , is written, from [28] and [29], as

$$SNR = \frac{P_r}{N} = \frac{P_t G_t G_r}{kTB} \left(\frac{\lambda}{4\pi r} \right)^2 \quad (48)$$

For digital communications, it often provides greater information to instead define a ratio of energy per bit, E_b , to noise power spectral density, N_0 . Starting with Equation (48), this ratio can be formed through the application of the bandwidth, B , to bit rate, R_b , ratio, from [28] and [29], as

$$\frac{E_b}{N_0} = SNR \left(\frac{B}{R_b} \right) \quad (49)$$

This relationship expands to provide additional insight as

$$\frac{E_b}{N_0} = \frac{P_t G_t G_r}{kTR_b} \left(\frac{\lambda}{4\pi r} \right)^2 \quad (50)$$

Polarization is also a concern in terms of communications link performance. Antennas transmit electromagnetic waves with a specific polarization. As an example, a wire antenna element will produce in the far field a wave with linear polarization where the electric field is parallel, and magnetic field is perpendicular in relation to the length of the antenna. In reception, antennas most efficiently transduce signals with polarization matching what they are capable of producing. In cases where polarization between the incoming signal and the receiver antenna are mismatched, the fraction of power received, ρ , is determined, from [16], by

$$\rho = \left| \hat{e}_i \bullet \hat{h}^* \right|^2 \quad (51)$$

where \hat{e}_i represents the unit vector for polarization of the incident electromagnetic wave and \hat{h}^* is the complex conjugate of the receive antenna polarization. From this ratio relationship, an antenna oriented with polarization perfectly matching the incoming wave will produce a 100% transduction of the sensed signal. Conversely, an antenna with polarization orthogonal to the incoming signal will produce no signal reception. Finally, the common case of graduated mismatch between wave and antenna transduces a portion of signal per the dot produce relationship in Equation (51).

Applying the polarization relationship to the communications link model, the power fraction can be applied directly to received power in Equation (46) plus the other losses factor, L_o , from [28], [29], and [16], as

$$P_r = \frac{P_t G_t G_r}{L_o} \left(\frac{\lambda}{4\pi r} \right)^2 \rho \quad (52)$$

Similarly, this quantity is applied to signal-to-noise ratio and energy per bit to noise power spectral density as

$$SNR = \frac{P_t G_t G_r}{kTB} \left(\frac{\lambda}{4\pi r} \right)^2 \rho \quad (53)$$

$$\frac{E_b}{N_0} = \frac{P_t G_t G_r}{kTR_b} \left(\frac{\lambda}{4\pi r} \right)^2 \rho \quad (54)$$

In order for signal reception to occur within the receiver, a decision is necessary in regards to the detection of the signal. Although signal detection can be simply applied though the use of a threshold power reception value, the consequences of setting such a threshold are critical. The threshold value is directly tied to the important system parameters of detection probability, P_D , and false alarm rate, P_{FA} . The detection probability is defined, from [30] and [18], as

$$P_D = P(\text{signal detected} / \text{signal present}) \quad (55)$$

and false alarm rate is defined, from [30] and [18], as

$$P_{FA} = P(\text{signal detected} / \text{no signal present}) \quad (56)$$

It is clear that a system with the primary purpose of signal detection will always detect a signal when it is present. The converse of detection in this case is the probability of a miss, P_M , which is defined, from [30] and [18], as

$$P_M = 1 - P_D = P(\text{signal not detected} / \text{signal present}) \quad (57)$$

Therefore, in order to maximize detection, minimizing the probability of missing a signal of interest, it would seem that the threshold should be set low. However, a low threshold would simultaneously increase the opportunity for false alarm due to spurious noise or events. Such false decisions may cause further issues within a system where detection initiates other operations requiring energy expenditure [31].

The Neyman-Pearson criterion is one of many ways to determine the optimal threshold for detection. As it will be the primary criterion used, for reasons discussed later, it is briefly presented here and used to further illustrate detection theory. Neyman-Pearson refines the concept of detection probability by basing the likelihood for a decision on a user determined false alarm rate. So, this criterion enables a system to be designed with a maximum available detection probability while limiting false alarms to a rate deemed acceptable in specifications.

Beginning with basic signal detection theory, a set of two hypotheses, H_0 indicating noise only and H_1 indicating signal plus noise, are defined, from [30], as

$$\begin{aligned} H_0 : m_1 &= n(t) \\ H_1 : m_2 &= s(t) + n(t) \end{aligned} \quad (58)$$

where m represents the detected energy, n is noise, and s is the signal. The probability set for each case is then defined, from [30], as

$$\begin{aligned} P(z | m_1) &= \text{probability of received energy given } m_1 \\ P(z | m_2) &= \text{probability of received energy given } m_2 \end{aligned}$$

and the threshold, T , is set based on the probabilities of received energy. The threshold can be considered in a likelihood ratio, LR , which demonstrates the proper detection decision based on the probabilities. The likelihood ratio is written, from [30], as

$$LR(z) = \frac{f(z | m_2) >_{d_2}}{f(z | m_1) <_{d_1}} T \quad (59)$$

where d_1 indicates a decision of H_0 and d_2 indicates a decision of H_1 . Considering the energy probabilities, they can be tied to the definitions of detection probability and false alarm probability, from Equations (55) and (56), as

$$P_D = P(d_2 | m_2) = \int_{Z_2} f(z | m_2) dz \quad (60)$$

and

$$P_{FA} = P(d_2 | m_1) = \int_{Z_2} f(z | m_1) dz \quad (61)$$

where the boundary of integration, Z_2 , is the space in the observation probability associated with H_1 , as shown in Figure 17.

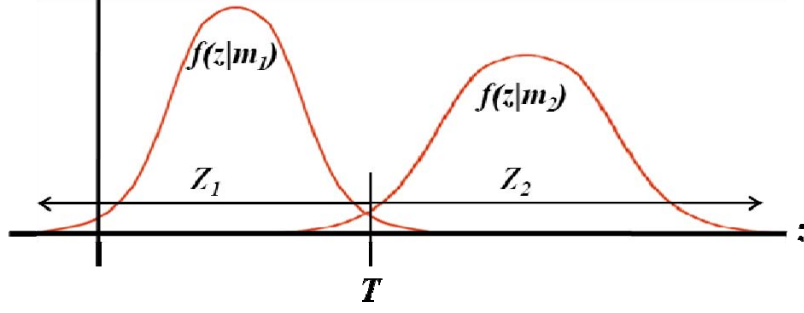


Figure 17. The probability space for signal detection. Note that although probabilities appear Gaussian, any probability distribution is possible.

Under Neyman-Pearson, the false alarm rate is set at an acceptable value in design. As a general value, P_{FA} will be chosen as the maximum false alarm rate. A solution to maximizing P_D with the constraint of P_{FA} is then constructed by applying LaGrange's method of undetermined multipliers, from [30], as

$$\Gamma = P_D - \Lambda (P_{FA} - \alpha_0) \quad (62)$$

where Λ is the LaGrange multiplier and Γ is the minimized value. Substituting in the relationships from Equations (60) and (61), this is rewritten as

$$\begin{aligned} \Gamma &= \int_{Z_2} f(z|m_2) dz - \Lambda \left(\int_{Z_2} f(z|m_1) dz - \alpha_0 \right) \\ &= \int_{Z_2} (f(z|m_2) - \Lambda f(z|m_1)) dz + \Lambda \alpha_0 \end{aligned} \quad (63)$$

In order to maximize the equation, the integrand must be positive

$$f(z|m_2) - \Lambda f(z|m_1) > 0 \quad (64)$$

Equation (64) can then be re-ordered as

$$\frac{f(z|m_2)}{f(z|m_1)} > \Lambda \quad (65)$$

This equation can then be compared to the likelihood ratio in Equation (59). From this comparison, it can be seen that the decision criteria for d_2 matches this equation when $\Lambda = T$. In this manner, the constraint that $P_{FA} = \alpha_0$ is applied and detection probability is maximized [30].

3. Array Beamforming

Based on the connection between antenna gain with respect to transmit and receive elements and free-space communications performance, as described in Section B.2 of this chapter, it would seem intuitively obvious that maximizing gain provides better link results or enables the system to relax other factors like transmission power. However, the physics of gain pattern as introduced earlier show that placing the brunt of gain directly into the communications link is not a simple task. Antenna gain patterns are directly dependent on the resonance length and shape of the element. The result is that antennas with very focused gain patterns tend to be very frequency specific or highly complex in construction [4] and [16].

In contrast, many applications require antennas to operate over broad ranges or be physically robust. Simple structures, such as monopole or dipole whip antennas, provide only a nominal gain above an isotropic model when oriented for maximum directivity. However, a technique known as coherent array beamforming is available to allow groups of antennas to operate together, increasing performance while remaining relatively robust and uncomplicated.

The concept of coherent array beamforming is based on combining waves. Stated plainly, multiple electromagnetic waves of the same frequency at the same point in space will interfere with one another. The interference can be viewed as a vector addition problem where vector amplitude is associated with wave component amplitude and vector direction is associated with component phase. In array reception, the same wave is received at two separate antennas that are spatially separate. The outputs from the arrays are then summed; however, since they are received at separate points, they will have different amplitudes and phases due to the path of transmission. So, in combining the waves the electric field and magnetic field components add like the vectors defined. The

result is either increased or decreased overall wave amplitude. The constructive or destructive interference in this combination can be described in terms of gain, identical to gain of a single element defined earlier [16]. Array transmission works in a similar manner.

Although arrays may be constructed of various elements with individual patterns and characteristics, it is common to consider construction by a single element type. Array performance, in the form of an array factor, will be discussed shortly. However, as a first step, elements will be considered isotropic.

A two element array with a target (source) in two-dimensional space is shown in Figure 18. An electromagnetic wave generated by the target is received at each node and then combined. Since the distance between each individual node and the target differ, the phase of the received wave will differ at each node. The goal of a coherent array is to constructively add the electric and magnetic component outputs of the individual elements to increase received wave amplitude. This can be accomplished through the use of a phase delay as shown in Figure 19. In order to combine the signals in a fully constructional manner, the phase delay is used to synchronize the signals [4] and [16]. It should be noted that a different phase offset may be used to provide fully destructive combination of the waves if so desired. Operation in this manner would generally be used to remove an interfering or jamming signal.

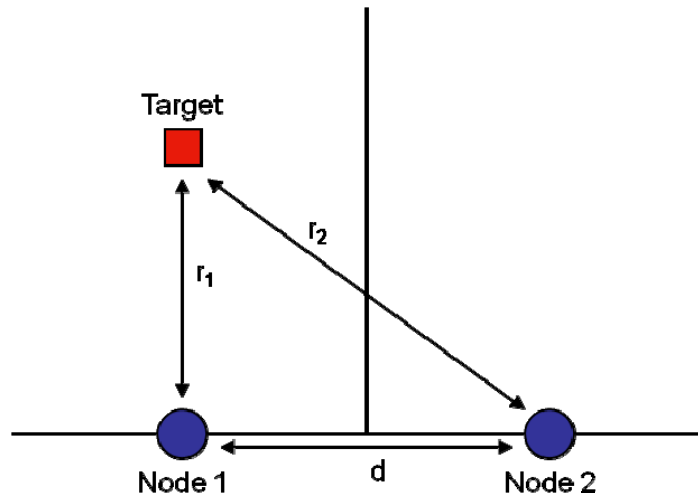


Figure 18. A two-element array with a target emitter in two-dimensional space.

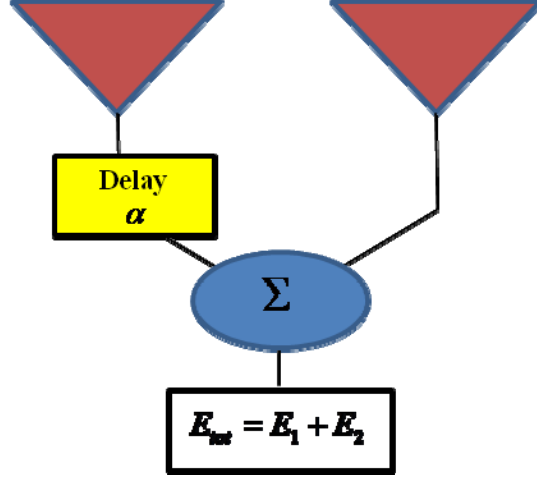


Figure 19. A system diagram of a two-element array.

As shown in Figure 19, the addition that takes place in array signal combination takes place with the electric (and magnetic) field components. The power in the individual electromagnetic waves is not directly summable. Let the electric field, E , of the wave transmitted by the target be described as

$$E = A_0 \cos(\omega t) \quad (66)$$

where A_0 is the initial field amplitude and t indicates the field is time varying. Assuming transmission in free-space, the electric field of the wave received at Node 1, E_1 , is

$$E_1 = A_1 \cos\left(\omega t - \frac{2\pi r_1}{\lambda}\right) \quad (67)$$

and at Node 2, the electric field of the received wave, E_2 , is

$$E_2 = A_2 \cos\left(\omega t - \frac{2\pi r_2}{\lambda}\right) \quad (68)$$

where the amplitude for each is subscripted to denote a difference based on the individual propagation distances. Combination of the electric field components can be done through direct addition to create a total electric field, E_{tot} , which is written, from [4] and [16], as

$$E_{tot} = E_1 + E_2 \quad (69)$$

Since the distance between the two nodes is known, the electric field at Node 2 can be rewritten as

$$E_2 = A_2 \cos \left(\omega t - \left(\frac{2\pi r_1}{\lambda} \right) - \alpha \right) \quad (70)$$

where the term α is, from [4] and [16]

$$\alpha = 2\pi \frac{(r_2 - r_1)}{\lambda} \quad (71)$$

So, α is the phase difference of the electric field between Node 2 and Node 1 due to the greater distance traveled by the wave. Therefore, in order to optimally construct the resultant signal, the signal received at Node 1 must be delayed by α , as was demonstrated in Figure 19 [4] and [16].

Based on the combining described, the resultant collection of electric fields increased the received electric to $A_1 + A_2$. Assuming the transmitter is in the far-field, then the distance r_1 is much, much greater than the space between the nodes, d , and the amplitude difference A_1 and A_2 is small. So assuming $A_1 \approx A_2$, the magnitude of the electric field component of the wave is increased by a factor of 2. Although the addition of E-fields for the target emitter in the desired direction is straightforward, determining gain is more complex procedure. Using Equations (40) and (41), the electric field pattern over the full 4π steradians around the array must be integrated. The result is an array gain pattern that varies over the available angles.

To illustrate, consider the two-element array with a constant phase delay applied to focus the array at a desired target. Then allow the target to drift in angle to the array. The array produces a beam with increased gain in the preferred direction while providing gain at a decreased level elsewhere. Alternately, the array can “follow” a target emitter by varying the phase delay, α , before combining signals when direction to the target signal is known or the array wishes to scan an area for active emitters. Figure 20 shows a basic example of the antenna pattern produced by a two element array. For this figure,

the elements are spaced half a wavelength apart, the wave amplitude is assumed equal at both elements, and phase delay of 45° is assigned. The figure reveals that the array has maximum gain for targets oriented at 120° or 240° under these conditions.

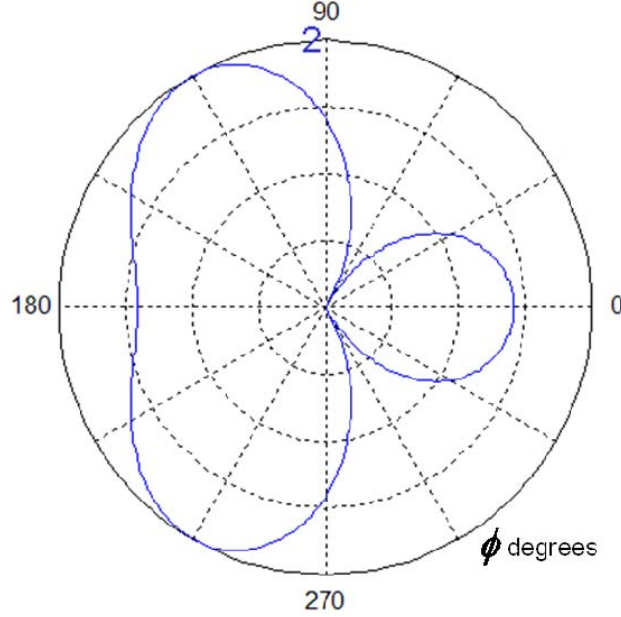


Figure 20. A two-element coherent array pattern in two dimensions.

The combination of electromagnetic waves from two elements can be expanded to additional elements with similar results. As shown in Figure 21, a combination of I nodes can be represented by a general structure, and the combination of electric field components in the preferred direction is then represented by the sum, from [4] and [16], as

$$E_{tot} = \sum_{i=1}^I E_i \quad (72)$$

Although the array system depicted shows an arrangement of elements in a linear pattern, the layout of specific nodes may be arbitrary, as shown in Figure 22. In each case, the delay is a function of the relative position of each node to the reference node. Alternatively, a reference point in space may be used instead of a reference node where every node has a delay applied based on its location related to the reference. Such an

arrangement may ease calculations in specific geometrical configurations, such as randomly dispersed or circularly constructed [16].

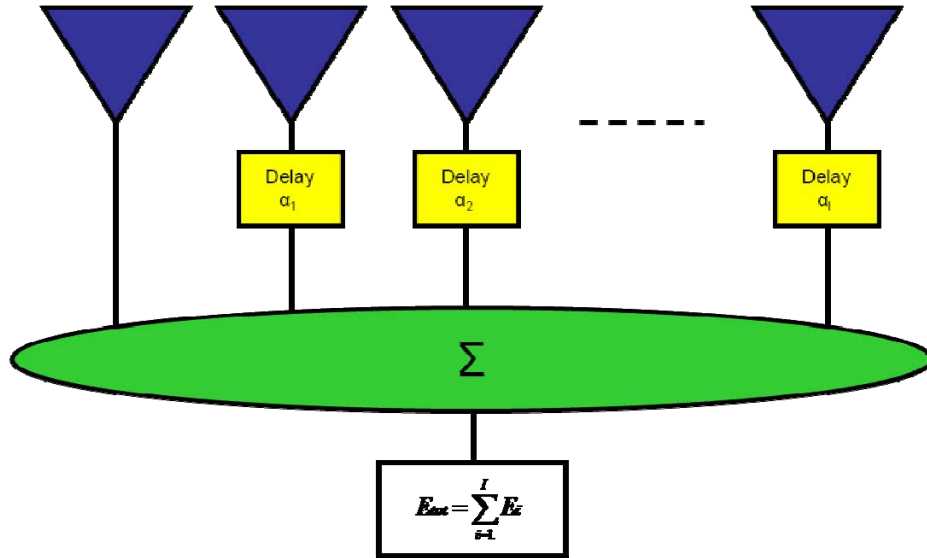


Figure 21. A generalized array structure with I elements.

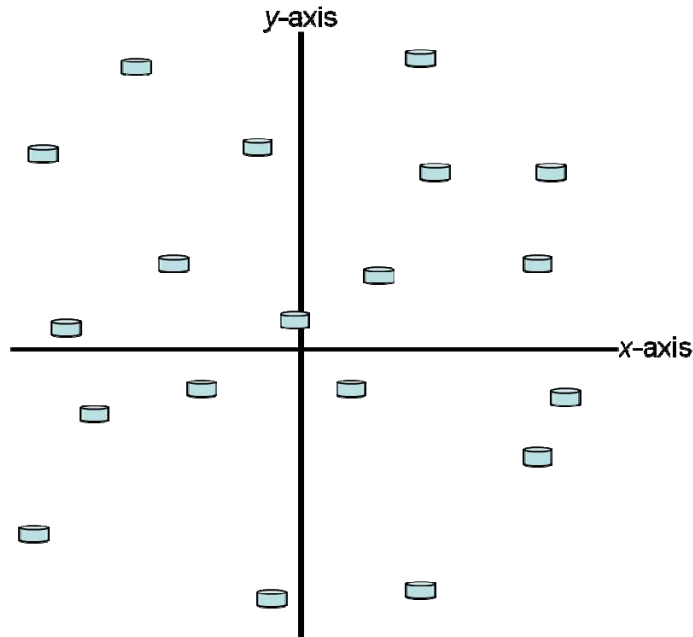


Figure 22. A multi-node array with random distribution in a two-dimensional space.

Arrays are generally designed with linear or planer node placements as the resultant patterns are predictable and provide optimal properties for implementation. The

solution for the general case with random distribution is sufficiently simple for later analysis. In constructing the solution, assumption of isotropic elements will continue. Obviously, real-world implementation does not allow for isotropic elements; however, the results obtained earlier remain useful through the concept of an array factor, AF . An array factor accounts for array element number, relative disposition, and excitation when calculating the pattern formed by an antenna array. It is formed by simply evaluating the pattern created by a distribution of isotropic elements, as was done with the two element example. So long as the individual elements of the array are the same, the total pattern for the array including elements, F , can be determined through multiplication of the individual element pattern, EF , with the array factor, from [4] and [16], as

$$F(\theta, \phi) = AF(\theta, \phi)EF(\theta, \phi) \quad (73)$$

Creation of array pattern in this manner also requires that elements hold the same orientation and that mutual coupling can be ignored. The concept of mutual coupling will be presented in Section B.3.c of this chapter. Various orientations of array elements result in variances in terms of individual element patterns and polarizations [32]. In common array construction, a technique known as the active element pattern analysis enables the estimation of array gain pattern. This technique analyzes individual element patterns with all other elements in parasitic mode. Individual patterns are then combined for the result. This technique is further simplified by assuming similar results from elements with similar disposition and in similar relative location (interior or exterior to the array) [33].

Although it is simple to consider the in phase addition of electric and magnetic field components of electromagnetic waves with an assumed known target location while introducing the concept of array formation, the general case of array operation does not assume a fixed, known location for the target emitter. As the target emitter's location, or in the case of transmission, the location of the target receiver, is unknown, coherent array beamforming focuses on beam direction. An array factor is, therefore, formed by the consideration of amplitude and phase differences of element excitation currents from target locations over the full range of potential angles summed with respect to element location. This is shown for an array with M elements, from [13], as

$$AF(\theta, \phi) = \sum_{m=1}^M I_m \iota_m e^{j\alpha_m} e^{j\zeta_m} \quad (74)$$

where the relative element locations are known in Cartesian coordinates and a phasing reference position is assigned at the origin that may (or may not) be associated with a node position. The term I_m represents the magnitude of element currents. Magnitude weights are included in the general equation as ι_m ; however, the task of equalizing magnitudes can be carried out through an equalizer. Therefore, this term will normally be ignored. The current phase factor, ζ_m , represents the differences in current phasing based on element position and is expanded, from [13], as

$$\zeta_m = \beta [x_m \sin \theta \cos \phi + y_m \sin \theta \sin \phi + z_m \cos \theta] \quad (75)$$

The phase weights, α_m , provide the synchronization required to direct the main beam as desired. Its solution is unsurprisingly similar to the current phase factor and is expanded, from [13] and [14], as

$$\alpha_m = -\beta [x_m \sin \theta_0 \cos \phi_0 + y_m \sin \theta_0 \sin \phi_0 + z_m \cos \theta_0] \quad (76)$$

where the angles (θ_0, ϕ_0) represent the desired angle for maximum gain. An example of a randomly dispersed array and its associated array factor are shown in Figure 23 and Figure 24, respectively. The distances between elements are shown in wavelengths, and the desired beam target is $\theta_0 = 90^\circ$ and $\phi_0 = 60^\circ$. The gain pattern for the array shown produces a maximum gain of 6.4 dB at the target angle.

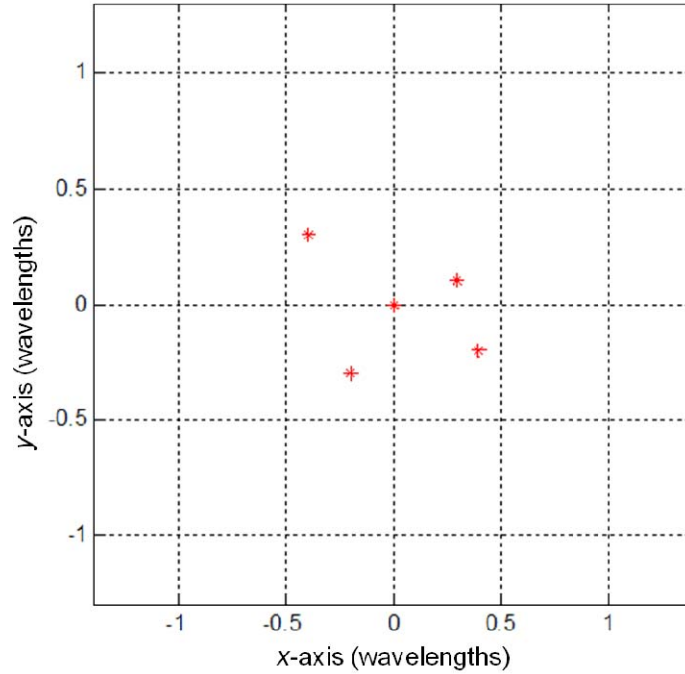


Figure 23. A five-element array with elements randomly distributed in two dimensions.

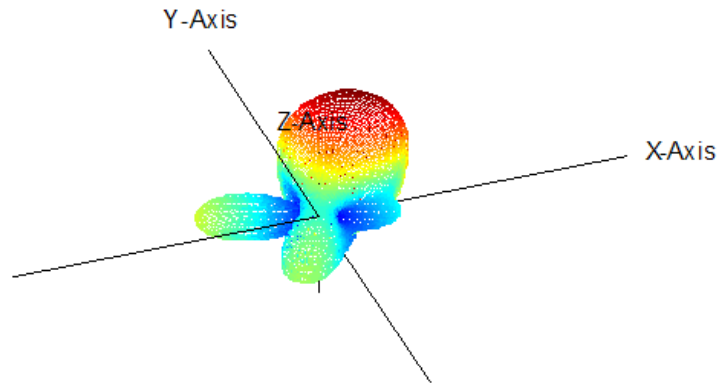


Figure 24. Gain pattern from the five-element, two-dimensional array in Figure 23.

a. Adaptive Beamforming

As array beamforming is a technique to improve antenna performance, it is appropriate to consider how the antenna may work in the context of the system. Pairing an array aperture with a receiver system, it is often the case where the general

shape of the power density of the received signal is known a priori. In such cases, or in any case where the received signal may be estimated, a method known as adaptive beamforming may be applied in order to further improve array performance [34].

Adaptive beamforming uses a comparison between the received signal and the expected signal to optimize phase weights, based on some given criteria. There are various algorithms to implement adaptive beamforming, and the most basic of these uses a least mean square comparison. In this implementation, the array uses the error, $e(t)$, between the expected signal, $a(t)$, and the output of the beamformer, $b(t)$, to further refine weights in an iterative manner, determining the mean square error, from [34], as

$$E[e^2(t)] = E[(a(t) - b(t))^2] \quad (77)$$

By minimizing the mean-squared error, $E[e^2(t)]$ by updating the weights involved in forming $b(t)$, an improved solution is obtained [34].

b. Grating Lobes

A phenomenon in array beamforming that must be monitored, and avoided in most applications, is grating lobes. Grating lobes refer to secondary maxima in an antenna pattern that offer equal or near equal magnitude as the main beam. Grating lobes occur in a linear array when array nodes are symmetrically equally spaced and element spacing, d , follows the relationship, from [35]

$$\frac{d}{\lambda} \geq \frac{1}{1 + |\sin \phi_o|} \quad (78)$$

where ϕ_o is the target azimuth. From [36], it is further known that for a planar array the linear relationship in Equation (78) must be false to avoid grating lobes in the x - y plane, and grating lobes in the x - z and y - z planes may be avoided with spacing $d < \lambda$. The principle maximum and grating lobes can be located in any planar array using the relations, from [36]

$$\begin{aligned}\sin \theta \cos \phi - \sin \theta_o \cos \phi_o &= \pm \frac{m\lambda}{d_x}, & m = 0, 1, 2, \dots \\ \sin \theta \sin \phi - \sin \theta_o \sin \phi_o &= \pm \frac{n\lambda}{d_y}, & n = 0, 1, 2, \dots\end{aligned}\tag{79}$$

Using these relations, distances may be set to avoid grating lobes at a specific target angle. However, in general, the following relationship is held to ensure against grating lobes, from [4], [13], [20], and [16],

$$d \leq \frac{\lambda}{2}\tag{80}$$

An example four element array is shown in Figure 25. In this case, the elements are 0.2 wavelengths away from their nearest adjacent nodes. The normalized azimuth of the pattern from this array is shown in Figure 26, where the target direction of $\theta_0 = 90^\circ$ and $\phi_0 = 90^\circ$ has been chosen. The cross-section is from the x - y plane due to the target direction. It can be seen in Figure 26 that the spacing of this array does not excite grating lobes.

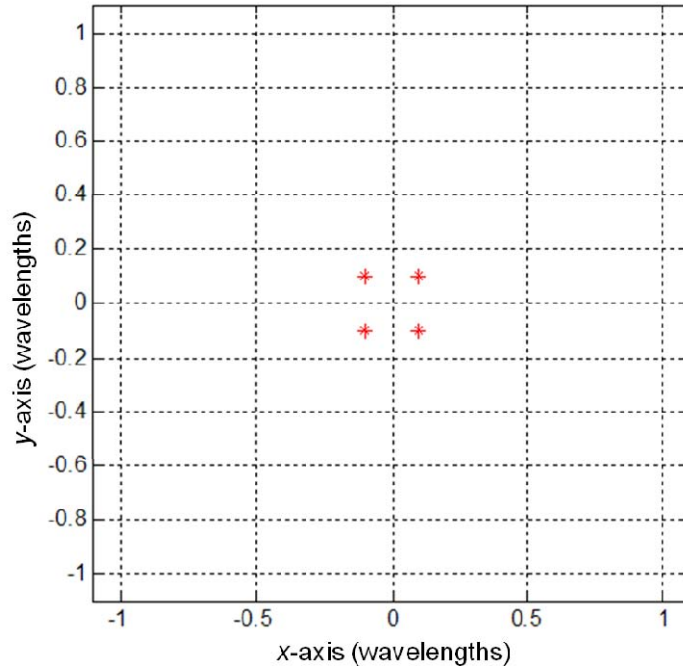


Figure 25. A four-element array with symmetrically placed nodes. Nodes have a distance $d = 0.2$ to nearest adjacent node.

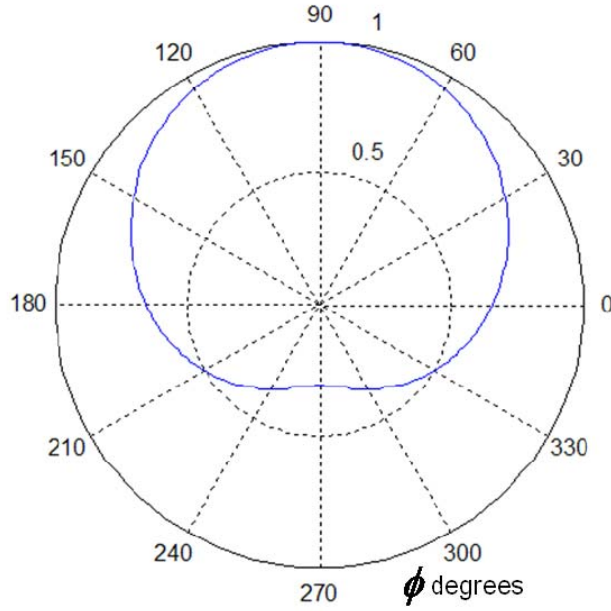


Figure 26. Azimuth of normalized pattern associated with the array in Figure 25 and a scan angle of $\phi_o = 90^\circ$.

The same four element array from Figure 25 is spread out as in Figure 27. In this case, the elements are spaced at 1.2 wavelengths from their adjacent nodes. The normalized azimuth of this array's pattern is shown in Figure 28. Based on the spacing of the elements, a grating lobe is expected and is shown at $\phi = 220^\circ$ and $\phi = 320^\circ$.

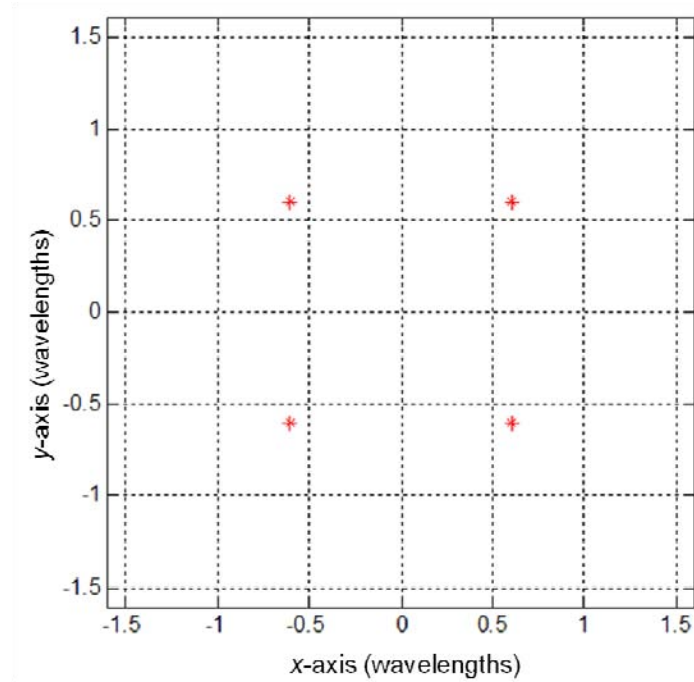


Figure 27. A four-element array with symmetrically placed nodes. Nodes have a distance $d = 1.2$ to nearest adjacent node.

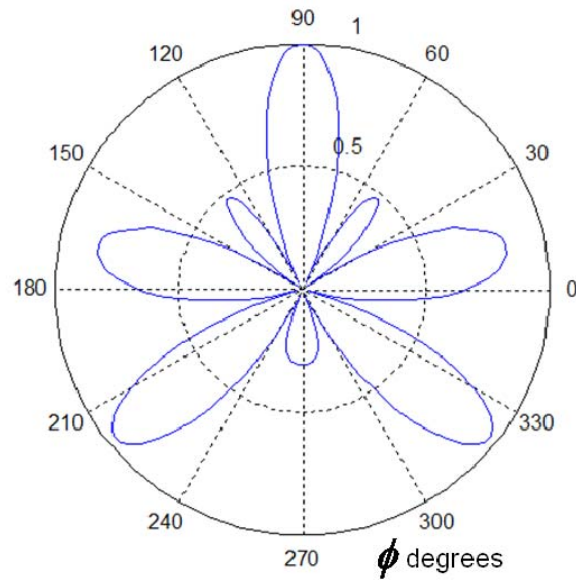


Figure 28. Azimuth normalized pattern associated with the array in Figure 27 and a scan angle of $\phi_o = 90^\circ$.

Further illustrative, the four element array is again recast with wavelength spacing of 3, as shown in Figure 29. As expected the normalized azimuth of this array's pattern, shown in Figure 30, displays several grating lobes.

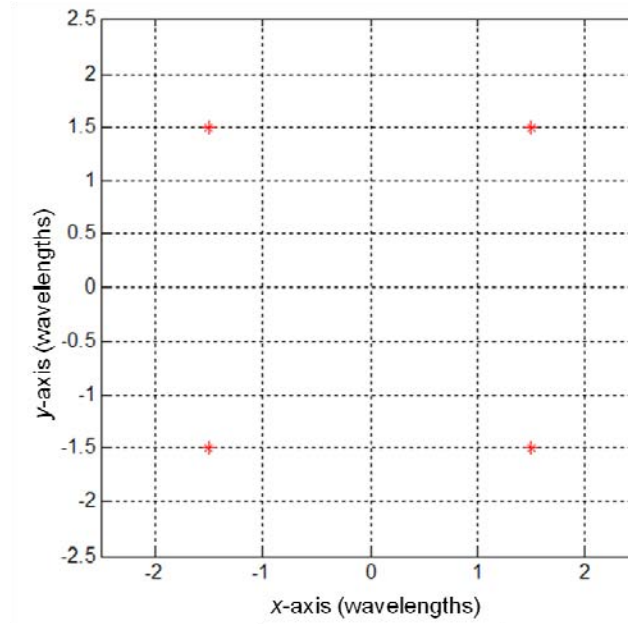


Figure 29. A four-element array with symmetrically placed nodes. Nodes have a distance $d = 3$ to nearest adjacent node.

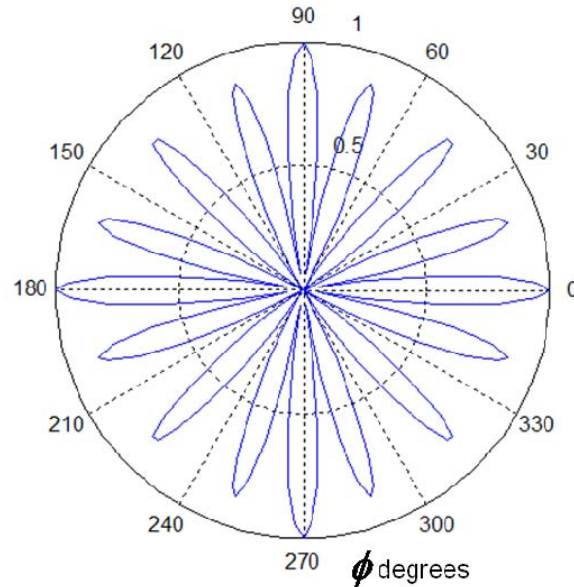


Figure 30. Azimuth of normalized pattern associated with the array in Figure 29 and a scan angle of $\phi_o = 90^\circ$.

c. Mutual Coupling

Another consideration in beam formation is the potential for mutual coupling. Mutual coupling occurs when antennas not only react to the designated current source but also to the reaction of adjacent antennas to the same current source. Simply explained in terms of a transmitting array, each element radiates a signal introduced at the antenna feed; however, the transmission from each antenna reaches every other antenna in the array where that transmission is received and re-radiated. The result is a cacophony of delayed (though lower power) signals at the targeted receiver. Although described for a transmitting situation, mutual coupling occurs when transmitting and receiving. Additionally, the effects of mutual coupling may occur due to coupling in the transmission line networks of wired arrays [37].

As described in the discussion on noise in Subsection 2, the nature of antennas is that they are subject to receiving undesired signals as well as desired signals. However, mutual coupling is a specific subset of this phenomenon because of the correlation of the received signal and mutually coupled signal. These two signals hold high correlation because the interferer is not a random undesired signal but instead it is the desired signal delayed in transmission. As such, techniques commonly used to filter noise are less effective in this instance [4].

Array elements tend to have similar structure and orientation. Additionally, the elements tend to be located in close proximity to one another. This being the case, the potential for mutual coupling through re-radiation exists. At a deeper level, the unintended received wave is inducing a current onto an element. This can be explored with a simplified example. Considering again a transmission scenario, the input voltage at the feed, V_1 , drives an input current, I_1 , intended for transmission. Using basic circuit theory, this can be modeled as an antenna impedance, Z_{11} , as shown from [16]

$$Z_{11} = \frac{V_1}{I_1} \quad (81)$$

Now including the induced current from a second element, it can be considered as an additional current, I_2 , driven by the input voltage, as shown from [16]

$$V_1 = Z_{11}I_1 + Z_{12}I_2 \quad (82)$$

where Z_{12} represents mutual impedance between the initial element and a second element. Mutual impedance can be solved in a two element case by measuring the first antenna's reaction to setting the second antenna to an open circuit (i.e., remove the second antenna) and with the second antenna present with a short circuit across its terminals. The resultant relation is, from [16],

$$Z_{12} = \sqrt{Z_{oc}(Z_{oc} - Z_{sc})} \quad (83)$$

where subscripts OC and SC refer to open circuit and short circuit, respectively. The change in impedance is accompanied by changes in current magnitude and phase for the element under observation and adjacent elements, distorting the original signal.

Returning to the general situation of mutual coupling in arrays, the determination of mutual impedances between multiple elements requires the solution of coupled integral equations. Therefore, determination of mutual coupling is generally done through numerical modeling methods such as the Method of Moments, a solution technique based upon systems of linear algebraic equations [4]. Alternative techniques such as pattern multiplication, active element patterns, or hybrid techniques also offer insight. However, as obtaining the solution may be resource intensive and does not offer a direct avenue to counteract the effects, avoiding significant mutual coupling is the general engineering response. From [16], the majority of effects caused by mutual coupling are removed keeping minimum element spacing as

$$d \geq \frac{\lambda}{3} \quad (84)$$

d. Beam Squint

Steering an array main beam is predicated upon a target frequency, as per Equation (74). However, electromagnetic waves carrying modulated signals operate over a range of frequencies. It is obvious that general practice trains an array by the center frequency. However, the upper and lower frequencies of a signal must also be considered, and since the direction of array main beam pointing is a function of

frequency, array response may be highly varied across the signal's spectrum. The result at the target direction may be varied gain levels across the signal bandwidth [20]. Such an event is known as beam squint. It is a common issue in phased array radar design, as modern radar signals tend to have wide bandwidths. However, beam squint may also be caused by frequency shifts in a signal, such as that caused by motion. Spreading through motion is known as Doppler shift and will be introduced in Section C of this chapter.

Figure 31 illustrates a randomly placed six-element array with element spacing in meters. At a frequency of 300 MHz, a normalized cross-section of the coherent array factor pattern targeted at $\theta_o = 90^\circ$ and $\phi_o = 60^\circ$ is shown in Figure 32. Additionally included in the figure are the cross-sections of the pattern at upper and lower frequencies of 272.2 MHz and 333.3 MHz, where they are normalized to the maximum gain at those frequencies. Beam squint is evident in the shifting patterns from the center frequency. An additional function of beam squint is the maximum gain associated with those patterns, which is 7.1 dB at 300 MHz, 7.06 at 272.7 MHz, and 7.08 dB at 333.3 MHz. It should be noted that differences of hundredths of dB are not statistically relevant for gain calculation, but the general trend shown is important.

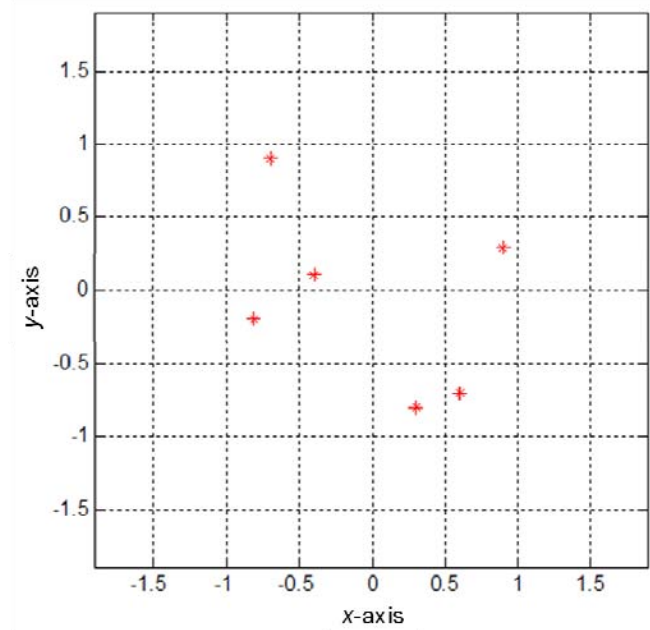


Figure 31. A six-element array with randomly spaced nodes. Spacing shown is in meters.

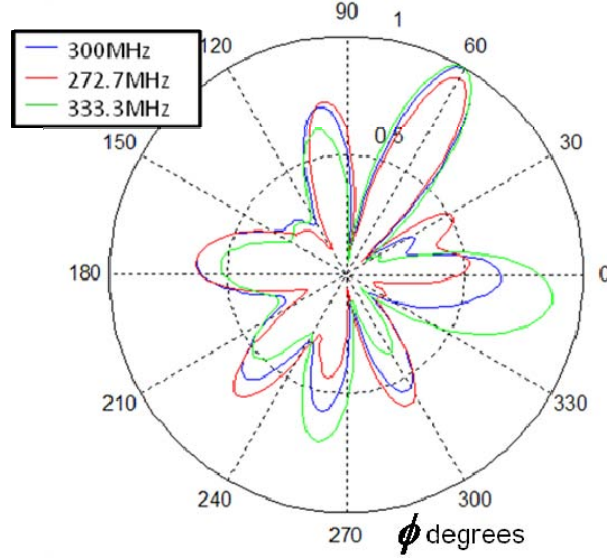


Figure 32. The array factor pattern for the array in Figure 31 at various frequencies.

4. Time Difference of Arrival

In addition to coherent beamforming, arrays also offer the ability to assist in location of the target emitter. Time difference of arrival (TDOA) is one of the techniques to determine target emitter geolocation, and the disposition of an array, requiring multiple receiver elements in different spatial locations, is common to beamforming and TDOA. Due to the spatial positioning of the receive antennas versus the transmitter, the path length from transmitter to each element may vary, resulting in individually associated signal arrival times. Since the speed of transmission, c , is known, this arrival time difference can then be used to determine the relative position of the transmitter.

With the position of the transmitter at an unknown location and a set of spatially separated receive nodes, as shown in Figure 33, a signal from the emitter reaches each node at a different time. The time difference of the signal from the transmitter to elements 1 and 2, $\Delta\tau_{12}$, can be determined from geometry, from [12], as

$$\Delta\tau_{12} = \frac{1}{c} \left(\sqrt{(x-x_1)^2 + (y-y_1)^2 + (z-z_1)^2} - \sqrt{(x-x_2)^2 + (y-y_2)^2 + (z-z_2)^2} \right) \quad (85)$$

Using the measured time difference, Equation (85) can be solved for emitter position. However, the resulting solution places the target emitter anywhere within two sides of a hyperboloid, as shown in Figure 34. Combining the results of three hyperboloids (from time differences to two elements) indicates a position where the solutions cross. Hyperboloid solutions from additional elements can help further refine the target position estimate. The accuracy of time difference measurements determines the accuracy of the TDOA geolocation, and the associated tolerance of the TDOA solution to timing inaccuracies is dependent on the angular spread of the receivers relative to the target emitter [12].

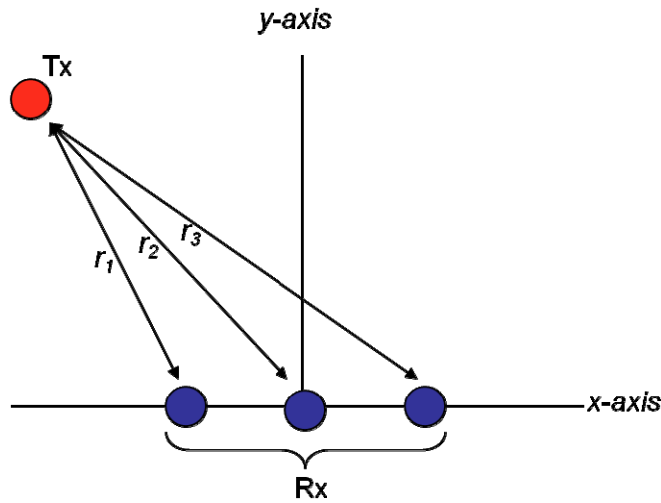


Figure 33. The basic setup for application of the time difference of arrival technique.

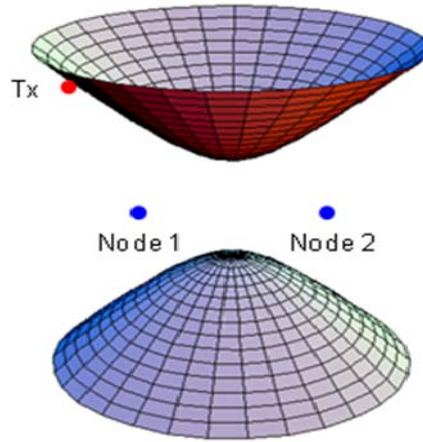


Figure 34. The two-sided hyperboloid formed by the TDOA solution from two elements.

As the processing for a precise position from TDOA can become intense where iterative methods are used to refine the solution, it is often the case that a Line of Bearing (LOB) to the target is enough for operational use. A LOB can be formed through simple estimation of the center of the TDOA error ellipse. Although the LOB will inherently have an associated error, it may be of greater practical use than the hyperboloid solutions.

C. WIRELESS SENSOR NETWORKS

The ability to create, maintain, and manage ordered communications among a group of nodes through wireless tethers and do so in an organized manner is the heart of wireless networking. The advancement of this area has enabled various applications and may be considered as a boon for implementations. However, it is important to understand the limitations and drawbacks of a wireless network. Physical layer issues of specific interest to the research will be the primary covered topic here, as well as some coverage of the medium access control layer.

The basics of physical layer data communications was covered earlier, resulting in Equation (54) for digital communications. This equation provides a specific relationship between signal parameters and a consequential ratio of energy per bit to noise density due to free space loss. Based on the type of signal sent, and how it is to be demodulated, the

energy per bit to noise density ratio can then be related to a probability of bit error for a transmission. Due to transmission over an unguided medium, external noise has greater access to the receiver than in a wired connection. Therefore, the potential for bit error in a transmission between two nodes is greater than in a wired network. Keeping the bit error low is certainly a goal of wireless communications, but this must be done in balance while optimizing energy usage and bandwidth. Therefore, some amount of bit error can be expected from wireless communications.

Further influencing wireless communications are the phenomena of multi-path fading and Doppler spreading. Multipath fading is a result of electromagnetic waves arriving at the receiver via different routes. As an example, a transmitted signal may take a direct path, reflect off of a surface, reradiate off a structure, scatter off an irregular surface, or may take any number of combinations in the transmission path to the receiver. From the receiver's point of view, the path is immaterial, what is important is that the received signal is distorted due to reception of time delayed, lower power versions of the intended signal. Reception of multiple time-delayed versions of the same signal is referred to as time dispersion. Multipath fading can be mitigated through management of coherence bandwidth, B_c . Coherence bandwidth reflects the size of the transmission band where the channel response can be expected to remain flat. It is a function of the root mean square (RMS) of the power delay spread, σ_τ , where each incoming signal is characterized by power, σ_i^2 , and delay, τ_i . The power delay spread can be determined, from [15], by

$$\sigma_\tau = \sqrt{\left(\frac{\sum_i \sigma_i^2 \tau_i^2}{\sum_i \sigma_i^2} \right) - \left(\frac{\sum_i \sigma_i^2 \tau_i}{\sum_i \sigma_i^2} \right)^2} \quad (86)$$

The coherence bandwidth is then determined directly from the power delay spread, from [15], by

$$B_c = \frac{1}{\gamma \sigma_\tau} \quad (87)$$

where γ represents the coherence factor and is determined by analysis in design with regards to channel correlation. Greater correlation results in smaller coherence bandwidth. Likewise smaller correlation results in a larger coherence bandwidth. By varying the coherence factor, relative values of correlation can be set based on application [15].

The phenomenon of the Doppler effect is a well-known and understood scientific concept. A shift in frequency of a signal occurs as a result of relative motion between the sender and the receiver of a message. In general, an increase in frequency indicates a closing relative distance. Conversely a decrease in frequency indicates growing relative distance [38].

Standard wireless transmission/reception presents a natural model for application of Doppler. In this arrangement a transmitter produces a signal, generally represented as a plane wave, which reaches the observer position at the receiver. With the addition of relative motion between transmitter and receiver, the transmitted wave is altered by a frequency shift dependent on the motion. This spreading has the ability to cause frequency dispersion, much like multi-path fading causes time dispersion. Due to this relative motion, the carrier frequency, f_c , undergoes a shift in frequency. The shift frequency, f_D , can be determined as related to the phase velocity in free space, c , relative velocity between transmitter and receiver, v , azimuth between direction of motion and direction from the transmitter to the receiver, ψ , and the elevation between direction of motion and direction from the transmitter to the receiver, ϑ . The relative geometry is demonstrated in Figure 35. The relationship between shift frequency and these factors can be written, from [38], as

$$f_D = \pm \frac{f_c}{c} v \cos \psi \cos \vartheta \quad (88)$$

Potential Doppler shift can be modeled as a random variable, but of specific importance to managing Doppler spreading is determination of maximum shift frequency, $f_{D_{Max}}$, which can be found, from [15], by

$$f_{D_{Max}} = \frac{v_{Max}}{\lambda} \quad (89)$$

Maximum shift frequency is related to coherence time, T_c , which sets the separation necessary between two symbols to mitigate the interference caused by frequency dispersion, and it can be found, from [15], by

$$T_c \approx \frac{0.423}{f_{D_{Max}}} \quad (90)$$

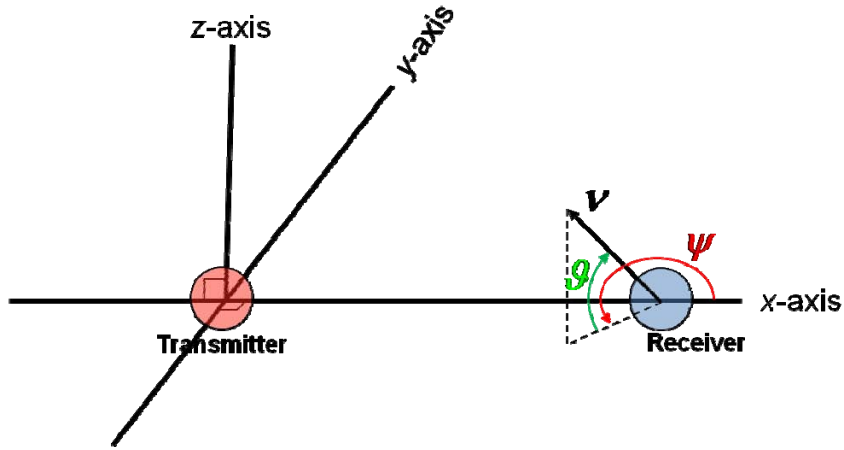


Figure 35. The relative angles in a Doppler effect problem.

Although both multipath fading and Doppler spreading can be managed as discussed, fading margins are generally included to account for expected loss. In doing so, expected probability of error calculations can continue to be used to account for potential bit errors.

This chapter covered background materials regarding random variables and stochastic models, communications phenomena, antenna and array operation, and basic wireless network issues. Each of these topics will play a role in assessing the dissertation topic of conducting coherent beamforming while array elements are in motion. The next chapter will provide basic analysis of beamforming to illuminate issues regarding imprecise element positioning, basic expectations with motion applied, the potential effect of Doppler, and the influence of intermittent participation due to wireless network connectivity.

III. BEAMFORMING USING WIRELESS NETWORK CONNECTIVITY

As described, sensor connectivity will be enabled through the employment of wireless sensor network technology, and while the use of a wireless sensor network assists to simplify the task of fielding the array, it also removes from traditional array formation the static nature of the nodes as well as careful array calibration to optimize operations. This chapter will analyze the effects that can be expected on the beamforming solution as a result of the more casual fielding technique. It will be seen that the issues covered under this circumstance are all a piece of the final implementation as an array with nodes expected to operate under constant random motion.

First, a study is presented on the ability to form array solutions from an imprecisely placed set of element nodes. The premise of this analysis is similar to that presented under [13]; however, the focus here is tailored to the topic of interest. The effects demonstrated will be necessary in the proposed solutions for managing sensor network operations. Then, a discussion is offered regarding beamforming with imprecise node locations. Within this topic, it will be shown how an assumption of imprecise node location is relevant even with high accuracy geo-location technology and how that assumption may be qualified based on target frequency band. In the company of wireless communications is the potential for data loss from any individual node. The result of such loss is the non-inclusion of that node in the beamforming solution. Therefore, the third section considers the expected result when elements are removed from the array. Penultimately, an analysis is presented on the reaction of the array to random motion applied to the array elements. This examination equips the research for future proposals to manage the array effects. Finally, a set of research proposals are made that present the set of major research challenges in confronting the wireless independently mobile sensor network array problem. Each proposal will be covered in detail in later chapters.

A. ARRAY PERFORMANCE WITH RANDOM NODE DISTRIBUTION AND IMPRECISE LOCATION INFORMATION

Although basic spatial stochastic distributions may be used to evaluate the idea of a randomly displaced array as in [14], the simple application of a uniform or Gaussian distribution against potential array elements is not directly fitting of the end goal where the tactical sensor field is not purely random. As described, a set of potential platforms are most likely related; therefore, they may have designated, vice arbitrary, positions. The question then becomes how close to the selected position a node resides. The applied model should account for relevant boundaries on random arrangement as much as possible. While certainly, these boundaries are not “hard” when applied to the real world, they are useful in determining most likely operational scenarios for optimization. Figure 36 illustrates a uniformly random set of nodes placed around the origin. In contrast, Figure 37 shows a moderately arranged set of nodes where the platforms reside in groups of two-to-three and are roughly placed in a pyramid-like configuration. While the exact placement of the elements retains a random nature, the noted structure needs to be accounted for to properly model.

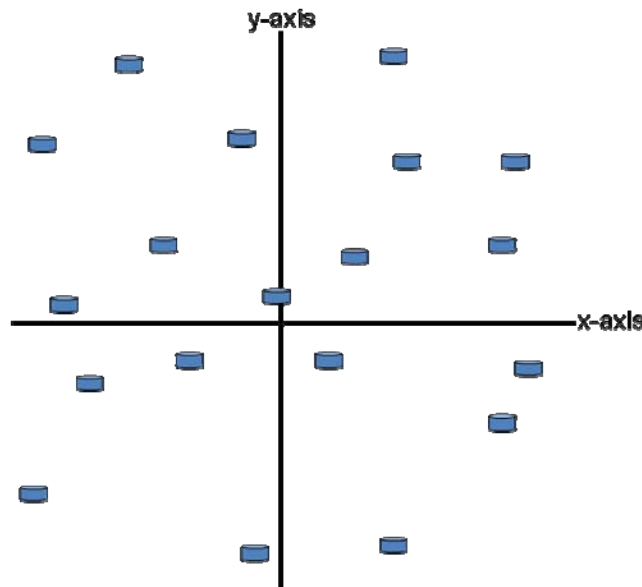


Figure 36. A uniformly random distribution of nodes in two dimensions.

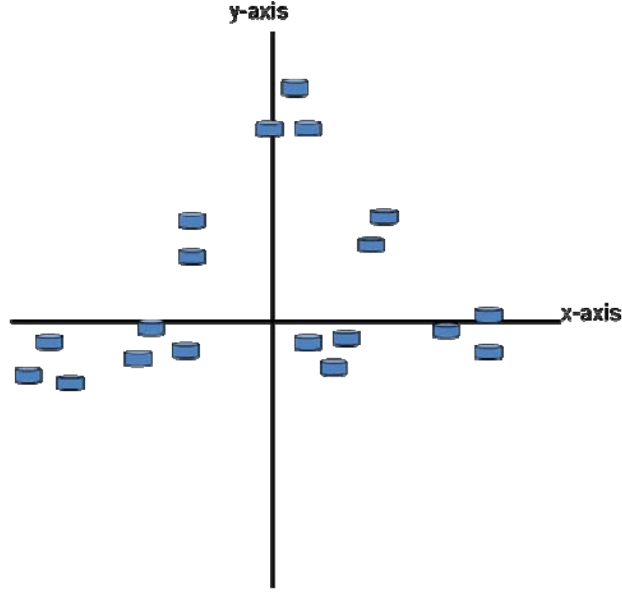


Figure 37. A moderately arranged set of nodes.

In each case, the distribution of elements can be used to form a coherent array beamforming solution using Equations (74), (75), and (76), as described in Chapter II.B [13] and [16]. However, the difference in considering a model with a desired arrangement resides in the internals of the mathematical description. In the case of a purely random set of elements, the node positions are unknown and must therefore be reported prior to array factor determination. In the case where a desired arrangement exists, the array factor may instead be formed based on the arrangement; however, the actual array factor pattern will be based on arrangement position plus error. Specifically, this affects the current phase factor, ξ_m , which is then written as

$$\zeta_m = \beta \left[(x_m + \delta x_m) \sin \theta \cos \phi + (y_m + \delta y_m) \sin \theta \cos \phi + (z_m + \delta z_m) \cos \theta \right] \quad (91)$$

where the variables δx , δy , and δz represent the position error for each node applied in Cartesian coordinates. This representation will be useful in Section B of this chapter when considering random motion. It is of further interest to note that the offsets are included with the spatial layout, where distances are converted to wavelengths for computation. Therefore, the positioning error elements are similarly sensitive to wavelength distances, vice pure distance measurements.

Figure 38 and Figure 39 illustrate basic formations that could be used as arrays with determined platform positions. Figure 38 is a basic three node configuration, and Figure 39 is a two dimensional structure with a greater number of nodes. Further describing the figures, coordinates shown correspond to wavelength distance from the origin. Using distances defined by numbers of wavelength allows the model to be flexibly applied in our scenario to a variety of target frequencies. Based on the basic relationship in Equations (31) and (32), resulting physical positioning between nodes can be derived as required.

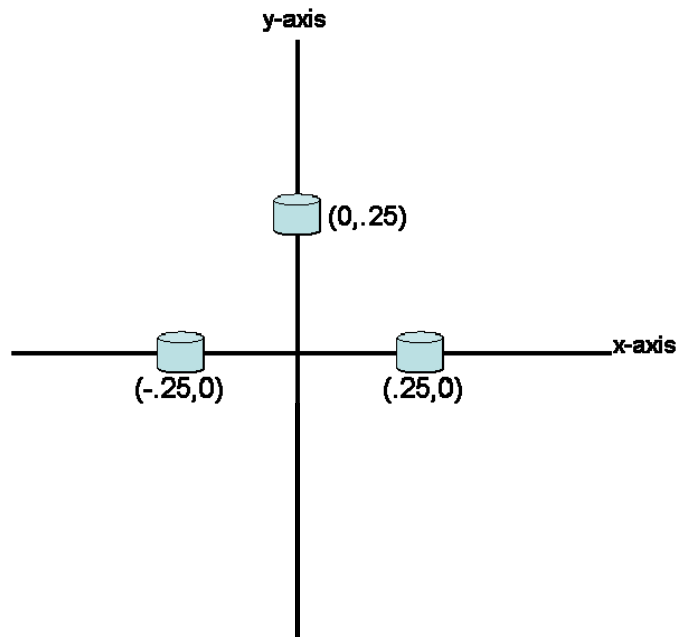


Figure 38. A three-node array (distance in wavelengths).

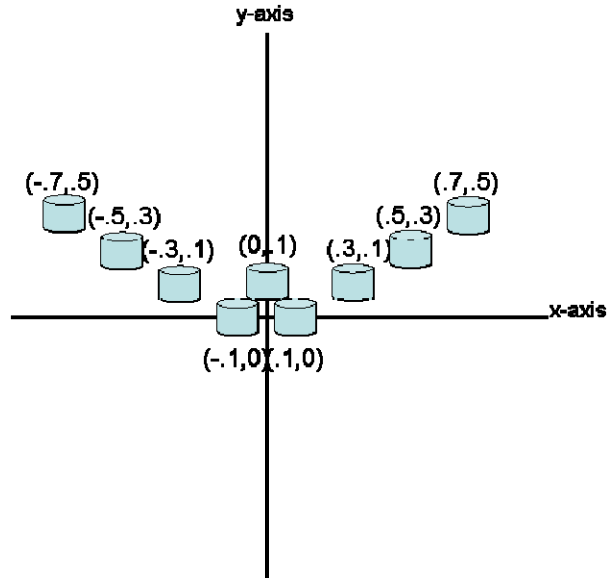


Figure 39. A nine-node array (distance in wavelengths).

The array factor for the arrays in Figure 38 and Figure 39 can be determined from Equation (74), as was shown in Chapter II, for any target angle defined by (θ, ϕ) . Applying a target located in the x - y plane at an angle of 60° from the x -axis, the three dimensional array factor patterns for each array are respectively shown in Figure 40 and Figure 41.

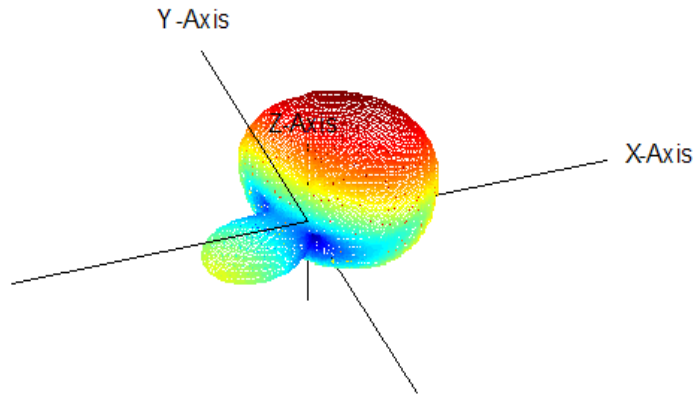


Figure 40. Normalized array factor pattern for array in Figure 38 with $\phi_o = 60^\circ$ and $\theta_o = 90^\circ$.

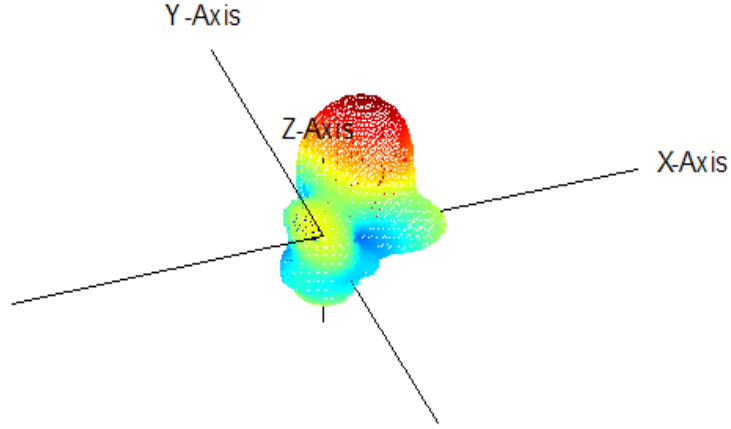


Figure 41. Normalized array factor pattern for array in Figure 39 with $\phi_o = 60^\circ$ and $\theta_o = 90^\circ$.

Since the element arrangement may create a complex set of side or grating lobes in the array factor pattern, viewing the three dimensional pattern provides a qualitative perspective on pattern structure. However, it is often of greater interest to evaluate the pattern only in the plane of interest. For both of the evaluated arrays, the target aim point resides in the x - y (azimuth) plane. A cross-section of each pattern is provided in Figure 42 and Figure 43. In each case, the array factor has been normalized. The maximum gain, associated with the maximum of the array factor, is 4.4 dBi and 7.6 dBi, respectively.

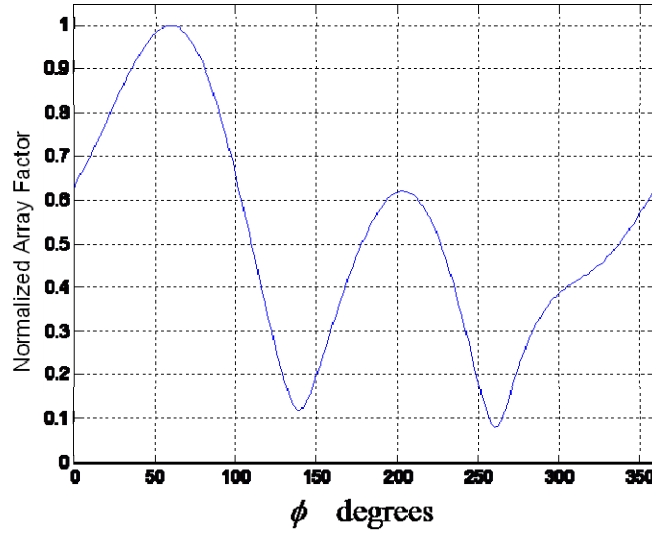


Figure 42. Normalized array factor azimuth pattern associated with Figure 40.

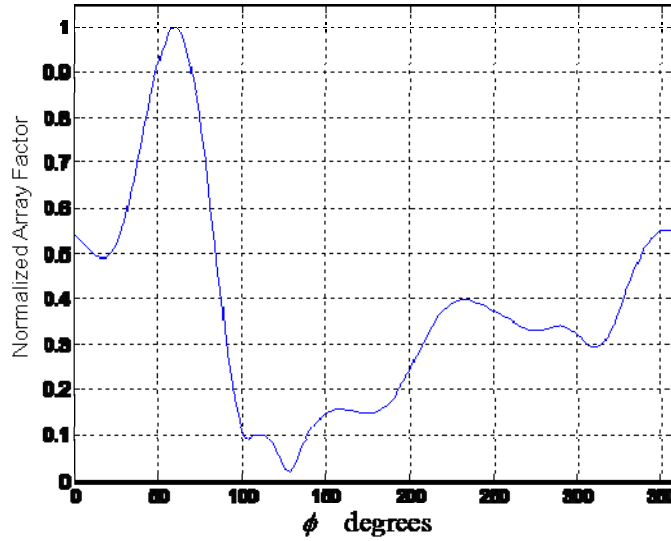


Figure 43. Normalized array factor azimuth pattern associated with Figure 41.

From the array factor formed by each array presented, or any array that may be considered, the general properties of multi-element arrays established by [13] are available. The coherent addition of array elements clearly provides increased targeted gain in a desired direction bracketed by the array factor beamwidth. From [13] and [14], general relationships are established for both gain, G , and beamwidth, BW , as

$$G \propto N \quad (92)$$

$$BW \propto \frac{\lambda}{D} \quad (93)$$

where N represents the number of elements and D is the spatial width of the array. Both are shown as proportionalities since the specific nature of gain and beamwidth is heavily dependent upon the spatial organization with respect to the target direction; however, the general proportionality remains in vogue. Further, the relationship in Equation (93) must also consider the effects of target signal wavelength, as the existence of grating lobes alters the effect of beamwidth after $D > \lambda$ [17]. Further, from [13], the pure concept of grating lobes is not present when elements are randomly spaced; however, individual sidelobes may remain high based on specific target and element location. The sparseness of an array and the presence of symmetry will increase these individual lobes, in effect allowing grating lobes with some loss against main beam performance [7].

With the concept of array formation using random element placement fully formed, positioning knowledge inaccuracy can be assessed. In the most general of terms, positioning knowledge inaccuracy is a result of errors in geolocation position finding techniques. There are a variety of options for position determination in wireless sensor networks. As discussed in [39] and [40], techniques can be divided into external positioning, internal localization, or hybrid approaches. External positioning uses some external service to determine node location, internal localization uses information within the network to establish node position relative to other nodes in the network, and hybrid techniques combine these methods. The most well-known external positioning technique is use of the Global Positioning System (GPS), and a fully implemented external positioning system on a wireless sensor network would have a GPS receiver on each node. Internal techniques include methods based on metrics like receiver signal strength or message time delay to establish relative node spacing. Typical hybrid techniques establish positions for a set of landmarks or a subset of nodes, then use internal location methods and landmark knowledge to establish the position of all others [41]. Each technique has benefits and detractors. External positioning is considered highly accurate

(more on this in the next paragraph) and available for continuous independent status update; however, the presence of an external process for positioning draws from a limited node power supply. Internal localization generally provides a less accurate position that is only referenced to other nodes. Additionally, it requires meta-data transfer in the network, but it provides a positioning service using only a few processor cycles and messages, saving network energy. Hybrid techniques provide a global reference for internal techniques. Therefore, positioning through internal or hybrid methods is attractive in cases where positioning is static or rarely required. Alternatively, when location is fluid and updates are necessary on a more frequent basis, external techniques are appropriate.

Regardless of positioning technique used, location errors may be introduced. GPS is greatly relied upon as a primary provider of external positioning or for setting landmarks in hybrid methods. However, typical commercial GPS systems are only noted as accurate to around 18.3 meters [42]. For a titular target frequency of 900 MHz, the wavelength is 0.3 meters – equating to an accuracy of 54.9 wavelengths — an extremely large number. However, this is only the starting point in terms of GPS accuracy. To further consider, a more precise definition of GPS accuracy is necessary. For military use, the measure of accuracy commonly used in GPS is Circular Error Probability (CEP). CEP provides the circular range around the area that has a 50% probability of containing the target [43]. Accuracy for positioning can certainly be described in different terms, such as increasing the percent probability included in a circular error measurement or simply providing mean bias and variance measures. However, most important to such a definition is ensuring which definition is being used at a given time [43]. Considering the large accuracy error noted for commercial GPS and the CEP definition, it is easy to believe that GPS is not an adequate positioning system, but that is not the case. Through analysis of the errors resident in a GPS location, additional techniques have been created to improve accuracy. From [44], the main causes of position error in GPS are:

- Ephemeris error
- Ionospheric delay error

- Tropospheric delay error
- Multipath error
- Receiver noise
- Satellite clock error

Many of these errors are correctable in that they affect two GPS receivers in relatively close vicinity to one another in the same way. These include ephemeris error, ionospheric and tropospheric delay, and satellite clock error. Correlation of data between two local receivers removes these errors, significantly improving performance [44]. Differential GPS (DGPS), a scheme using GPS stations at known locations to provide correction data to mobile users, has proven flexible and easy to implement. Results from a low cost commercial DGPS demonstrate an accuracy of 1.18 meters CEP [45]. With a far narrower baseline error in positioning, further techniques can be attached to refine position. Since the context of the scenario emphasizes the knowledge of relative positioning, exchanges between mobile users can be used to assist in position estimation. GPS gross knowledge of position, time of arrival, and time difference of arrival knowledge can potentially be used to further improve accuracy. Studies indicate possible improvement with hybrid methods but has focused on degraded GPS initial solutions [46].

Further bolstering the use of GPS is its ability to provide very accurate time synchronization within the 10-20 nanosecond range [21]. This level of time synchronization is much tighter than methods available internal to the network, such as the Network Time Protocol (NTP) [47], Reference Broadcast System (RBS) [48], Efficient RBS [49], Timing-sync Protocol for Sensor Networks (TSPN) [50], Time-Diffusion Synchronization Protocol (TDP) [51], or Cluster-wise Clock Synchronization [52]. The result is, therefore, a very precise time synchronization and continuously available positioning within centimeters relative to the network. GPS also provide a frequency reference with a traceable accuracy better than 10^{-12} available in off the shelf commercial systems [53].

Considering this error in terms of available positioning accuracy, beamforming conducted must expect errors. Research in [5] and [54] demonstrates the robustness of beamforming with multiple nodes and position errors limited to within wavelength parameters. Demonstrating these results, the arrays in Figure 38 and Figure 39 have been re-formed with a single node position error as shown in Figure 44 and Figure 45. A cross-section of the array factor pattern in each case displays that the pattern remains robust and the main beam does not vary greatly from the target despite the small positioning error, as shown in Figure 46 and Figure 47. The comparisons shown display each pattern individually normalized. In the case of the three node array, array gain towards the target is 4 dBi in the altered case. Contrasted with the desired arrangement, a loss of 0.4 dBi was observed for this positioning error. This is a specific value to the scenario shown, and 0.4 dBi is small in terms of antenna performance measurement. As discussed in [5], array gain change due to positioning error tends to have a mean of only slightly below that of the array without error. Further, variance of that change decreases with the addition of elements. Considering that result, it can be expected that, in general, the main beam of the nine element array will remain close to the desired position beam. It proves true in this scenario, as shown in Figure 43. Further, gain on target drops from the previous 7.6 dBi to 7.5 dBi.

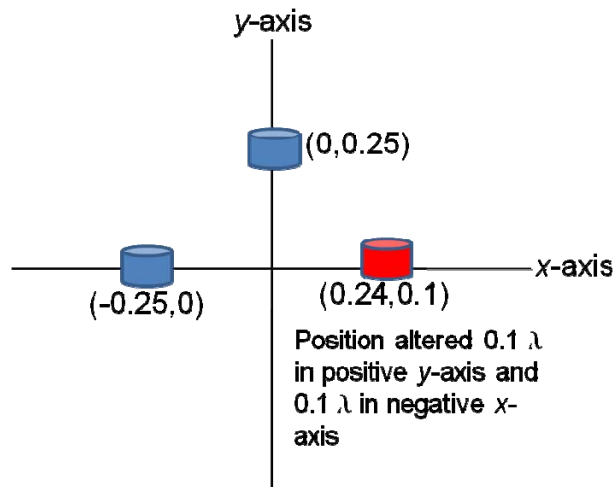


Figure 44. Array from Figure 38 with a 0.1 wavelength positioning error in the negative y-axis direction applied to the red node.

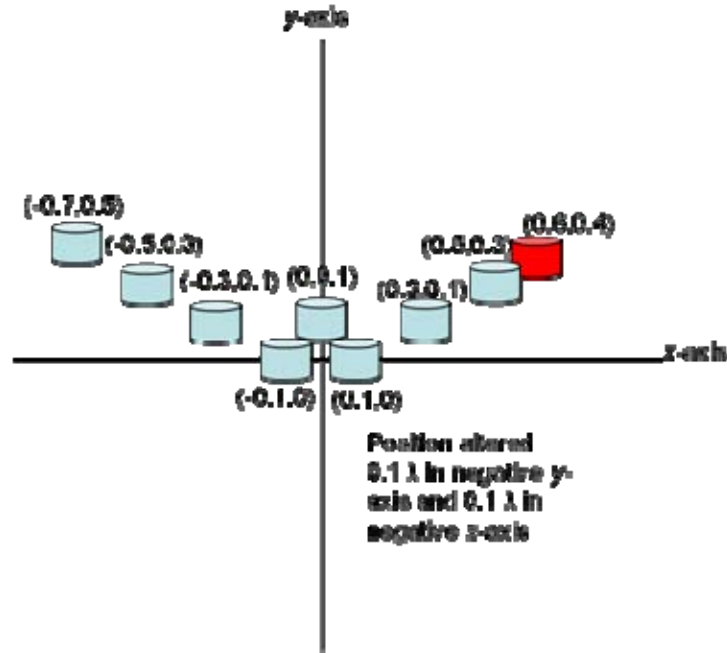


Figure 45. Array from Figure 39 with a 0.1 wavelength positioning error in the negative y-axis direction applied to the red node.

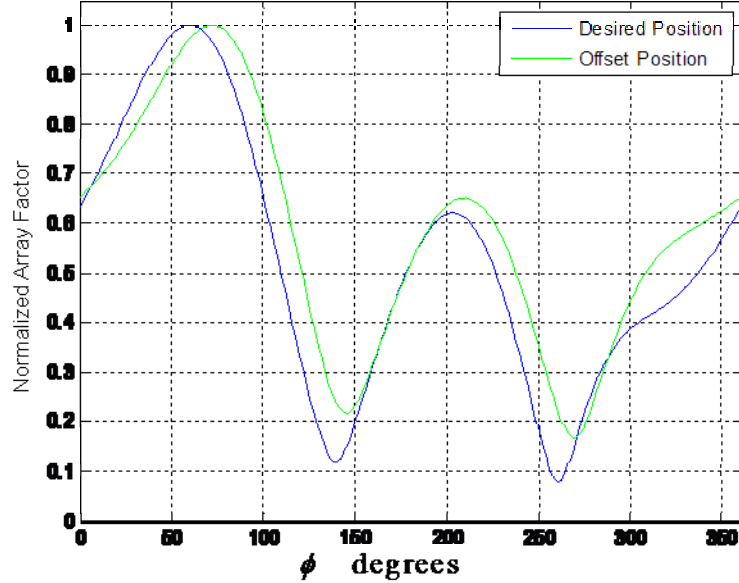


Figure 46. Cross-section comparison of normalized array factor patterns for the array in Figure 38 versus array with node offset shown in Figure 44.

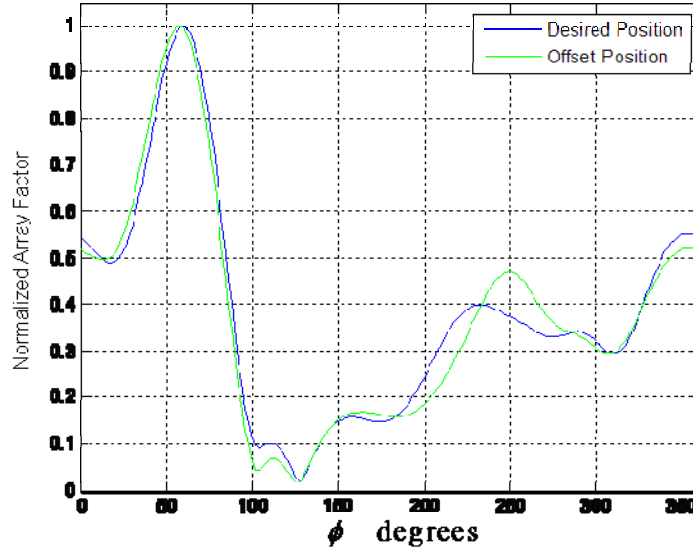


Figure 47. Cross-section comparison of normalized array factor patterns for the array in Figure 39 versus array with node offset shown in Figure 45.

Therefore, it is known that positioning errors can be treated as offsets in the formation equation. Based on this treatment, the error distances are important in terms of target signal wavelength distance and not pure distance. Additionally, positioning errors can be expected in array factor formation, even when using high accuracy external positioning systems like GPS. Further, and consistent with the findings of [5] and [54], the array factor results can be expected to remain robust when positioning errors are present. Per [5], when errors are cumulative over the array and assumed Gaussian, they are tolerable to 30% for production of gain, but this is not a hard limiting factor. In [54], a similar assumption of cumulative Gaussian error is taken.

B. ARRAY PERFORMANCE WITH NODES IN STOCHASTIC MOTION

Element motion within a beamforming array is not commonly considered in applications because the weights required for coherence requires element spatial positioning at the time of intercept. Therefore, traditional engineering associated with the design and fielding of arrays immediately assumes fixed element positions. As discussed in [18] and [16], which individually cover general beamforming and beamforming in radar applications, the static assumption is valid for the vast majority of phased array

applications. Although the field of sensors may be strategically placed, assembled from a random arrangement, or opportunistically formed from available sensors in random positions, once locations are defined weights are applied with consistent results. To this point, research in beamforming using distributions of ad hoc or sensor networks has similarly adopted this same assumption. Beginning with [7], investigations have shown that coherent beamforming is a viable method to exfiltrate data from a sensor network. The study in [8] improved on this position by defining a specific implementation for removing sensor data from a locally networked field using a coherently beamformed radio frequency signal. This further demonstrated how sensor nodes in a randomly distributed field could form a viable main beam and track to a relay or destination position. In both of these cases, known spatial location is assumed; however, research in [5] expanded the ability to implement when precise positioning data is not available. This work was used in defining the analysis shown in Section A of this chapter. Connected to this idea, analysis presented in [6] demonstrated resilience to synchronization errors. Each of these research efforts were primarily focused on data exfiltration. While reciprocity applies, specific research regarding usefulness and providing employment methodologies for wireless sensor network arrays as radio frequency detection and reception arrays is also of interest. The analysis in [9] provides initial insight into this application while focusing on the performance of the sensors in forming an adequate beamformed solution. This study was further codified in [11], which expanded on details of the analysis. A separate study in [55], applying to both array operations for data exfiltration and sensor beamforming, considered the random element node deployment in a wireless radio frequency array to match a Gaussian distribution. This analysis is relevant as general investigation had assumed a uniform distribution across the deployment area. However, it also demonstrates in its applicability that each study continues to assume spatial location as static after initial fix.

Considering random motion to the individual sensors in a field, the motion model applied in a complex simulation should follow the tenants defined in Chapter II.A.5. However, initial inspection should consider the simplest motion and array configuration available. Limiting motion to basic parameters and motion models will in fact be

necessary to determine effects that may be a result of more synchronized motion. Starting simple, an initial motion model will be based on a basic one-dimensional random walk. The background previously provided on beam patterns from randomly displaced arrays can now be used to evaluate a series of discrete time models for evaluation. Single time-distance steps provide insight for discussion. A two node array is a simple array to begin analysis. Because two points with any placement obviously define a line, two node arrays can be viewed as simple linear arrays. The benefit of considering a two element array in this fashion is that lobe patterns are symmetrical around the linear axis, and the interesting facets of the array formation only occur in the plane of the linear axis and the target.

Along with of motion, the potential for frequency shift due to the Doppler effect must also be considered. Analysis of both the initial motion and Doppler effect are provided in the following subsections.

1. Analysis of Simple Motion in a Two-element Array

Considering a two element array formation, shown in Figure 48, and neglecting the amplitude difference in a received wave at each individual element, the array factor can be formed using equation (74). Ignoring the amplitude difference due to the difference in range from the target to each element is valid as this difference can be restored with proper amplitude weights in the summation. Further, unless spacing is very wide, or the medium is very lossy, the amplitude differences should be minimal. So, the array factor for this case, AF_{2-node} , can then be written as

$$AF_{2-node}(\theta, \phi) = I_1 e^{j\alpha_1} e^{j\zeta_1} + I_2 e^{j\alpha_2} e^{j\zeta_2} \quad (94)$$

Clearly, this is the simplest array case as the two node model can also be considered along a line in a single dimension as well.

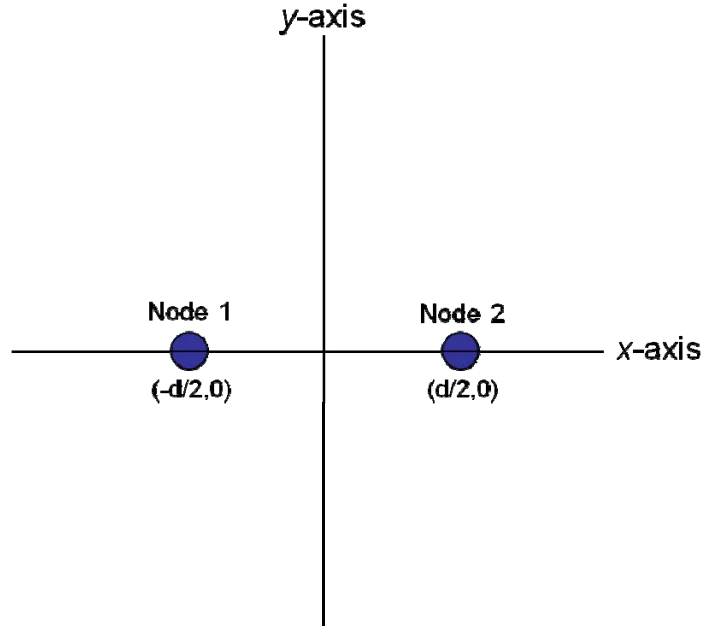


Figure 48. A two-element array with element spacing, d .

The creation of the spatial factor and phase weights for each node is similarly simple for the two node model. These are written, respectively, as

$$\zeta_1 = \beta [x_1 \sin \theta \cos \phi] \quad (95)$$

$$\zeta_2 = \beta [x_2 \sin \theta \cos \phi] \quad (96)$$

$$\alpha_1 = -\beta [x_1 \sin \theta_0 \cos \phi_0] \quad (97)$$

$$\alpha_2 = -\beta [x_2 \sin \theta_0 \cos \phi_0] \quad (98)$$

The simple form of the spatial factors and phase weights allows the expansion of Equation (94) for general inspection as

$$AF_{2-node}(\theta, \phi) = e^{j\beta x_1 (\sin \theta \cos \phi - \sin \theta_0 \cos \phi_0)} + e^{j\beta x_2 (\sin \theta \cos \phi - \sin \theta_0 \cos \phi_0)} \quad (99)$$

where the current magnitudes have been normalized. It should be noted that at the target angle, $\theta = \theta_0$ and $\phi = \phi_0$, the phase terms disappear and magnitudes add directly. By holding spatial distance inside 0.5λ , further interesting observations can be made in regards to the angle terms. For θ equal to any other angle (recall that θ is limited between 0° and 180°), the phases will not match. However, ϕ varies between 0° and

360° and the odd symmetry of the sine function then allows for main beam formation at complementary angles. The βx_n terms in Equation (99) define the distance between the elements in spatial frequency. Therefore, increased distance between two nodes results in increased spatial frequency in the phase terms, repeating the results of each angle contribution, and creating grating lobes in three dimensions.

Consider element motion by the second node along the x -axis with target angle held constant. In this assumption, the motion will not be accounted for in creating beamforming weights, so the weights will remain as calculated in the original positions of x_{1_0} and x_{2_0} . So, the array factor will be perturbed as the spatial factors are altered. In order to further simplify the analysis, node 1 is held constant at position x_{1_0} . The array factor can then be reformed to display the structure after the second node is moved to position x_2 , as

$$AF_{2\text{-node}}(\theta, \phi) = e^{j\beta x_{1_0}(\sin\theta \cos\phi - \sin\theta_0 \cos\phi_0)} + e^{j\beta(x_2 \sin\theta \cos\phi - x_{2_0} \sin\theta_0 \cos\phi_0)} \quad (100)$$

Comparing Equations (99) and (100), a difference in summation, Δ , can be expected due to the motion. The cause of the error is based on the spatial frequency distance between x_{2_0} and x_2 , as

$$\Delta(\theta, \phi) = e^{-j\beta x_{2_0} \sin\theta_0 \cos\phi_0} \left(e^{j\beta x_2 \sin\theta \cos\phi} - e^{j\beta x_{2_0} \sin\theta \cos\phi} \right) \quad (101)$$

By observation of the difference terms, the primary perturbation factors are considered. Specifically, it is evident that physical distance changes in one dimension result in cyclical errors in weight phasing. Additionally, increasing physical distance may result in both phase weight errors and addition of grating lobes. These observations from the difference equation match the results for the general case from [13].

The array factor pattern for the two node array formation of Figure 48 can be calculated to increase understanding of the results of motion. Assuming element spacing of 10 meters and target center frequency of 900 MHz, the nodes are spaced well past the parameters of Equation (80), so grating lobes are expected. The wave magnitude difference at each of the nodes will be assumed minimal since free space loss over the

distance between the nodes is negligible. Therefore, this difference will be ignored. Instead of aiming the pattern at a target, the phase difference in combining the signal, α , will be adjusted per Equation (71), demonstrating how this adjustment affects beam pattern. Figure 49 displays the array pattern when a phase difference, α , of 0° is applied.

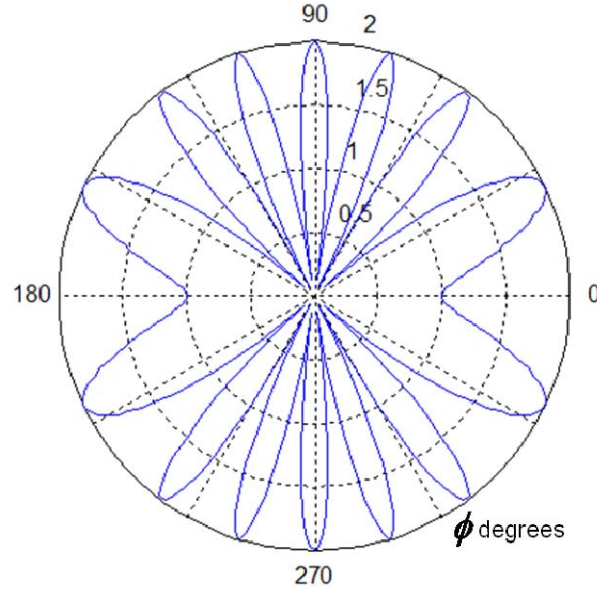


Figure 49. Array pattern in x - y plane for two-element array in Figure 48 with $\alpha = 0^\circ$.

The pattern without phase application demonstrates the presence of grating lobes and the natural positions of array gain and nulls. Adjusting the phase delay to 250° , the array beam formation is aimed at a target direction of 0° . This resultant pattern is shown in Figure 50. This pattern will be used as a basis for analysis of the effect of elements in motion described.

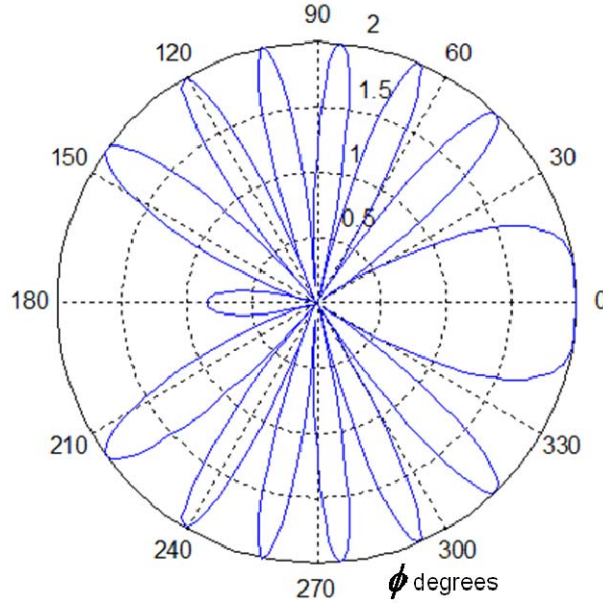


Figure 50. Array pattern in x - y plane for the two-element array in Figure 48 with $\alpha = 250^\circ$.

Assuming motion of node two as per the earlier analysis of the array factor equation, it is simple to simulate the change in array factor after one time step of motion; however, at this point it is unknown what time step size is proper. Figure 51 illustrates the geometry of the first variation to be evaluated, where node two has been moved 0.5 m in the positive direction along the x -axis. As this is a two element array, this motion has the net effect of increasing the spatial distance between the nodes. The important factor to consider is the separation between nodes in terms of wavelengths. In this case, the change is equivalent to 1.5λ ; therefore, a radial error of 3π can be expected in the Δ term of Equation (101). The result should then be to move the main beam aim point off of the target; the grating lobes will remain, and a new aim point can be predicted through partial derivative analysis. Further, since the array is linear, analysis can discount the effect of the θ variable, since the pattern will be symmetric around the array, which has been aligned with the x -axis.

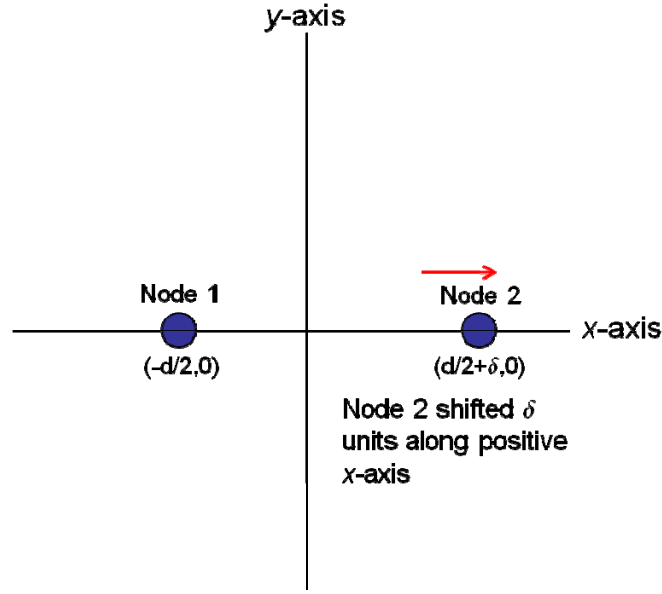


Figure 51. The two-element array from Figure 48 modified by positive x -axis motion of node two.

Considering the partial derivative analysis, Equation (99) can be re-written to reflect the new position of node two as $x_2 + \delta$. It should be noted that this representation is similar to that of Equation (91) evaluating position errors. The revised form of the array factor equation for this specific example is then

$$AF_{2-node}(90^0, \phi) = e^{j\beta x_1(\cos\phi - \sin\theta_0 \cos\phi_0)} + e^{j\beta x_2(\cos\phi - \sin\theta_0 \cos\phi_0)} e^{j\beta\delta(\cos\phi)} \quad (102)$$

where θ has been set to 90^0 . With this simplified form, a derivative with respect to ϕ can determine local maximum and minimum angles as

$$0 = \frac{dAF_{2-node}(\phi)}{d\phi} = -j\beta x_1 e^{j\beta x_1(\cos\phi - \sin\theta_0 \cos\phi_0)} \sin\phi - j\beta(x_1 + \delta) e^{j\beta x_2(\cos\phi - \sin\theta_0 \cos\phi_0)} e^{j\beta\delta \cos\phi} \sin\phi \quad (103)$$

Like terms can then be canceled, and Equation (103) here can be reordered to isolate the ϕ term to one side of the equation as

$$e^{j\beta(x_1 - x_2 - \delta)\cos\phi} = -\frac{x_2 + \delta}{x_1} e^{j\beta(x_1 - x_2)\sin\theta_0 \cos\phi_0} \quad (104)$$

In order to solve for ϕ without a complex angle, the phase terms on each side are equated. The resulting solution is then

$$\phi = \cos^{-1} \left[\frac{x_1 - x_2}{x_1 - x_2 - \delta} \sin \theta_0 \cos \phi_0 \right] \quad (105)$$

The beam pattern, shown in Figure 52, demonstrates the changed array factor based on the motion in Figure 51. A significant loss of gain towards the original aim point direction is evident as a result of the motion applied. Further, since the power removed from the target direction must be applied elsewhere in the array pattern, the potential for increased interference is introduced. Grating lobe positions have remained relatively stable.

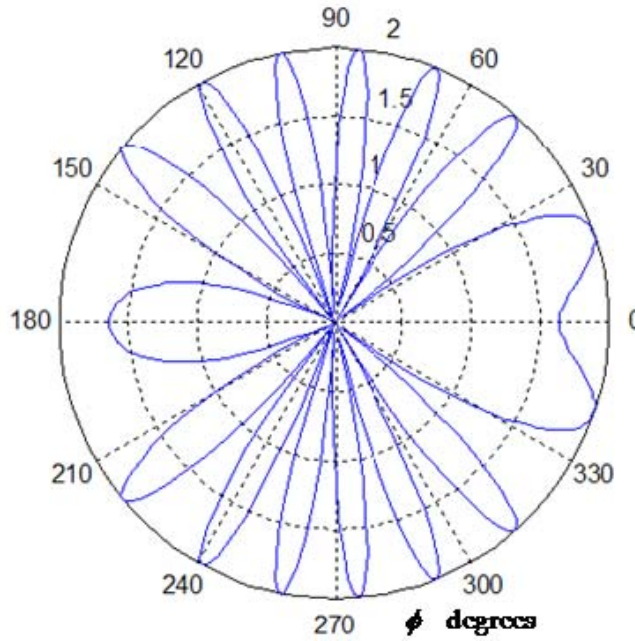


Figure 52. Array pattern in x - y plane of the modified two-element array in Figure 51.

Next consider motion of node two along the y -axis by 0.5 m in the positive direction. The assumptions of node one's position held constant at x_1 and the target aim point at 0° in the x - y plane will continue. This geometry is shown in Figure 53. The two node array formation after motion step must now account for the existence of node two in the y -plane. Stated another way, the array axis has shifted in respect to keeping the target in constant position. Therefore, the array factor of Equation (99) can be re-written to include the y -axis term after motion as

$$AF_{2-node}(\theta, \phi) = e^{j\beta x_1(\sin\theta\cos\phi - \sin\theta_0\cos\phi_0)} + e^{j\beta(x_2(\sin\theta\cos\phi - \sin\theta_0\cos\phi_0) + y_2(\sin\theta\sin\phi))} \quad (106)$$

where the position x_2 has not been altered from the original location, and the position y_2 is a result of the motion applied.

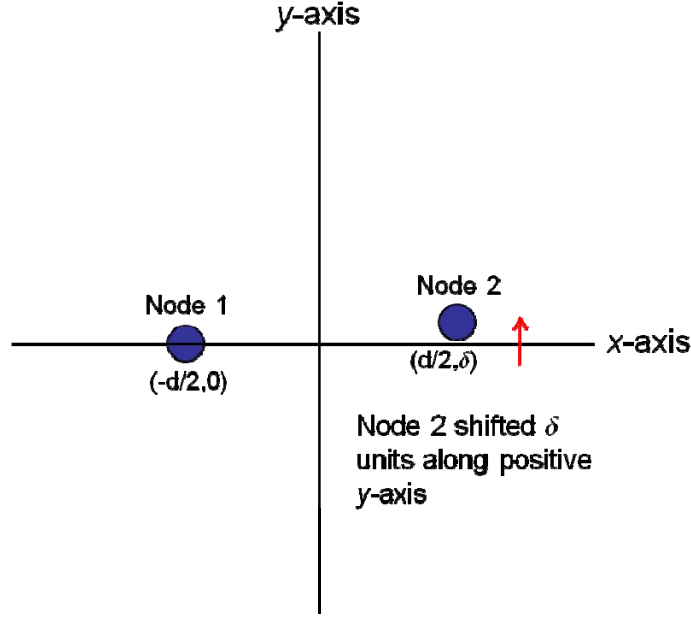


Figure 53. The two-element array from Figure 48 modified by positive y-axis motion of node two.

Again, a phase error can be immediately detected from comparison of Equation (99) with Equation (106). From this comparison, the difference due to motion along the y-axis, Δ , is written as

$$\Delta(\theta, \phi) = e^{j\beta x_2(\sin\theta\cos\phi - \sin\theta_0\cos\phi_0)} (1 - e^{j\beta y_2 \sin\theta\sin\phi}) \quad (107)$$

In itself, this term is not very instructive, but the two element geometry can be exploited to better understand the expected results that match the mathematical result. With a shift in y-axis position, the Pythagorean theorem can be directly applied to determine the distance between the nodes. The array will then continue to operate as a linear array along its axis but with an altered target aim point, due to both the change in array axis and change in node spacing. Determination of the new aim point is again possible by analysis of partial derivatives similar to the previous derivation shown in Equations (103)

– (105), but the axis rotation must be accounted for as well. An additional point to note from the equations from y-axis motion is that relative motion between the nodes is important while correlated motion is not. If two elements rotate but retain their respective position to one another, and the aim point is based on relative geometry (vice absolute), then no change in array pattern is noted. Change occurs only due to perturbation of relative position or rotation in absolute geometry if aim point must remain constant in that geometry. This is consistent with array theory as described in [4] and [16].

The effect on the two element array from the 0.5 m motion of node two along the positive y-axis is both a rotation of the array axis and a slight lengthening of the distance between the nodes. Therefore, rotation of the array and modified aim point due to extending the node spatial difference is expected. From simple geometry, we know the new distance between the nodes is 10.01 meters and rotation is about 2.8° . Since the motion of node two is slight in relative terms (0.03λ), the aim point with respect to the rotated array axis should also be minimal. The resulting array pattern in Figure 54 confirms this expectation, further, it shows that although the main beam direction is no longer focused on the original target, the resulting gain remains very near the maximum available. The grating lobe positions have rotated with the array, changing the effect of any nearby interferers.

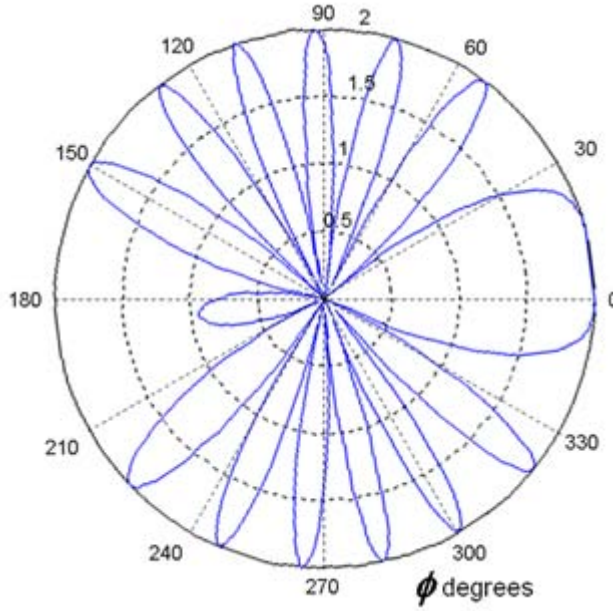


Figure 54. Array pattern in x - y plane of modified two-element array.

Considering the results for motion isolated along the x -axis and y -axis, the effects of different motion have drastic effects on the resulting pattern depending on the relative motion of the nodes to one another. The length of spacing in the motion has not been linked to time step, so the effect of velocity remains an open topic to be covered in Chapter IV. However, as a significant difference in drop in directivity towards the target is evident between the two motion analyses, this effect must be approached in a non-absolute manner.

2. Analysis of Doppler Effect on Array Factor Due to Independent Motion

The phenomenon of the Doppler effect is a well-known and understood scientific concept. In prosaic terms, a shift in the frequency of a signal occurs as a result of relative motion between the source and the observer of a wave, [38]. Standard wireless transmission and reception presents a natural model for application of the Doppler effect. In this arrangement, a transmitter produces a signal, generally represented as a plane wave, which reaches the observer position at the receiver. With the addition of relative motion between transmitter and receiver, the transmitted wave is altered by a frequency

shift dependent on the motion. The frequency shift, f_D , can be determined, as shown in Equation (88). There are additional factors that can be analyzed in terms of a successful transfer of signal from transmitter to receiver. Research has demonstrated in a dispersive medium that the connection between frequency increase or decrease and their related relative motion may be reversed [56] and [57]. For an electromagnetic problem, this same reversal of shift to relative motion association, known as inverse Doppler Effect, has been shown to exist in the near-field of an antenna in free space [58]. Although the altered shifts in the near-field offer additional information, it is the far field reaction that is of most interest, as that is where applications reside for array operations. From a transmitter's standpoint, motion of self or of the receiver is not necessarily a concern in terms of signal creation and transmission. However, for coherent detection and demodulation in a communications receiver in the far field, a signal received with an offset center frequency will result in degradation of signal-to-noise ratio (or equivalently E_b/N_0 for digital communications).

Conventional antenna arrays are formed between elements with known, non-varying relative positioning. Based on the static relative motion between antennas within a transmitting or receiving array, Doppler effect is easily accounted for by considering each array as an individual element. Considering general array reception geometry, as shown in Figure 55, array elements are generally spatially located at different distances and angles with respect to the transmitter. Since $r \neq r_1 \neq r_2 \neq r_3 \neq r_4$, the received signals at each element vary both in terms of amplitude and phase. These differences can be coherently corrected, as discussed in Chapter II.B. Then the phase centers of the arrays can be used to determine any relative motion.

Motion of array phase centers is a common issue when considering phased array radar applications even though relative element spatial positions are fixed [19] and [18]. Such motion is generally associated with electronic sweeping over a wide bandwidth. Since such a sweep is extremely fast, within the time period of a radar pulse, the phase center motion is enough to cause dispersion that must be corrected. Research in [19] showed how time-varying weights can be used to reduce dispersion and increase the operating bandwidth.

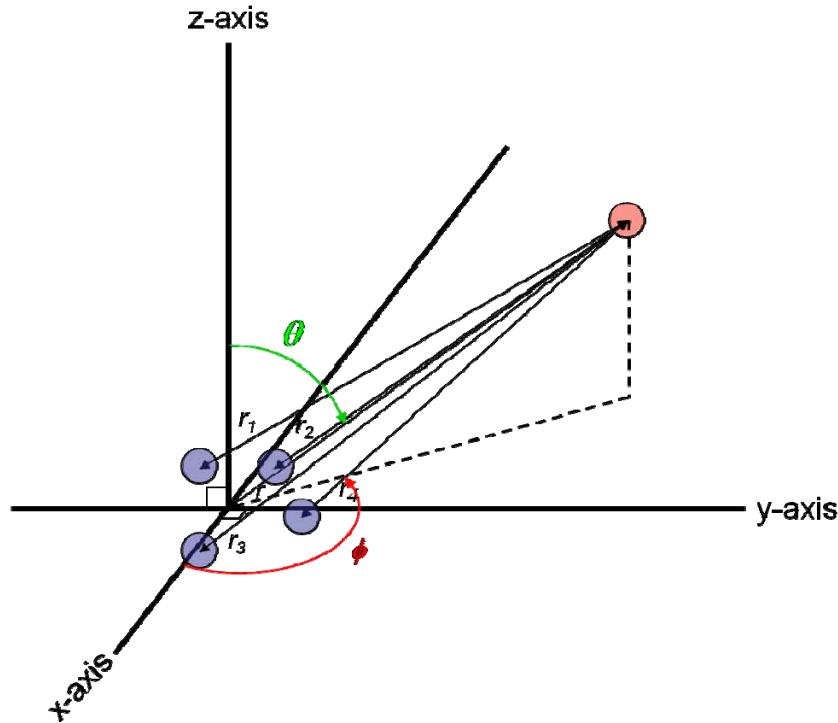


Figure 55. General reception array geometry with respect to a target transmitter.

However, allowing independently mobile elements within an array creates a separate problem in terms of Doppler effect. Independent motion among elements within the array means that physical motion, vice phase center motion, must be considered and the approximations that apply to static element arrays may no longer be valid. Therefore, the question to be considered is if the physical motion in an array with independently mobile elements is great enough to require correction.

First, evaluating shift in an array with static element positions, some important relationships are revealed. Geometry shows that a transmitter in motion with reference to a receiving array produces a differing angle with respect to each individual element than to the array reference point. It is then clear using Equation (88) that the differences in angle result in a difference in Doppler shift at each element. Yet, the influence of a Doppler shift from relative motion in the far field can often be ignored. This can be explained for general applications using the common far-field definition from Equation

(35) [16]. Therefore, the physical construct of the problem can be assembled as shown in Figure 56, and the angle, χ , can then be solved as

$$\chi = \arctan\left(\frac{D}{2R}\right) \quad (108)$$

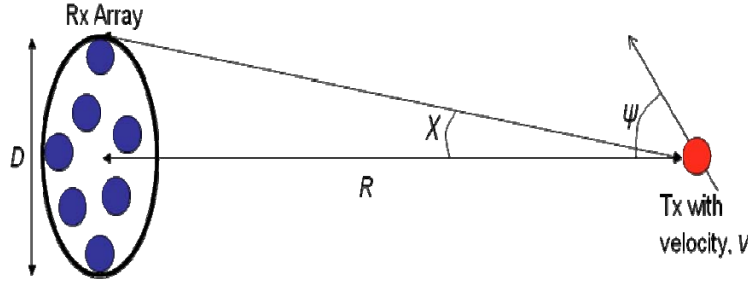


Figure 56. Geometry of reception array with transmitter in motion.

Evaluating this geometry at the far-field boundaries, it is calculated that $\chi \leq 2.86^\circ$ from the boundary of the far-field to distances beyond. This can then be related back to Equation (88) such that a limit on Doppler shift variation, $f_{D_{LM}}$, is set, as

$$f_{D_{LM}} = \frac{v}{\lambda} \cos(\psi \pm 2.86^\circ) \quad (109)$$

The point where maximum Doppler shift takes place is then dependent on the relative motion angle, ψ , motion velocity, v , and signal wavelength, λ . Rewriting Equation (109), this relationship is demonstrated more clearly as

$$f_D = \frac{v}{\lambda} (0.999 \cos(\psi) \pm 0.0498 \sin(\psi)) \quad (110)$$

So, the maximum difference between array elements occurs when the relative motion angle is perpendicular to the receiver; however, the overall effect of Doppler shift is at a minimum to the array center at that same motion angle. Additionally, the maximum difference during perpendicular motion is bounded at $0.1(v/\lambda)$. Conversely, when Doppler shift is at a maximum (with relative motion parallel to the receiver), the maximum difference between elements is at a minimum. Most importantly, unless the relative motion is near perpendicular to the receiver, all elements are shifting together to

either increase or decrease frequency, and in the case where the elements are shifting in opposite directions, the overall shift effectiveness is at a minimum.

In a time snapshot, an antenna array with mobile elements will operate very much like an array with randomly placed elements. Despite the random configuration, coherent detection can be achieved with increased gain (versus non-coherent operation), beamwidth related to aperture size, and manageable sidelobe levels. Additionally, the random configuration dampens grating lobes [13]. However, relative motion between the array aperture and target transmitter becomes an expanded problem, even with a constant velocity assumed. As shown in Figure 57, individual motion by elements complicates weight calculations. It should be noted that motion in Figure 57 is limited to two dimensions for graphical depiction only. Considering this type of motion, relative direction of motion to target is now element specific. Positioning of the elements with respect to the array reference point is no longer the dominant coordinating factor in regards to Doppler shift and, Doppler shift may vary from increasing in frequency to decreasing in frequency between adjacent elements. Therefore, the mobile element case is not limited by Equation (109) and must be specifically modeled regarding effects on array factor formation.

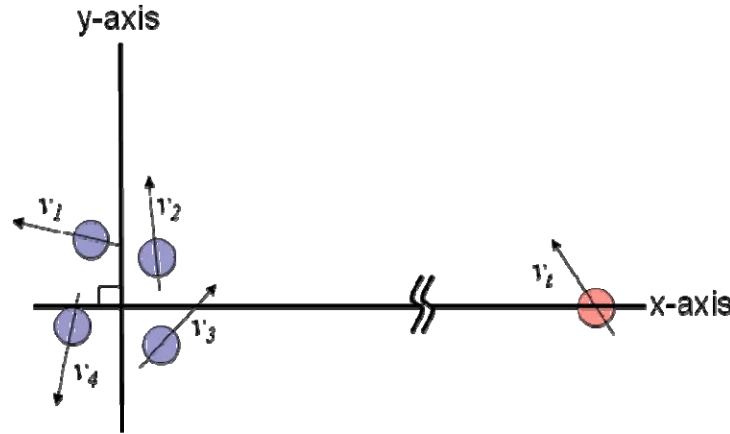


Figure 57. An array with elements and target transmitter in two-dimensional random motion.

So, considering a specific model for the changes in array factor due to Doppler effect, an initial case is offered. The ten-element array in Figure 58 will be considered as

a baseline with aim point $\theta = 90^\circ$ and $\phi = 60^\circ$. The x - y plane cross-section of the static array factor pattern under these parameters is shown in Figure 59.

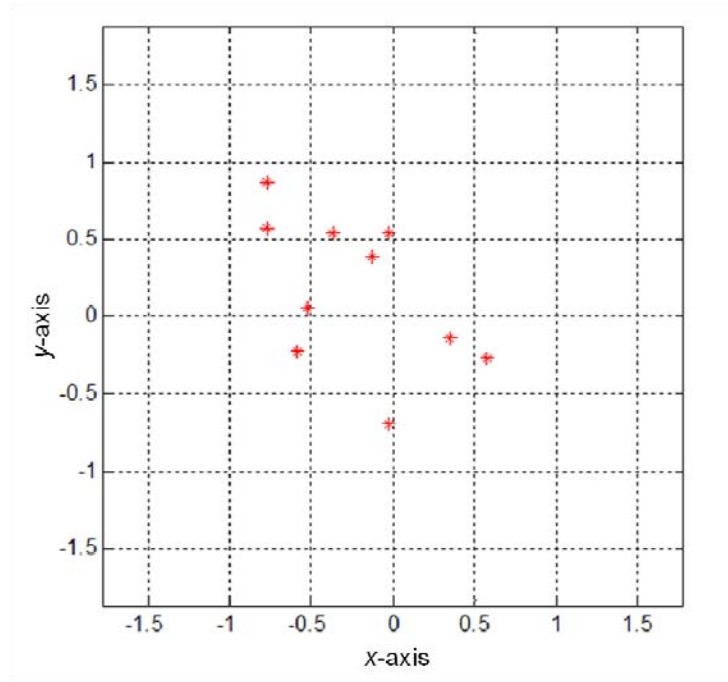


Figure 58. A ten-element array with Uniform random distribution (distance in wavelengths).

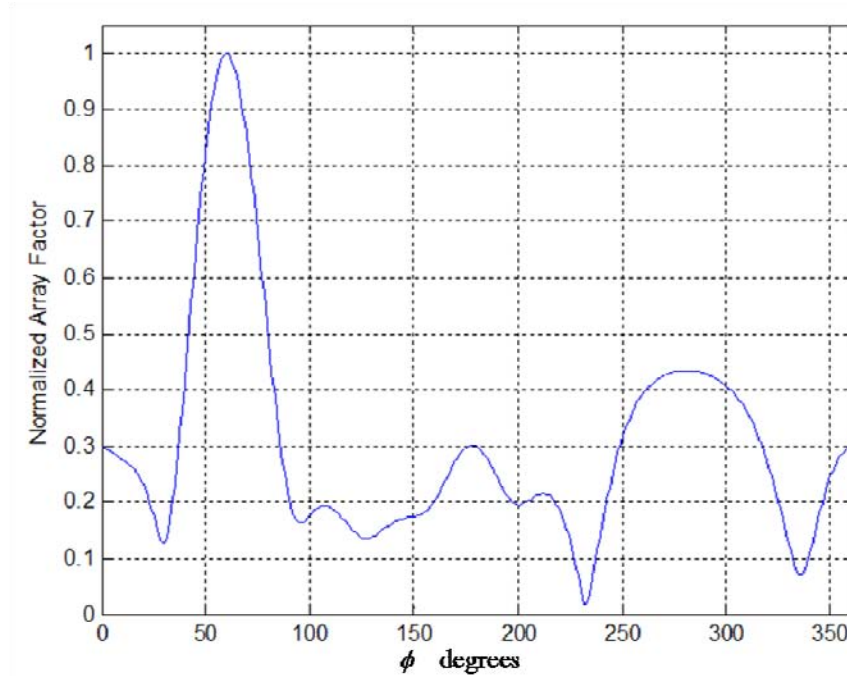


Figure 59. Cross-section along the x - y plane of the normalized array pattern from the array in Figure 58.

Under an initial set of arbitrary element velocities and directions, where velocity is considered as uniformly distributed below a threshold in wavelengths per second and direction is considered as uniform in three dimensions, the Doppler shift to each element is determined, and the resultant array factor compared with the array factor with static elements is shown in Figure 60. The velocities were limited below a speed of 29.8 mph considering a target signal at 900-MHz. This speed is much faster than possible by a pedestrian. The difference between the two patterns at each angle is shown in Figure 61. It should be noted that both patterns were normalized to the same reference value. It is noted that Doppler shift has produced minimal perturbation for this case, with the maximum difference at 3.88×10^{-8} , which is insignificant.

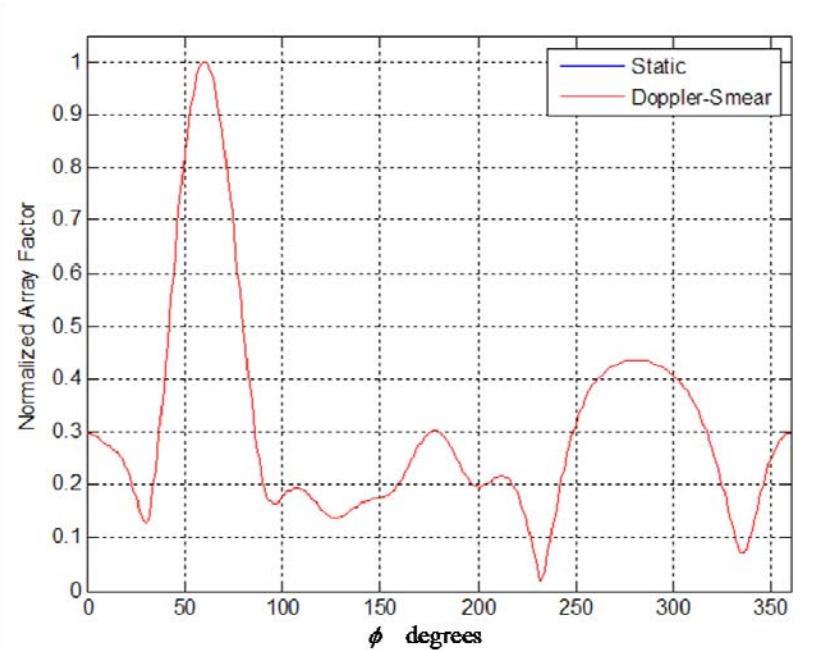


Figure 60. Cross-section along the x - y plane of the normalized array pattern from the array in Figure 58 with Doppler smear compared with the pattern from static elements.

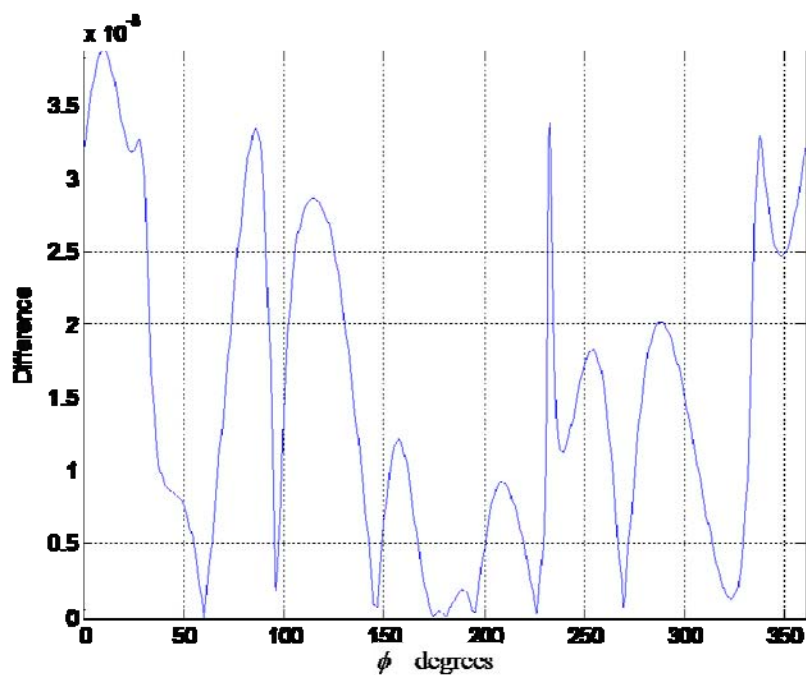


Figure 61. Absolute difference between the normalized array pattern in the x - y plane for the array with static elements and with Doppler smear.

Generalizing the result, a set of individual test cases is considered. Holding the number of elements and aim point constant, each run considers a random initial distribution and random element velocities. The pattern produced in the x - y plane cross-section is then compared to the pattern produced without Doppler smear. Table 1 displays the mean and variance of the maximum difference under different sets of maximum velocities applied with reference to the 900-MHz target signal. Maximum difference is considered here to observe worst case. From this table, it is evident that array factor pattern perturbation is not prevalent due to physical motion until motion velocities are well beyond reasonable limits for platform motion. Therefore, array factor smearing due to the Doppler effect is disregarded.

Table 1. Array pattern differences due to Doppler smear over various velocities.

Max Velocity (mph)	Max Difference	
	Mean	Variance
29.8	6.69E-08	5.70E-16
74.6	1.67E-07	3.57E-15
372.8	8.39E-07	9.15E-14
745.6	1.67E-06	3.48E-13
74565	1.66E-04	3.61E-09

C. ARRAY PERFORMANCE WITH INTERMITTENT NODE PARTICIPATION

The application of a wireless sensor network as a host for coherent beamforming in radio frequency signal detection depends directly on the ability of the network to relay collected data through a wireless channel. However, as discussed in Chapter II.C, wireless communications are subject to a variety of interfering phenomena, including multipath fading and Doppler spreading. Therefore, an assumption of near perfect data exchange cannot be made, where such an assumption is normally valid for static array formations. For the purposes of beamforming, a constant stream of updates from the individual elements is necessary to form a solution. So, an individual dropped packet

from any given element could be considered the same as a dropped node for aperture pattern formation. Further, a near-real time quality of service demands that packets be delivered without bit errors, and therefore packets received with errors can be considered dropped for the sake of array formation. This means that at any given time, the array may drop an element or gain back an element previously lost. The question is how the array reacts to such variations in element participation, or how data loss sensitive array formation is on a sample by sample basis.

Due to the tyranny of distance, the most likely node(s) lost to a network drop would be the furthest from a central information sink, as shown in Figure 62, in a multi-hop scenario. This accounts for both the distance required to form the necessary links and the number of hops. In a single-hop scenario, distance remains the prime factor in determination of potential communications errors given transmission power as a constant, based on the relationship in Equation (54).

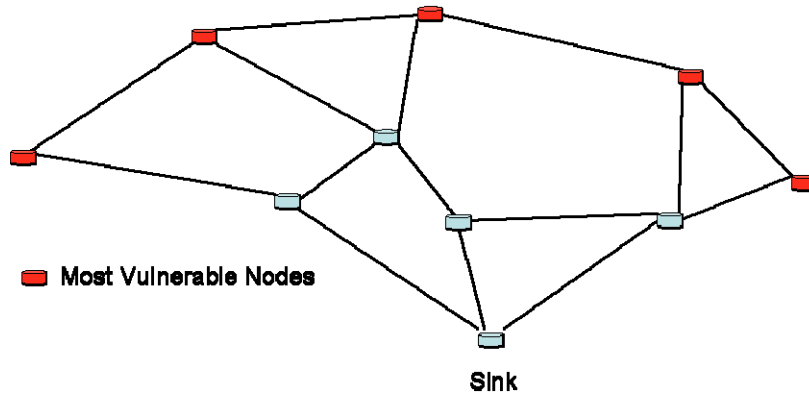


Figure 62. Vulnerable Nodes.

From the relationships in Equations (92) and (93), some insight is gained regarding the loss of a node in array formation. In general, node loss will affect gain and loss of an exterior node will have a greater effect on beamwidth than loss of an interior node. While these relationships are general, the importance of relative geometry between the nodes themselves and the array to the target are also driving factors.

The previously evaluated array formations, shown in Figure 38 and Figure 39, will be used as initial baselines. Although these node locations may not be optimal for

network operations, they will work well to demonstrate the basic mechanics involved when nodes are lost. The array configuration, shown in Figure 38, resulted in the pattern previously shown in Figure 40 with the designated aim point. This array can be considered sparse and relatively balanced towards the target. There are a minimal number of elements and spacing between elements varies between 0.35λ and 0.5λ . With respect to the target, the array aperture is 0.5λ wide. Consider this same array with a dropped node resulting in two element array pattern. Figure 63 shows a new geometry with a node removed.

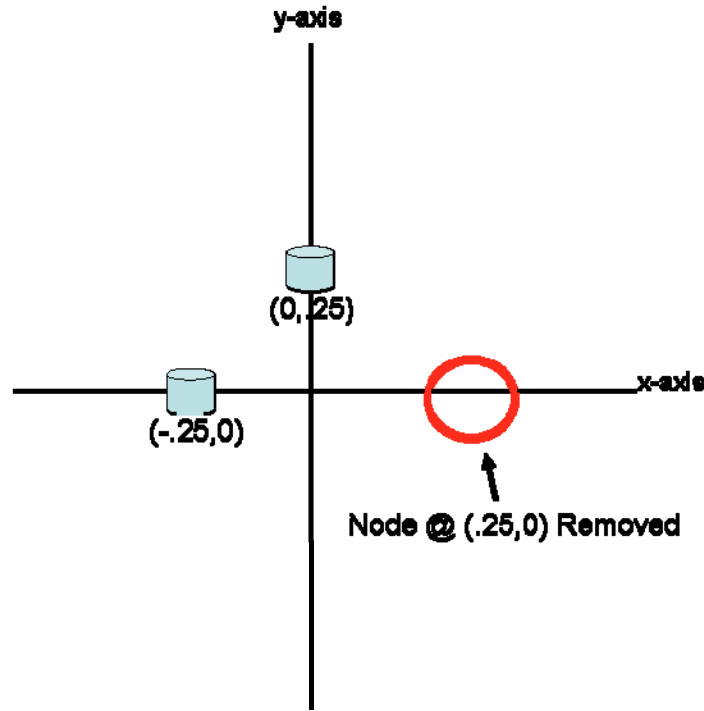


Figure 63. The array from Figure 38 modified to show one node intermittent (distance in wavelengths).

Focusing first on the original array, the array factor, AF_{3-node} , can be written (numbering nodes from left to right) as

$$AF_{3-node}(\theta, \phi) = e^{j\alpha_1} e^{j\zeta_1} + e^{j\alpha_2} e^{j\zeta_2} + e^{j\alpha_3} e^{j\zeta_3} \quad (111)$$

In contrast to the motion analysis, the phase weight parameters, α_i , and position factors, ξ_i , for the nodes are not changed. Therefore, in the array factor for the missing node case, $AF_{(3-1)-node}$, these weights do not change for the included nodes as shown

$$AF_{(3-1)-node}(\theta, \phi) = e^{j\alpha_1} e^{j\xi_1} + e^{j\alpha_2} e^{j\xi_2} \quad (112)$$

Since the weights do not change, array aim point should remain constant, and it is then obvious that the array factor difference between the two arrays, Δ , is solely based on the contribution of the lost node, isolated by subtracting Equations (111) and (112), as

$$\Delta(\theta, \phi) = -e^{j\alpha_3} e^{j\xi_3} \quad (113)$$

Equation (113) has been set negative to indicate the loss of an array element, but of specific importance is how contribution of the intermittent node remains a direct function of the aim point and observation angles. Expanding this equation and separating x and y terms, it is written as

$$\Delta(\theta, \phi) = -e^{j\beta x_3(\sin \theta \cos \phi - \sin \theta_0 \cos \phi_0)} e^{jy_3(\sin \theta \sin \phi - \sin \theta_0 \sin \phi_0)} \quad (114)$$

It is evident that at the target angle the contribution of full phase addition is available; indicating the inclusion of additional elements generally increases the ability to focus energy towards the target. However, it is more important to analyze the contribution off target, because the off target parameters determine contribution to main beam width and sidelobe magnitude. For off target analysis, the differences between the addends are based on size of the phase term in the exponentials. In isolation, the greater the phase terms, the faster the radial frequency; however, the size of the phase term is a function of both the x - y location of the node and the θ - ϕ variation from the target angle. Equation (114) can be simplified by condensing the angular dependent terms as

$$f(\theta, \phi) = \sin \theta \cos \phi - \sin \theta_0 \cos \phi_0 \quad (115)$$

$$g(\theta, \phi) = \sin \theta \sin \phi - \sin \theta_0 \sin \phi_0 \quad (116)$$

Equation (115) projects the angle of interest with reference to the target axis onto the x -axis. It is then multiplied into the x component of the node location. In doing this, the phase term, with an initial size of x , is then weighted based on alignment between a given

angle and the target direction. As the differences in the angles increase, the phase terms follow along their sinusoidal path. A simple partial derivative of Equation (115) with respect to θ and ϕ demonstrates the rate of change based on motion around the array remains sinusoidal as

$$\frac{\delta^2 f(\theta, \phi)}{\delta \theta \delta \phi} = -\cos \theta \sin \phi \quad (117)$$

Similar results can be found in considering the rate of change along the y-axis with Equation (116).

Summarizing the expected results then, Equations (92) and (93) indicate in general a loss of gain with the loss of total elements and an increase in beamwidth, particularly when overall aperture size is affected. The derivatives of the angular terms, as demonstrated in Equation (117) show that the contribution of a single node is greatly based on spatial positioning to target and observation point through a sinusoidal relationship. Finally, the aim point for the array will remain constant, despite the intermittent node. Applying this knowledge to the array in Figure 63, the resultant array factor pattern can be expected to have a wide beamwidth and a loss of gain in comparison to the original configuration but remain on target. Figure 64 shows the comparison of the cross-section of the normalized array factor pattern. As expected, beamwidth has increased, gain has dropped minimally from 4.4 dBi to 3.9 dBi, and aim point has remained at 60° .

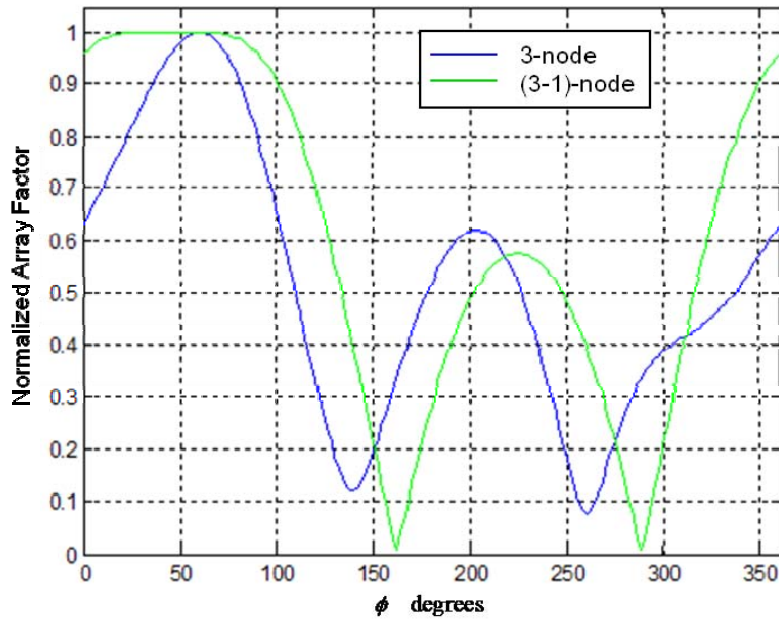


Figure 64. Cross-section along the x - y plane of the normalized array pattern from the array in Figure 63 where one node is intermittent compared with the pattern from the full array in Figure 38.

Considering the more complex array configuration from Figure 39, there are two variations to the intermittent node problem that can be tested — intermittent interior node and exterior node. Figure 65 shows an array configuration created after removing an interior element of the base array.

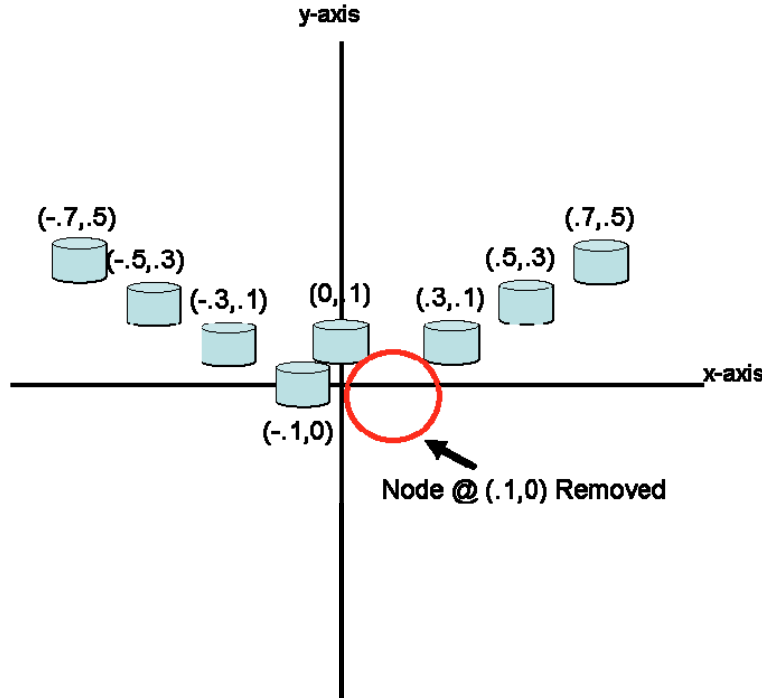


Figure 65. The array from Figure 39 modified to show one interior node intermittent (distance in wavelengths).

Figure 66 displays the pattern results from the modified configuration. The pattern result in this case is unusual in that the removal of the chosen interior node has not produced a great effect on the produced array performance. Indeed, the array gain for the original nine-element case was 7.6 dBi and the altered case produces gain that is not significantly different from that case. Most importantly, the aim point has remained constant, as before, further confirming the main issue that aim point is not altered. The result for the pattern does help illustrate the issue that element geometry relative to each other and aim point is of great importance in beamforming. In order to illustrate the unusualness of this result, a Monte Carlo simulation with 10000 realizations was run comparing randomly spaced nine element arrays with the same boundary constraints as in Figure 65 versus their interior element removed counterparts, and a mean difference of 0.2 dB was obtained.

However, this type of result, where geometry produces a superior result against a chosen aim point, is used in the practice of sub-array formation. Sub-array formation

uses select elements from a larger array while applying beamforming in a chosen target direction. The sub-array used for a specific direction may have characteristics, such as small sidelobes or nulls at specific angles, which make it comparable to using a larger structure [59]. Sub-arrays also can provide a level of tolerance to positioning errors used for phase weight determination. Breaking two-dimensional arrays into linear arrays with large apertures towards the target has been shown as an effective method to deal with positioning or calculation issues, since linear arrays are more tolerant of phase imperfections [5]. This approach has also been proven to be successful in minimizing grating lobe effects [11].

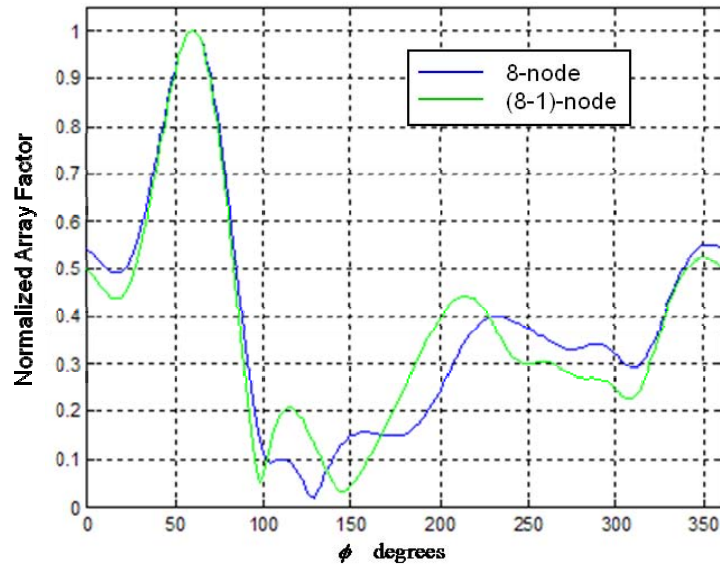


Figure 66. Cross-section along the x - y plane of the normalized array pattern from the array in Figure 65 where one interior node is intermittent compared with the pattern from the full array in Figure 39.

The results in Figure 66, where an interior node was intermittent, are interesting to contrast with a case where an exterior node is selected. Since exterior nodes are directly related to antenna aperture size, it is presumed that beamwidth will be affected to a greater degree. Figure 67 shows an array configuration that allows us to test this case, and the array pattern results are depicted in Figure 68. Beamwidth of the main beam has

expanded. The pattern result in this case also is a half decibel lower in maximum gain, which is lowered to 7.1 dBi. The major role of the exterior nodes in shaping array response has thus been demonstrated.

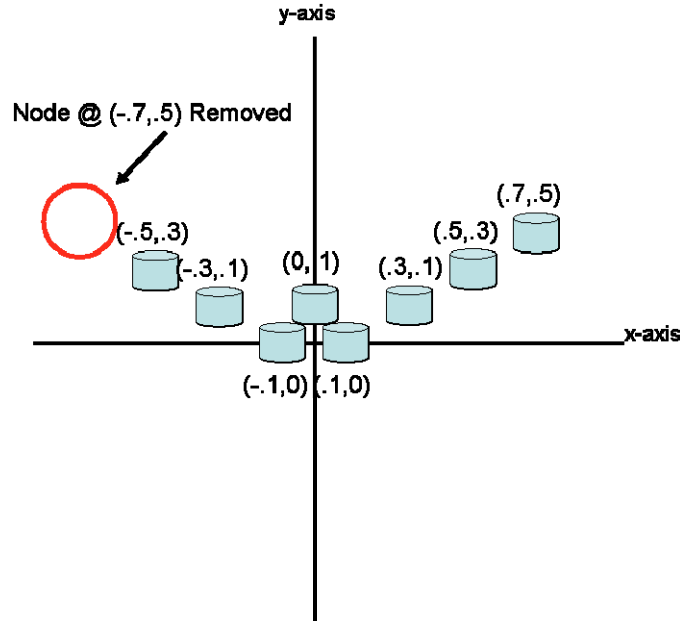


Figure 67. The array from Figure 39 modified to show one exterior node intermittent.

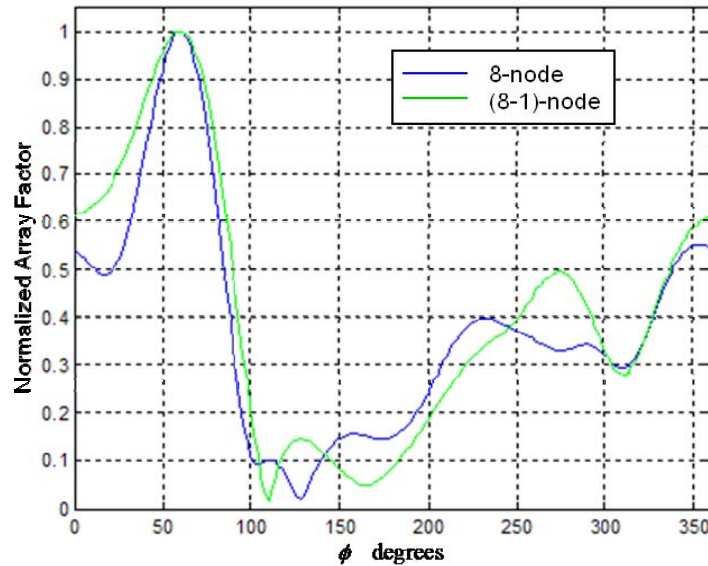


Figure 68. Cross-section along the x - y plane of the normalized array pattern from the array in Figure 67 where one exterior node is intermittent compared with the pattern from the full array in Figure 39.

As shown in the results of array pattern after the removal of an internal node, employing sub-arrays has been shown as a method with the potential to provide performance increase. Research in this area has focused primarily on improving performance of designated arrays or establishing stability for array calculations, which include positional errors. Using iterative methods to determine required phase weights is an alternative technique to deal with stability concerns. This process has proven effective but has the drawback of iterative calculation expense [54]. An Eigen-based solution was previously proposed, which is computationally simpler than the iterative method but not as effective [60]. Non-linear solutions have also been proposed with improved results but include the issues that accompany non-linearity [61].

This chapter investigated issues related to beamforming with elements connected via a wireless network. Specific attention was given to imprecise element positioning, basic motion application, Doppler shift, and the potential of intermittent participation due to wireless network connectivity. These findings will be applied in the next chapter, which attempts to mitigate remaining issues through management or other novel techniques.

THIS PAGE INTENTIONALLY LEFT BLANK

IV. RADIO FREQUENCY WIRELESS SENSOR NETWORK WITH INDEPENDENTLY MOBILE NODES

The central argument of this dissertation is that it is possible to use a wirelessly networked set of sensor nodes attached to mobile platforms as a system for the detection and follow-on processing of radio frequency signals. Such a system would fuse the collected data from each sensor to achieve the effect of a beamforming array, enhancing aperture gain towards a targeted direction while deemphasizing (in comparison) signals from alternative spatial directions. The system is envisioned to be typically employed for passive sensing of a radio frequency environment to detect signals present and to conduct reception of signals detected. This concept includes the idea of the system intercepting the signal as an unintended recipient or in reception from a cooperative transmitting source.

In order to achieve the stated goal, a variety of issues must be overcome to realize such a system. Many of the problems facing implementation of a wireless sensor network with independently mobile nodes constructed for detection and reception of radio frequency signals are answered in the analysis presented in Chapter III. It was demonstrated that array formation is robust in terms of not having precise positioning knowledge. The analysis presented, commensurate with other available research, demonstrated that minor position errors in the spatial reference term do not pose a major issue when the position change are fractions of wavelength away from original position. The examination of simple motion in a two-node scenario demonstrated that a major perturbation of array pattern does occur as elements drift; however, the direction of drift and wavelength rotation in the array factor phase terms are key factors that may exacerbate or mitigate the motion based on target and element spatial construct. Within the topic of motion, consideration of the effect of Doppler shift due to physical motion was shown to exhibit no discernable perturbation on array factor formation under velocities achievable by physical platforms. Therefore, the Doppler Effect can be disregarded in this sense. Study of the effect of an intermittently operating node in array factor formation confirmed the result of literature with regards to gain and beamwidth

[13]; however, the analysis additionally illustrated that aim point is unaffected. Therefore, the main beam solution is not subject to being slewed due to the loss (or recovery) of a given node.

With the knowledge gained, significant issues remain regarding system implementation of the radio frequency wireless sensor network. The primary of the remaining issues will be addressed in this chapter. A vital component to system implementation is the ability to operate the network in an efficient manner. Sensors must be able to produce collected data to meet operational requirements, but they must also conserve energy in order to provide a useful network lifetime. So, the issues involved with operating such a system will be initially considered, to include a proposal to optimize energy usage and primary functional requirements. The second question to consider is the possibility of continuing to operate a coherent beamforming solution when array nodes are independently mobile. Extending the previous analysis, a proposal to solve this problem will be offered and shown to produce an implementable solution that meets operational standards. In the third question, a most favorable timing pattern is proposed to produce a final implementable vision. This timing is necessary to establish a system capable of producing the required beamforming solution while conserving energy versus alternative approaches. Finally, as individual nodes are independently mobile, the question of node orientation rectitude is considered. Although unsteady orientation's effect on array factor formation may be mitigated based on application technique, the result of this uncertainty is diminished interior network communications, leading to the intermittent node results previously described. Therefore, a proposal to improve this network physical layer issue will be provided, enabling a mean consistent communications channel without expending excess energy.

A. MANAGEMENT METHODOLOGY EMPHASIZING SIGNAL DETECTION IN RADIO FREQUENCY SENSOR NETWORK NODES

The consideration of the most advantageous operation of a wireless sensor network inherently demands a focus on energy usage across the network as a figure of merit. Wireless sensor networks are typically defined to be composed of autonomous nodes with self-contained sensors, communications, processing, and power supply. Of

these component pieces, the power supply is generally considered the limiting factor. This is because batteries offer a limited amount of energy for system use [15] and [8]. Based on this limiting factor, optimization in wireless sensor network operation is a considerably active area in research.

Operation of a sensor network to achieve operational goals and conserve energy may be considered in two ways. The most general approach is to take into account network communications requirements, optimizing protocol usage as in [62] or sleep determinations as in [63]. This approach assumes the general case where sensor data is constantly available but not continuously required, so communications network efficiency is the main factor in energy economy. The alternate method bases the power cycle operation of the nodes around sensor activity. Operations in this case are more specialized to the sensor type and the data sought; however, it does offer the ability to save energy under tight operational constraints.

The system operation envisioned for the considered radio frequency wireless sensor network requires continuous sensor data update from all active sensors at each data sample. The data must be transmitted to a remote operating station for follow-on processing and examination. As this requirement demands a continuously open communications channel, an operations methodology seeking energy thrift through sensor requirements is the preferred path.

Study in this area has occurred considering a closely related wireless sensor network application. Research regarding a radio frequency wireless sensor network, which uses data from sensors to create a beamforming sensor aperture, was the subject of [10], where a methodology is introduced based on fast direction finding of the target signal. In this analysis, the elements are statically positioned but randomly distributed. It is assumed that the deployment scenario places the sensor network in a position that is either isolated or unfriendly (in military parlance). The nodes, distributed randomly in a defined area, form an ad hoc network for the ultimate purpose of directing radio frequency sensors towards a signal of interest. In order to accomplish this, a local central controller manages the sensor network by first detecting a signal of interest on its own, second selecting and energizing sensor node participants to assist in receiving the signal,

third using participating node signal reception data to form Time Difference of Arrival (TDOA) and Line of Bearing (LOB) information about the signal of interest, and fourth applying the LOB information to form an adaptive beamforming array using sensor nodes for sustained reception of the signal. The research demonstrates this method as superior to a method of serially beam scanning to find a target. The use of a local central controller is a key factor in [10] to synchronize node operations, process follow-on data, and provide initial signal detection. The requirement for the controller to provide initial detection requires that the controller be local to the sensor network. As an example, the controller could be one of the nodes in the network, a person within close distance, an aircraft, or a satellite connected to the network for control, queuing, and receipt of data. While this arrangement has applications, the availability of a local controller to spur operations limits when the network may be used. Further, using a single node for initial detection of emitters limits the ability to identify an emitter that may be in the gain pattern of the array but not an individual element.

Although the methodology proposed in [10] was for static element placement, the considerations for energy conservation in the mobile platform case are no different. In both cases, energy must be conserved due to limited battery power and the function of beamforming is consistent. However, the emphasis in [10] is to conserve energy above all other operational concerns. Therefore, a methodology is proposed, as documented in [31], which emphasizes system operation and then concerns itself with how to conserve energy under that constraint. Since the system of interest is focused on reception of radio frequency signals, the detection of a signal of interest is the primary emphasis for the sensor network. This is because without initial signal detection, no other process can initiate. The proposed methodology is structured to maximize detection probability, as defined in Equation (55), to meet operational requirements and remove reliance on a local central controller in detection and processing, allowing control and data processing from a remote position. A communications relay, a satellite for example, may still be required to enable control and synchronization of the network nodes; however, basic communications relay assets are of greater availability than a specialized node participant.

Of course, removing the central controller's participation in initial signal detection means that the network nodes are responsible for that action. Therefore, a set of wireless sensor nodes must be in full operational posture during the detection process, vice in sleep mode. Obviously, an energy cost will exist for operating nodes (versus sleep). However, the proposed methodology's flow associated with processing after initial detection uses the additional information available from the node-level detection to minimize additional work by the nodes in follow-on processing. The result will be shown as energy saved during operations when a target emitter is active and a shortened timeline to initial beamformed signal reception versus the alternative method offered in [10]. Indeed, the worst case of the proposed methodology will always be equal to or better (depending on node wake-up protocol) than the alternative method.

A basic assumption regarding the deployment of the above mentioned wireless sensor network is that the target emitter resides in the far field of the array; the far field is defined in Equation (35). This provides the basis for deployment of the sensor network. If a single element were capable of meeting operational requirements for both target signal detection and reception, the complexity of a network operation would not be necessary.

A radio frequency sensor array must have a process for signal detection in order to then conduct post-detection operations, such as emitter geolocation or signal demodulation. However, design must take into account that post-processing initiated by a false alarm may energize network operations, unnecessarily spending energy. External to the network, a detection false alarm may also initiate processes that expend energy or resources. As an example, a military situation may call for anything from maneuver to live fire based on warning. Therefore, consideration of the probability of false alarm, as defined in Equation (56), is of great importance in terms of operational requirements. It is due to the constraint of false alarm rate that use of the Neyman-Pearson criterion is proposed in constructing the operation methodology. As described in Chapter II.B, Neyman-Pearson enables the false alarm rate to be dictated in design with a corresponding maximum detection probability under the constraint. It will be shown that the detection process may then be associated with the required aperture gain to meet operational needs.

The general result of the Neyman-Pearson criterion can be applied to the specific issue of signal detection in the case of a signal reception unit. The hypotheses in Equation (58) result in the general expected values and variances of

$$\begin{aligned} E[z|m_1] &= E[n] = m_n \\ E[z|m_2] &= E[s+n] = m_s + m_n \end{aligned} \quad (118)$$

and

$$\begin{aligned} \text{Var}(z|m_1) &= \text{Var}(n) = \sigma_n^2 \\ \text{Var}(z|m_2) &= \text{Var}(s+n) = \sigma_s^2 + \sigma_n^2 \end{aligned} \quad (119)$$

where Equation (119) assumes the signal and noise are uncorrelated. The probabilities of these hypotheses match the concept of signal detection probability demonstrated in Figure 17. As shown in the figure, the threshold factor, T , marks the division between the decision regions. Determination of the threshold is dependent on the decision criterion, and using Neyman-Pearson it is known that $T = \Lambda$ to maximize detection with a given false alarm rate. It can be assumed that the primary contributing noise is additive white Gaussian noise, i.e., $m_n = 0$, and the signal of interest is deterministic. These assumptions are realistic in terms of a signal on the air. With these assumptions, the probabilities required to form the likelihood ratio in Equation (65) can be written as

$$f(z|m_1) = \frac{1}{\sqrt{2\pi\sigma_n^2}} \exp\left[\frac{-z^2}{2\sigma_n^2}\right] \quad (120)$$

$$f(z|m_2) = \frac{1}{\sqrt{2\pi\sigma_n^2}} \exp\left[\frac{-(z-s)^2}{2\sigma_n^2}\right] \quad (121)$$

where m_s is simplified to the constant s , and the signal variance, σ_s^2 , is zero due to the deterministic assumption. The factor Λ is still needed in order to operate the likelihood ratio. However, P_D and P_{FA} can be determined through application of Equations (60) and (61), respectively. Initially focusing on false alarm rate, the Gaussian assumption of noise allows this probability to reduce to a familiar form of

$$P_{FA} = \int_{Z_2} f(z|m_1) dz = Q(\beta_0) \quad (122)$$

where the function $Q(x)$ is defined as

$$Q(x) = \frac{1}{\sqrt{2\pi}} \int_x^\infty e^{-u^2/2} du \quad (123)$$

and β_o is defined as

$$\beta_o = \frac{T - m_n}{\sigma_n} \quad (124)$$

Solving for detection probability, a similar form can be obtained as

$$P_D = \int_{Z_2} f(z|m_2) dz = Q\left(\beta_0 - \frac{s}{\sigma_n}\right) \quad (125)$$

Recalling that the Neyman-Pearson criterion maximizes P_D with respect to a chosen false alarm rate, $P_{FA} = \alpha_o$, the factor β_o can be determined from Equation (122), and this factor may then be used with Equation (125) to determine the maximum probability of detection. Now considering the received signal-to-noise ratio as defined in Equation (53) with respect to the factor s/σ_n , critical transmission and reception parameters can be linked directly to detection probability.

For the radio frequency wireless sensor network, it has been assumed that signal detection using a single element is insufficient to meet requirements. Considering P_D with unity signal to noise ratio as a boundary for a signal element reception, the probability of detection can be analyzed for increasing gain for the receiving aperture. The resulting detection probabilities under various false alarm rate constraints are shown in Figure 69. Initial receive antenna gain is set at 2.15 dBi for this simulation, which is equivalent to a single half wave dipole at resonance. It should be stressed that this study considers only white noise and ignores the ability of the array to diminish the effect of interferers from spatial geometry outside of the target beam.

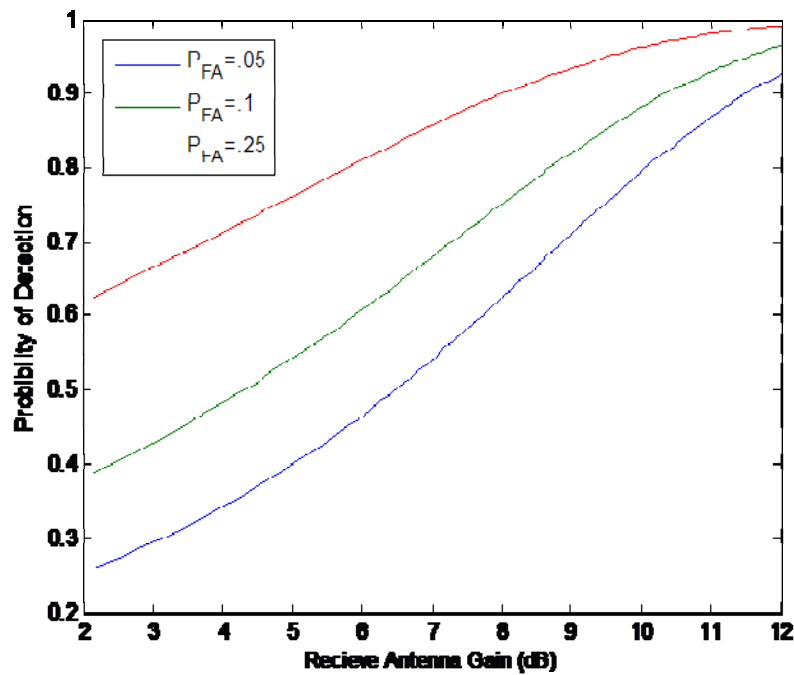


Figure 69. Probability of detection versus receive antenna gain under differing levels false alarm constraint.

Clearly increased gain results in increased probability of signal detection. In a typical signal reception problem, increased gain may be realized by using a high gain antenna element or constructing an array of elements operating coherently. That principle can similarly be applied to the radio frequency wireless sensor network; however, using wireless sensor nodes to detect and process an emitted signal presents a unique situation. A random deployment of nodes does not support the use of a specified high gain element. At issue would be both the orientation of the beam pattern from the high gain element after deployment and the energy cost associated solely with that element node. Therefore, using the power of beamforming in the array is the better alternative.

Fixed fielded arrays do not have energy limitations at each element. Further, aperture size is constant and known. Additionally, all elements tend to be active full time, providing highest available gain. In the wireless sensor network case being considered, there is a fundamental requirement to keep energy costs low and spread these

costs over the network, as each node only has a limited amount of power. The proportional relationships shown in Equations (92) and (93) become useful in setting up an array of the dispersed elements to achieve gain necessary for detection under Neyman-Pearson. As discussed when these relationships were introduced, they operate as general proportionalities because specific spatial geometry must be accounted for in each case.

The methodology for operating a wireless sensor network as a radio frequency sensor array emphasizing initial probability of target signal detection can then be formed. A group of nodes are deployed in a random fashion in the operating area such that K nodes are distributed over an area A . The nodes self organize and are in contact with a controlling station. Their locations are determined using location discovery techniques and are reported back to the controller. The controller then determines a subarea, A_s , from the overall distribution area, A . The dimensions of the subarea are dependent on desired beamwidth and gain of an array pattern. The desired gain is based on the required probability of detection from Equation (125) with the constraining false alarm rate and the gain increase due to number of array elements as described in Equation (92). Similarly, the desired beamwidth is based on the relationship in Equation (93); however, the density of node distribution also impacts. It can be assumed that a sufficient node density is available such that a subarea contains a large multiple of nodes greater than the number, N , necessary to meet gain requirements. If that is not the case, the subarea can be expanded (increasing aperture size and number of available nodes) resulting in a narrower beamwidth. It is, therefore, imperative to distribute nodes with sufficient density to avoid expansion to the point where grating lobes form. It should be noted that beamforming with random element distribution in a set aperture area, the beamwidth in any target direction is roughly the same [13]. Therefore, beams can be created for 360° coverage simultaneously in the central processor without additional messaging from the network nodes for each beam since the same samples may be used (with alternate weights associated with different aim points) in multi-processing at the data sink. As an example, a beamwidth of 45° can simultaneously form 16 beams overlapping roughly at their 3 dB beamwidth points from a single input by the target elements. This is not exact, so over-determination of the beams in processing may be required.

The nodes in the subarea, A_s , are then used to form a signal detection array in accordance with the random array process in [9]. To enter this process, the number of nodes used to form an iteration of nodes, N_i , is determined based on the gain necessary to meet the required detection probability with a constraining false alarm rate. Therefore, N_i is equal to N for array factor formation. Designating N_s as the total number of nodes within A_s , it is assumed that $N_s \gg P_i$ such that multiple iteration runs can be made against a subarea of nodes before a new subarea is designated (assuming each node is used only once). This is consistent with the assumption on node distribution density when forming A_s . Iterations are then formed from the designated nodes, N_i , in the subarea. Other nodes in the subarea are in active stand-by awaiting the opportunity to contribute to each iteration, and nodes outside of the subarea may be in a sleep cycle. After beamforming iterations have covered the nodes in a subarea, a new subarea within the total area, A , is formed and the process continues. It should be noted that the new subarea may overlap space with previous subarea selections. With this method, simultaneous array beams in desired directions are thus formed at the central controller using inputs from the wireless sensor network nodes. The parameters involved in this structure are demonstrated in Figure 70.

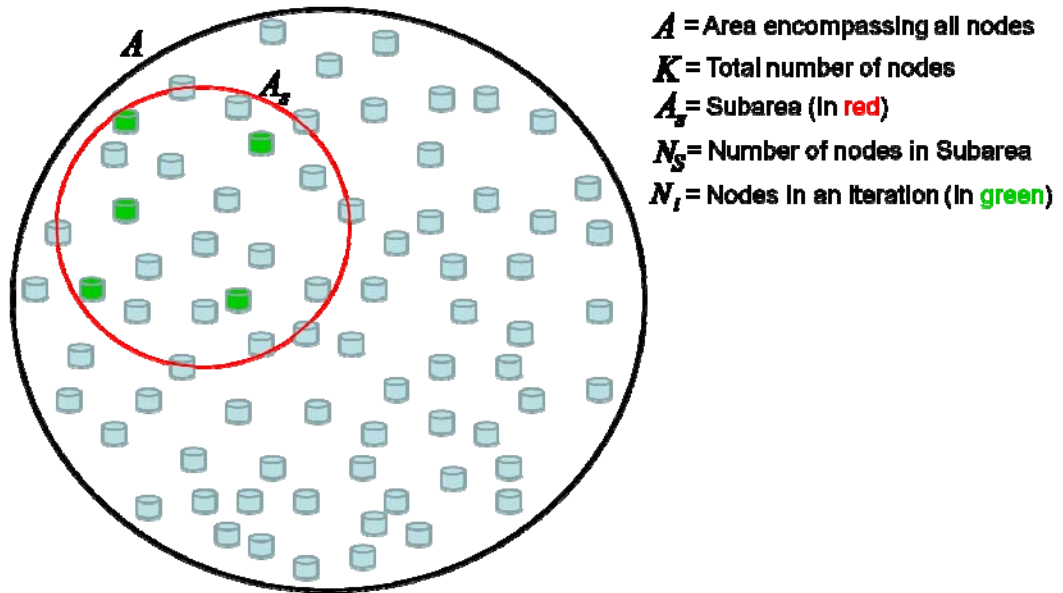


Figure 70. The structure of parameters in the system methodology.

Operation of the radio frequency wireless sensor network extends past the formation of the array to processing a signal after detection has occurred. Based on the purpose of the system, there are a small variety of actions, which may be attempted post-detection, and these may vary based on the purpose of the network, type of signal received, or simply due to operator desires. Considering the most likely post-detection processing options, the operator may desire a detected signal to set off an alarm, demodulate and record the signal, geolocate the emitter, or a combination of those options. A flow chart of post-detection actions is shown in Figure 71. It bears noting that central controller has knowledge of which beam detects the signal, indicating a rough azimuth to the target, allows some ease of follow-on processing. If multiple beams detect the signal, the central controller has information on which beam provided best signal to noise ratio.

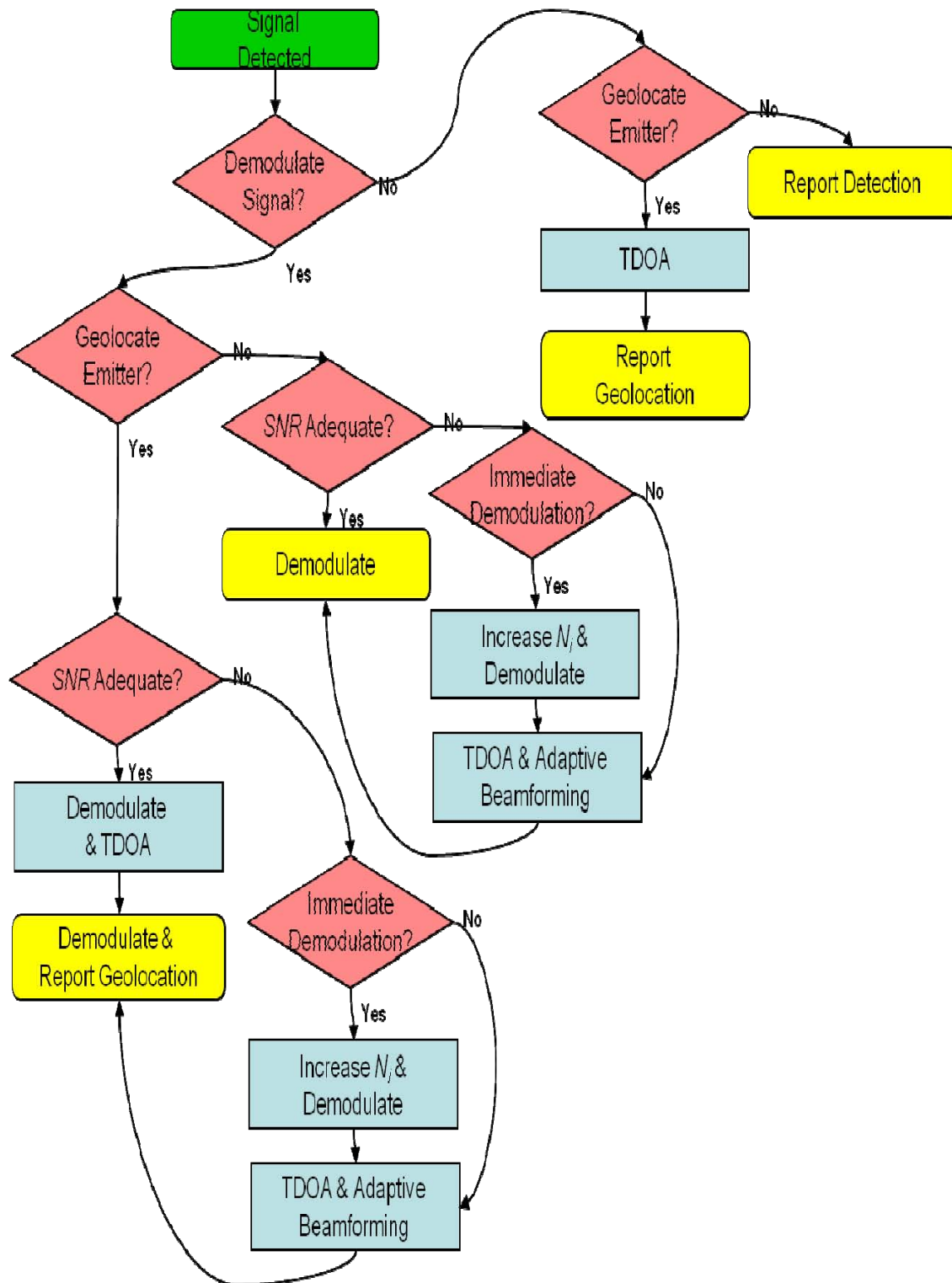


Figure 71. Flow chart depicting post-detection processing for the wireless sensor network array.

As is shown in the figure, there are branches where “immediate demodulation” is available. This is based on the option to increase the available gain by increasing the number of elements in an iteration, N_i . Such an action may be necessary in cases where signal-to-noise ratio allows detection but follow-on processing requires additional signal power. In such cases, it is assumed that the additional nodes within the subarea can immediately contribute, and that once processing of the signal has completed, the system returns to the previously set parameters. Additionally, when the number of nodes in an iteration, N_i , is increased for immediate demodulation, there is an associated increase in sensor energy usage; therefore, this practice is for use temporarily until a formal scheme can be assembled, perhaps through adaptive beamforming. Finally, it should be noted that the detection process can continue in alternate beams during any follow-on processing, where the already detected signal may be regarded as an interferer for detection of other signals. Such an operation is held to the constraints of frequency and spatial separation.

In order to consider the effectiveness of the proposed system, it is necessary to evaluate the associated cost. As previously discussed, cost in a wireless sensor network typically relates to energy efficiency, and that holds here as well. Additionally, cost in time to reaction to a present emitter is an important metric considering the value of system operations. Therefore, time must also be measured.

There are two specific assumptions related to energy cost in system operations. The first is that expected signal of interest activity in the deployed region will be moderate; therefore, extensive sleep periods for sensor nodes are not available. This assumption is based on the idea that deployment to a region where signal activity is infrequent may not be a proper use of resources, or an operational methodology that emphasizes sleep over signal operations may be preferable.

There are three important states to consider when evaluating energy usage in a wireless sensor network. The transmit state indicates a node is active and transmitting collected data. The idle state indicates a node is active but waiting to transmit data. The sleep state indicates a minimal energy usage condition; however, there is additional

energy expended in transitioning from a sleep state to idle. Basic quantities can be delineated to capture the energy costs associated with these states. Define δ as the energy cost per transmission (joules/transmission), χ_1 as the energy expended when a node is on and waiting to transmit (joules), and χ_2 as the energy expended in waking up a node for operations and transmission. Because they tend to be smaller in magnitude, the quantities χ_1 and χ_2 are often considered as a percentage of δ . The energy expended to beamform the detection array, Γ_D , is made up of energy to wake up nodes in A_s , Γ_{wake} , energy while nodes sit idle, Γ_{idle} , and energy to transmit data to the controller, Γ_{xmit} . Sleep energy will be ignored in this calculation as analysis is focused on energy use of the operating nodes. However, sleep energy must be included when assessing a projected lifetime of the network. Thus, the energy expended to beamform is

$$\Gamma_D = \Gamma_{wake} + \Gamma_{idle} + \Gamma_{xmit}. \quad (126)$$

With the number of nodes in A_s known as N_s , the first two terms can be defined as

$$\Gamma_{wake} = N_s \chi_2 \quad (127)$$

$$\Gamma_{idle} = (N_s - 1) \chi_1 \quad (128)$$

As the process described in [9] is used to provide a low-sidelobe array solution, the third term in Equation (126) can be obtained as

$$\Gamma_{xmit} = \delta \sum_{i=1}^L N_i \quad (129)$$

where L indicates the number of iterations required to produce the desired array factor. Therefore, through simple substitution into Equation (126), the energy required to operate the detection array in A_s , Γ_D , can be explicitly expressed as

$$\Gamma_D = \delta \sum_{i=1}^L N_i + (N_s - 1) \chi_1 + N_s \chi_2 \quad (130)$$

This energy cost is spread over the network as the subarea is redefined. It should be noted again that the number of beams created for detection does not impact the energy cost because beams are created in processing at the central controller using already

collected data instead of through additional work by the element nodes. The central controller is not a contributing part of the sensor network; therefore, its energy usage is not a concern.

Post-detection processing not requiring additional node participation, including TDOA and LOB calculation, also does not require additional energy cost as node communication levels are not altered. However, increasing N_i and/or A_s for an adaptive beamforming solution after LOB determination or increasing N_i for immediate collection increases energy usage since additional nodes are required to wake. This refers to the concept of increasing gain immediately to respond to immediate needs in signal processing when additional gain is required. Designating the potentially increased factors with primes, the new energy cost, Γ' , can be written as

$$\Gamma' = \delta \sum_{i=1}^L N'_i + (N'_s - 1)\chi_1 + N'_s \chi_2 \quad (131)$$

The increase in energy costs under various constraints on N_s is demonstrated in Figure 72 for the increased node option. For this simulation, energy associated with transmission, idling, and waking up is assumed equal. Although this is not a realistic assumption, it does not affect the curve trends. Additionally, an initial value for N_s is chosen to provide a numeric solution. The figure shows a linear relationship between N_i and energy cost, and the slope the curves vary due the increase in N_s . Creation of a strict definition for the increase of N_s due to increasing N_i would require specific knowledge of the deployment density. For the simulation, this increase is assumed linear associated with a uniform distribution. Although a Gaussian distribution may be more fitting for a random deployment, as discussed in [55], the distributions in the subarea can be described as uniform when they represent a small section of a much larger distribution. It is obvious then that the density of sensor deployment is an important factor. In cases where N_s does not require increase for increased N_i , the energy slope is more modest during active beamforming.

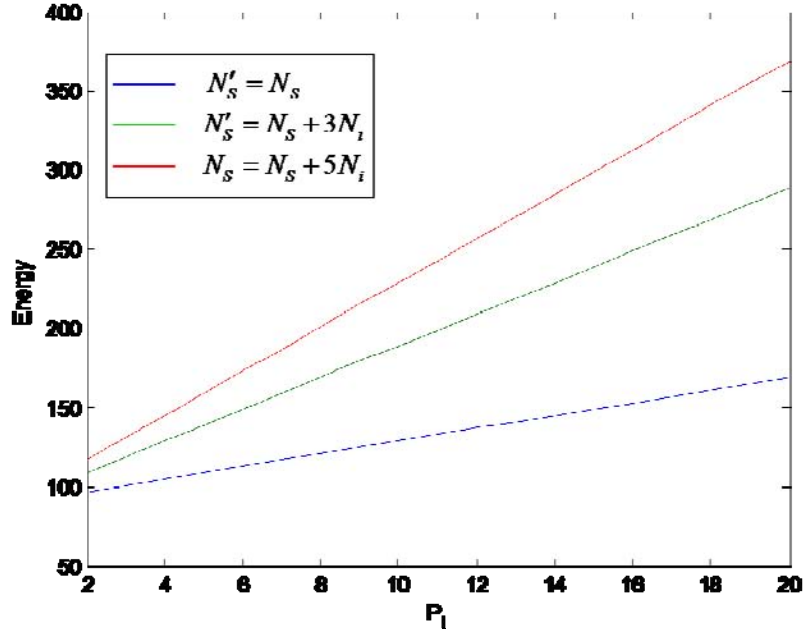


Figure 72. Energy cost versus number of nodes in an iteration where cost is constrained with respect to the additional nodes.

In order to facilitate immediate signal demodulation when the detection signal to noise ratio is not adequate for this action, an increase in N_i without a corresponding increase in A_s can form a temporary solution until a TDOA/LOB/adaptive beamforming solution is available. Using the same prime notation, the temporary energy required can be defined as

$$\Gamma_{temp} = \delta \sum_{i=1}^L N'_i + (N_s - 1)\chi_1 + N_s\chi_2 \quad (132)$$

To demonstrate the energy usage of the proposed method, a comparison to the method in [10] is offered. In the method proposed in [10], all nodes with the exception of a local central controller are in sleep (conserving energy) prior to signal of interest detection. This has the benefit of extending network life during periods of target emitter inactivity. However, based on the assumption of moderate signal activity, energy usage during periods of active emitter operation is of primary interest. The comparison of energy required methods during emitter operation is shown as

$$\delta \sum_{i=1}^L N_i + (N_s - 1)\chi_1 + N_s \chi_2 < \delta \sum_{i=1}^L N_i + (N_s - 1 + \Omega Y - Y)\chi_1 + (\Omega + N_s)\chi_2 + \delta \Omega Y \quad (133)$$

where the energy required in [10] is on the right hand side. In this equation, Ω indicates the number of nodes in the TDOA solution and Y represents the number of data samples from each node involved in TDOA. The inequality accounts for the energy required to wake up selected nodes, the energy from nodes in operating status but waiting to transmit, the energy from each transmission required to form the TDOA solution, and the energy required to beamform after a LOB is established. Cancelling like terms, the increased amount of energy expended in [10], Γ_δ , is determined as

$$\Gamma_\delta = (\Omega Y - Y)\chi_1 + \Omega \chi_2 + \delta \Omega Y \quad (134)$$

This difference is displayed in Figure 73 as linear when the number of nodes involved increases. The slope of the increase is $Y\chi_1 + \chi_2 + \delta Y$. It is evident that the energy costs for node wake up and performing TDOA/LOB prior to beamforming marks where the energy difference between the two methods resides.

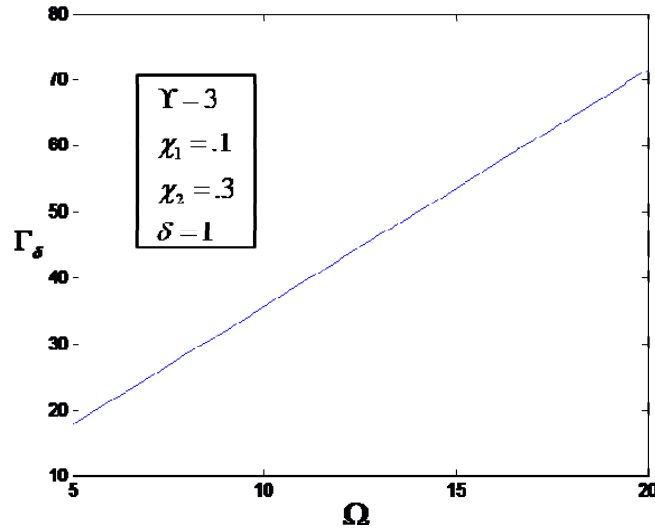


Figure 73. The difference in energy cost between the proposed method and the method in [10] versus the number of nodes involved in TDOA.

Considering time to signal demodulation after detection for the proposed method, it is clear that in cases where the signal to noise ratio is adequate to enable reception there

is no delay imposed. Further, when immediate signal demodulation is required following detection but signal-to-noise ratio is not adequate for that action, the time to enable the additional nodes is solely based on a logical decision at the controller. This can again be compared to the method in [10]. Since the method in [10] requires signal detection by the single central controller prior to awakening any network nodes, time in [10] between detection and demodulation can, therefore, be quantified as lag behind the proposed method.

Therefore, a measurable network delay in the proposed method is only evident in the event that the array formed for detection does not have an adequate signal-to-noise ratio for follow-on demodulation and demodulation is not necessary until an adaptive beamforming solution is formed. In such a worst case, the delay, t_{delay} , is dependent on both network delay in feeding the central controller and processing delay in the controller, as

$$t_{delay} = \Omega Y \zeta + \Omega \varepsilon + (\Omega Y + N_s) t_1 + (N'_s - N_s) t_2 + t_\psi \quad (135)$$

where ζ indicates the time to create a cross-ambiguity function for TDOA, ε represents the time to create a LOB from the TDOA pair solution, t_1 represents the time to transmit from each node, t_2 indicates wake-up time, and t_ψ represents processing time. A serial wake-up protocol is assumed in Equation (135) in order to match the analysis from [10], which assumes a serial wake-up in time calculations. Strict comparison of the two methods during this worst case event (again with the method from [10] on the right hand side) shows

$$\Omega Y \zeta + \Omega \varepsilon + (\Omega Y + N_s) t_1 + (N'_s - N_s) t_2 + t_\psi < \Omega Y \zeta + \Omega \varepsilon + (\Omega Y + N_s) t_1 + N_s t_2 + t_\psi \quad (136)$$

The method in [10] assumes no nodes operating prior to signal detection; so, the difference in the two methods is set by the wakeup time required for fewer nodes in the case of the proposed method. If parallel wake-up is assumed, the two methods would have no difference with the possible exception of t_ψ , which may be only slightly shorter for the proposed method in choosing which nodes to wake up because fewer nodes are

chosen in this method since an initial set exists. Therefore, the proposed methodology will, in general, have less lag in comparison with the alternative method even under worst-case constraints.

Therefore, the proposed methodology for employing a remotely deployed wireless sensor network as an array for radio frequency signal detection, geolocation, and demodulation compares better than the related alternative method in terms of energy and time delay costs. The design takes advantage of array gain and detection criterion during signal detection to increase detection probability and reduce false alarm activity. Further, the methodology enables multiple options during post-process without increasing energy usage, except under specified circumstances. Energy usage remains spread through the network, as was true with previously proposed techniques, in order to extend network lifetime.

B. BEAMFORMING WITH DISTRIBUTED MOBILE ELEMENTS IN A WIRELESS SENSOR NETWORK

The ability to connect receiver nodes through wireless technology not only eases the burden of wired connections in harsh environments, but it also allows designers to consider the implications of the freedoms offered by wireless connections. The topic of the ensuing analysis in this section will consider the effects of independent node mobility, where each node represents an element that is used in the formation of a radio frequency coherent beamforming array for sensing the environment and propose a novel method to operate under this condition, as documented in [64]. Such an arrangement is not standard in traditional arrays.

In the case of radio frequency beamforming using an antenna array, the primary algorithm involved to coherently aim the aperture in a target direction is a direct function of element positioning. It is by adding phase weights to the signal received at each element that a resultant signal with the gain effect from the array can be formed [13]. When independent motion is introduced to individual elements, this motion directly perturbs the intended coherent array factor beam pattern. Classical design of an array reception aperture uses a wired approach to connect the elements to a central processing

location for coherent signal reception of a preferred azimuth and elevation; therefore, traditional array formation does not account for motion because wired antenna arrays are assumed to have static element positions. Literature, such as [7], supporting wireless sensor networks using arrays to exfiltrate data investigated usefulness and implementation of a transmission array and analyzed effects and mitigation strategies regarding imperfect position or phase knowledge for randomly deployed nodes, as previously discussed. However, fixed position elements remain standard despite growing applications for mobile platforms. Mobile element implementation requires further investigation for potential applications in mobile communications or radio intercept operations.

Also previously discussed, sensor network energy efficiency is generally a key factor in the operation of a wireless sensor network since individual nodes have a limited power supply. Therefore, it is necessary to apply schemes designed to reduce energy usage, extending network life. Just as node communication processes and operational sleep-wake cycles (such as demonstrated in Section A of this chapter) are engineered to reduce energy requirements, energy savings are available in the reduction of sensor associated meta-data. Using a wirelessly networked reception array, the dynamic of random motion applied to the nodes will be developed, demonstrating the motion's effect on array factor formation under various conditions. A model is then proposed that connects the random node motion to array factor formation. The relationship is shown to be assessable and useful for reducing network traffic and processing overhead while producing operationally acceptable gain towards the target. This connection metric is then exploited in order to remove the need to continuously update node positions in coherent beamforming while maintaining gain above a pre-determined level towards the target vector. Implementation of this strategy allows reduction of node transmitted meta-data as a function of the network node speed of motion.

Motion by platforms in the wireless sensor network may occur for any operational rationale including improvement of reception position, motion of a supporting platform, or to honor other considerations. Of greater interest is the result of that motion. Equations (75) and (76) show that the element positions, with reference to azimuth and

elevation desired and measured, respectively, are multiplied by the phase constant, β , of the signal of interest. So, the array factor formed by Equation (74) is a function of distance in wavelengths between elements in specific geometry. From this relationship, it can be noted that sensor network motion that holds relative element positioning static has no effect on array pattern formation, as was shown in Chapter III.B.1. This remains true for sensor field rotation as well, assuming that the desired target aim point is relative to the array vice to a global position.

Further consideration with regards to motion is also due with respect to the influence of past motion on current motion decisions. As described in Chapter II.A.5, random walk attributes allow for motion in any direction, although potentially with greater probability in some directions and distances. However, research reveals that previous position and velocity of motion are critical to determination of next position. This relationship is a Markov process of sorts, as the influence of only the last motion is of importance. Specifically, the dynamics created will have the greatest influence on next position probabilities [26].

Applying motion to the coherent array factor in Equation (74) may be considered on a sample by sample basis. Position updates for each element can be applied for each sample, indicating the array factor and gain associated with that sample. With position updates provided, array factor weights from Equation (76) are recalculated to assure optimal azimuth and elevation weights. Although the beam pattern in each iteration will be altered due to the change in element geometry, the coherently formed main beam will remain focused on target. This is indeed the case when deterministic motion is applied to individual elements.

Applying independent random motion to each node has the effect of perturbing the main beam aim-point away from the desired target. This was also shown in Chapter III.B.1, and it occurs because the phase weights are not be updated due to unknown element positioning. Figure 74 provides an x - y plane cut comparison of array gain provided by a randomly distributed 10-element array with static elements and where each

element has independent random motion applied. The array is aimed at an azimuth of 60° and elevation of 0° . The perturbation is clear, reinforcing the conclusions from Chapter III.

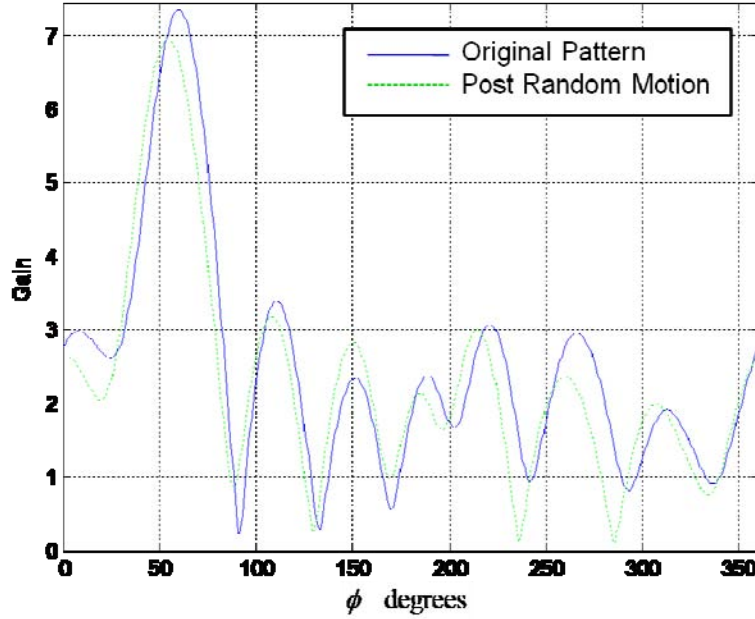


Figure 74. A comparison of array gain for a randomly distributed 10-element array versus the same array after random motion is applied to the elements.

The resultant change in geometry of the array, with regards to the target azimuth and elevation, alters the phase relationships between the elements, perturbing array factor formation. The motion of interest is based on wavelength changes vice purely physical speed. The relationship between the two is

$$Z = 100 \left(\frac{vt}{\lambda} \right) \quad (137)$$

where Z represents the percentage of wavelength moved over time, t , speed corresponds to the symbol v , and λ represents the signal wavelength of interest. Figure 75 demonstrates this relationship. Speeds shown correspond to potential node platforms: 23 mph roughly represents the fastest human sprint time or a slow moving land vehicle; 50 mph is for a fast moving land vehicle; slow and fast moving Unmanned Air Vehicles (UAV) are roughly associated with velocities of 135 mph and 404 mph, respectively. It

is clear from Equation (137) and the figure that speed of element motion relative to frequency of interest will drive the rapidity of change in the array factor. However, as non-deterministic motion involves uncertainty in the relative motion direction vector as well as relative speed, a direct linkage is not available through this avenue.

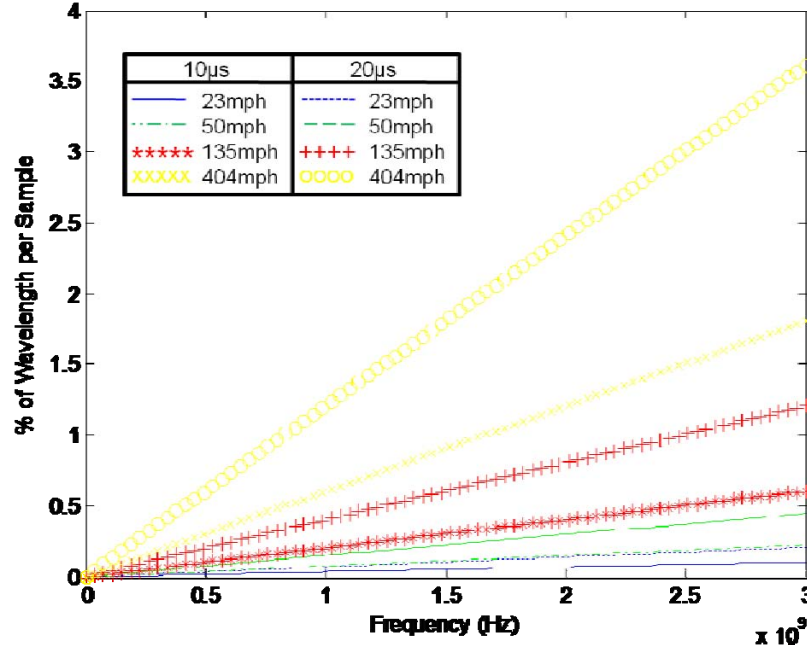


Figure 75. A comparison of motion at different node speeds in terms of the percentage of wavelength per sample versus frequency of interest.

The independent movement of elements is most interesting for analysis in determining the random nature of pattern perturbation. Consider the difference in array factor formation at discrete times. Assuming an array with N elements, the full array factor equation can be expanded and written directly as

$$AF(\theta, \phi) = \sum_{i=1}^N e^{j\beta[x_i \sin \theta \cos \phi + y_i \sin \theta \sin \phi + z_i \cos \theta]} e^{-j\beta[x_i \sin \theta_0 \cos \phi_0 + y_i \sin \theta_0 \sin \phi_0 + z_i \cos \theta_0]} \quad (138)$$

Applying component random velocities (v_x, v_y, v_z) to Equation (138) and considering at time t , this relationship is now expressed as

$$AF(\theta, \phi) = \sum_i^N e^{j\beta[(x_i + v_{x_i}t) \sin \theta \cos \phi + (y_i + v_{y_i}t) \sin \theta \sin \phi + (z_i + v_{z_i}t) \cos \theta]} e^{-j\beta[x_i \sin \theta_0 \cos \phi_0 + y_i \sin \theta_0 \sin \phi_0 + z_i \cos \theta_0]} \quad (139)$$

The difference between Equations (138) and (139), ΔAF , can then be determined for any direction (θ, ϕ) . However, the behavior difference at the target aim point (θ_o, ϕ_o) is clearly of the most interest. At original position, the array factor in Equation (138) sums to N under this condition. The difference is then simplified through like term combination

$$\Delta AF(\theta_o, \phi_o) = N - \sum_i^N e^{j\beta[v_{x_i}t \sin \theta_o \cos \phi_o + v_{y_i}t \sin \theta_o \sin \phi_o + v_{z_i}t \cos \theta_o]} \quad (140)$$

From Equation (140), it is clear that the main beam array factor is dependent directly on the independent element speed and direction. Translating to gain, a difference can be determined between the two states as

$$\Delta G(\theta_o, \phi_o) = G(\theta_o, \phi_o, t=0) - G(\theta_o, \phi_o, t=t_1) \quad (141)$$

Applying this equation, a relationship in gain difference over time when element nodes are in random motion can be considered. Using the two element array, a distribution of gain changes for randomly distributed arrays with random component velocities applied independently to each node is shown in Figure 76, resulting in random speed and direction. The percentage of gain lost is shown with respect to the target direction (θ_o, ϕ_o) over time for separate realizations of simulation. For this simulation, the speed was set as a uniform random variable with overall maximum speed limited below 60.35 wavelengths per second — corresponding to the roughly defined speed of a slow moving UAV (135 mph) at the target frequency of interest. Initial distributions were also considered as a uniform random variable inside a defined area. The figure shows multiple realizations indicting how beamforming performance alters in each. As expected the result is generally increasing perturbation over time regardless of initial distribution or applied velocities. However, the appearance of some natural clustering is evident in the distribution of the realizations. As the two-element case is harsh in terms of individual motion affecting outcome, the simulation was also considered with respect to $N = 5$, $N = 10$, and $N = 40$. The results of these are respectively displayed in Figure 77, Figure 78, and Figure 79. These simulations illustrate that a given random distribution occurs with regards to gain lost across realizations, and that the number of

elements involved in array formation delineates the variance of the gain changes at any point in time. Further simulations confirm that changes in maximum velocity, velocity random distribution type, initial node distribution type, or defined area of distribution do not remove the effect of a defined random distribution. Therefore the change in gain towards the target, despite the application of random velocity vectors, appears to be predictable.

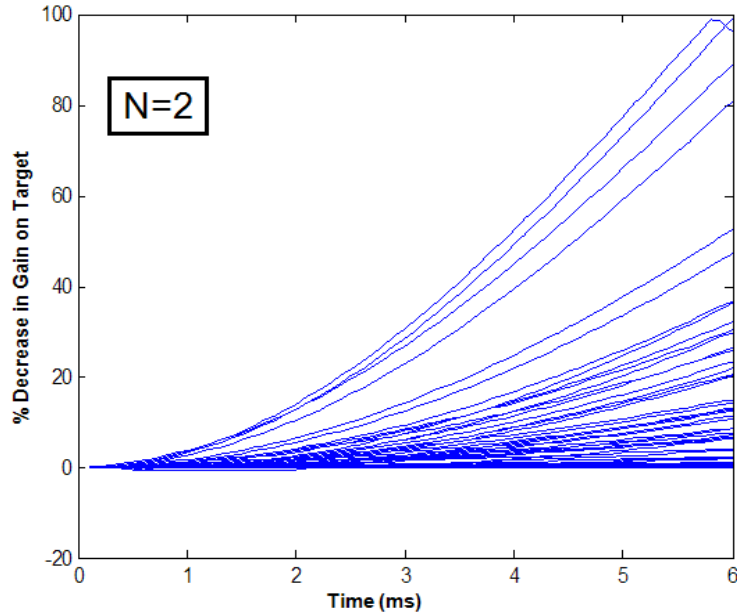


Figure 76. Percentage of gain lost in the target direction over time where $N = 2$ in the case of random element motion. Each line represents a separate instance of 100 iterations.

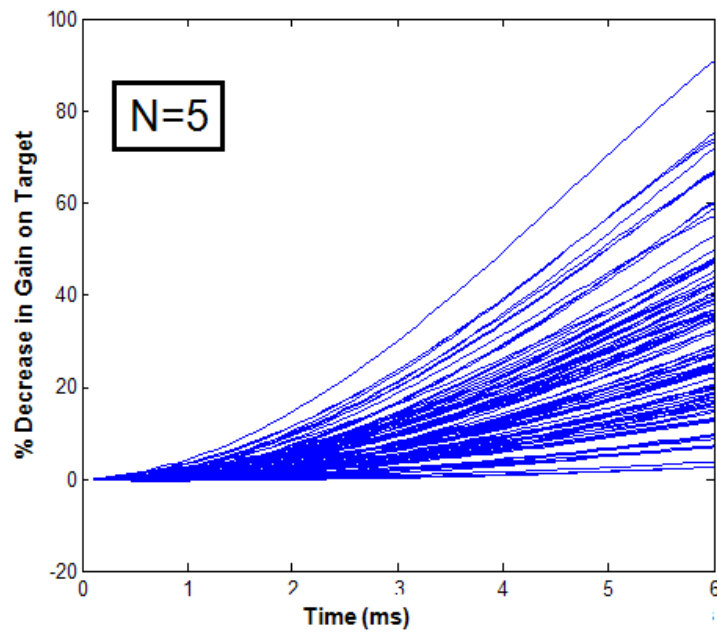


Figure 77. Percentage of gain lost in the target direction over time where $N = 5$ in the case of random element motion. Each line represents a separate instance of 100 iterations.

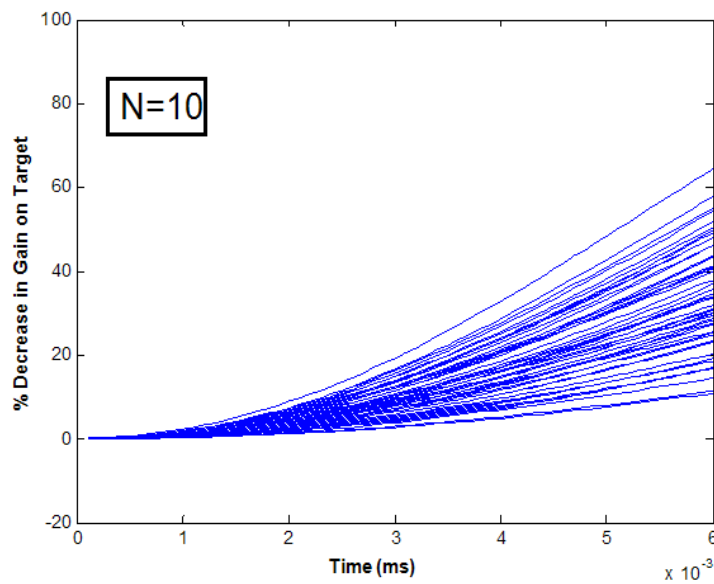


Figure 78. Percentage of gain lost in the target direction over time where $N = 10$ in the case of random element motion. Each line represents a separate instance of 100 iterations.

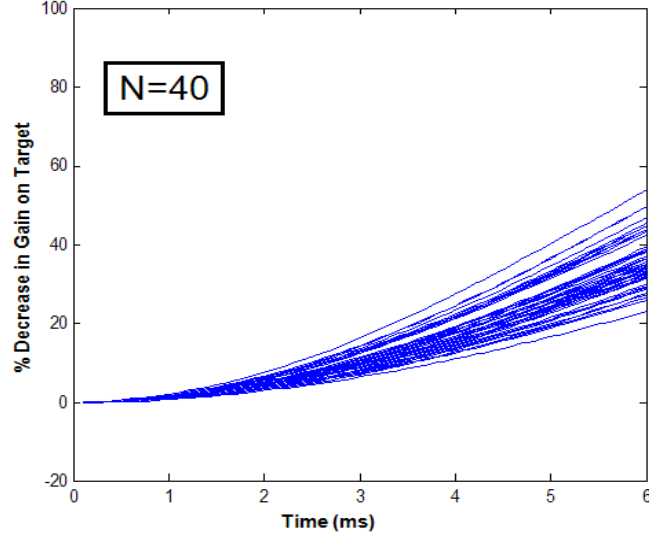


Figure 79. Percentage of gain lost in the target direction over time where $N = 40$ in the case of random element motion. Each line represents a separate instance of 100 iterations.

With the existence of a defined random distribution in mind, it is evident that knowledge of the distribution's characteristics would be useful to determine the time point at which position updates are necessary to reapply array weight factors. In order to characterize the distribution, the gain difference formula in Equation (141) must be reconsidered and expanded. First expand the second term, as

$$G(\theta_o, \phi_o, t=0) = \frac{(4\pi) \left| \frac{1}{N} \sum_{i=1}^N e^{j\zeta_i(\theta_o, \phi_o)} e^{j\alpha_i(\theta_o, \phi_o)} \right|^2}{\int_0^{2\pi} \int_0^\pi \left| \frac{1}{N} \sum_{i=1}^N e^{j\zeta_i(\theta, \phi)} e^{j\alpha_i(\theta, \phi_o)} \right|^2 \sin \theta d\theta d\phi} \quad (142)$$

Note that in this expansion, the factors for current signal phase, ζ , and weight, α , from Equations (75) and (76), respectively, are shown as functions of their particular angle. Further, each is assumed to be referenced to node original positions (x_i, y_i, z_i) . Based on the adherence to the target direction, Equation (142) then simplifies to $G(\theta_o, \phi_o, t=0) = G_m$, which is maximum gain at aim point for $t=0$. Next expand the first term, as

$$G(\theta_o, \phi_o, t) = \frac{(4\pi) \left| \frac{1}{N} \sum_{i=1}^N e^{j\zeta_i(x_i + v_{x_i}t, y_i + v_{y_i}t, z_i + v_{z_i}t, \theta_o, \phi_o)} e^{j\alpha_i(\theta_o, \phi_o)} \right|^2}{\int_0^{2\pi} \int_0^\pi \left| \frac{1}{N} \sum_{i=1}^N e^{j\zeta_i(x_i + v_{x_i}t, y_i + v_{y_i}t, z_i + v_{z_i}t, \theta, \phi)} e^{j\alpha_i(\theta_o, \phi_o)} \right|^2 \sin \theta d\theta d\phi} \quad (143)$$

where N is approximately the maximum value for normalization. The current signal phase is shown as a function of updated position. In the numerator, this accounts for the array factor change. In the denominator, it accounts for the overall change in array gain due to updated positioning. Based on this understanding of the array factor perturbation due to motion, the desired result can be achieved, that result being determination of time allowed before position reset is required. Reflecting the change in percentage assists in design decisions based on relative beam pattern perturbation. Assigning the variable \mathbb{C} to reflect the percent change, the quantity is

$$\mathbb{C} = 100 \left(\frac{\Delta G(\theta_o, \phi_o, t)}{G(\theta_o, \phi_o, t=0)} \right) \quad (144)$$

Simplifying this expression allows the final expression as

$$\mathbb{C} = 100 \left(1 - \frac{1}{N^2} \left| \sum_{i=1}^N e^{j\zeta_i(x_i + v_{x_i}t, y_i + v_{y_i}t, z_i + v_{z_i}t, \theta_o, \phi_o)} \right|^2 \frac{G_{m_t}}{G_m} \right) \quad (145)$$

where G_{m_t} represents the maximum gain of the perturbed array at time t . With the percent change in hand, a determination can then be made as to the probability of a percentage of change occurring at a given time when the velocity vectors are unknown. Reflecting a threshold percentage as T , this is

$$\Pr(\mathbb{C}(\theta_o, \phi_o, t) \geq T) = \Pr \left(100 \left(1 - \frac{1}{N^2} \left| \sum_{i=1}^N e^{j\zeta_i(x_i + v_{x_i}t, y_i + v_{y_i}t, z_i + v_{z_i}t, \theta_o, \phi_o)} \right|^2 \frac{G_{m_t}}{G_m} \right) \geq T \right) \quad (146)$$

Reordering this probability to remove functions not dependent on random variables from the left hand side, it can be rewritten as

$$\Pr(\mathbb{C}(\theta_o, \phi_o, t) \geq T) = \Pr \left(\left| \sum_{i=1}^N e^{j\zeta_i(x_i + v_{x_i}t, y_i + v_{y_i}t, z_i + v_{z_i}t, \theta_o, \phi_o)} \right|^2 \leq \gamma \right) \quad (147)$$

where

$$\gamma = G_m N^2 (1 - T / 100) \quad (148)$$

Therefore, the distribution of interest has been narrowed. Considering only this portion, the random distribution is expanded, using Equations (143) and (147), as

$$G_{m_t} \left| \sum_{i=1}^N e^{j\zeta_i(x_i+v_{x_i}t, y_i+v_{y_i}t, z_i+v_{z_i}t, \theta_o, \phi_o)} \right|^2 = \frac{4\pi \left| \sum_{i=1}^N e^{j\zeta_i(x_i+v_{x_i}t, y_i+v_{y_i}t, z_i+v_{z_i}t, \theta_o, \phi_o)} \right|^2}{\int_0^{2\pi} \int_0^\pi \left| \frac{1}{N} \sum_{i=1}^N e^{j\zeta_i(x_i+v_{x_i}t, y_i+v_{y_i}t, z_i+v_{z_i}t, \theta, \phi)} e^{j\alpha_i(\theta, \phi)} \right|^2 \sin \theta d\theta d\phi} \quad (149)$$

In Figure 80, distributions of the random result attributed to the modified percent change, \mathbb{C} , are shown where $N = 2$. This is repeated in Figure 81, Figure 82, and Figure 83 matching arrays with $N = 5$, $N = 10$, and $N = 40$, respectively. This corresponds to the previously considered percentage of gain lost array configurations while focusing on the threshold inequality shown in Equation (147) with the random factors shown in Equation (149). Keeping the parameters of the defined model, elements are initially randomly distributed and each element then has a stochastically determined motion direction and speed applied. The limiting factor in this construct is again a maximum node speed of 60.35 wavelengths per second, which is uniformly distributed.

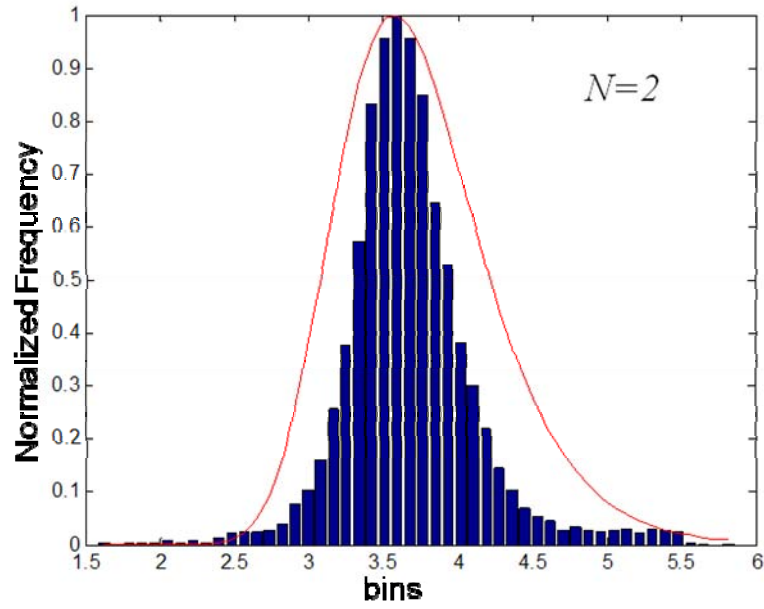


Figure 80. Histogram of modified change percentage, \mathbb{C} , for wirelessly connected arrays with element nodes in independent random motion for $N = 2$ and Rician ratio distribution line.

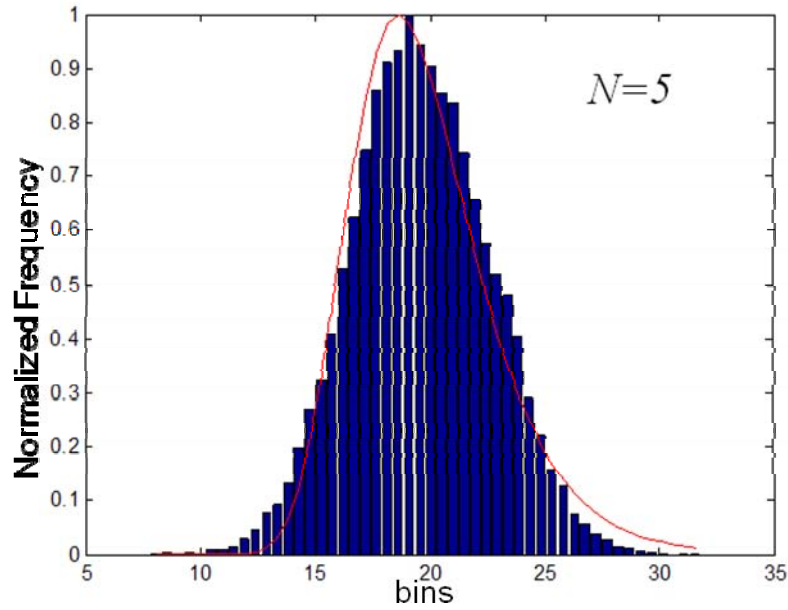


Figure 81. Histogram of modified change percentage, \mathbb{C} , for wirelessly connected arrays with element nodes in independent random motion for $N = 5$ and Rician ratio distribution line.

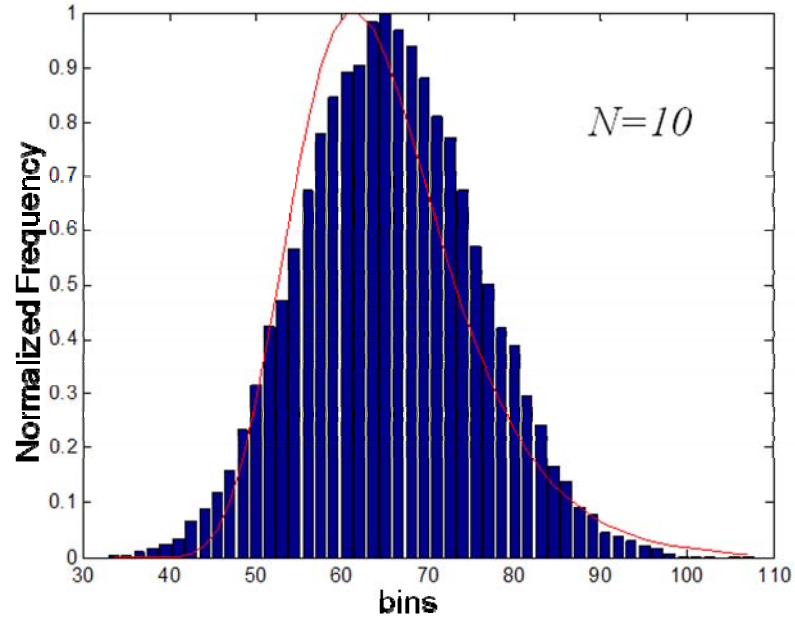


Figure 82. Histogram of modified change percentage, \mathbb{C} , for wirelessly connected arrays with element nodes in independent random motion for $N = 10$ and Rician ratio distribution line.

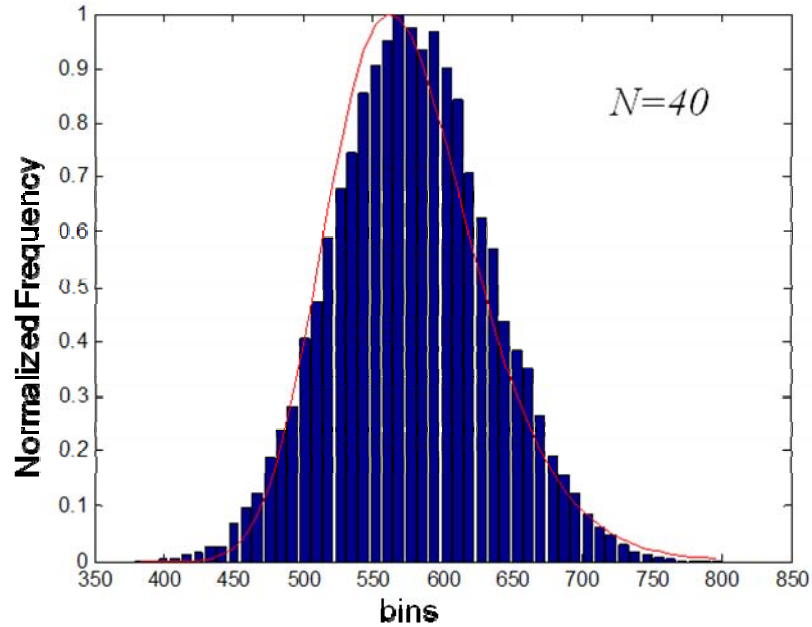


Figure 83. Histogram of modified change percentage, \mathbb{C} , for wirelessly connected arrays with element nodes in independent random motion for $N = 40$ and Rician ratio distribution line.

A general distribution shape can be observed in the change percentage, providing a concrete result for design parameters. The shape of the histogram appears initially familiar as similar to Gaussian, and an association of the Gaussian distribution seems to increase with an increasing number of element nodes. Pragmatically, this increasing association is appropriate for applications, as the overhead required to operate an array with two elements may not be offset by the gain achieved. However, the limits of the factor do not enable a Gaussian random variable to represent the distribution. Indeed, instead of Gaussian, the distribution is related to the Rician random variable, which as was previously noted and from [22], is very similar to Gaussian when the ratio of mean to standard deviation is large. The Rician random variable is generally associated with the multipath problem with a single dominating signal, as in Rician fading. Further, sums of squared Gaussian random variables is a general source for creation of a Rician random variable [23]. However, in this case, it is not a strict Rician random variable, but it is instead a ratio of individual Rician random variables as the best approximation. This can be determined theoretically by initially considering the distributions of the numerator and denominator of Equation (149) separately. Identifying the summation in the numerator as Ξ and evaluating, it is noted that the random variable resides in the power term with the numerator result a sum across the factors with each addend having an independent random variable in the power. Because of the cyclic nature of the addends and the interest only in the distribution of the magnitude of the sum based on complex number addition, it is an acceptable approximation to combine terms and consider the numerator summation as a uniform random variable, w , over the span of $[0, 2\pi]$, written as

$$\Xi = k \sum_{i=1}^N e^{jw_i} \quad (150)$$

where k is simply a constant. Although the magnitude of the addends are set at unity due to assumptions in beamforming, a magnitude random variable, r , will be added to the summation for a general case by rewriting Equation (150) as

$$\Xi = k \sum_{i=1}^N r_i e^{jw_i} \quad (151)$$

With this notation, analysis of the numerator for a case of $N = 2$ similar to that done in [65] follows. Since the random variables r and w are independent of one another and each addend is an independent case, the joint density function for each is

$$f_{R,W}(r, w)_i = \frac{1}{2\pi} f_R(r)_i \quad (152)$$

Summation is then accomplished considering the resultant convolution of the density functions, accomplished through transform, resulting in a probability density function, $f_R(r)_{\sum_{i=1}^2}$, of

$$f_R(r)_{\sum_{i=1}^2} = r \int_0^{\infty} \rho \Phi(\rho)_{\sum_{i=1}^2} J_0(\rho r) d\rho \quad (153)$$

where $\Phi(\cdot)$ represents the transformed version of each density function and $J_0(\cdot)$ is the Bessel function of order zero. Since it is known that the magnitudes are actually fixed in the summation, density function for $i=1$ can then be considered as a delta function, resulting in the form of a general Rician density function as [65]

$$f_R(r)_{\sum_{i=1}^2} = \frac{r}{2\pi} \int_{|r-r_o|}^{r+r_o} \frac{f_R(a)_2}{\Delta(a, r_o, r)} da \quad (154)$$

where a is used to distinguish magnitude in the density function of the second addend, r_o marks the position of the delta function, and $\Delta(\cdot)$ is a triangle area function, which can be solved using Heron's formula in [66].

This result can then be generalized for N addends using either a product of transforms as

$$\Phi(\rho)_{\sum_{i=1}^N} = \prod_{i=1}^N \Phi(\rho)_i \quad (155)$$

or performing two addend summation iteratively. The final density function is then only a minor variation from Equation (154), as [65]

$$f_R(r)_{\sum_{i=1}^N} = \frac{r}{2\pi} \int_{|r-r_o|}^{r+r_o} \frac{f_R(a)_{\sum_{i=1}^{N-1}}}{\Delta(a, r_o, r)} da \quad (156)$$

such that $f_R(a)_{\sum_{i=1}^{N-1}}$ is the density function of the previous iterations. The general form of Rician remains. It can be noted that the distribution in the numerator of the result in Equations (154) and (156) are initially associated with a delta function since the magnitude is invariant. That distribution is replaced with generalized Rician functions over subsequent iterations but still may be expected to be slightly perturbed by the delta function input.

Considering the denominator of the modified percent change, \mathfrak{M} , it can be taken from Equation (149) as

$$\mathfrak{M} = \int_0^{2\pi} \int_0^\pi \left| \frac{1}{N} \sum_{i=1}^N e^{j\zeta_i(x_i + v_{x_i}t, y_i + v_{y_i}t, z_i + v_{z_i}t, \theta_o, \phi_o)} e^{j\alpha_i(\theta, \phi)} \right|^2 \sin \theta d\theta d\phi \quad (157)$$

Focusing on the effects of the random variables, a similar analysis to the one performed on the numerator can be done. First, the representation is simplified to one similar to Equation (150) by approximating the integration as summation. By a similar argument, the result follows suit as a general Rician distribution. Numerical analysis of the distribution of the numerator and the reciprocal of the denominator demonstrate that the two quantities are independent. This is determined through observation of the mean, μ , and variance, σ^2 , of the factors and resultant product, which exhibit the following relationships

$$\mu = \mu_\Xi \mu_{\mathfrak{M}^{-1}} \quad (158)$$

$$\sigma^2 = \sigma_\Xi^2 \sigma_{\mathfrak{M}^{-1}}^2 + \mu_\Xi^2 \sigma_{\mathfrak{M}^{-1}}^2 + \mu_{\mathfrak{M}^{-1}}^2 \sigma_\Xi^2 \quad (159)$$

Since these random variables are independent, the distributions of the numerator to the denominator must also be independent. Therefore, the final distribution is available through the ratio, from [22], as

$$f_{\Xi/\mathfrak{M}}(u) = \int_0^\infty r_{\mathfrak{M}} f_{\mathfrak{M}}(r_{\mathfrak{M}}) f_\Xi(ur_{\mathfrak{M}}) dr_{\mathfrak{M}} \quad (160)$$

The resulting distribution therefore statistically remains related to a Rician distribution, and the ratio distribution was solved for the general case by Oetting [67] resulting in

$$f_{x/y}(z) = \frac{2zK_1}{(K_1 + z^2)^2} e^{-\left(\frac{K_2 z^2 + K_1 K_3}{K_1 + z^2}\right)} \left[\left(1 + \frac{K_1 K_2 + K_3 z^2}{K_1 + z^2}\right) I_0(\alpha(z)) + \alpha I_1(\alpha(z)) \right] \quad (161)$$

where $K_1 = \sigma_x^2 / \sigma_y^2$, $K_2 = \mu_y^2 / 2\sigma_y^2$, $K_3 = \mu_x^2 / 2\sigma_x^2$, $I(\cdot)$ is the modified Bessel function, and $\alpha(\cdot) = \sqrt{4K_1 K_2 K_3 (\cdot)^2 / ((\cdot)^2 + K_1)}$. The graphs in Figure 80 to Figure 83 demonstrate the Rician ratio distribution with respect to the associated histograms.

In order to further evaluate and associate the resultant distributions with the statistic of a ratio of Rician random variables, the Kolmogorov-Smirnov goodness-of-fit test, as defined in [68] and computed using [69], is applied to the distribution shapes. The mean and standard deviation associated with each array and the results of the Kolmogorov-Smirnov goodness-of-fit test are presented in Table 2. It is clear from the table that the histograms quickly associate to the Rician ratio distribution when the numbers of element nodes are in a region useful for significant gain. Employing the probability distribution as the operational metric, a determination of the time allowed prior to resetting array factor weights is the result. This enables beamforming to meet operational gain requirements while minimizing meta-data transfer through the network and minimizing weight re-processing.

Table 2. Mean, standard deviation and Kolmogorov-Smirnov goodness-of-fit data for the arrays in Figure 80, Figure 81, Figure 82, and Figure 83.

	Number of Elements			
	2	5	10	40
Mean	3.8	20.5	66.9	578.7
Std Dev	0.4	2.6	10	54.4
D	0.2	0.12	0.08	0.06
Fit	0.179	0.716	0.997	0.998

With the model available, it is now appropriate to consider basic application and the cost associated. As discussed earlier, for a wireless sensor network, the key factor is energy consumption. The data requirement from elements in an array to the central

processor is generally constant. For each signal sample, the element must sample and forward data and meta-data from the reception at a frequency of interest. Consider a wireless network where all N nodes are in an active and transmit state. Because of the high rate of data arrival, a contention-free medium access technique, such as time division multiple access, would be preferred. In such a scheme, there is no wait time for medium access prior to transmission; therefore, the energy expended within the network is driven by the cost of each transmission only. Additionally, the energy cost of each transmission is based on the payload of data and meta-data. Therefore, reduction of meta-data assists to reduce energy requirements across the network.

It is assumed that each node is capable of transmitting data to the processing center with the same amount of transmission power, and the energy cost of a full data and meta-data transmission is defined as δ . The energy to then transmit data to the processing node for a single sample is

$$\Gamma = \delta N \quad (162)$$

In this case, the meta-data in each transmission contains a position update necessary to calculate array weights. When such position updates are provided with each sample, recalculation of weights can occur on a sample by sample basis. Such an approach removes any perturbation due to motion. As an alternative approach proposed using the technique presented, recalculation of weights can be delayed by a time τ with a probability that array gain towards the target will not degrade beyond a desired threshold.

Define the quantity χ as the amount of energy less than δ required to transmit data and meta-data not including the node position update. Therefore, the energy to transmit this packet for a single sample is

$$\Gamma = (\delta - \chi) N \quad (163)$$

The resultant energy savings are consistent and predictable during network operation. Using the proposed methodology, a number of samples, \mathbb{N} , can be determined prior to weight recalculation. Considering transmissions over the full period of samples, it can be seen that the cumulative energy used with the proposed approach will always be less than

the continuous update method as shown where energy for the proposed approach is on the left hand side of the following equation:

$$\delta N + \sum_{i=1}^{N-1} (\delta - \chi) N \leq \sum_{j=1}^N \delta N \quad (164)$$

This inequality is further illustrated in a normalized fashion in Figure 84. The energy using the proposed metric is consistently below that of the continuous update technique. As the above analysis presents a general case, this may be further improved based on the implementation scheme. Further, the energy saved increases with increasing number of elements, which coincides with the region where the metric is most consistent.

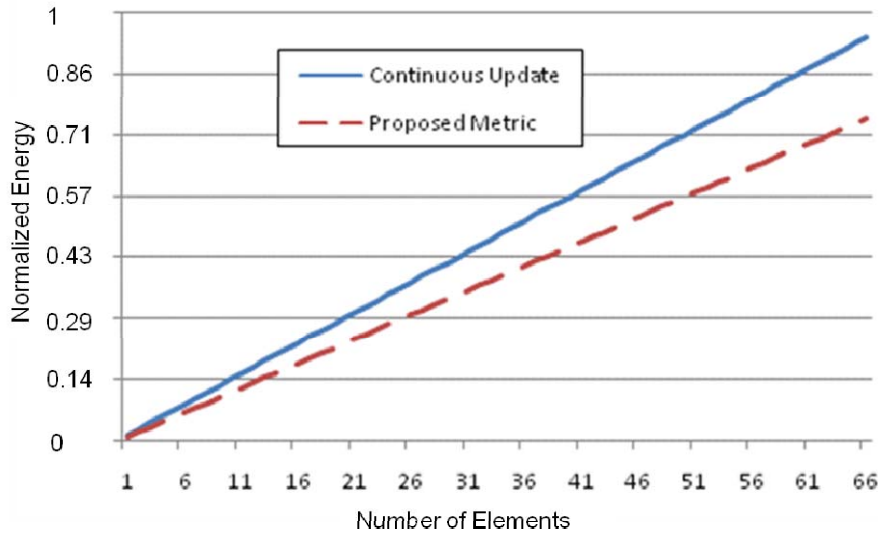


Figure 84. A comparison of transmission energy between a method using the proposed metric and a method with continuous updates over a single cycle, N . The energy per transmission is normalized, so unit size is arbitrary.

So, the effect of random motion by independently mobile sensor nodes to radio frequency coherent array formation is based on a predictable relationship through the method proposed. Analysis of the effects of motion application to the problem has shown a relationship between element motion and array gain that is then utilized to reduce the overhead and processing traditionally associated with motion of array elements. The results of this proposed relationship model are shown to reduce network overhead and therefore node energy consumption in a wireless network structure.

C. DETERMINING WEIGHT RESET TIMING IN A WIRELESS SENSOR NETWORK WITH INDEPENDENTLY MOBILE ELEMENTS

Section A in this chapter presented a method for managing a wireless sensor network constructed to form a beamforming array for the purpose of sensing radio frequency signals. The assembled network is managed through a process emphasizing its ability to detect a signal within the sensitivity range of the beamformed array while conserving energy in operations. Section B explored the concept of the radio frequency sensing wireless sensor network possessing independently mobile nodes, and it proposed a model in array factor formation connected to independent node motion that indicated the ability to conserve energy through the application of periodic, vice continuous, position updates. This relationship may be used to reduce network meta-data overhead and associated energy use in the network, but it requires proper timing to achieve this goal on a consistent basis. A process is then necessary to optimally choose update timing to reset the array factor phase weights.

This section demonstrates a methodology, as documented in [70], to employ a probabilistic relationship tying the networked array's performance to an operational requirement for system usability. A new algorithm is proposed to connect system operational performance in signal detection to phase weight resets while managing network energy usage under the concept of a wireless mobile element array. Consistent with the system management methodology in Section A, probability of detection against a target signal will be used as the key performance parameter of the proposed method, and in this case, it is used to determine the resultant timing for when to reset array weights. As before, using probability of detection as the operational requirement allows for results to be exercised in support of either a communications partner or unintended recipient scenario. The primary consideration in constructing the proposed method is then to determine reset timing around energy usage in the network balanced against the ability to meet gain requirements toward the target.

In general operations, receivers do not have detailed knowledge of the reception pattern provided by their apertures. Such information would be available only through continuous measurement, which would be burdensome. Knowledge of the transmitter

parameters, providing insight on reception pattern gain in the direction of the target, may be known in the case of a communications partner relationship. However, this information would not be available to the unintended recipient. Therefore, forming and maintaining beam pattern by a transmitter or receiver is based on mathematical estimation. The stochastic relationship between gain and element motion shown in Equation (147) can be used to determine the most likely effect of independent element motion on a coherent array. Although it is clear from Chapter III.B.1 and Section B of this chapter that the perturbation of array pattern requires correction in order to maintain target focus, the need remains to determine when to reset array weights. Without detailed knowledge of the array pattern from constant measurement or the target transmitting parameters, a methodology can be determined based on determined gain threshold and a desired probability to remain above that threshold. The determination of these controlling factors will remain arbitrary to design and operational requirement. Further, as described in Section A, determination of receiver gain for use with Equation (125) is not a simple substitution. Maximum gain is altered based on changes in element geometry, even in cases where main beam direction is allowed to remain focused. This will need to be addressed in the proposed methodology.

In constructing the proposed process, a starting array configuration with an associated gain, G_1 , can be determined. Likewise from the gain, an associated detection probability, P_{D_1} , can be located along the edge of the detection envelope. As gain is decreased, the associated slide down the detection envelope can also be found. Based on the operational requirement for signal detection, these parameters can be determined at a minimum detection probability threshold, P_{D_r} . Considering Equations (145) and (147), the array's ability to stay above that threshold within a specified time duration can be determined. Concurrently, through operation on the percentage threshold, T , a timescale can be drawn to determine maximum available time before the probability of gain change has exceeded parameters.

The proposed methodology for implementing the array gain probability and detection probability in the design and operation of an array with wirelessly connected elements is thus described. It is assumed that a target signal at a wavelength, λ , and array aim point (θ_o, ϕ_o) is given.

- **Step 1:** Establish a set of operating parameters. These parameters are not a set of receiver specifications, but instead they provide the context for operational employment. At a minimum, the required probability detection, P_D , for a signal on the edge of the operating envelope should be specified. A probability of false alarm, P_{FA} , may also be specified. This false alarm rate may be reduced if post-detection processing spurs additional energy concerns and other requirements can still be met.
- **Step 2:** Determine the number of participating element nodes, N . This may be based on the number of potential node locations provided. Alternatively, if the number of participating nodes is available for specification, this may be chosen in any manner preferred, i.e., arbitrarily or based on maximum or minimum gain provided in a particular distribution pattern. A maximum velocity of movement and potential distribution of that movement for the nodes should also be determined.
- **Step 3:** Calculate the weights for the selected nodes at their initial location and implement. Equation (76) is applicable.
- **Step 4:** Determine the gain in a desired target direction from the array using Equation (41).
- **Step 5:** Establish the Probability of Detection curve appropriate for the desired false alarm rate. Equation (125) is applicable. Based on the gain provided in step three, determine the acceptable loss of gain to the required detection probability. This is the threshold T when translated into a percentage of the initial gain.
- **Step 6:** Determine γ from Equation (148).

- **Step 7:** Applying Equation (147), the probability the array can maintain gain above threshold after a period of time can be determined.
- **Step 8:** Determine the time between reset of weights based on the probability threshold to be maintained.
- **Step 9:** Implement determined delay. Following delay period, a new set of positions are received. Then return to step 3.

The result of implementing this methodology is a reset time, which is updated dynamically. The rewards then associated with this result are a confidence in array operations and an energy savings in comparison with other methods. This is where the benefit of the proposed method must be measured. The proposed method is clearly preferable for management of independently mobile element nodes in a radio frequency detection receiver compared to an alternative of continuous position update. Indeed, a comparison of energy usage between techniques using continuous position updates versus a method employing probability relationships in Equation (147) was provided in Section B. However, the analysis in Section B did not propose an implementation method for determining the reset timing. Therefore, only the general result of increased energy savings in the wireless network was shown. Defining δ as the energy cost of a full data and meta-data transmission, χ as the amount of energy less than δ required to transmit data and meta-data not including the node position update, and N as the number of samples between weight reset, the cumulative energy used with the proposed approach will always be less than the continuous update method as shown previously in Equation (164).

As it is then established that delaying reset in general provides an energy savings in network communications, it is far more interesting to consider an alternate scheme of determining reset time for comparison with the proposed method for reset time determination. The most obvious case that can be made for an alternate method is a system that arbitrarily assigns reset timing. In such a case, specific reset timing through an alternate method would be designed into the system based on any engineering considerations in design. As such, there are three possible cases that must be considered

of the arbitrarily assigned reset timing model: 1) The first case assumes the arbitrarily assigned timing is much smaller than the time it would take for array performance degradation. 2) The second case assumes the assigned timing is much larger than the time it would take for array performance degradation. 3) Finally, the third case assumes the arbitrarily assigned timing is correct to reset weights with a maximum time prior to array performance degradation for the initial element distribution, but, as the timing remains static for follow-on iterations, it will vary between being longer or shorter than necessary in terms of array performance.

For the first case, an analysis similar to that for the continuous update case is appropriate. Defining \mathbb{N}_{A_1} as the number of samples between weight reset where $\mathbb{N}_{A_1} < \mathbb{N}$ is consistent, then the energy expended over \mathbb{N} samples can be compared. The energy for the proposed case, E_p , can be taken from Equation (164) as

$$E_p = \delta N + \sum_{i=1}^{\mathbb{N}-1} (\delta - \chi) N \quad (165)$$

The energy associated with the arbitrary method, E_{A_1} , can be solved from three summation parts. The first part represents the whole number of times a full set of samples must be repeated with the arbitrary case timing, $E_{A_{1a}}$, as

$$E_{A_{1a}} = \sum_{j=1}^{\left\lfloor \frac{\mathbb{N}}{\mathbb{N}_{A_1}} \right\rfloor} \left[\delta N + \sum_{i=1}^{\mathbb{N}_{A_1}-1} (\delta - \chi) N \right] \quad (166)$$

The second part represents the energy from additional messages where a full set of meta-data is required, $E_{A_{1b}}$, as

$$E_{A_{1b}} = \sum_{i=1}^{\left\lfloor \frac{\mathbb{N}}{\mathbb{N}_{A_1}} \right\rfloor \left\lceil \frac{\mathbb{N}}{\mathbb{N}_{A_1}} \right\rceil} [\delta N] \quad (167)$$

And the third part accounts for the energy required from messages that do not include the position meta-data set, $E_{A_{1c}}$, as

$$E_{A_{lc}} = \sum_{i=1}^{\mathbb{N} - \left\lfloor \frac{\mathbb{N}}{\mathbb{N}_{A_l}} \right\rfloor} [(\delta - \chi)N] \quad (168)$$

In this notation, when the lower bound of summation is greater than the upper bound of summation, the summation is zero. A comparison between the energy from the proposed method and the arbitrary method can then be made. Since it has been established that $\left\lfloor \frac{\mathbb{N}}{\mathbb{N}_{A_l}} \right\rfloor \geq 1$ in the case definition, the task of determining the equality relationship is academic, as shown:

$$\delta N + \sum_{i=1}^{\mathbb{N}-1} (\delta - \chi)N \leq E_{A_{la}} + E_{A_{lb}} + E_{A_{lc}} \quad (169)$$

Energy required for the proposed method is clearly less. The quantities in Equation (169) can be rewritten as a difference as

$$\Delta = (E_{A_{la}} + E_{A_{lb}} + E_{A_{lc}}) - E_p \quad (170)$$

This difference in energy is shown in Figure 85 at increasing settings for arbitrary reset, \mathbb{N}_{A_l} . The curves indicate increased energy savings as the distance between arbitrary and proposed reset values increases with increased general slope when the arbitrary reset is smaller. While both methods would provide prescribed beamforming performance, the energy savings from the proposed method is clear. Therefore, the proposed method provides both energy savings and operational confidence.

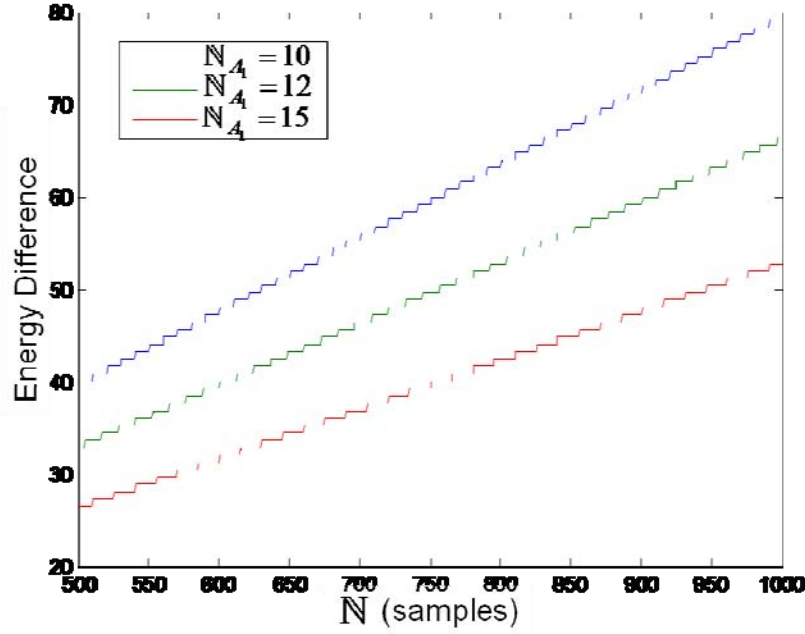


Figure 85. Energy difference (arbitrarily scaled based on application) between the proposed method and the first alternate method at various settings for \mathbb{N}_{A_1} . For analysis, settings of $\delta = 1$, $\chi = 0.1$, and $N = 8$ were applied.

In the second case, where arbitrarily assigned timing is much larger than the time it would take for array performance degradation, the issue of energy savings is reversed; Equation (164) applies. Therefore, the arbitrarily assigned timing method would have an advantage in energy savings over the proposed method. However, the ability of the array to meet the operational requirement using the arbitrarily assigned timing method is severely compromised. Define t_{A_1} as the reset timing for this arbitrarily assigned case and t_p as the timing for the proposed method, where $t_{A_2} > t_p$ is consistent. Applying Equation (147) for $t = t_{A_2}$ and taking the expectation of the change value, $\mathbb{C}(\theta, \varphi, t)$, using Equation (144), a relationship of threshold probabilities can be formed, where the value of the proposed relationship is on the left hand side, shown as

$$E\left[\mathbb{C}(\theta_o, \varphi_o, t = t_p)\right] < E\left[\mathbb{C}(\theta_o, \varphi_o, t = t_{A_2})\right] \quad (171)$$

The result of this relationship is demonstrated in Table 3, showing the mean percent change, $\mathbb{C}(\theta, \phi, t)$, for three cases of random distributions with N equal to five, eight, and ten. The mean percent change is formed through the application of random velocity vectors for individual nodes in each run. In the table, t_p has been chosen as the time between reset associated with $N = 30$. This result is compared to the same array at arbitrary times in this case, t_{A_2} , as shown.

Table 3. Mean percent change $(\mathbb{C}(\theta, \phi, t))$.

	t_p	Time Segments			
		t_{A_2}			
		35	40	45	50
Case 1	6.1%	8.2%	10.6%	13.3%	16.2%
Case 2	6.8%	9.1%	11.8%	14.7%	17.9%
Case 3	7.1%	9.6%	12.4%	15.5%	18.8%

Equation (171), as demonstrated in the table, states that the mean value of percent change, $\mathbb{C}(\theta, \phi, t)$, for the arbitrarily assigned case with $t_{A_2} > t_p$ is greater than that for the proposed method. As the proposed method assigns this value to maximize timing while remaining within the prescribed operational parameters, the arbitrary method then resides outside of those parameters. Therefore, the arbitrarily assigned case is not able to provide consistent array gain above the operational requirement over the time period.

In the case where the arbitrarily assigned timing, t_{A_3} , is correct to reset weights with a maximum time prior to array performance degradation for the initial element distribution but the timing remains static for follow-on iterations, the comparison will be in both energy expended and in gain produced. With random motion of the elements assumed, the shape and distribution of the elements will vary for each iteration. As such, the time to reset in each iteration will also vary when using the proposed method. For two successive nodes, if the time of the second iteration, t_2 , is determined to be less than the time of the first iteration, t_1 , then the energy expended over the two arbitrary time

periods, t_{A_3L} , will be greater in the proposed method than in the arbitrarily assigned case, but the array will vary outside of operational parameters given by

$$E\left[\mathbb{C}(\theta_o, \varphi_o, t = t_2)\right] < E\left[\mathbb{C}(\theta_o, \varphi_o, t = t_{A_3L})\right] \quad (172)$$

If instead the time of the second iteration, t_2 , is determined to be greater than the time of the first iteration, t_1 , then both methods will meet operational requirements, but the energy expended by the arbitrarily assigned case will be greater than the proposed method. This is the same situation as in case one and is shown where \mathbb{N}_{A_3S} represents the number of samples between resets for the arbitrary method with shorter time and \mathbb{N} is the timing for the proposed method as

$$\delta N + \sum_{i=1}^{\mathbb{N}-1} (\delta - \chi) N \leq \sum_{j=1}^{\left\lfloor \frac{\mathbb{N}}{\mathbb{N}_{A_3S}} \right\rfloor} \left[\delta N + \sum_{k=1}^{\mathbb{N}_{A_3S}-1} (\delta - \chi) N \right] + \sum_{l=1}^{\left\lfloor \frac{\mathbb{N}}{\mathbb{N}_{A_3S}} \right\rfloor} \left[\frac{\mathbb{N}}{\mathbb{N}_{A_3S}} \right] \left[\frac{\mathbb{N}}{\mathbb{N}_{A_3S}} \right] [\delta N] + \sum_{m=1}^{\mathbb{N} - \left\lfloor \frac{\mathbb{N}}{\mathbb{N}_{A_3S}} \right\rfloor \mathbb{N}_{A_3S} - 1} [(\delta - \chi) N] \quad (173)$$

where again any sum is assessed to be zero when the lower bound of summation is greater than the upper bound of summation.

So, the proposed methodology to determine reset time has the best performance in terms of operational array performance and network energy usage. Analysis of the proposed technique demonstrated that application of the method is clearly preferable to alternate methods. Direct comparison to a continuous position updating method demonstrated that the proposed technique is superior in saving energy within the network, which is a key operational parameter for wireless sensor networks. Evaluation versus a trio of models involving arbitrarily determined reset timing implemented in system design established the proposed method as superior dependent on the arbitrary timing assigned. In the case where the arbitrary timing is always shorter than that of the proposed method, energy savings in the proposed method dominate the comparison. In the case where the arbitrary timing is always longer than that of the proposed method, the arbitrary method is unable to meet the operational array requirements specified. Finally, in the case where the arbitrary timing is on target for an initial iteration (but timing

remains static for follow-on iterations), a combination of energy and operational array effects, dependent on element motion, decrease efficiency of the arbitrary method against the proposed method. The result of this proposed methodology is then a suitable balance between operational requirement and energy efficiency in the network – both extending network life and meeting operational gain needs.

D. PAIR-WISE WIRELESS COMMUNICATIONS PERFORMANCE WITH UNSTEADY NODE ORIENTATION IN A SENSOR NETWORK

Where Section A of this chapter focused on how to manage the nodes in a wireless sensor network in order to optimize energy expenditures referenced to the requirements for sensor input in beamforming, and Sections B and C considered the ability to beamform using a wireless sensor network with independently mobile nodes and derive weight reset timing for implementation, none of these addresses the question of errors in the wireless link between nodes in the network. As was discussed in Chapter II.C, there are a variety of issues in wireless networking resulting in increased bit error occurrence over a simple free-space loss model, and Chapter III.C reviewed the direct effect of packet loss in communications as an intermittently participating node in the creation of a coherent beamforming array. The result of that analysis was that the array with the loss of a node could still be effectively created with the target aim point remaining as desired; however, the array gain is generally decreased. Therefore, as this is a tangible performance effect, options to reduce bit error rate are generally necessary.

Considering the problem of a wireless sensor network with independently mobile nodes, the problems generally associated with a wireless scenario continue to influence behavior. However, the specific introduction of independent mobile elements carries an additional complicating factor with regards to system operation, that being the potential for node element orientation to behave unsteadily with respect to a desired point of reference. Orientation of a node mounted on an independently mobile platform may be affected due to a variety of conditions including vibration, natural motion, material flexibility, terrain, or weather. Thus, unsteady orientation must be considered in terms of both effect on sensors attempting coherent beamforming and inter-node communications. Inter-node communications may be greatly affected by element orientation, so a proposal,

as documented in [71], is presented to minimize the influence of unsteady orientation without expending exaggerated network energy.

Antenna orientation affects the alignment of its pattern, polarization and mutual coupling properties. Mutual coupling can generally be ignored for the scenarios being considered due to the random and relatively large element separations in wavelengths. The effect of antenna rotations in azimuth and elevation angles are well documented in texts under static conditions. Analysis in [72] and [73] discuss the assumption of stability in orientation as hindrances to accuracy and realistic modeling. As described in [16] and [28], the physical condition of an antenna transmission pattern and the associated effect on a communications link can be mathematically described in a two antenna situation. Specifically for sensor networks, research in [73], [75], and [76] provide insight on measured sensor communications with various polarization properties. The end effect of each of these studies is insight on propagation loss under specific constraints including placement and frequency in static deployment, but they demonstrate a single static deployment fielding and do not expand the general fielding knowledge set in terms of dynamic orientation. In more complex circumstances, like multiple antenna scenarios, research in [32] does provide a baseline to understand combinatory effects caused by polarization differences, and the method proposed in [33] uses the active element pattern to address individual polarization, mutual coupling, and element patterns. However, these treatments are also primarily suited for static applications, where orientations remain fixed after initial setup. The increase of fielding scenarios and the physical reality of platform instability do not make this a realistic condition, necessitating analysis under randomly varying orientation.

Array factor formation for a coherent beamforming solution is dependent on the induced currents on the individual array elements being coherently combined as shown in Chapter II.B.3. As a signal arriving from the aim point must travel different distances to reach each element, as was shown in Figure 18, there is a resultant difference in amplitude and phase of the induced currents. Coherence of currents is then reliant on proper weights, where weights are based on the spatial configuration of the elements.

However, amplitude differences are generally small as they are based on path loss due to strict physical distance while phase differences are a function of wavelength, so phase weights are constructed using Equation (76).

Amplitude differences due to orientation can present an issue in coherent combination. One method to deal with differences due to orientation is equalization; however, this affects the ability to consider array factor gain as a multiplicative term to element gain [16]. In cases where providing equalization is difficult, it is also common to ignore amplitude differences. It will be assumed that amplitude issues are not a factor in this study. The introduction of an orientation offset in an array does not alter the spatial structure of the array, so a signal from the desired aim point continues to arrive at each element with the same phase delay and path loss difference; however, the altered pattern of the element with offset orientation will further influence the received amplitude of the induced current due to the polarization and pattern of the element. Since for an ideal dipole the received phase is unaffected, given that the array equalizes all induced current prior to combination, there is no change in array factor, unless orientation results in no signal received. If amplitudes are not equalized in array pattern calculation, then methods such as those discussed in [33] are in vogue.

For communications, a wireless sensor network consists of a set of spatially separated sensor nodes that exchange information over a wireless path. Data forwarding methods, such as the ones offered in [8], require nodes to form a coherent beam to pass data to a central processor. Alternatively, nodes may simply pass data to a relay node for forwarding. Both methods require the ability to pass data to adjacent nodes, setting up pair-wise links to reach a central processor. Individual nodes continue to consist of a sensor assembly, a transceiver for network participation, an on-board processor, and a battery. Generalization of the sensor package has been done purposefully, as analysis focused on data exchange need not be tied to the sensor beamforming and is instead for common application. Although analysis will clearly be valid for any linear polarization producing communications element, each node's communications antenna will be

assumed as a dipole near resonance for purposes of modeling. Dipoles are chosen here as they represent a general case. The gain pattern, $G(\theta)$, for a half-wave dipole antenna at resonance is [16]

$$G(\theta) \approx 1.64 f_{norm}^2(\theta, \phi) = 1.64 \left(\frac{\cos\left(\frac{\pi}{2} \cos(\theta)\right)}{\sin(\theta)} \right)^2 \quad (174)$$

An additional angle, ϕ , describes the azimuth angle of rotation from the x -axis in a standard spherical coordinate system where the dipole resides on the z -axis. It is evident from this relationship that the gain pattern for a dipole is not dependent on the azimuth angle but only the polar angle. In terms of polarization, the relationship in Equation (51) continues to hold; however, for a pair of dipoles the polarization efficiency, ρ , simplifies to the more usable form, from [16],

$$\rho = \cos^2(\aleph) \quad (175)$$

where \aleph represents the angle between dipole axes in common reference.

As this is a wireless sensor network question, the efficient consumption of energy continues to be a primary concern. This must be balanced against the required bit error performance determined for desired system operation. Thinking first about the wireless network, the deployment method or platform operations may result in a random or intended distribution across the target area, as before, and node positions may be found using self-location techniques, such as described in [40], or other means such as GPS as previously described. However, specific position knowledge will not be required in forming the general model. Communications between the nodes assumes free-space position and transmission. More complex propagation environments may be considered, but it is important to note that the proposed model ignores the effects of shadowing, multi-path or “polarization altering” transmission factors as these factors are not predictable in a general environment.

Most importantly, nodes are assumed to have a preferred orientation matched to the adjacent elements considered as a specified reference; however, as each platform is

unstable, orientation varies from the preferred in a random manner. So, an element may tip randomly in any direction. The amount of tilt will be characterized as a Gaussian random variable with a mean of zero. An estimate of the tilt standard deviation can be made from physical conditions. This parameter is monikered the “wobble factor” for the element, w . Wobble factor can range 0° to 90° for a dipole in free-space and is based on physical measurements of stability and velocity in tilt. As noted, the motion of an unstable platform allows movement equally in the full range of the upper hemisphere. Therefore, a uniform random variable is appropriate to represent tilt direction.

Forming a model to consider communications, assume a link between nodes B and C in the sensor network where the orientation of each element is off normal, as shown in Figure 86. Tilt angles, (θ_B, θ_C) , and associated azimuth angles, (ϕ_B, ϕ_C) , exist in the global coordinate system at a specific instant in time. In a static system, this state can be solved to determine the expected free-space power transfer between the two nodes when specific knowledge of all angles in the global coordinate system exists, allowing application of Equations (174) and (175) to account for gain pattern and polarization. However, random dynamic orientation cases require further analysis.

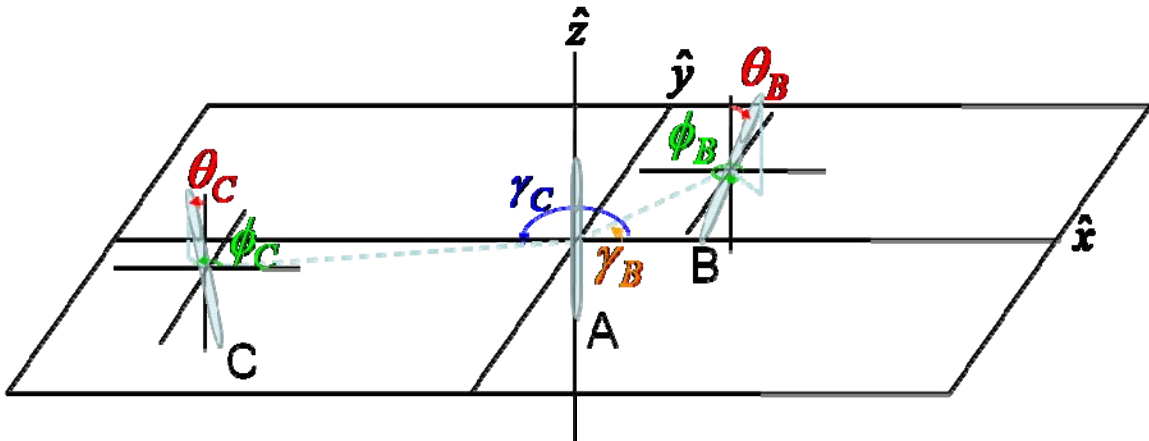


Figure 86. Arrangement of a pair of nodes (Nodes B and C) in communication plus a check node (Node A), which exhibits desired orientation.

The establishment of a reference or “check” node is convenient for the model. Establish Node A as adjacent to Nodes B and C. Node A, also included in Figure 86, is assumed fixed in the preferred reference orientation and is located at the origin of a

coordinate system in the plane containing the three nodes. Angles of rotation from the x -axis to Node B and Node C, designated γ_B and γ_C , respectively, can be found using a tangent function from the known geometry at a given time. Node A's position and the orientation of Node B, rotated to the x -axis, are shown in Figure 87. This figure demonstrates the angle for polarization, \aleph , and introduces the angle, ψ , used for gain pattern, which represents the elevation from the system transmission plane. The relationship of angles ψ and \aleph to the orientation angles of θ and ϕ for a node located on the x -axis adjusting for required angle limitations can be approximated using

$$\phi = \tan^{-1} \left(\frac{\aleph}{\frac{\pi}{2} - \psi} \right) \quad (176)$$

and

$$\theta = \frac{\aleph}{\sin \phi} \quad (177)$$

where these approximations are valid for small (less than 30°) values of θ . Figure 88 depicts how the approximation applies with respect to arc-length projections. From this figure, it can be seen that

$$\tan \aleph = \frac{v}{w} = \frac{\sin \theta \sin \phi}{\cos \theta} = \tan \theta \sin \phi \quad (178)$$

therefore, solving for ϕ , the connection to Equation (177) is

$$\sin \phi = \frac{\tan \aleph}{\tan \theta} \approx \frac{\aleph}{\theta} \quad (179)$$

Additionally, it is noted that

$$\tan \psi = \frac{w}{u} = \frac{\cos \theta}{\sin \theta \cos \phi} = \frac{1}{\tan \theta \cos \phi} \quad (180)$$

Therefore, using trigonometric identities to solve for $\tan \phi$, the approximation in Equation (176) is shown as

$$\tan \phi = \tan \theta \sin \phi \frac{\cos\left(\frac{\pi}{2} - \psi\right)}{\sin\left(\frac{\pi}{2} - \psi\right)} \approx \frac{\aleph}{\frac{\pi}{2} - \psi} \quad (181)$$

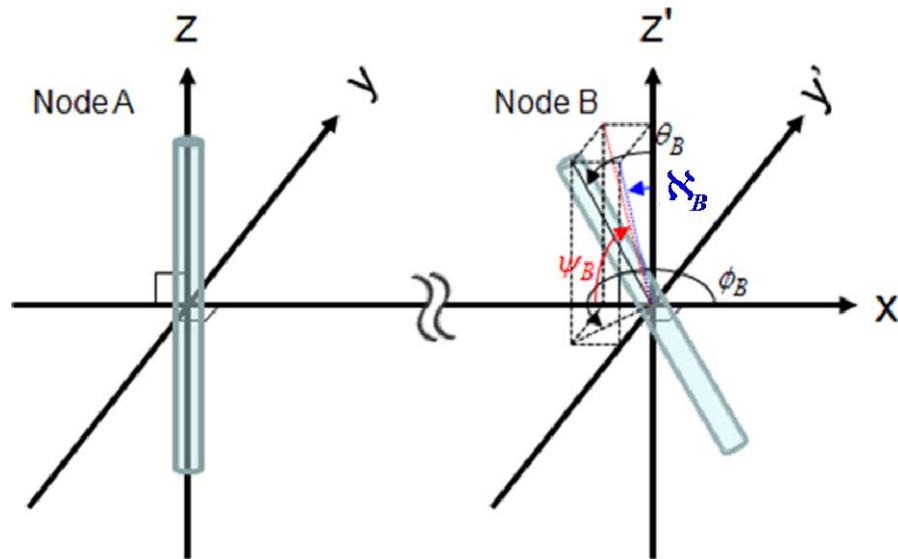


Figure 87. Check Node A and Node B with Node B rotated to the x-axis. Note: Axes y' and z' are parallel to the y and z axes and are shown for convenience.

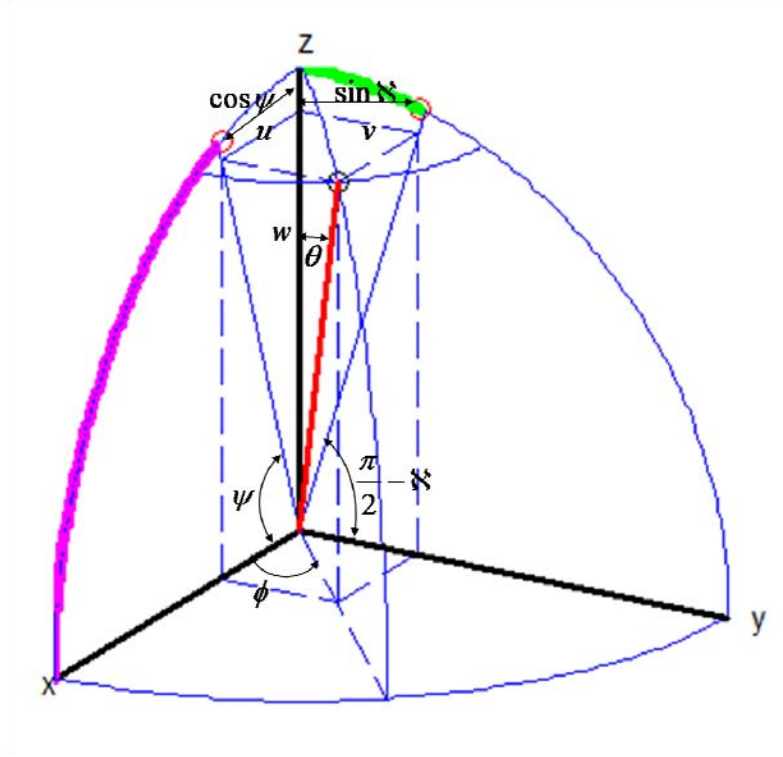


Figure 88. Arc-length element rotation compared to approximation using angle projection.

First considering paired communications between the check Node A and Node B, the ideal power transfer in free-space transmission can be determined from Equation (52) by neglecting orientation factors, which would alter transmit element gain, G_t , receiving element gain, G_r , and polarization, ρ . Actual power transfer may be measurably less than the ideal value, and the difference is (for this model) attributed to orientation. A single element's projected gain efficiency, $f_{norm}(\pi/2 - \psi)$ from Equation (174), or polarization, $\rho(\aleph)$ from Equation (175), where ψ and \aleph are as shown in Figure 87 can be used to display in Figure 89 how the gain efficiency and polarization mismatch factor change by applied angle, are thus associated to the difference between ideal and actual transmission.

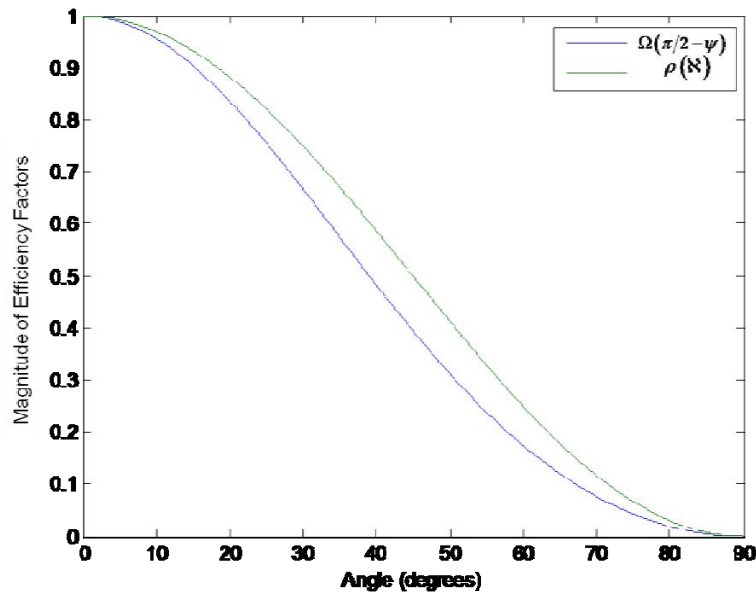


Figure 89. Magnitude of efficiency factors for gain pattern and polarization versus function angles ψ and \aleph , respectively.

Conversely, a range of potential angles, ψ and \aleph , can be determined from the power difference when the orientation is unknown. Figure 90 shows the ranges of potential angles with a variety of magnitude drops.

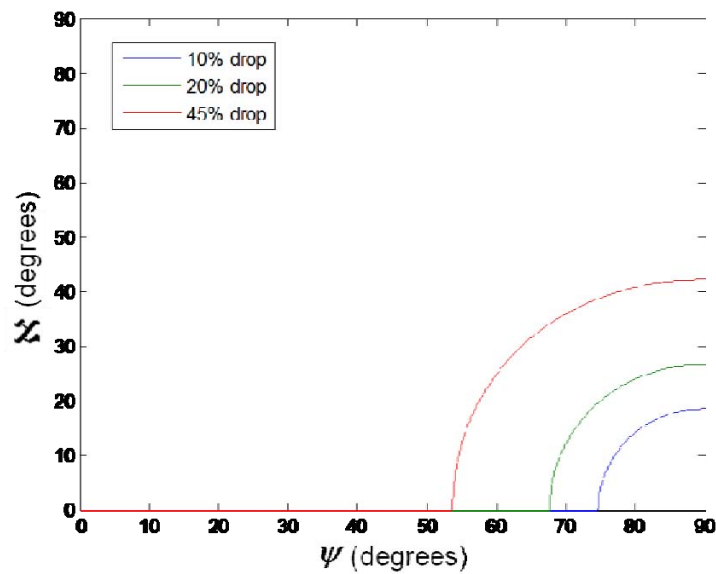


Figure 90. Example of potential function angles for pattern and polarization in a communications pair with a variety of drops from ideal.

In the static case where the specific orientations for Node B and Node C are known in reference to Node A, simple geometry may be used to determine their orientation with respect to one another. A set of elevation and polarization angles for Node B (ψ_B, \aleph_B) and Node C (ψ_C, \aleph_C) can be translated back into the spherical system $(\theta_B, \phi_B, \theta_C, \phi_C)$ with respect to Node A, using Equations (176) and (177). The azimuth angle for each can then be rotated by γ_B and γ_C , respectively, to reflect geometric position. These angles are not in the calculations, but instead within the algorithm connecting the two elements to the reference plane. The coordinates of Node B and Node C may then be rectified, placing Node B at the center of the local coordinate system. Again, a tangent function may be used to determine the angle from the x -axis to Node C, denoted as γ_{BC} . Rotating azimuth angles for both nodes by γ_{BC} to place Node C on the x -axis, the angles (ψ_{BC}, \aleph_{BC}) and (ψ_{CB}, \aleph_{CB}) are determined from Equations (176) and (177). Based on these angles, a transmission factor, \mathbb{F} , between Node B and Node C may be formed based on the gain pattern of the transmitting element, the gain pattern of the receiving element, and the cross-polarization of the pair. The transmission factor can be written using Equations (174) and (175), as

$$\mathbb{F} = f_{norm_t}(\psi_{BC}) f_{norm_r}(\psi_{CB}) \rho(|\aleph_{BC} - \aleph_{CB}|) \quad (182)$$

where Equation (52) is re-written as

$$P_r = \frac{(1.64)^2 P_t}{\left(\frac{4\pi d}{\lambda}\right)^2 L_o} \mathbb{F}(\psi_{BC}, \aleph_{BC}, \psi_{CB}, \aleph_{CB}) \quad (183)$$

Returning to an evaluation without known orientations for Nodes B and C, a stochastic distribution applied using the wobble factor provides greater insight into the system, and it is from the following method that behavior is evaluated. First, assignment of respective wobble factors (w_B, w_C) for Nodes B and C is necessary. As noted, this is based on physical parameters of motion. The wobble factors are then translated into expected pitch and polarization factors against the reference element using a reference 45° azimuth angle and Equations (176), (177), and (182). It should be noted that

Equation (182) is applied against the reference node in this instance vice between Nodes B and C. The reference factors are then re-applied to determine the expected magnitudes of each to the reference node using a Gaussian random tilt angle (θ_B, θ_C) and a uniformly random azimuth angle (ϕ_B, ϕ_C) . The next step takes the determined magnitude and, using a newly determined value for azimuth angle (ϕ_B, ϕ_C) from a uniform distribution, establishes the associated tilt angle (θ_B, θ_C) . This second step decouples the initial magnitude assignment from the original determination angles. With the tilt and azimuth angles with respect to the reference node defined through the first two steps, the third step uses the known angles and locations to establish orientation between Nodes B and C, (θ_{BC}, ϕ_{BC}) . This information is then used to solve for relative pitch and polarization between the two nodes, $(\psi_{BC}, \psi_{CB}, \aleph_{BC}, \aleph_{CB})$. Finally, the transmission factor in Equation (182) is re-applied for the specific instance solution.

The transmission factor for wobble factors $w_B = 5^\circ$ and $w_C = 5^\circ$ were first evaluated, with the results from 50,000 runs shown in Figure 91.

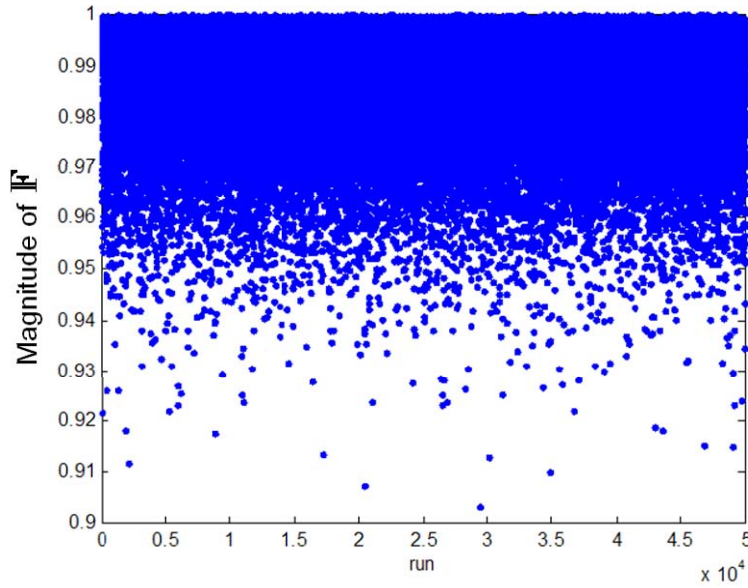


Figure 91. Transmission Factor over 50,000 runs for $w_B = 5^\circ$ and $w_C = 5^\circ$.

It is clear from the figure that the transmission factor does not vary greatly in the $w_B = 5^\circ$ and $w_C = 5^\circ$ case. Considering further cases allows this to become constructive. Figure 92, Figure 93, and Figure 94 respectively demonstrate cases for $w_B = 8^\circ$ and $w_C = 10^\circ$, $w_B = 15^\circ$ and $w_C = 15^\circ$, $w_B = 15^\circ$ and $w_C = 20^\circ$.

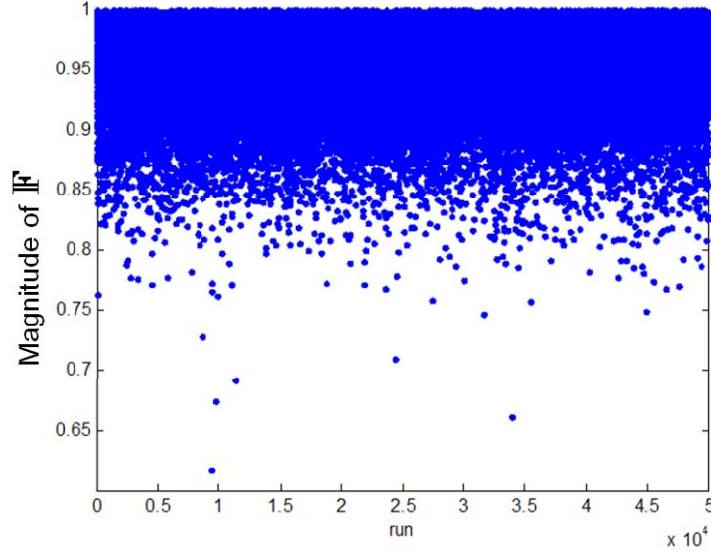


Figure 92. Transmission Factor over 50,000 runs for $w_B = 8^\circ$ and $w_C = 10^\circ$.

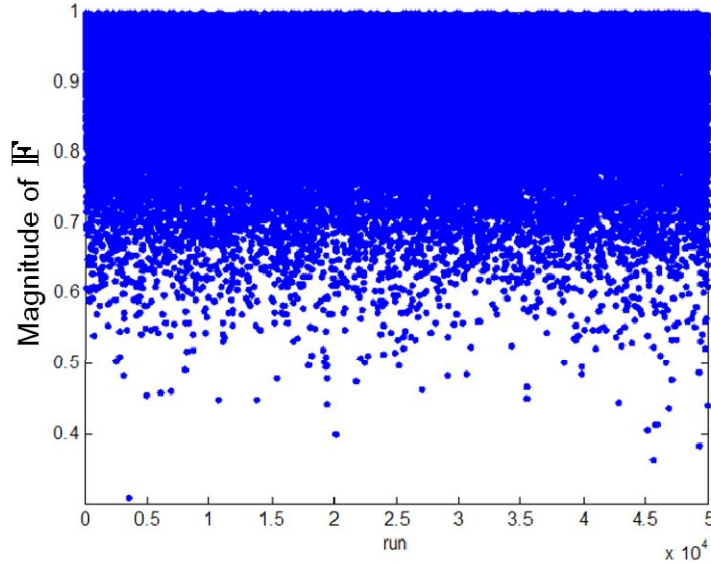


Figure 93. Transmission Factor over 50,000 runs for $w_B = 15^\circ$ and $w_C = 15^\circ$.

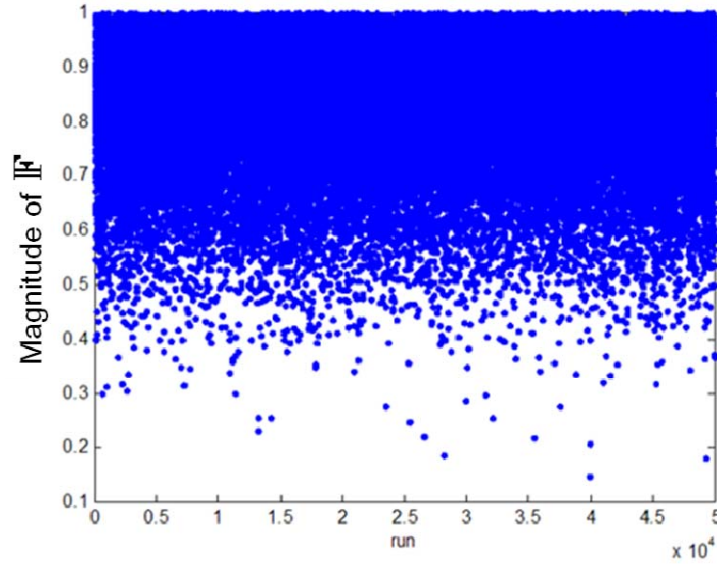


Figure 94. Transmission Factor over 50,000 runs for $w_B = 15^\circ$ and $w_C = 20^\circ$.

Observing the figures created, the transmission factor appears to reside within a random distribution when element orientation stability reflects the physical properties described. A histogram of the individual cases shows this to be true as illustrated in Figure 95 – Figure 98. The histograms are compared to a beta distribution (See Chapter II.A.3). The red line indicates the progression of the normalized beta stochastic distribution with mean and variance parameters matched to the collected data. The Beta distribution appears to provide a tight fit to the model data for the angles shown.

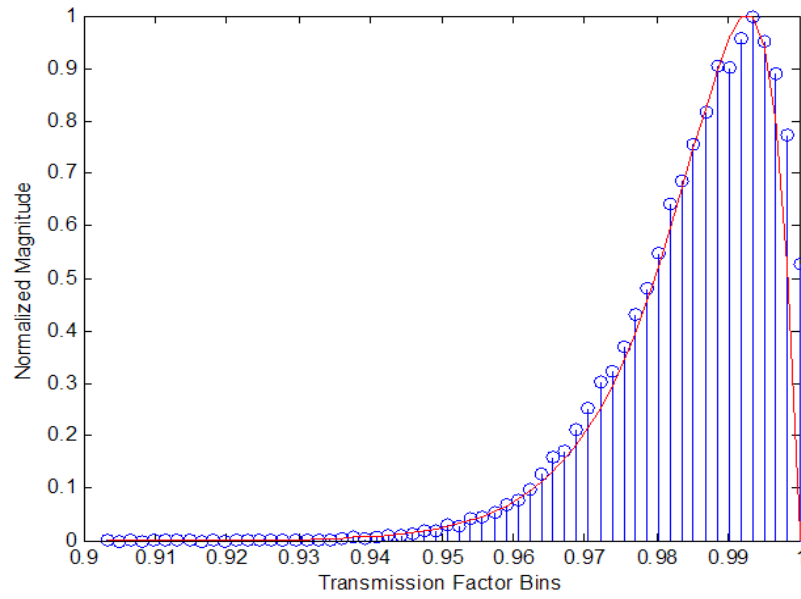


Figure 95. Histogram of transmission factor, \mathbb{F} , compared with a beta distribution, where $w_B = 5^0$ and $w_C = 5^0$.

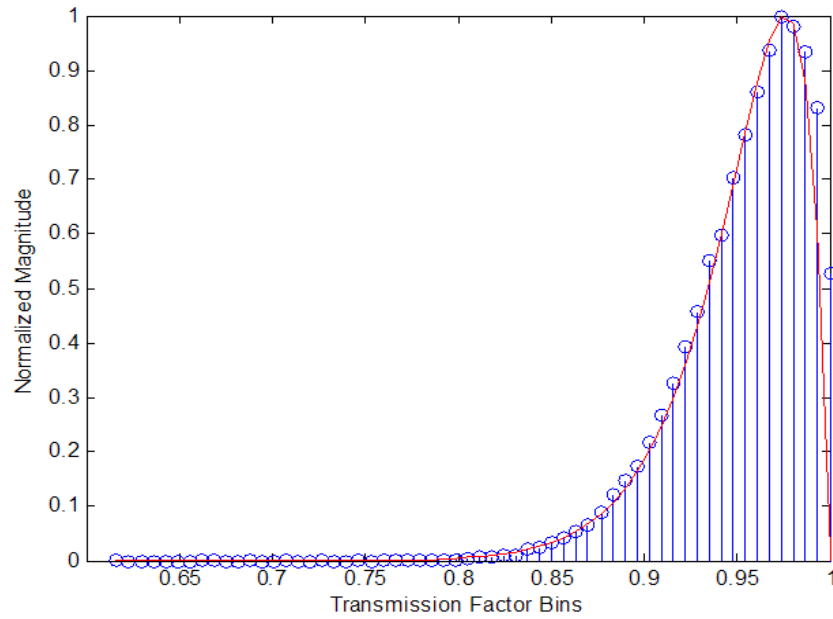


Figure 96. Histogram of transmission factor, \mathbb{F} , compared with a beta distribution, where $w_B = 8^0$ and $w_C = 10^0$.

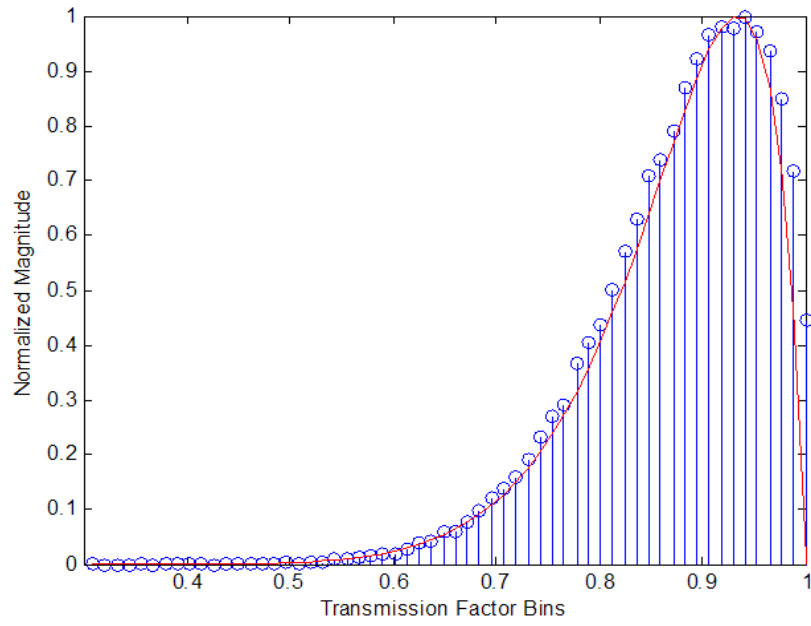


Figure 97. Histogram of transmission factor, \mathbb{F} , compared with a beta distribution, where $w_B = 15^\circ$ and $w_C = 15^\circ$.

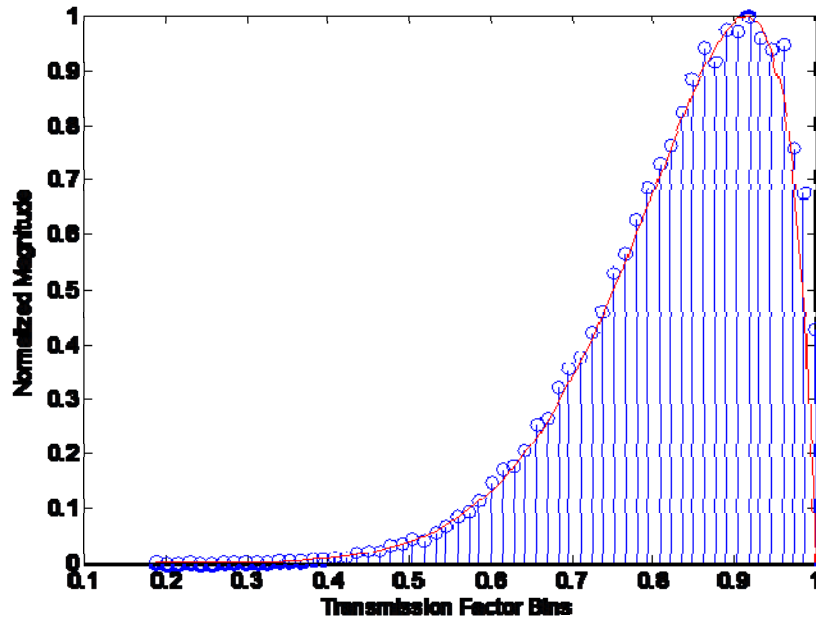


Figure 98. Histogram of transmission factor, \mathbb{F} , compared with a beta distribution, where $w_B = 15^\circ$ and $w_C = 20^\circ$.

Formalizing the association of the beta distribution, a goodness-of-fit comparison can be performed. The chi-squared test to determine goodness-of-fit, from [22], is appropriate for this comparison. Using the tools available on [69], the beta distribution demonstrates an extremely tight fit in each case, with a p-value of 1 for each case shown over 58 bins. Therefore, the measured beta distribution is a suitable model for the transmission factor, \mathbb{F} , in the pair-wise connection.

Two additional factors of the model to note are that the physical distribution of the nodes is only used to determine rotation factors for the elements, and, since the azimuth angles of the respective elements are varied through a uniform random variable, the specific positions have no bearing on the resulting distribution. Further, the check node, Node A, is only used to mathematically determine the beta distribution, so there is no need to physically realize the check node to implement. The result is a model distribution that may be implemented on any pair-wise communications involving unstable orientations without respect to position.

The need to conserve energy in the network demands a balance between transmission energy and bit errors allowed. Determining the energy per bit over noise power spectral density, E_b/N_o , as an indicator of robustness is appropriate, because it can be related to bit error rate dependent on the modulation technique employed. Therefore reaching a desired mean E_b/N_o will be considered for an operational goal.

Establishment of a blanket transmission power increase within a network due to orientation concerns is a general engineering response to managing the link budget across a connectionless network. This tactic provides a safe cushion to assure a desired signal quality to the receiver. However, application of the proposed model on a pair-wise basis offers the opportunity to tailor an individual transmission power for each link, maintaining a desired mean for E_b/N_o at an energy savings compared to the blanket margin method.

Consider a sensor network containing K sensors. A subset of k sensors may be required in a multi-hop scenario when communications must link back to a data sink in that manner. Without regard to orientation, transmit power levels for each hop can be

determined by distance between nodes using Equation (52) to meet the P_r necessary for a desired E_b/N_o . Total transmission power expended is determined by summing transmission power in each link as

$$P_{TOT} = \sum_{i=1}^{k-1} P_{T_i} \quad (184)$$

In a blanket increase scenario, the transmitted power for each link is increased by a uniform percentage, η , to compensate for expected loss due to orientation mismatch. This percentage is generally chosen to address expected or measured worst case scenario. The resulting total power due to transmission when using this blanket method, P_{TOT_B} , can be written as

$$P_{TOT_B} = \eta \sum_{i=1}^{k-1} P_{T_i} \quad (185)$$

Using the proposed model, a transmission power increase, Φ , can be determined for each hop. Considering a simple increase to maintain the mean of received power, the increase can be determined as

$$\Phi = \frac{1}{E[\mathbb{F}]} \quad (186)$$

where Φ must determined for each hop. Multiplication by this factor resets received power to a proper mean. Figure 99 demonstrates this shift of the histogram by subtracting the power associated with the uncorrected example where $w_B = 15^\circ$ and $w_C = 20^\circ$ shown in Figure 98 from a signal corrected using Φ . The resulting signal histogram has a mean approaching zero.

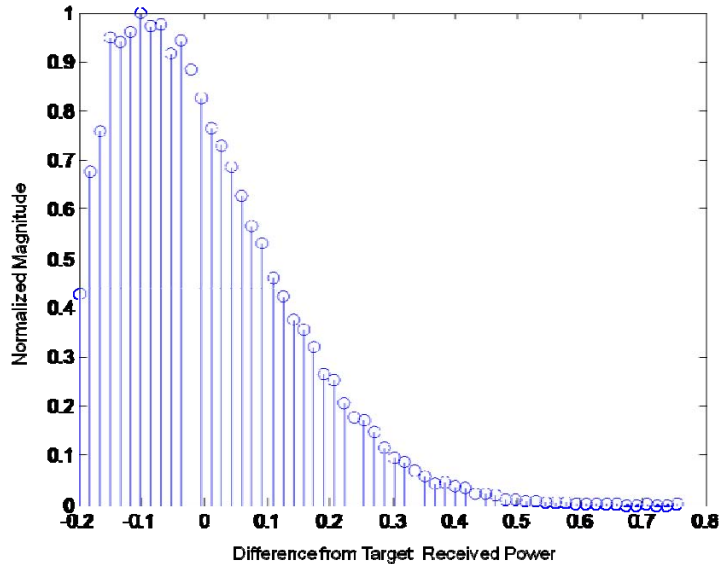


Figure 99. Histogram of normalized signal magnitude distribution in a signal hop with the model based correction factor, Φ . Target received power is arbitrary power units based on application.

Now, considering the total power due to transmission using the proposed model and increase from Equation (186), it may be written as

$$P_{TOTP} = \sum_{i=1}^{k-1} \Phi_i P_{T_i} \quad (187)$$

Since the blanket increase percentage, η , was determined to assure margin over the worst case, we know $\eta \geq \Phi$ for all hops. So the power savings, ΔP , is

$$\Delta P = \sum_{i=1}^{k-1} P_{T_i} (\eta - \Phi_i) \quad (188)$$

Therefore, the proposed method is preferable for meeting desired transmission goals in terms of energy cost and moderating potential bit errors.

The proposed model and compensation technique are therefore applicable when considering pair-wise communications between elements that have unsteady orientation. This model is easily applicable between any two nodes and can be done on a link by link basis in a multi-hop scenario. Application of the proposed model and compensation technique effectively shifted the mean of the received signal back to the intended

location. Direct comparison between this technique using the proposed model and the general case of a margin increase across the network demonstrated the savings of the proposed technique while meeting mean performance goals. The result of this effort is a model, which may be generally applied to meet physical layer requirements in a sensor network while preserving node energy – extending network life while meeting operational requirements.

This chapter submitted novel proposals to contend with noted issues in beamforming in a wireless sensor network with independently mobile elements. A management method, stochastic relationship between element motion and beamforming solution, algorithm for asynchronous timing update determination, and stochastic relationship between orientation and communications link performance are presented. The individual proposals are demonstrated to assist the system in meeting operational requirements while reducing system energy requirements versus alternative methods. The next chapter will apply these methods to an operational scenario in order to demonstrate a titular application.

THIS PAGE INTENTIONALLY LEFT BLANK

V. CAPSTONE SIMULATION USING THE PROPOSED TECHNIQUES

Analysis of specific aspects regarding the operation of an sensor network for reception of radio frequency signals through use of beamforming techniques has thus far resulted in increased insight into the beamforming process and a set of proposed techniques to mitigate issues that have been identified when sensor nodes are independently mobile. The techniques in Chapter IV have been demonstrated to enable specific results necessary to meet the goals attributed to them. In this chapter, the operational setting from Chapter I will be used to demonstrate application of the individual techniques cooperatively within a simulation demonstrating both the effectiveness of implementation and the ability of each technique to harmonize within the system. It will be shown that the broad methods proposed can be implemented for a specific target based on scenario boundaries and operational goals.

The role of a radio frequency signal intercept operator supporting unit operations was described in Chapter I. In brief, a radio frequency signal intercept operator has the responsibility of providing indications and warning of potential threats to his unit based on his surveillance of the radio frequency spectrum. As further described, the ability of the operator is limited due to the requirement to operate only equipment that is man-portable in a potentially hostile environment. From a physical layer point of view, this may translate into a limitation in terms of available apertures such that the radio frequency environment is only viewable through an omni-directional element. In an effort to provide access to the radio frequency spectrum offering greater directivity and gain, the use of an array was discussed; however, the operational array must still meet the constraints of the operational environment, including man-portability, while introducing the constraints associated with beamforming arrays, such as known positions for phase weights. Through application of the techniques proposed, the ability to operate such an array in this manner is demonstrated. It is important to note that this simulation is not offered as an all-encompassing collection of potential operational scenarios. The scenario applied is instead chosen as an academic tool for physical demonstration of the

proposed techniques within a single environment. Clearly specific target signal and operational constructs are the driving factors in the determination of use for any method.

A. MODEL SETUP

The operational setting shown in Figure 1 can be used to set the operational tone. A unit consisting of multiple members is advancing towards a common geographical goal. In an ideal situation, unit members are arranged and remain in formation as they advance towards the goal. Such an ideal situation discounts varying member speeds, ability to locate and maintain position, non-homogenous terrain, and potential interaction within the unit, among other numerous rationale for non-ideal individual motion. A comprehensive description of the non-ideal case of motion is beyond the scope of this research, but it is enough to state that the reality of motion in such a case is that unit member motion will vary individually in terms of speed and direction. While a variety of models could be used to simulate the random actions of this motion, the interaction of unit members regarding motion makes pinning down expected motion difficult; therefore, the concept of an agent based model is necessary.

As introduced in Chapter II.A.5, agent based models use interaction rules to determine a most-likely outcome based on randomized conditions. The U.S. Army and U.S. Marine Corps have a variety of agent based models, which they use in the development of scenarios to evaluate tactics, techniques, and procedures in warfighting. Since the target scenario supposes movement in a military operations setting, use of one of these models is appropriate. The U.S. Army Training and Doctrine Analysis Center in Monterey, California, part of the Army's Training and Doctrine Command headquartered at Fort Leavenworth, Kansas, provided access to the modeling tool Pythagoras [77]. Pythagoras is agent based simulation software designed to integrate both physical aspects and human reaction into combat scenario modeling. Therefore aspects such as terrain, individual ability, and decision making in combat are available in considering motion for individual unit members.

The basic scenario considered, that of a unit crossing a field, was entered into Pythagoras in order to determine the most likely motion and formation. This information

is then used as the driver in the simulation. Limitations in the software prevent a direct entry and retrieval of soldier positions at minute definition levels. This is primarily because Pythagoras limits the operational field to a set of two-dimensional pixels sized 1000×1000 . The meaning of individual pixels in terms of size is at the user's discretion; however, it is obvious that assignment of one meter to each pixel results in a field of 1000 meters in length and width. Smaller pixel sizes necessary to capture more diminutive motion then has the effect of shrinking the field. An example of this is assignment of the distance 0.0001 meter per pixel results in a field of only 0.1 meters in length and width, too small for use in this scenario. Further complicating entry is the software requirement that mean speed be represented as an integer.

It is at this point that the potential target signal must first be considered. It has already been established that motion as minute as 0.0001 pixels per meter creates a field too small for physical motion modeling with multiple agents; so, larger distances must be assigned to pixels. Consideration of the target signal must again be considered to assure that distance translation does not model motion too gross for analysis. As an example, if a target signal has a wavelength of 0.5 m, then movement of 1 meter per pixel creates too great a change in array pattern to be of use. For simulation use, a target signal is selected. A channel is selected with a center frequency of 37.5-MHz, common for push-to-talk radio. This center frequency translates into a wavelength of 8 m, using Equation (31) assuming a propagation velocity at free-space. Considering wavelength to remove overly gross pixel distance assignment and field size to limit overly minute assignment, a determination of 0.02 meters per pixel is chosen. This results in a field size of 20×20 square meters.

Assignment of time steps within the model is the next issue. Again, the target signal must be considered in this determination as analysis is concerned with position changes on a sample-by-sample basis. Considering the choice of an analog the push-to-talk target, a bandwidth of 4 kHz is assumed. Obviously, larger bandwidths may be applied for specific simulations. A sampling rate of 10 kilo-samples per second, two and a half times maximum frequency, is used; the sampling period is then 0.0001 seconds.

Using the information regarding sample interval and pixel distance, the speed of motion is then considered. As noted, mean speed within the model must be an integer, representing the number of pixels traversed per time step. As the scenario considers pedestrian speeds assigned to a military unit, a mean transit velocity of seven miles per hour (roughly 3.13 m/s) is chosen. The result is 0.01565 pixels per time step, which is obviously not an integer. In order to reach integer status, the time step must be extended and interpolated for smaller steps. Therefore, time step is chosen as 0.01 seconds resulting in a model velocity of 1.5 pixels per time step, rounded up to two pixels per time step. The result is a mean velocity of almost nine miles per hour. Although this speed is fast, the model allows compensation through terrain selection.

Further addressing the size of the perspective field, it will be assumed that the proposed unit is comprised of over 50 members. Unit members must have adequate spacing to assume formation and maneuver towards the geographic goal. Since the selected pixel distance does not allow for necessary spacing, an alternative method for introducing the unit in total to the model is necessary. In order to accomplish placing all members within the model, the unit was broken into individual details, small groups of unit members, such that overall motion is evaluated in two phases. In the first phase, the motion scenario for individual agents in each detail is considered. An example of a scenario run in this phase is shown in Figure 100. Then each detail is entered into the model as a group so that motion between details is captured, as shown in Figure 101. The results from the position and motion in the second phase ripples back to adjust positions for each unit member. In this way, full unit motion is captured at a level allowing for motion analysis within the context of the scenario and proposed operations.

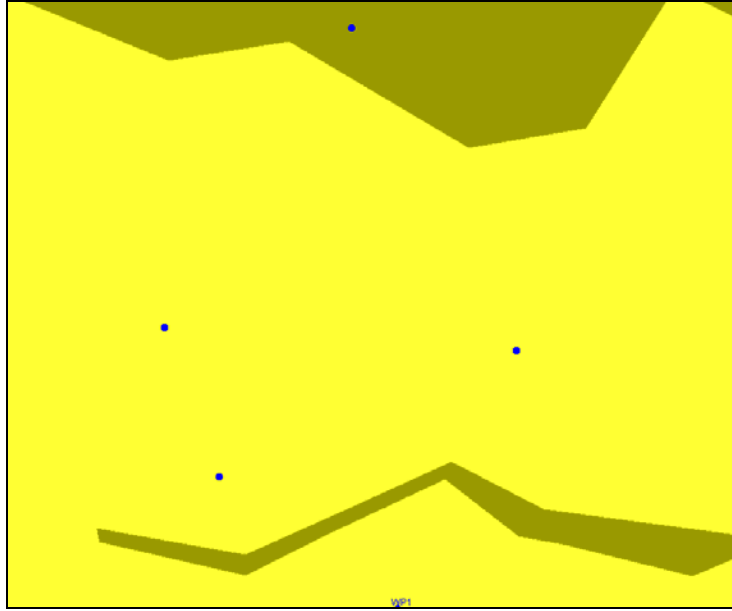


Figure 100. Agent position in Pythagoras modeling in first phase level showing individual unit member interaction where each dot is an individual agent, the yellow background indicates terrain, and the brown notes terrain changes (in this case, “road” conditions).

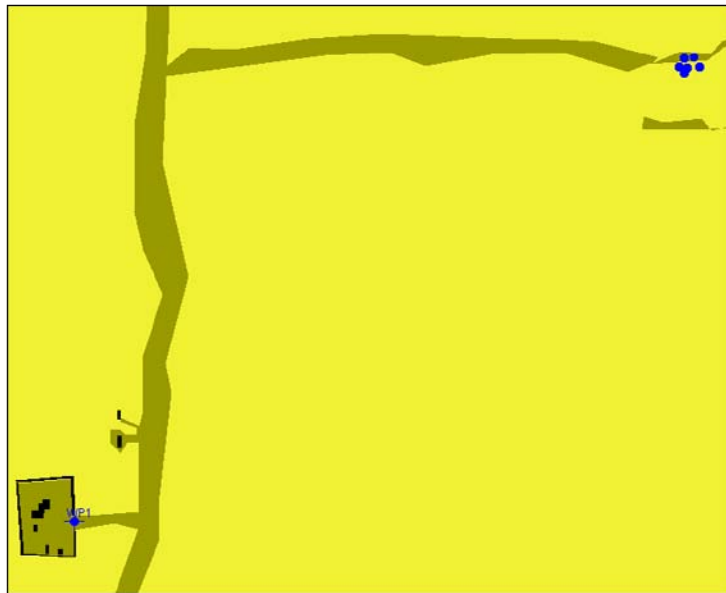


Figure 101. Detail position in Pythagoras modeling in second phase showing detail group interaction where each blue dot is a unit with multiple agents, the yellow background indicates terrain, and the brown notes terrain changes (in this case, “road” conditions).. The blue dot on the lower left represents the way-point motion goal.

The specific positions for each agent at individual time steps is available from the modeling software. Table 4 displays an abbreviated listing of agent position, indicating pixel positions at time steps for four separate agents. Translation to elapsed time, physical distance, and rectification to a reference point is necessary in applying this data to the scenario.

Table 4. An abbreviated listing of agent position versus time step.

timestep	1		2		3		4	
	X	Y	X	Y	X	Y	X	Y
1	63	845	679	275	99	431	543	464
2	63	844	679	274	100	430	544	464
3	63	844	678	272	101	430	544	464
4	63	844	678	272	102	430	544	464
5	63	844	678	272	103	430	544	464
6	63	844	678	272	104	429	544	464
7	63	844	678	272	105	429	544	464
8	63	843	678	272	106	429	544	463
9	63	843	677	271	107	428	544	463
10	63	843	677	271	108	427	544	463
11	63	843	677	271	108	427	544	462
12	63	843	677	271	109	426	544	462
13	63	843	677	271	110	425	544	461
14	63	843	676	270	111	424	544	461
15	63	843	676	269	111	424	544	461
16	63	843	676	269	112	424	544	461
17	63	843	676	268	113	423	544	460
18	63	842	676	267	114	423	544	460
19	63	842	676	267	115	422	544	460
20	63	842	676	267	116	421	544	460

B. APPLICATION OF TECHNIQUES

Of greatest initial interest is the management of resources in the sensor network to effect beamforming. As described in Chapter IV.A, management is a factor of the ability to divide the overall sensor network into groups that are optimized for signal detection based on established probability of detection and false alarm rate criteria. In order to establish an initial groups, a couple of factors are considered. The first of these is

considering the far field region of the array. From Equation (35), the general far field division can be found after the aperture size, D , is established.

The second factor to consider is the extent of signal propagation at the frequency of interest. This distance of propagation is not expressly used in the management algorithms from Chapter IV.A or Chapter IV.C, but it is helpful in understanding distance locations for potential targets. The target signal center frequency resides in the lower end of the Very High Frequency (VHF) range. Communications in VHF tend to be limited by line of sight propagation. Diffraction caused by curved earth may extend propagation slightly further than line of sight distance. From [15], a general extended line of sight distance equation is available based on geometry, as

$$d = 3.57 \left(\sqrt{kh_1} + \sqrt{kh_2} \right) \quad (189)$$

where h represents the height of each aperture in meters, the result d is in kilometers, and k is a factor representing refraction and is typically assumed to equal $4/3$ for standard atmospheric conditions. Assuming $h_1 = h_2 = 1.8\text{m}$, the extended line of sight distance over a smooth earth can then be expected to be about 11,060 m.

The next critical factors requiring consideration are detection probability and false alarm rate. These are both operational specifications in terms required in the algorithms proposed. Using the Neyman-Pearson detection criterion, the false alarm rate will be set below an allowable level and the probability of detection will then be maximized for that condition. From the proposed technique, a normalized communications scheme will be considered such that the gain necessary to reach the desired detection probability can be formed. From this gain, the number of array nodes is determined, which is used in turn to define the sub-area for selection in conjunction with the desired beamwidth. For the simulation, a required false alarm rate of $P_{FA} = 0.25$ and desired detection probability of $P_D = 0.8$ are selected. Considering the solution set, as shown in Figure 69, the receive aperture requires a gain slightly over 6 dBi in order to achieve detection. As noted in Chapter IV.A, array factor gain does not have a direct relationship with the number of elements unless the array geometry is considered. As the potential geometry is random, the proportional relationship is instead required. Further, it is obvious that element

participation can only be made available in integer numbers, so a gross figure is chosen to meet specifications. Relating the required gain solely to the array factor component and considering the expected relative spacing of elements, a value of $N = 6$ is chosen.

The sub-area, A_s , within the sensor network is then determined allowing for an adequate number of available elements with respect to the desired beamwidth. From the motion simulation, the initial positioning of the agents is depicted in Figure 102. The sub-area is selected as shown in Figure 103, where the reference point for location has been shifted to the center of the area. In this case, there are enough nodes for three separate node iterations in the sub-area. The nodes colored red are selected for the initial beamforming iteration.

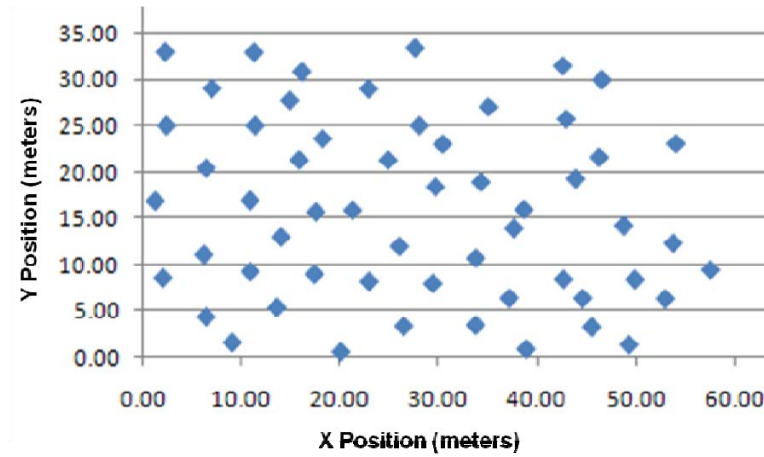


Figure 102. Agent positions translated to meters with a single reference point.

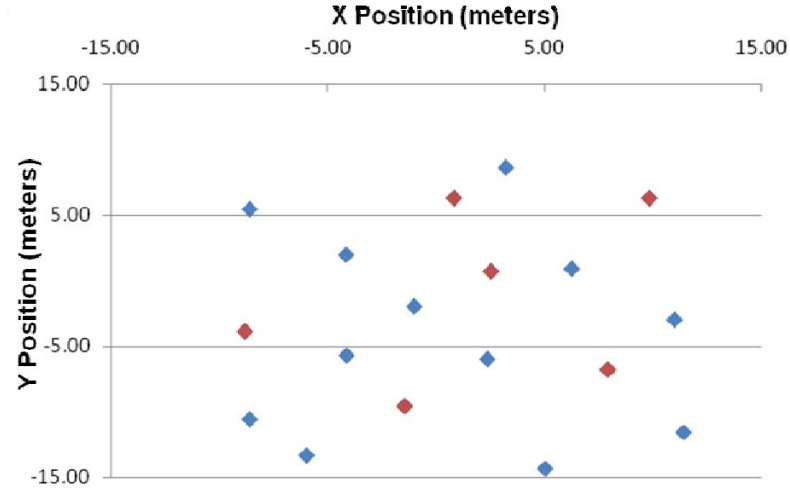


Figure 103. Sub-area agent positions with reference point shifted to the center of the sub-area. Agents depicted in red are selected for the initial iteration.

Considering the greatest distance between exterior nodes in the iteration for a conservative measure of aperture size, it can be determined that $D = 21.23$ m. Referring to Equation (35) and the determined wavelength of 8 m, the beginning of the far field region for the array, d , can be estimated as 212.3 m. Further, considering the spacing between nodes and the grating lobe relationships shown in Chapter II.B.3, it can be expected that some large sidelobes off the main beam will exist. These lobes will not be of the magnitude of grating lobes as the distribution of the elements are not symmetrical; however, they may be very large.

Considering the initial distribution of the first iteration, the coherent array beam formation in free space can be calculated and is shown in Figure 104. This array factor result assumes the target angle resides in the x - y plane and is at an azimuth of along the negative y axis. This iteration, without motion, provides an array factor maximum gain of 7.4 dBi. Figure 105 shows the normalized cross-section of array factor pattern in the plane of interest.

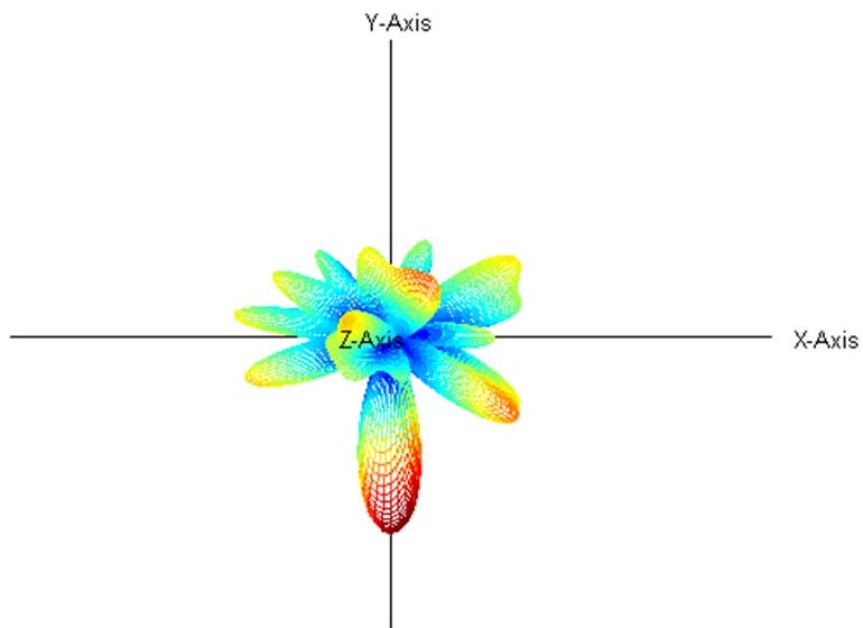


Figure 104. A three-dimensional depiction of the coherent array beamforming result from the first iteration.

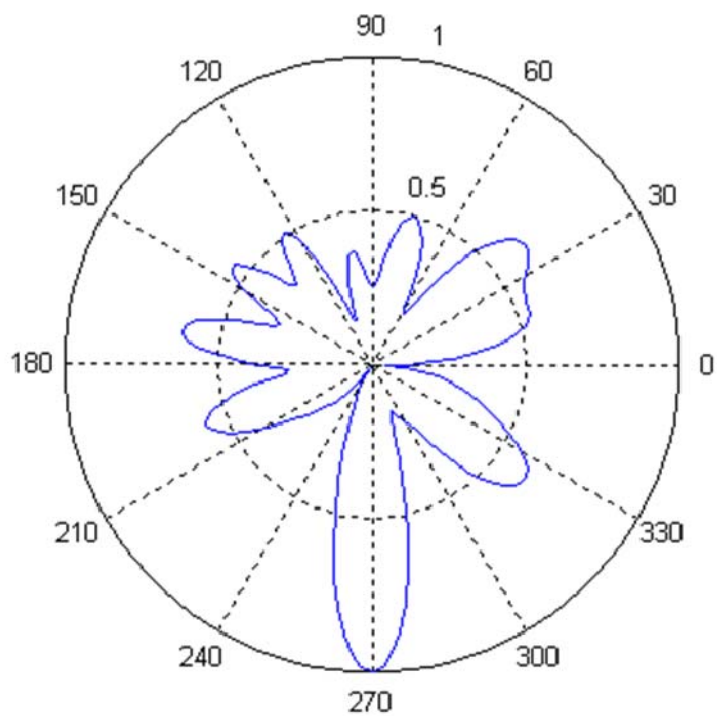


Figure 105. The normalized array pattern in the x - y plane from the first iteration.

The percent change, \mathbb{C} , as defined in Chapter IV.B is the next important parameter to consider. Choosing percent change threshold as 10%, a determination of time allowed until weight reset can be estimated according to the proposed method in Chapter IV.C. Of further importance is the selection of the constraint affect regarding the threshold value. As the potential random motion of each agent will be used to form a probability space against the threshold, the desire to remain above the threshold is subjective to design. A desire to remain above the threshold at all times would translate a physical situation of constant position updates. In converse, the flexibility to bypass the threshold by too great a measure makes the requirement lax. In order to maintain a useful and physically understandable simulation, the requirement to remain above the modified threshold will be placed approximately at the probability density function median, such that reset occurs when

$$\Pr\left(G_{m_i} \left| \sum_{i=1}^N e^{j\zeta_i(x_i+v_{x_i}t, y_i+v_{y_i}t, z_i+v_{z_i}t, \theta_o, \phi_o)} \right|^2 \leq \gamma\right) = 0.5 \quad (190)$$

It should be noted that this simulation does not include alternating between iterations as is part of the proposed method. This is because simulation of that aspect increases the complexity of description, and it is not a critical piece for demonstration.

The choice of \mathbb{C} allows for the determination of the modified threshold constant, γ , from Equation (148). This value is calculated as $\gamma = 29.7$ and must then be used in the probability determination in Equation (190). Within the solution for the timing, it is important that maximum velocity of the agents be specified based on potential relative maximum motion in components. As discussed in Chapter III.A, only motion relative to the element space is of interest compared to motion relative to an external fixture. Therefore, for the scenario applied based on relative motion of agents, the estimated weight reset time value is $t = 125$ msec. With the sampling rate identified, this timing is equivalent to resetting phase weights after 1250 samples. Clearly, this is a savings in terms of provision of meta-data. It is assumed, as discussed in Chapter IV.A, that the processing of weight rest and signal reception is performed in post-processing equipment without the constraints of energy associated with the forward nodes.

Agent motion from the Pythagoras model scenario at reset time indicates a percent change of 9.1%. A cross-section of the array factor compared with the initial array factor is shown in Figure 106. For further comparison, Table 5 shows the percent change, \mathbb{C} , associated with all three iterations in the sub-area due to agent motion from the Pythagoras scenario. The resultant change at the reset time is also visible in the cross-section comparisons from the second and third iterations shown in Figure 107 and Figure 108.

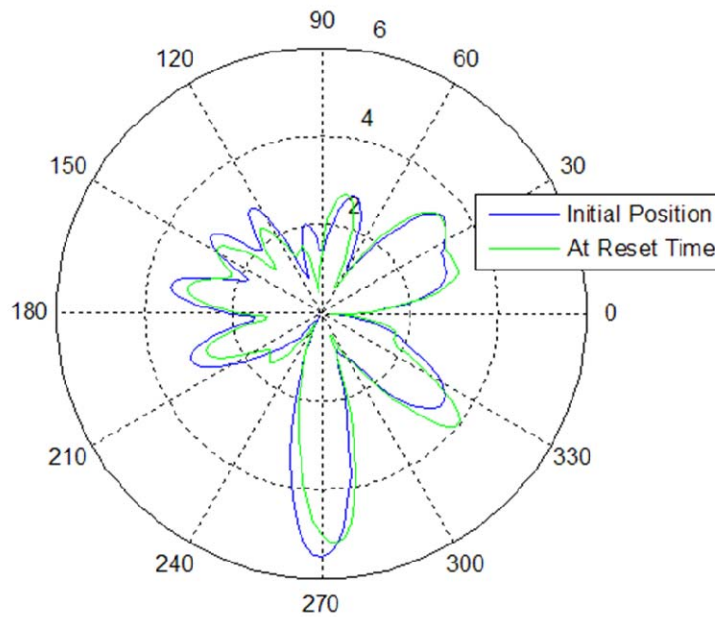


Figure 106. The two-dimensional cross-section of the array factor result at the time step indicated for change versus the initial configuration of the first iteration.

Table 5. Estimated reset time values and associated change percentage from Pythagoras agent motion.

Iteration	Initial AF Gain	Change Percentage at Reset
1	7.4 dBi	9.1%
2	7.1 dBi	8.9%
3	7.7 dBi	11.2%

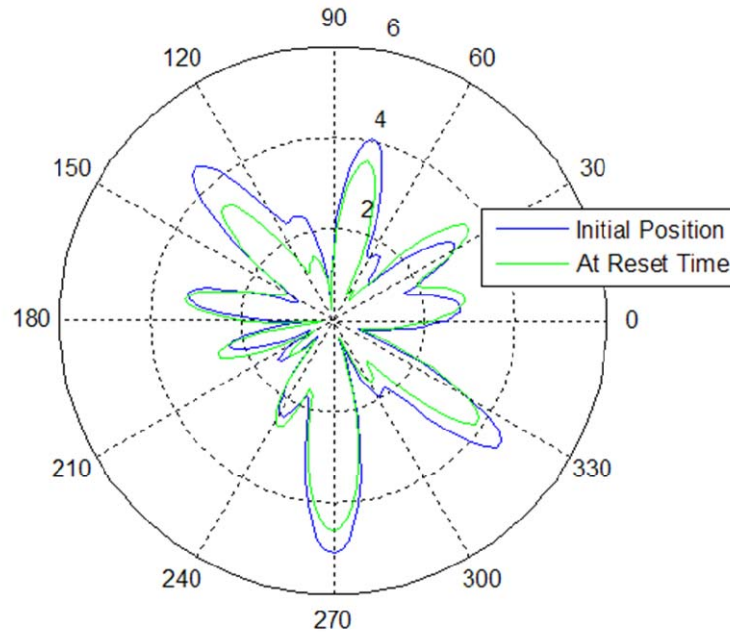


Figure 107. The normalized two-dimensional cross-section of the array factor result at the time step indicated for change versus the initial configuration of the second iteration.

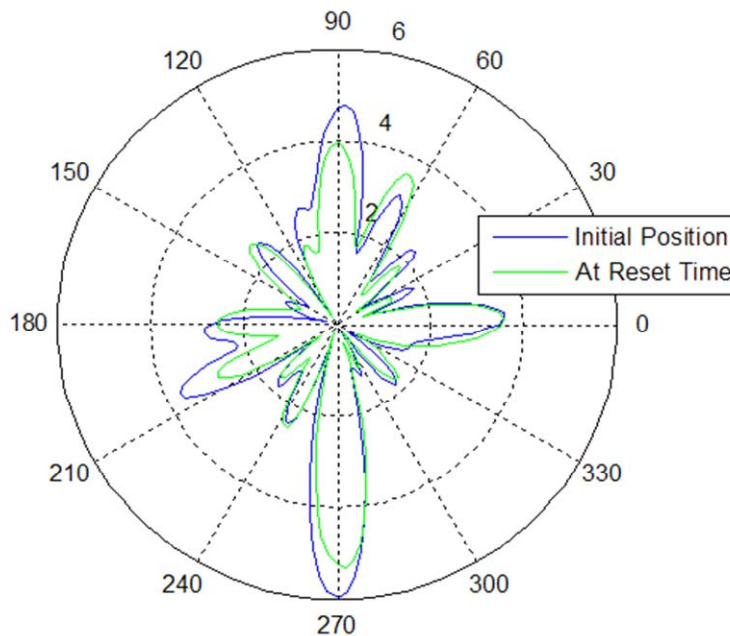


Figure 108. The normalized two-dimensional cross-section of the array factor result at the time step indicated for change versus the initial configuration of the third iteration.

Simulation modeling of unsteady tilt with regards to intra-node communications is less interesting because the Pythagoras model does not add further information for consideration. Although Pythagoras does use variations regarding agent health, motion, and surrounding terrain to determine progression within a model, it does not consider the posture of the agent in motion. Therefore, physical determinations regarding orientation are not uniquely available within the scenario.

In the model, agents are humans on foot moving toward a destination. Since the physical act of human motion does not lend itself to maintaining rigidly straight orientation, motion away from the desired orientation is certainly evident. However, the wobble factor associated to a soldier in combat gear with an estimated velocity requires physical science estimation. Based on the constraints of the scenario and the proposed method, interior network communications is then comprised of a pair of nodes with similar wobble factors. Alternatively, exterior communications to a tower or vehicle would instead indicate dissimilar wobble factors. Neither of these scenarios provides information past the models presented earlier in Chapter IV.D. However, Table 6 shows the resulting mean and variance for the beta distribution when wobble factors for agent to agent communications and agent to base station communications are assigned. In each case, the resulting beta distribution is expected.

Table 6. Beta distribution factors arising from assigned wobble factors for agent to agent and agent to base station links.

	Wobble Factor		Beta Distribution	
	Element 1	Element 2	Mean	Variance
Agent-Agent	17	17	0.84	0.011
Agent-Base	17	2	0.92	0.005

The results of this overarching simulation demonstrate that the individual proposed techniques can be applied cooperatively within a single scenario for operational efficacy. While, to some degree, they may be implemented on limited or individual basis contingent upon design goals, they are also able to operate in harmony against a specific target.

VI. CONCLUSION

In this research effort, the problem of constructing a coherent beamforming array was considered within the operational construct of a wireless sensor network. In a general sense, such an application requires a unique management methodology based upon the data requirement while maximizing network life. Further to the problem, each individual node may be assumed capable of independent motion. In such a case, the motion applied may be unrelated to the task of the sensors nodes such that coherent aggregation of the data may be difficult or communication among the nodes may limit participation.

Study focused on the ability to meet the operational goals of beamforming within the constraints provided. Initial analysis and literature review revealed insights regarding beamforming using random element distributions and the affect of imprecise knowledge of location. Although this research considered the array in a static sense, many of the related findings led to the dynamic case considered later. In the case of random element distribution, positive attributes were gained in acknowledgement of the existence of a generalized beamforming approach and the elimination of grating lobes. Of course, negative aspects accompanying random distribution, including sub-optimization of potential array factor gain effects, were also recognized. Further, research on imprecise element placement provided a scaling with regards to error in coherent combination.

The next step introduced motion among nodes. Considering a two-element model, basic motion effects on the beamforming solution were investigated. Study of stochastic motion by array elements provided information regarding the connection of node wavelength geometry to the target vector. From this information, deductions were made regarding the response of an array to motion. Available literature was helpful in providing the underpinnings of this analysis. Continuing the study of motion in an array, Doppler shift due to physical motion was found to be negligible in this particular application.

Research into array operation, due to intermittent node operation, demonstrated the direct effect of node loss during coherent signal combination. Particularly affected was the array factor gain; however, it was also noted that the beamforming solution was not slewed from the target aim point due to this phenomenon.

As a result of the background literature and analysis, a set of particular issues were selected, which required additional study and led to proposals of novel techniques for alleviation. These issues were overall system management of nodes in the wireless sensor network, degradation of beamforming with element motion, the need for a method to determine when to apply new weights, and the effect of unsteady antenna orientation on network communications. Novel methods for conducting coherent beamforming in a wireless sensor network with independent motion were then presented to address these issues. The proposed methods were demonstrated to produce better results than alternative techniques.

Finally, a simulation representative of a typical operational scenario was conducted to demonstrate the effectiveness of the proposed methods. The simulation was set up as a mobile array for a radio frequency intercept operator supporting a military transit across a field. This scenario does not limit applications of the proposed techniques but instead demonstrates how they may be applied against a specific problem.

A. CONTRIBUTIONS

The primary contributions of this dissertation come from the investigation of the beamforming problem with node motion and the novel techniques proposed to deal with the effects of motion on array pattern. These contributions can be seen in the conclusion reached on the negligible effect of Doppler shift due to physical motion in this application, the novel management system for the wireless sensor network focusing on sensor data requirements, the novel analysis of the effects of independent node motion on beamforming performance, the methodology proposed in determining weight reset times for the beamforming array, and the investigation and novel analysis developed regarding unsteady antenna orientation in pair-wise communications. Further contributions are also evident in the analysis of system energy cost and extending battery life.

The work demonstrated that Doppler shift due to physical motion of array elements provides negligible perturbation of the beamforming solution. This conclusion was based on simulation that showed negligible change in beam pattern in the specific application in which phase center is held constant. This result assisted in simplifying the solution methods developed to address other issues caused by nodes in random motion.

Management of resources in a wireless sensor network is a critical issue revolving around effectiveness of the radio frequency sensor scheme, optimization of individual node energy costs, and lifetime of the network power source. Previous research confirmed that sensor networks operate to their maximum potential only when all network nodes are available to participate. As such, in this work, two methods have been identified in management of sensor network resources. One method focuses on communications, since the act of transmitting data is generally a heavy drain on available energy. The other method centers on required sensor data. Since the operation of a coherent beamforming array is data intensive, communications links are stressed; therefore, a novel management method emphasizing node usage for sensor data is necessary and was proposed. The proposed method considered the primary operational metrics for a signal reception array and emphasized performance towards those goals. Specifically, signal detection is emphasized in system operations, and energy conservation across the network is then assembled based on that initial goal. Compared to alternative methods, the proposed method provided enhanced signal detection and better energy efficiency when a target signal was present.

The ability to operate a coherent beamforming array while array elements are independently mobile is a major thrust of this research. Although efficient management of individual sensor nodes allows such an array to exist, overhead from meta-data and constant array weight recalculation make operation untenable. The research on beamforming algorithms and their operation under non-ideal conditions enabled the proposed novel method of using a probability based scheme to manage this issue. The research demonstrated its contribution in that although the nodes exhibit independent motion, when combined with the beamforming structure a predictable pattern emerges based on a Rician ratio distribution. Knowledge of this distribution allows for delay in

resetting array weights for coherent combination. This revealed the potential to conserve energy in meta-data transfer as a further contribution, preserving energy in the network while continuing to provide array factor gain at the required level.

With the knowledge of a proposed management structure to operate a radio frequency signal sensor network and the distribution associated with an array with nodes in independent motion, consideration of the entire problem of a signal sensor array with mobile nodes was undertaken. A technique for implementation of these methods was thus required. The proposed algorithm was based upon an eight-step procedure. This novel method enables the previously proposed management method and the defined beamforming percent change distribution algorithm to work together in determining an optimal time for weight reset and demonstrates specific energy savings and/or performance improvement compared to alternative methods.

Proper function of a data intensive wireless sensor network requires solid communications links. In order to assist in improving data exchange when nodes are mobile, node orientation was considered. Antenna polarization and tilt may have a specifically deleterious effect on communications links, but they are often considered in a static sense. The proposed method combines physical motion and element attributes in a free-space link in order to assess the most-likely loss of power due to these factors. With this knowledge, a mitigation strategy was developed that successfully improved transmission performance. This method provided energy savings compared to alternative techniques while keeping required bit error rate at a desired level.

Each of the novel methods proposed within this research performs better than the alternative methods available in literature. Obviously each proposed method may be applied in unison or individually based on design intent.

B. AREAS OF FUTURE RESEARCH

Although the research covered numerous aspects of the problem concerning operations of a radio frequency signal reception wireless sensor network with independently mobile nodes and provided novel techniques to manage the most egregious issues, there are other areas available as potential follow-on research.

The array factor gain considered in formation of the proposed method for coherent combination assumes elements with similar orientation and specification. Indeed, it is known that mixing element types or orientations changes the effectiveness of the array. As mobile elements may hold unsteady orientation, consideration of how dynamic physical orientation affects combination is the next logical step in research. The model considering element orientation in link quality provides some insight but does not yet fully address coherent combination without returning to an element by element analysis or the active element pattern method.

Motion modeling in the array factor gain analysis did not consider predictive algorithms to extend reset timing. Analysis using predicative models, such as Kalman filtering or swarm behavior theory, may offer further opportunities to increase usefulness of the proposed stochastic method.

The model regarding unsteady orientation provides significant insight in the assignment of correction or margin transmission power values; however, the model was specifically created to consider communications in free-space with dipole elements. Since the model is based on fundamental physics within these models, the information promises to be transferable to more complex transmission scenarios. Application and effectiveness measurements within dispersive or multi-path environments would assist in physical implementation of this algorithm and increase potential applications well beyond the sensor network realm.

Synchronization in terms of time and frequency, while attributed to GPS in this study, have a number of remaining facets for actual implementation across a physically dispersed array. Analysis solely in synchronization techniques and errors in specified processing, instead of gross algorithm construction, will be necessary for eventual implementation. Additionally, while considering data loss and post-processing in this study, the concept of data latency may offer further considerations for analysis.

Implementation of the proposed methods in various circumstances promises to provide intriguing results. While the scenario of soldiers walking across a battlefield dominates the application wisdom in this research, a slew of potential independent

mobile platforms may be available for wide or narrow-spaced implementation, include mounting on a variety of sizes of unmanned vehicles.

A major issue across wireless sensor networks is determination of data quality for any given sensor. This effects performance in that data from a “bad” sensor affects the solution, and bad sensor data riding over the network expends energy in transfer, draining the overall network without providing usable input. Study on this aspect, with an eye towards high data rate sensor requirements necessitated in the proposed function would be of great value.

Finally, consideration of energy expenditures in the wireless sensor network may be taken further within the proposed framework. Contemplation of the potential for over-performance in provided gain in return for longer reset times may be considered against the additional energy necessary to provide over performance in an iteration. Such a study would need to be grounded in a specific implementation.

LIST OF REFERENCES

- [1] "Joint Vision 2020," U.S. Government Printing Office, June 2000, <http://www.dtic.mil/jointvision/jvpub2.htm>, last accessed November 2008.
- [2] "Joint Publication 1-02: Department of Defense Dictionary of Military and Associated Terms," U.S. Government Printing Office, April 2001 as amended September 2008, http://www.dtic.mil/doctrine/jel/new_pubs/jp1_02.pdf, last accessed November 2008.
- [3] I. F. Akyildiz, T. Melodia, and K. R. Chowdhury, "A Survey on Wireless Multimedia Sensor Networks," *Computer Networks (Elsevier)*, Vol. 51, November 2006.
- [4] R. E. Collin, *Antennas and Radiowave Propagation*, McGraw-Hill, Inc., 1985.
- [5] W. Chen, D. Wang, and W. Wang, "Beamforming for Information Transfer in Wireless Sensor Networks without Perfect Positioning," in *Asia-Pacific Microwave Conference (APMC 2005)*, Suzhou, China, December 2005.
- [6] R. Mudumbai, G. Barriac, and U. Madhow, "On the Feasibility of Distributed Beamforming in Wireless Networks," *IEEE Transactions on Wireless Communications*, Vol. 6, Issue: 5, pp. 1754-1763, May 2007.
- [7] H. Ochiai, P. Mitran, H. Poor, and V. Tarokh, "Collaborative Beamforming in Ad Hoc Networks," in *IEEE Information Theory Workshop (ITW 04)*, San Antonio, TX, U.S.A., October 2004, pp. 396-401.
- [8] P. J. Vincent, M. Tummala, and J. McEachen, "A New Method for Distributing Power Usage Across a Sensor Network," in *IEEE Conference on Sensor and Ad Hoc Communications and Networks (SECON 06)*, Reston, VA, U.S.A., vol. 2, September 2006, pp. 518-526.
- [9] M. S. Batson, J. C. McEachen, and M. Tummala, "Enhanced Collection Methodology for Distributed Wireless Antenna Systems," in *IEEE International Conference on System of Systems Engineering (SoSE 07)*, San Antonio, TX, U.S.A., April 2007, pp. 1-6.
- [10] M. S. Batson, J. C. McEachen, and M. Tummala, "A Method for Fast Radio Frequency Direction Finding Using Wireless Sensor Networks," in *41st Hawaii International Conference on System Sciences (HICSS-41)*, Waikoloa, HI, U.S.A., January 2008, pp. 495-505.

- [11] M. S. Batson, "Enhanced Radio Frequency (RF) Collection with Distributed Wireless Sensor Networks," Ph.D. dissertation, Naval Postgraduate School, Monterey, CA, U.S.A., June 2007.
- [12] H. H. Loomis, "Geolocation of Electromagnetic Emitters," Naval Postgraduate School, Monterey, CA, Tech. Rep. NPS-EC-00-003 rev. 4, October 2007.
- [13] Y. T. Lo, "A Mathematical Theory of Antenna Arrays with Randomly Spaced Elements," *IEEE Transactions on Antennas and Propagation*, Vol. 12, Issue: 3, May 1964.
- [14] Y. T. Lo and R. Simcoe, "Experiment on Antenna Arrays with Randomly Spaced Elements," *IEEE Transactions on Antennas and Propagation*, Vol. 15, Issue: 2, pp. 257-268, March 1967.
- [15] W. Stallings, *Wireless Communications and Networks, 2nd Edition*, Prentice-Hall, Inc., 2004.
- [16] W. L. Stutzman and G. A. Thiele, *Antenna Theory and Design*, John Wiley & Sons, Inc., 1998.
- [17] D. King, R. Packard, and R. Thomas, "Unequally-Spaced, Broad-Band Antenna Arrays," *IEEE Transactions on Antennas and Propagation*, Vol. 8, Issue: 4, July 1960, pp. 380-384.
- [18] M. I. Skolnik, *Introduction to Radar Systems, 3rd Edition*, McGraw-Hill, Inc., 2001.
- [19] R. G. Plumb, "Antenna Array Beam Steering Using Time-Varying Weights," *IEEE Transactions on Aerospace and Electronic Systems*, Vol. 27, Issue 6, pp. 861-865, November 1991.
- [20] D. P. Scholnik and J. O. Coleman, "Optimal Design of Wideband Array Patterns," in *IEEE International Radar Conference (RADARCON 2000)*, Alexandria, VA, U.S.A., May 2000, pp. 172-177.
- [21] T. A. Clark, R. M. Hambly, and R. Abtahi, "Low-cost, High Accuracy GPS Timing," presented at Institute of Navigation's GPS Conference, Salt Lake City, UT, U.S.A., September 2000.
- [22] P. Z. Peebles, *Probability, Random Variables, and Random Signal Principles, 4th Edition*, McGraw-Hill, Inc., 2001.
- [23] M. Schwartz, *Information transmission, Modulation, and Noise, Second Edition*, McGraw-Hill, Inc., 1970.
- [24] E. Nelson, *Dynamical Theories of Brownian Motion, 2nd Edition*, Princeton University Press, 2001.

- [25] C. W. Therrien, *Discrete Random Signals and Statistical Signal Processing*, Prentice Hall, Inc., 1992.
- [26] J. Farrell, "Accuracy in More than Position Only," *GPS World*, Vol. 19, Issue: 2, pp. 8-10, February 2008.
- [27] E. Bonabeau, "Agent-based Modeling: Methods and Techniques for Simulating Human Systems," *Proceedings of the National Academy of the Sciences*, Vol. 99, No. Suppl. 3, pp. 7280-7287, May 2002.
- [28] B. Sklar, *Digital Communications Fundamentals and Applications*, 2nd Edition, Prentice Hall, Inc., 2001.
- [29] W. Stallings, *Data and Computer Communications*, 5th Edition, Prentice-Hall, Inc., 1997.
- [30] J. L. Melsa and D. L. Cohn, *Decision and Estimation Theory*, McGraw-Hill, 1978.
- [31] W. A. Lintz and J. C. McEachen, "A Method for Emphasizing Signal Detection in Wireless Sensor Network Radio Frequency Array Operation," in *Hawaii International Conference on System Sciences (HICSS-42)*, Kona, HI, U.S.A., January 2009, pp. 1-10.
- [32] L. B. Preiser, "Polarization Diversity of the General Non-Uniformly Spaced Adaptive Array," in *International Symposium of Antennas and Propagation (ISAP 88)*, Syracuse, NY, U.S.A., June 1988.
- [33] H. Rogier and D. DeZutter, "The Active Element Pattern Method for Beamforming with Nonuniform Arrays," in *IEEE International Symposium of the Antennas and Propagation Society*, Columbus, OH, U.S.A., Vol. 1, pp. 73-76, June 2003.
- [34] J. Litva and T. K. Y. Lo, *Digital Beamforming in Wireless Communications*, Artech House, 1996.
- [35] R. J. Mailloux, *Phased Array Antenna Handbook*, Artech House, 1994.
- [36] C. A. Balanis, *Antenna Theory Analysis and Design*, Harper and Row, Publishers, Inc., 1982.
- [37] D. F. Kelley and W. L. Stutzman, "Array Antenna Pattern Modeling Methods That Include Mutual Coupling Effects," *IEEE Transactions on Antennas and Propagation*, Vol. 41, Issue: 12, pp. 1625-1632, December 1993.
- [38] E. N. Da and C. Andrade, "Doppler and the Doppler Effect," *Endeavour*, Vol. 18, No. 69, January 1959.

- [39] D. Niculescu, "Positioning in Ad Hoc Sensor Networks," *IEEE Network*, Vol. 18, No. 4, pp. 24-29, July-August 2004.
- [40] M. Youssef, A. Nouredin, A. F. Yousif, and N. El-Sheimy, "Self-Localization Techniques for Wireless Sensor Networks," in *IEEE/ION Position, Location and Navigation Symposium (PLANS 2006)*, San Diego, CA, U.S.A., April 2006, pp. 179-186.
- [41] D. Niculescu and B. Nath, "Error Characteristics of Ad-Hoc Positioning Systems (APS)," in *ACM Fifth International Symposium on Mobile Ad-Hoc Networking and Computing (Mobihoc 2004)*, Tokyo, Japan, 2004, pp. 20-30.
- [42] R. Bajaj, S. L. Ranaweera, and D. P. Agrawal, "GPS: Location-Tracking Technology," *Computer*, Vol. 35, Issue: 4, pp. 92-94, March 2002.
- [43] T. McGurn, "Does Anybody Really Know What Accuracy Is?" *GPS World*, Vol. 18, Issue: 11, pp. 13-14, November 2007.
- [44] M. R. Mosavi, "Frequency Domain Modeling of GPS Positioning Errors," in *Eighth International Conference on Signal Processing (ICSP 06)*, Vienna, Austria, Vol. 4, December 2006.
- [45] M. Matosevic, Z. Salcic, and S. Berber, "A Comparison of Accuracy Using a GPS and a Low-Cost DGPS," *IEEE Transactions on Instrumentation and Measurement*, Vol. 55, No. 5, pp. 1677-1683, October 2006.
- [46] H. C. Son, J. G. Lee, and G. I. Jee, "Mobile Station Location Using Hybrid GPS and a Wireless Network," in *57th IEEE Vehicular Technology Conference (VTC 2003-Spring)*, Vol. 4, Jeju, Korea, April 2003, pp. 2716-2720.
- [47] D. Mills, "Internet Time Synchronization: The Network Time Protocol," *IEEE Transactions on Communications*, Vol. 39, Issue: 10, pp. 1482-1493, October 1991.
- [48] J. Elson, L. Girod, and D. Estrin, "Fine-Grained Network Time Synchronization using Reference Broadcasts," in *Fifth Symposium on Operating Systems Design and Implementation (OSDI 02)*, Boston, MA, U.S.A., December 2001.
- [49] H. Lee, W. Yu, and Y. Kwon, "Efficient RBS in Sensor Networks," in *Third International Conference on Information Technology: New Generations (ITNG 2006)*, Las Vegas, NV, U.S.A., April 2006, pp. 279-284.
- [50] S. Ganeriwal, R. Kumar, and M. B. Srivastava, "Time-sync Protocol for Sensor Networks," in *First ACM international Conference on Embedded Network Sensor Systems (SenSys 03)*, Los Angeles, CA, U.S.A., August 2003, pp. 138-149.

- [51] W. Su and I. F. Akyildiz, "Time-Diffusion Synchronization Protocol for Wireless Sensor Networks," *IEEE/ACM Transactions on Networking*, Vol. 13, Issue: 2, pp. 384-397, April 2005.
- [52] K. Sun and C. Wang, "Fault-Tolerant Cluster-wise Clock Synchronization for Wireless Sensor Networks," *IEEE Transactions on Dependable and Secure Computing*, Vol. 2, Issue: 3, pp. 177-189, July-September 2005.
- [53] "Using a Global Positioning System (GPS) Receiver as a NIST Traceable Frequency Reference," National Institute of Standards and Technology, <http://tf.nist.gov/service/gpscal.htm>, last accessed 3 June 2009.
- [54] J. H. Lee and C. Wang, "Adaptive Array Beamforming with Robust Capabilities Under Random Sensor Position Errors," *IEE Proceedings – RADAR, SONAR, and Navigation*, Vol. 152, No. 6, pp. 383-390, December 2005.
- [55] M. Ahmed and S. Vorobyov, "Performance Characteristics of Collaborative Beamforming for Wireless Sensor Networks with Gaussian Distributed Sensor Nodes," in *IEEE International Conference on Acoustics, Speech, and Signal Processing* (ICASSP 2008), Las Vegas, NV, U.S.A., March 2008, pp. 3249-3252.
- [56] I. M. Frank, "Doppler Effect in a Refractive Medium," *Journal of Physics U.S.S.R.*, Vol. 2, 1943.
- [57] K. S. H. Lee, "Radiation from an Oscillating Source Moving Through a Dispersive Medium with Particular Reference to the Complex Doppler Effect," *Radio Science*, vol. 3, 1968.
- [58] N. Engheta, A. Mickelson, and C. Papas, "On the Near-Zone inverse Doppler Effect," *IEEE Transactions on Antennas and Propagation*, Vol. 28, Issue: 4, pp. 519-522, July 1980.
- [59] V. Varadarajan and J. Krolik, "Target Detection Using Dynamically Reconfigurable Sensor Arrays," in *IEEE International Conference on Acoustics, Speech, and Signal Processing* (ICASSP 2005), Philadelphia, PA, U.S.A., Vol. 4, March 2005, pp. 1009-1012.
- [60] C. Lee and J. Lee, "Eigenspace-Based Adaptive Array Beamforming with Robust Capabilities," *IEEE Transactions on Antennas and Propagation*, Vol. 45, Issue: 12, pp. 1711-1716, December 1997.
- [61] J. Lee and K. Cheng, "Adaptive Array Beamforming with Robust Capabilities Under Random Phase Perturbations," *IEEE Transactions on Signal Processing*, Vol. 53, Issue: 1, pp. 365-371, January 2005.

- [62] T. O. Walker, M. Tummala, and J. McEachen, "Distributed Medium Access Control with Flow-Based Priority for Cooperative Multi-hop Wireless Sensor Networks," in *41st Hawaii International Conference on Science Systems (HICSS 41)*, Waikoloa, HI, U.S.A., January 2008, pp. 493-503.
- [63] W. Hoferkamp and S. Olariu, "A Power and Mobility-Aware Wireless Protocol for Ad-hoc Networks," in *Military Communications Conference (MILCOM 2000)*, Los Angeles, CA, U.S.A., October 2000, pp. 292-296.
- [64] W. A. Lintz, J. C. McEachen, and M. Tummala, M., "Sensor Beamforming with Wirelessly Networked Distributed Mobile Elements," in *22nd Canadian Conference on Electrical and Computer Engineering (CCECE 09)*, St. John's, Newfoundland and Labrador, Canada, May 2009.
- [65] D. M. Drumheller, "General Expressions for Rician Density and Distribution Functions," *IEEE Transactions on Aerospace and Electronic Systems*, Vol. 29, Issue: 2, pp. 580-588, April 1993.
- [66] W. H. Beyer (Ed.), *CRC Standard Mathematical Tables, 27th Edition*, CRC Press, 1984.
- [67] J. D. Oetting, "The Effects of Fading on Antijam Performance Requirements," *IEEE Journal on Selected Areas in Communications*, Vol. 5, Issue: 2, pp. 155-161, February, 1987.
- [68] I. M. Chakravarti, R. G. Laha, and J. Roy, *Handbook of Methods of Applied Statistics, Vol. 1*, John Wiley and Sons, Inc., 1998.
- [69] "Statistics Online Computational Resource," University of California, Los Angeles, <http://www.socr.ucla.edu/SOCR.html>, last accessed 30 December 2008.
- [70] W. A. Lintz, J. C. McEachen, and M. Tummala, "A Method for Determining Weight Reset Timing in a Wirelessly Networked Array with Independently Mobile Elements," in *IEEE 23rd International Conference on Advanced Information Networking and Applications (AINA 09)*, Bradford, United Kingdom, May 2009.
- [71] W. A. Lintz, J. C. McEachen, and D. Jenn, "Sensor network Pair-wise Wireless Communications Performance with Unsteady Node Orientation," in *IEEE Sarnoff Symposium*, Princeton, NJ, U.S.A., March 2009.
- [72] D. Kotz, C. Newport, R. S. Gray, J. Liu, Y. Yuan, and C. Elliot, "Experimental Evaluation of Wireless Simulation Assumptions," in *Seventh ACM International Symposium on Modeling, Analysis, and Simulation of Wireless and Mobile Systems (MSWiM 2004)*, Venice, Italy, October 2004, pp. 78-82.

- [73] T. Stoyanova, F. Kerasiotis, A. Prayati and G. Papadopoulos, "Evaluation of Impact Factors on RSS Accuracy for Localization and Tracking Accuracy," in *Fifth ACM International Workshop on Mobility Management and Wireless Access (MobiWac 07)*, Chania, Greece, 2007, pp. 9-16.
- [74] W. W. Merrill, H. L. N. Liu, J. Leong, K. Sohrabi, and G. J. Pottie, "Quantifying Short-Range Surface-to-Surface Communications Links," *IEEE Antennas and Propagation Magazine*, Vol. 46, Issue: 3, pp. 36-46, June 2004.
- [75] K. Phaebua, C. Phongcharoenpanich, D. Torrungrueng, and J. Chinrungrueng, "Short-Distance and Near-Ground Signal Measurements in a Car Park of Wireless Sensor Network System at 433 MHz," in *International Conference in Electrical Engineering/Electronics, Computer, Telecommunications, and Information Technology (ECTI-CON 2008)*, Krabi, Thailand, May 2008, pp. 241-244.
- [76] C. H. See, R. A. Abd-Alhameed, Y. F. Hu, and K. V. Horoshenkov, "Wireless Sensor Transmission Range Measurement within the Ground Level," in *Loughborough Antennas and Propagation Conference (LAPC 2008)*, Loughborough, United Kingdom, March 2008, pp. 225-228.
- [77] "Pythagoras, Version 1.10.2," developed for the U.S. Marine Corps by Northrop-Grumman Corporation, points of contact Z. Henscheid and D. Middleton, Northrop Grumman Corporation, {zoe.henscheid, donna.middleton}@ngc.com, received April 2008.

THIS PAGE INTENTIONALLY LEFT BLANK

APPENDIX A. BETA DISTRIBUTION

```
% This program displays the distribution of a Beta random variable
% under various alpha and beta influences
%
% Alpha and Beta are hardcoded for consistency, but can be altered
% within
%
% Shows Plot for a variety of Beta configurations
%
% By W. A. Lintz

clear;

alpha= [1 3 3 2.5];
beta=[3 3 1 1.7];
x=linspace(0,1);

fx1=(gamma(alpha(1)+beta(1))/(gamma(alpha(1))*gamma(beta(1))))...
    *(x.^(alpha(1)-1)).*((1-x).^(beta(1)-1));
fx2=(gamma(alpha(2)+beta(2))/(gamma(alpha(2))*gamma(beta(2))))...
    *(x.^(alpha(2)-1)).*((1-x).^(beta(2)-1));
fx3=(gamma(alpha(3)+beta(3))/(gamma(alpha(3))*gamma(beta(3))))...
    *(x.^(alpha(3)-1)).*((1-x).^(beta(3)-1));
fx4=(gamma(alpha(4)+beta(4))/(gamma(alpha(4))*gamma(beta(4))))...
    *(x.^(alpha(4)-1)).*((1-x).^(beta(4)-1));

plot(x,fx1,x,fx2,x,fx3,x,fx4)
legend(texlabel('alpha=1 and beta=3'),texlabel('alpha=beta=3'),...
    texlabel('alpha=3 and beta=1'),...
    texlabel('alpha=2.5 and beta=1.7'))
```

THIS PAGE INTENTIONALLY LEFT BLANK

APPENDIX B. ANTENNA EFFICIENCY

```
% This is a program that considers antenna efficiency as carrier
% shifts
%
% Show Plot efficiency vs. carrier
%
% Minimal effect noted at chosen frequencies.
%
% By W.A. Lintz

clear all;

fc=linspace(149999500,150000500,100);

Rohmic=(3e8./(8*pi*fc*.005)).*(pi*fc*(pi*4e-7)/(59.6e6)).^.5;

Rrad=((3e8*fc*(pi*4e-7)^2)/480).*(1-cos(pi*fc/3e8));

eff=Rrad./(Rrad+Rohmic);

plot(fc,eff)
xlabel('Carrier Frequency (MHz)')
ylabel('Antenna Efficiency')
```

THIS PAGE INTENTIONALLY LEFT BLANK

APPENDIX C. SIMPLE PATTERNS

```
% This is a program computes 2-D Normalized Patterns for a 2-Element
% Array composed of Symmetric Dipole Antennas.
%
% Independently entered factors:
%     Length of dipoles in wavelengths
%     Distance between elements in wavelengths
%     Current magnitude ratio
%     Phase difference in degrees
%
% Shows Polar Plots for: (1) Single Dipole
%                        (2) Space Factor,
%                        (3) Composite Product Pattern
%
% By M.A. Morgan, Naval Postgraduate School, ECE Department 2/12/96
% TeX symbol updates 13 Mar 2003

clear all
Nphi=360; % Use Default Increment
dphi=2*pi/Nphi; phi=(0:dphi:2*pi); theta=abs(pi/2-phi);
ct=cos(theta); st=sin(theta+eps); % eps avoids indeterminate
sp=sin(phi); cp=cos(phi);
figure(1)
% Symmetric Dipole Pattern
L=input('Enter Dipole Element Lengths in Wavelengths: '); BH=pi*L;
CBH=cos(BH);
E=abs((cos(BH*ct)-CBH)./st+eps); % E-Plane Dipole Pattern
Emax=max(E); En=E/Emax; % Normalized Pattern
clf reset; polar(phi,En);
title(['|E_n(\theta)| for a Symmetric Dipole: L=',num2str(L),...
'\lambda'],'FontSize',18);
text(-.65,-1.25,'Polar Angle Is From Array Axis');

figure(2)
% Two-Element Space Factor Pattern
d=input('Enter Array Spacing of Dipoles in Wavelengths: ');
Bd=2*pi*d;
IMR=input('Enter |I_1|/|I_0| Magnitude Ratio: ');
dalpha=input('Enter Alpha1-Alpha0 Phase Difference ...
in Degrees: ');
alpha=pi*dalphi/180; % Convert to Radians
Iratio=IMR*exp(j*alpha); % Complex I1/I0 Ratio

F2=abs(1+Iratio*exp(j*Bd*cp)); % Space Factor Magnitude
clf reset; polar(phi,F2);
title(['|F_2(\phi)|: d=',num2str(d),'\lambda; |I_1|/|I_0|='...
,num2str(IMR),'; \Delta\alpha=',num2str(dalphi),'^0'],'FontSize',18);
text(-1.3,-2.5,'Polar Angle Is From Array Axis');

figure(3)
EF2=F2.*En; % Composite Array Pattern
EF2n=EF2/(max(EF2)); % Normalized Pattern
```

```

clf reset; polar(phi,EF2n);
title(['E-Plane |F_2|*|E_n|: L=',num2str(L),' \lambda;...
d=',num2str(d),' \lambda; |I_1|/|I_0|=',num2str(IMR),...
'; \Delta\alpha=',num2str(dalpha),'^0'], 'FontSize',18);
text(-.65,-1.25,'Polar Angle Is From Array Axis');

```

APPENDIX D. NON-COHERENT

```

% This is a program that computes the 3 dimensional array pattern from
% a user input 3 dimensional array that is non-coherent
%
% Independently entered factors:
%         Number of elements
%         Element location
%
% Assumed factors:
%         Isotropic elements
%         Identical polarization
%         Identical current magnitude
%
% Shows Plots for
%         Array Positions
%         Normalized Array Factor pattern (2 separate view angles)
%         Polar cross-section of normalized Array factor pattern
%             in x-y plane
%         Linear cross-section of normalized Array factor pattern
%             in x-y plane
%
% By W. A. Lintz

% Set up problem space for spherical coordinates

clear all;

Ntheta=input('Enter Number of Theta Segments (default is 90): ');
if isempty(Ntheta)
    Ntheta=90;
end;
dtheta=pi/Ntheta;          % Changes to radians
theta=(0:dtheta:pi)';      % Theta vector (0-pi in Ntheta steps)

Nphi=input('Enter Number of Phi Segments (default is 180): ');
if isempty(Nphi)
    Nphi=180;
end;
dphi=2*pi/Nphi;            % Changes to radians
phi=(0:dphi:2*pi);         % Phi vector (0-2pi in Nphi steps)

Theta=theta*ones(1,Nphi+1); % Creates a Theta array Nt x Np
ST=sin(Theta)+eps;         % Projection on xy plane
CT=cos(Theta);              % Projection on z axis

Phi=ones(Ntheta+1,1)*phi;  % Creates a Phi array Nt x Np
SP=sin(Phi);               % Projection on y axis
CP=cos(Phi);               % Projection on xy plane

xa1=[1.5 0 0]; ya1=[0 0 0]; za1=[0 0 0]; % Axis coordinates
xa2=[-1.5 0 0]; ya2=[0 0 0]; za2=[0 0 0];

```

```

xa3=[0 0 0]; ya3=[1.5 0 0]; za3=[0 0 0];
xa4=[0 0 0]; ya4=[-1.5 0 0]; za4=[0 0 0];
xa5=[0 0 0]; ya5=[0 0 0]; za5=[1.5 0 0];
xa6=[0 0 0]; ya6=[0 0 0]; za6=[-1.5 0 0];

% N-Element Array Entry

N=input('Enter Number of Elements (Must be >1. Default is 2): ');
if isempty(N), N=2;
elseif N<=1, N=2;
end;

disp(' ')
disp('* Next you will enter information on element location.')
disp('* All information entered will be relative to the origin.')
disp('* Element locations will be in x,y,z coordinates,...
      and distances')
disp('are in wavelenghts.')

for n=1:N
    disp(' ')
    disp(sprintf('Element %d', n))
    X(n)=input('    Enter element "X" coordinate: ');
    Y(n)=input('    Enter element "Y" coordinate: ');
    Z(n)=input('    Enter element "Z" coordinate: ');
end

% N-element Array Display

figure(1)
clf reset
plot3(X,Y,Z,'r*')
axis([-1*max(abs(X))-1 max(abs(X))+1 -1*max(abs(Y))-1 max...
      (abs(Y))+1 -1*max(abs(Z))-1 max(abs(Z))+1])
axis('square')
grid
title([int2str(N),'-Element Array Arrangement - Distance...
      in Wavelengths'], 'FontSize', 14);
xlabel('X-Axis')
ylabel('Y-Axis')
zlabel('Z-Axis')

% N-Element Array Normalized Space Factor

n=1; AF=0; % Set initial loop conditions
for n=1:N
    AF=AF+ exp(j*2*pi*(X(n)*(ST.*CP)+Y(n)*(ST.*SP)+Z(n)*(CT)));
end
AF=abs(AF/(max(max(AF))));
AF2=AF.*AF.*ST;
D=4*pi/((sum(sum(AF2)))*dtheta*dphi);
DdB=10*log10(D);

% N-Element Array Normalized Space Factor Pattern Display

```

```

figure(2)
AFx=AF.*ST.*CP; AFy=AF.*ST.*SP; AFz=AF.*CT;% 3-D Plotting Coordinates
clf reset;
mesh(AFx,AFy,AFz,AF);
hold on
plot3(xa1,ya1,za1,'k',xa2,ya2,za2,'k',xa3,ya3,za3,'k',xa4,ya4,...
      za4,'k',xa5,ya5,za5,'k',xa6,ya6,za6,'k');

axis off
view([340,60]);
text(1.6,0,0,'X-Axis');
text(-.1,1.8,0,'Y-Axis');
text(-.2,0,2,'Z-Axis');
title([int2str(N),'-Element Array Space-Factor,...
      D_{dB}=',num2str(DdB)], 'FontSize',14);
hold off

figure(3)
AFx=AF.*ST.*CP; AFy=AF.*ST.*SP; AFz=AF.*CT; % 3-D Plotting Coordinates
clf reset;
mesh(AFx,AFy,AFz,AF);
hold on
plot3(xa1,ya1,za1,'k',xa2,ya2,za2,'k',xa3,ya3,za3,'k',xa4,ya4,...
      za4,'k',xa5,ya5,za5,'k',xa6,ya6,za6,'k');
text(1.6,0,0,'X-Axis');
text(-.1,1.6,0,'Y-Axis');
text(-.2,0,1.7,'Z-Axis');
axis off
view([0,90]);
title([int2str(N),'-Element Array Space-Factor,...
      D_{dB}=',num2str(DdB)], 'FontSize',14);
hold off

% x-y plane cut

AFxd=AFx(1+round(Ntheta/2),1:(Nphi+1));
AFyd=AFy(1+round(Ntheta/2),1:(Nphi+1));
R=(AFxd.^2+AFyd.^2).^5;
BW=.707*ones(size(phi));
figure(4)
polar(phi,R);
hold on
polar(phi,BW,'r');
hold off
title([int2str(N),'-Element Array Pattern (Polar)'], 'FontSize', 14);
figure(5)
plot((phi*(360/(2*pi))),R,(phi*(360/(2*pi))),BW,'r');
axis([0 360 0 1.05]);
grid
title([int2str(N),'-Element Array Pattern...
      (x-y Plane vs. Phi)'], 'FontSize', 14);
xlabel('Phi')
ylabel('Normalized Gain')
legend('Array Pattern', '3 dB line')

```

THIS PAGE INTENTIONALLY LEFT BLANK

APPENDIX E. ITERATIVE COMPARISON

```
% This program tests the difference in the creation of an array factor
% pattern using a single 15 element array versus iterative pattern
% creation using three element groups
%
% For comparison purposes, a single array is hardcoded with random
% elements, but array configuration can be changed or randomized
% within to include grouping, numbers, locations, and aim point
%
% Shows Plots for
%   Array Positions (broken down by iteration groups)
%   Normalized Array Factor pattern for large array (two views)
%   Polar cross-section of normalized Array factor pattern in
%       x-y plane for large array
%   Linear cross-section of normalized Array factor pattern in
%       x-y plane for large array
%   Normalized Array Factor pattern for iteration groups
%       (two views)
%   Polar cross-section of normalized Array factor pattern in
%       x-y plane for iteration groups
%   Linear cross-section of normalized Array factor pattern in
%       x-y plane for iteration groups
%
% By W. A. Lintz

clear all;

Ntheta=90;
dtheta=pi/Ntheta; % Changes to radians
theta=(0:dtheta:pi)'; % Theta vector (0-pi in Ntheta steps)

Nphi=180;
dphi=2*pi/Nphi; % Changes to radians
phi=(0:dphi:2*pi); % Phi vector (0-2pi in Nphi steps)

Theta=theta*ones(1,Nphi+1); % Creates a Theta array Nt x Np
ST=sin(Theta)+eps; % Projection on xy plane
CT=cos(Theta); % Projection on z axis

Phi=ones(Ntheta+1,1)*phi; % Creates a Phi array Nt x Np
SP=sin(Phi); % Projection on y axis
CP=cos(Phi); % Projection on xy plane

xa1=[1.5 0 0]; ya1=[0 0 0]; za1=[0 0 0]; % Axis coordinates
xa2=[-1.5 0 0]; ya2=[0 0 0]; za2=[0 0 0];
xa3=[0 0 0]; ya3=[1.5 0 0]; za3=[0 0 0];
xa4=[0 0 0]; ya4=[-1.5 0 0]; za4=[0 0 0];
xa5=[0 0 0]; ya5=[0 0 0]; za5=[1.5 0 0];
xa6=[0 0 0]; ya6=[0 0 0]; za6=[-1.5 0 0];

% N-Element Array Entry
```

```

N=15;

for n=1:N
    X(n)=(2*rand)-1;
    Y(n)=(2*rand)-1;
end

MBTo=90;
MBPo=60;
MBTo=(pi/180)*MBTo;          % Convert to Radians
MBPo=(pi/180)*MBPo;
SMBTo=sin(MBTo); CMBTo=cos(MBTo); % Handy for alpha determinations
SMBPo=sin(MBPo); CMBPo=cos(MBPo);

% N-element Array Display

for n=1:5
    X1(n)=X(n);
    X2(n)=X(5+n);
    X3(n)=X(10+n);
    Y1(n)=Y(n);
    Y2(n)=Y(5+n);
    Y3(n)=Y(10+n);
end

figure(1)
clf reset
plot(X1,Y1,'*',X2,Y2,'*',X3,Y3,'*')
axis([-1*max(abs(X))-1 max(abs(X))+1 -1*max(abs(Y))-1 max(abs(Y))+1])
axis('square')
grid
title(['15-Element Array Arrangement - Distance in Wavelengths'],...
    'FontSize', 14);
legend('Group 1', 'Group 2', 'Group 3')
xlabel('X-Axis')
ylabel('Y-Axis')

%%%%%%%%%%%%%%%%%%%%%%%%%%%%%%%%%%%%%%%%%%%%%%%%%%%%%%%%%%%%%%%%%%%%%%%%%%%%%%
% 15-Element Array Normalized Space Factor
%%%%%%%%%%%%%%%%%%%%%%%%%%%%%%%%%%%%%%%%%%%%%%%%%%%%%%%%%%%%%%%%%%%%%%%%%%%%%%

n=1; AF=0; % Set initial loop conditions
for n=1:N
    alpha=-(2*pi)*(X(n)*SMBTo*CMBPo + Y(n)*SMBTo*SMBPo); % Determine
    alpha
    AF=AF+ exp(j*alpha)*exp(j*2*pi*(X(n)*(ST.*CP)+Y(n)*(ST.*SP)));
end
AF=abs(AF/(max(max(AF)))));
AF2=AF.*AF.*ST;
D=4*pi/((sum(sum(AF2)))*dtheta*dphi);
DdB=10*log10(D);

```

```

%%%%%%%%%%%%%%%%%%%%%%%%%%%%%%%%%%%%%%%%%%%%%%%%%%%%%%%%%%%%%%%%%%%%%%%%%%%%%%
% 15-Element Array Normalized Space Factor Pattern Display
%%%%%%%%%%%%%%%%%%%%%%%%%%%%%%%%%%%%%%%%%%%%%%%%%%%%%%%%%%%%%%%%%%%%%%%%%%%%%%

figure(2)
AFx=AF.*ST.*CP; AFy=AF.*ST.*SP; AFz=AF.*CT; % 3-D Plotting Coordinates
clf reset;
mesh(AFx,AFy,AFz,AF);
hold on
plot3(xa1,ya1,za1,'k',xa2,ya2,za2,'k',xa3,ya3,za3,'k',xa4,ya4,za4,...
      'k',xa5,ya5,za5,'k',xa6,ya6,za6,'k');

axis off
view([340,60]);
text(1.6,0,0,'X-Axis');
text(-.1,1.8,0,'Y-Axis');
text(-.2,0,2,'Z-Axis');
title([int2str(N),'-Element Array Space-Factor, D_{dB}=',...
      num2str(DdB)], 'FontSize',14);
hold off

figure(3)
AFx=AF.*ST.*CP; AFy=AF.*ST.*SP; AFz=AF.*CT; % 3-D Plotting Coordinates
clf reset;
mesh(AFx,AFy,AFz,AF);
hold on
plot3(xa1,ya1,za1,'k',xa2,ya2,za2,'k',xa3,ya3,za3,'k',xa4,ya4,za4,...
      'k',xa5,ya5,za5,'k',xa6,ya6,za6,'k');
text(1.6,0,0,'X-Axis');
text(-.1,1.6,0,'Y-Axis');
text(-.2,0,1.7,'Z-Axis');
axis off
view([0,90]);
title([int2str(N),'-Element Array Space-Factor, D_{dB}=',...
      num2str(DdB)], 'FontSize',14);
hold off

% x-y plane cut

AFxd=AFx(1+round(Ntheta/2),1:(Nphi+1));
AFyd=AFy(1+round(Ntheta/2),1:(Nphi+1));
R=(AFxd.^2+AFyd.^2).^5;
figure(4)
polar(phi,R);
title([int2str(N),'-Element Array Pattern (Polar)'], 'FontSize', 14);
figure(5)
plot((phi*(360/(2*pi))),R);
axis([0 360 0 1.05]);
grid
title([int2str(N),'-Element Array Pattern (x-y Plane vs. Phi)']...
      , 'FontSize', 14);
xlabel('Phi')
ylabel('Normalized Gain')

```

```

%%%%%%%%%%%%%%%%%%%%%%%%%%%%%%%%%%%%%%%%%%%%%%%%%%%%%%%%%%%%%%%%%%%%%%%%%%%%%%
% 5-Element Array Normalized Space Factors Combined
%%%%%%%%%%%%%%%%%%%%%%%%%%%%%%%%%%%%%%%%%%%%%%%%%%%%%%%%%%%%%%%%%%%%%%%%%%%%%%

AF_1=0;          % Set initial loop conditions
for n=1:5
    alpha=-(2*pi)*(X1(n)*SMBTo*CMBPo + Y1(n)*SMBTo*SMBPo); % Alpha
    AF_1=AF_1+ exp(j*alpha)*exp(j*2*pi*(X1(n)*(ST.*CP)+Y1(n)*(ST.*SP)));
end

AF_2=0;          % Set initial loop conditions
for n=1:5
    alpha=-(2*pi)*(X2(n)*SMBTo*CMBPo + Y2(n)*SMBTo*SMBPo); % Alpha
    AF_2=AF_2+ exp(j*alpha)*exp(j*2*pi*(X2(n)*(ST.*CP)+Y2(n)*(ST.*SP)));
end

AF_3=0;          % Set initial loop conditions
for n=1:5
    alpha=-(2*pi)*(X3(n)*SMBTo*CMBPo + Y3(n)*SMBTo*SMBPo); % Alpha
    AF_3=AF_3+ exp(j*alpha)*exp(j*2*pi*(X3(n)*(ST.*CP)+Y3(n)*(ST.*SP)));
end

AF_C=AF_1+AF_2+AF_3;

AF_C=abs(AF_C/(max(max(AF_C))));
AF2_C=AF_C.*AF_C.*ST;
D_C=4*pi/((sum(sum(AF2_C)))*dtheta*dphi);
DdB_C=10*log10(D_C);

%%%%%%%%%%%%%%%%%%%%%%%%%%%%%%%%%%%%%%%%%%%%%%%%%%%%%%%%%%%%%%%%%%%%%%%%%%%%%%
% Combined 5-Element Array Normalized Space Factor Patterns Display
%%%%%%%%%%%%%%%%%%%%%%%%%%%%%%%%%%%%%%%%%%%%%%%%%%%%%%%%%%%%%%%%%%%%%%%%%%%%%%

figure(6)
AFx_C=AF_C.*ST.*CP; AFy_C=AF_C.*ST.*SP; AFz_C=AF_C.*CT;
clf reset;
mesh(AFx_C,AFy_C,AFz_C,AF_C);
hold on
plot3(xa1,ya1,za1,'k',xa2,ya2,za2,'k',xa3,ya3,za3,'k',xa4,ya4,za4,...
      'k',xa5,ya5,za5,'k',xa6,ya6,za6,'k');
axis off
view([340,60]);
text(1.6,0,0,'X-Axis');
text(-.1,1.8,0,'Y-Axis');
text(-.2,0,2,'Z-Axis');
title(['5-Element Array Space-Factor, D_{dB}=',num2str(DdB_C)]...
      , 'FontSize',14);
hold off

figure(7)
AFx_C=AF_C.*ST.*CP; AFy_C=AF_C.*ST.*SP; AFz_C=AF_C.*CT;
clf reset;
mesh(AFx_C,AFy_C,AFz_C,AF_C);
hold on
plot3(xa1,ya1,za1,'k',xa2,ya2,za2,'k',xa3,ya3,za3,'k',xa4,ya4,za4,...

```

```

        'k',xa5,ya5,za5,'k',xa6,ya6,za6,'k');
text(1.6,0,0,'X-Axis');
text(-.1,1.6,0,'Y-Axis');
text(-.2,0,1.7,'Z-Axis');
axis off
view([0,90]);
title(['5-Element Array Space-Factor Combined, D_{dB}=',...
    num2str(DdB_C)], 'FontSize',14);
hold off

% x-y plane cut

AFxd_C=AFx_C(1+round(Ntheta/2),1:(Nphi+1));
AFyd_C=AFy_C(1+round(Ntheta/2),1:(Nphi+1));
R_C=(AFxd_C.^2+AFyd_C.^2).^5;
figure(8)
polar(phi,R_C);
title(['5-Element Array Pattern Combined (Polar)'], 'FontSize', 14);
figure(9)
plot((phi*(360/(2*pi))),R_C);
axis([0 360 0 1.05]);
grid
title(['5-Element Array Pattern Combined (x-y Plane vs. Phi)'],...
    'FontSize', 14);
xlabel('Phi')
ylabel('Normalized Gain')

```

THIS PAGE INTENTIONALLY LEFT BLANK

APPENDIX F. DOPPLER SHIFT

```
% This is a program that considers Doppler Shift and Carrier for
% multiple relative velocities.
%
% Show Plot Doppler Shift vs. carrier
%
% By W. A. Lintz

clear all;

fc=linspace(1,3000000000,1000);

% v1=10mph -> 4.47 m/s
% v2=30mph -> 13.41 m/s
% v3=60mph -> 26.82 m/s
% v4=120mph -> 53.64 m/s

v=[4.47 13.41 26.82 53.64];

fd1=(fc/3e8)*v(1);
fd2=(fc/3e8)*v(2);
fd3=(fc/3e8)*v(3);
fd4=(fc/3e8)*v(4);

plot(fc/1000000,fd1,fc/1000000,fd2,fc/1000000,fd3,fc/1000000,fd4)
xlabel('Carrier Frequency (MHz)')
ylabel('Doppler Shift (Hz)')
legend('10mph','30mph','60mph','120mph')
```

THIS PAGE INTENTIONALLY LEFT BLANK

APPENDIX G. DOPPLER SMEAR

```
% This is a program that computes the array factor smear caused by the
% Doppler effect on an array with elements in motion
%
% Array configuration is random but set for general run. Can be
% modified.
%
% Shows Plots for
%     Array Positions
%     Normalized Array Factor pattern (2 separate view angles)
%     Polar cross-section of normalized Array factor pattern
%         in x-y plane
%     Linear cross-section of normalized Array factor pattern
%         in x-y plane
%     Normalized Array Factor pattern (2 separate view angles)
%         for smeared pattern
%     Polar cross-section of normalized Array factor pattern
%         in x-y plane for smeared pattern
%     Linear cross-section of normalized Array factor pattern
%         in x-y plane for smeared pattern
%     Difference between original and smeared pattern
%
% Physical velocities used are random but provided - a wide sampling
% is performed at random velocities to find smear at speed.
%
% By W. A. Lintz

% Set up problem space for spherical coordinates

clear all;

for set=1:5000

Ntheta=180;          % Number of Theta segments
dtheta=pi/Ntheta;    % Changes to radians
theta=(0:dtheta:pi)'; % Theta vector (0-pi in Ntheta steps)

Nphi=360;            % Number of Phi segments
dphi=2*pi/Nphi;      % Changes to radians
phi=(0:dphi:2*pi);   % Phi vector (0-2pi in Nphi steps)

Theta=theta*ones(1,Nphi+1); % Creates a Theta array Nt x Np
ST=sin(Theta)+eps;        % Projection on xy plane
CT=cos(Theta);             % Projection on z axis

Phi=ones(Ntheta+1,1)*phi; % Creates a Phi array Nt x Np
SP=sin(Phi);               % Projection on y axis
CP=cos(Phi);               % Projection on xy plane    % Projection on x axis

% N-Element Array Entry
```

```

N=10;                % Number of elements
for n=1:N

    X(n)=2*rand-1;    % Position of elements around origin x
    Y(n)=2*rand-1;    % Position of elements around origin y

    %%%%%%%%%%%%%%%%%%%%%%%%%%%%%%%%%%%%%%%%%Velocity%%%%%%%%%%%%%%%%%%%%%%%%%%%%%%%%%%%%%%%%
    Vm(n)=100000*rand; % Velocity magnitude of element in
                        % wavelengths per second
    Vaz(n)=2*pi*rand;  % Velocity Phi azimuth angle
    Vel(n)=pi*rand;    % Velocity theta elevation angle

end

% Set aim point
MBTo=90;
MBPo=60;
MBTo=(pi/180)*MBTo; % Convert to Radians
MBPo=(pi/180)*MBPo;
SMBTo=sin(MBTo); CMBTo=cos(MBTo); % Handy for alpha determinations
SMBPo=sin(MBPo); CMBPo=cos(MBPo);

% N-Element Array Normalized Space Factor - Normal (non-smeared)
% N-Element Array Normalized Space Factor - Normal (non-smeared)

n=1; AF=0; % Set initial loop conditions
for n=1:N
    alpha=-(2*pi)*(X(n)*SMBTo*CMBPo + Y(n)*SMBTo*SMBPo); % Alpha
    AF=AF+ exp(j*alpha)*exp(j*2*pi*(X(n)*(ST.*CP)+Y(n)*(ST.*SP))); % AF
end

AF=abs(AF/(max(max(AF)))));
AF2=AF.*AF.*ST;
D=4*pi/((sum(sum(AF2)))*dtheta*dphi);
DdB=10*log10(D);

% N-Element Array Normalized Space Factor Pattern Display

xa1=[1.5 0 0]; ya1=[0 0 0]; za1=[0 0 0]; % Axis coordinates for plots
xa2=[-1.5 0 0]; ya2=[0 0 0]; za2=[0 0 0];
xa3=[0 0 0]; ya3=[1.5 0 0]; za3=[0 0 0];
xa4=[0 0 0]; ya4=[-1.5 0 0]; za4=[0 0 0];
xa5=[0 0 0]; ya5=[0 0 0]; za5=[1.5 0 0];
xa6=[0 0 0]; ya6=[0 0 0]; za6=[-1.5 0 0];

AFx=AF.*ST.*CP; AFy=AF.*ST.*SP; AFz=AF.*CT;% 3-D Plotting Coordinates

% x-y plane cut

AFxd=AFx(1+round(Ntheta/2),1:(Nphi+1));

```

```

AFyd=AFy(1+round(Ntheta/2),1:(Nphi+1));
R=(AFxd.^2+AFyd.^2).^5;

%%%%%%%%%%%%%%%%%%%%%%%%%%%%%%%%%%%%%%%%%%%%%%%%%%%%%%%%%%%%%%%%%%%%%%%%%%%%%%
% N-Element Array Normalized Space Factor - Doppler Smeared
%%%%%%%%%%%%%%%%%%%%%%%%%%%%%%%%%%%%%%%%%%%%%%%%%%%%%%%%%%%%%%%%%%%%%%%%%%%%%%

n=1; AFD=0;          % Set initial loop conditions
for n=1:N
    alpha=-(2*pi)*(X(n)*SMBTo*SMBPo + Y(n)*SMBTo*SMBPo); % Alpha
    AFD=AFD+ exp(j*alpha)*exp(j*2*pi*(X(n).*(1./(1+(Vm(n)*...
        cos(Vaz(n)-Phi)).*sin(Vel(n)-Theta))/3e8)).*(ST.*CP)...
        +Y(n).*(1./(1+(Vm(n)*sin(Vaz(n)-Phi)).*sin(Vel(n)-...
        Theta))/3e8)).*(ST.*SP)); % Determine AF
end

AFD=abs(AFD/(max(max(AFD)))));
AF2D=AFD.*AFD.*ST;
D=4*pi/((sum(sum(AF2D)))*dtheta*dphi);
DdB=10*log10(D);

% N-Element Array Normalized Space Factor Pattern Display

AFxD=AFD.*ST.*CP; AFyD=AFD.*ST.*SP; AFzD=AFD.*CT;% 3-D Plotting Coords
% x-y plane cut
AFxD=AFxD(1+round(Ntheta/2),1:(Nphi+1));
AFyD=AFyD(1+round(Ntheta/2),1:(Nphi+1));
RD=(AFxD.^2+AFyD.^2).^5;

Diff(set)=max(abs(R-RD));

set

end

mean(Diff)
var(Diff)
Maxvel=100000*(3e8/900e6)*2.236936

```

THIS PAGE INTENTIONALLY LEFT BLANK

APPENDIX H. ARRAY FACTOR PATTERN

```
% This is a program that computes the 3 dimensional array pattern
% from a user input 3 dimensional array
%
% Independently entered factors:
%     Number of elements
%     Element location
%     Desired aim point
%
% Assumed factors:
%     Isotropic elements
%     Identical polarization
%     Indentical current magnitude
%
% Shows Plots for
%     Array Positions
%     Normalized Array Factor pattern (2 separate view
%         angles)
%     Polar cross-section of normalized Array factor pattern
%         in x-y plane
%     Linear cross-section of normalized Array factor pattern
%         in x-y plane
%
% By W. A. Lintz (Graphing based on code by M.A. Morgan '05)

% Set up problem space for spherical coordinates

clear all;

Ntheta=input('Enter Number of Theta Segments (default is 90): ');
if isempty(Ntheta)
    Ntheta=90;
end;
dtheta=pi/Ntheta;      % Changes to radians
theta=(0:dtheta:pi)';  % Theta vector (0-pi in Ntheta steps)

Nphi=input('Enter Number of Phi Segments (default is 180): ');
if isempty(Nphi)
    Nphi=180;
end;
dphi=2*pi/Nphi;        % Changes to radians
phi=(0:dphi:2*pi);     % Phi vector (0-2pi in Nphi steps)

Theta=theta*ones(1,Nphi+1); % Creates a Theta array Nt x Np
ST=sin(Theta)+eps;        % Projection on xy plane
CT=cos(Theta);            % Projection on z axis

Phi=ones(Ntheta+1,1)*phi; % Creates a Phi array Nt x Np
SP=sin(Phi);              % Projection on y axis
CP=cos(Phi);              % Projection on xy plane
```

```

xa1=[1.5 0 0]; ya1=[0 0 0]; za1=[0 0 0]; % Axis coordinates
xa2=[-1.5 0 0]; ya2=[0 0 0]; za2=[0 0 0];
xa3=[0 0 0]; ya3=[1.5 0 0]; za3=[0 0 0];
xa4=[0 0 0]; ya4=[-1.5 0 0]; za4=[0 0 0];
xa5=[0 0 0]; ya5=[0 0 0]; za5=[1.5 0 0];
xa6=[0 0 0]; ya6=[0 0 0]; za6=[-1.5 0 0];

% N-Element Array Entry

N=input('Enter Number of Elements (Must be >1. Default is 2): ');
if isempty(N), N=2;
elseif N<=1, N=2;
end;

disp(' ')
disp('* Next you will enter information on element location.')
disp('* All information entered will be relative to the origin.')
disp('* Element locations will be in x,y,z coordinates,...
      and distances')
disp('are in wavelenghts.')

for n=1:N
    disp(' ')
    disp(sprintf('Element %d', n))
    X(n)=input('    Enter element "X" coordinate: ');
    Y(n)=input('    Enter element "Y" coordinate: ');
    Z(n)=input('    Enter element "Z" coordinate: ');
end
disp('')
disp('Enter desired main beam pointing direction in degrees')
MBTo=input('Enter Theta (between 0 and 180 degrees -...
          default is 90): ');
if isempty(MBTo), MBTo=90;
elseif MBTo<0, MBTo=90;
elseif MBTo>90, MBTo=90;
end
MBPo=input('Enter Phi (between 0 and 359 degrees -...
          default is 60): ');
if isempty(MBPo), MBPo=60;
elseif MBPo<0, MBPo=60;
elseif MBPo>359, MBPo=60;
end

MBTo=(pi/180)*MBTo; % Convert to Radians
MBPo=(pi/180)*MBPo;

SMBTo=sin(MBTo); CMBTo=cos(MBTo); % Handy for alpha deteminations
SMBPo=sin(MBPo); CMBPo=cos(MBPo);

% N-element Array Display

figure(1)
clf reset
plot3(X,Y,Z,'r*')

```

```

axis([-1*max(abs(X))-1 max(abs(X))+1 -1*max(abs(Y))-1 ...
      max(abs(Y))+1 -1*max(abs(Z))-1 max(abs(Z))+1])
axis('square')
grid
title([int2str(N),'-Element Array Arrangement - Distance in...
       Wavelengths'], 'FontSize', 14);
xlabel('X-Axis')
ylabel('Y-Axis')
zlabel('Z-Axis')

% N-Element Array Normalized Space Factor

n=1; AF=0; % Set initial loop conditions
for n=1:N
    alpha=-(2*pi)*(X(n)*SMBTo*CMBPo + Y(n)*SMBTo*SMBPo + Z(n)*CMBTo);
    % Alpha
    AF=AF+ exp(j*alpha)*exp(j*2*pi*(X(n)*(ST.*CP)+Y(n)*(ST.*SP)...
        +Z(n)*(CT)));
end
AF=abs(AF/(max(max(AF))));
AF2=AF.*AF.*ST;
D=4*pi/((sum(sum(AF2)))*dtheta*dphi);
DdB=10*log10(D);

% N-Element Array Normalized Space Factor Pattern Display

figure(2)
AFx=AF.*ST.*CP; AFy=AF.*ST.*SP; AFz=AF.*CT; % 3-D Plotting Coordinates
clf reset;
mesh(AFx,AFy,AFz,AF);
hold on
plot3(xa1,ya1,za1,'k',xa2,ya2,za2,'k',xa3,ya3,za3,'k',xa4,ya4,za4,...
      'k',xa5,ya5,za5,'k',xa6,ya6,za6,'k');

axis off
view([340,60]);
text(1.6,0,0,'X-Axis');
text(-.1,1.8,0,'Y-Axis');
text(-.2,0,2,'Z-Axis');
title([int2str(N),'-Element Array Space-Factor, D_{dB}=...
      ',num2str(DdB)], 'FontSize',14);
hold off

% N-Element Array Normalized Space Factor Pattern Display
%(alternate angle)

figure(3)
AFx=AF.*ST.*CP; AFy=AF.*ST.*SP; AFz=AF.*CT; % 3-D Plotting Coordinates
clf reset;
mesh(AFx,AFy,AFz,AF);
hold on
plot3(xa1,ya1,za1,'k',xa2,ya2,za2,'k',xa3,ya3,za3,'k',xa4,ya4,za4,...

```

```

    'k',xa5,ya5,za5,'k',xa6,ya6,za6,'k');
text(1.6,0,0,'X-Axis');
text(-.1,1.6,0,'Y-Axis');
text(-.2,0,1.7,'Z-Axis');
axis off
view([0,90]);
title([int2str(N),'-Element Array Space-Factor, D_{dB}=...
    ',num2str(DdB)], 'FontSize',14);
hold off

% x-y plane cut polar display

AFxd=AFx(1+round(Ntheta/2),1:(Nphi+1));
AFyd=AFy(1+round(Ntheta/2),1:(Nphi+1));
R=(AFxd.^2+AFyd.^2).^5;
BW=.707*ones(size(phi));
figure(4)
polar(phi,R);
hold on
polar(phi,BW,'r');
hold off
title([int2str(N),'-Element Array Pattern (Polar)'], 'FontSize', 14);

% x-y plane cut linear display

figure(5)
plot((phi*(360/(2*pi))),R,(phi*(360/(2*pi))),BW,'r');
axis([0 360 0 1.05]);
grid
title([int2str(N),'-Element Array Pattern (x-y Plane vs. Phi)']...
    ',FontSize', 14);
xlabel('Phi')
ylabel('Normalized Gain')
legend('Array Pattern', '3 dB line')

```

APPENDIX I. OFFSET POSITIONS

```
% This is a program that computes difference in array factor pattern
% for a 2 dimensional array when an offset to expected position is
% applied. The original array element locations and perturbed
% positions are entered by the user.
%
% Independently entered factors:
%     Number of elements
%     Element location
%     Desired aim point - Offset measurement is set for X-Y
%     plane aim point
%
% Assumed factors:
%     Isotropic elements
%     Identical polarization
%     Identical current magnitude
%
% Shows Plots for
%     Array Positions (original and offset locations)
%     Normalized Array Factor pattern for original configuration
%     (2 separate view angles)
%     Polar cross-section of normalized Array factor pattern in
%     x-y plane for original configuration
%     Linear cross-section of normalized Array factor pattern
%     in x-y plane for original configuration
%     Normalized Array Factor pattern for offset configuration
%     (2 separate view angles)
%     Polar cross-section of normalized Array factor pattern in
%     x-y plane for offset configuration
%     Linear cross-section of normalized Array factor pattern
%     in x-y plane for offset configuration overlaid with
%     pattern for original configuration
%
% By W. A. Lintz

% Set up problem space for spherical coordinates

clear all;

Ntheta=input('Enter Number of Theta Segments (default is 90): ');
if isempty(Ntheta)
    Ntheta=90;
end;
dtheta=pi/Ntheta;      % Changes to radians
theta=(0:dtheta:pi)';  % Theta vector (0-pi in Ntheta steps)

Nphi=input('Enter Number of Phi Segments (default is 180): ');
if isempty(Nphi)
    Nphi=180;
end;
dphi=2*pi/Nphi;        % Changes to radians
```

```

phi=(0:dphi:2*pi);          % Phi vector (0-2pi in Nphi steps)

Theta=theta*ones(1,Nphi+1); % Creates a Theta array Nt x Np
ST=sin(Theta)+eps;          % Projection on xy plane
CT=cos(Theta);              % Projection on z axis

Phi=ones(Ntheta+1,1)*phi;   % Creates a Phi array Nt x Np
SP=sin(Phi);                % Projection on y axis
CP=cos(Phi);                % Projection on xy plane

xa1=[1.5 0 0]; ya1=[0 0 0]; za1=[0 0 0]; % Axis coordinates
xa2=[-1.5 0 0]; ya2=[0 0 0]; za2=[0 0 0];
xa3=[0 0 0]; ya3=[1.5 0 0]; za3=[0 0 0];
xa4=[0 0 0]; ya4=[-1.5 0 0]; za4=[0 0 0];
xa5=[0 0 0]; ya5=[0 0 0]; za5=[1.5 0 0];
xa6=[0 0 0]; ya6=[0 0 0]; za6=[-1.5 0 0];

% N-Element Array Entry

N=input('Enter Number of Elements (Must be >1. Default is 2): ');
if isempty(N), N=2;
elseif N<=1, N=2;
end;

disp(' ')
disp('* Next you will enter information on element location.')
disp('* All information entered will be relative to the origin.')
disp('* Element locations will be in x,y coordinates, and distances')
disp('are in wavelenghts.')

for n=1:N
    disp(' ')
    disp(sprintf('Element %d', n))
    X(n)=input('    Enter element "X" coordinate: ');
    Y(n)=input('    Enter element "Y" coordinate: ');
end

disp(' ')
disp('* Now you will enter information on element location for')
disp('* a set of element offset from desired location.')
disp('* All information entered will be relative to the origin.')
disp('* Element locations will be in x,y coordinates, and distances')
disp('* are in wavelenghts.')

for n=1:N
    disp(' ')
    disp(sprintf('Element %d', n))
    Xdel(n)=input('    Enter element "X" coordinate: ');
    Ydel(n)=input('    Enter element "Y" coordinate: ');
end

disp('')
disp('Enter desired main beam pointing direction in degrees')
MBTo=input('Enter Theta (between 0 and 180 degrees -...
    default is 90): ');

```

```

if isempty(MBTo), MBTo=90;
elseif MBTo<0, MBTo=90;
elseif MBTo>90, MBTo=90;
end
MBPo=input('Enter Phi (between 0 and 359 degrees -...
           default is 60): ');
if isempty(MBPo), MBPo=60;
elseif MBPo<0, MBPo=60;
elseif MBPo>359, MBPo=60;
end

MBTo=(pi/180)*MBTo;           % Convert to Radians
MBPo=(pi/180)*MBPo;

SMBTo=sin(MBTo); CMBTo=cos(MBTo); % Handy for alpha determinations
SMBPo=sin(MBPo); CMBPo=cos(MBPo);

% N-element Array Display

figure(1)
clf reset
plot(X,Y,'r*',Xdel,Ydel,'g*')
axis([-1*max(abs(X))-1 max(abs(X))+1 -1*max...
      (abs(Y))-1 max(abs(Y))+1])
axis('square')
grid
title([int2str(N),'-Element Array Arrangement - Distance in...
        Wavelengths'], 'FontSize', 14);
xlabel('X-Axis')
ylabel('Y-Axis')
legend('Desired Location','Offset Location')

% N-Element Array Normalized Space Factor - Desired

n=1; AF=0;           % Set initial loop conditions
for n=1:N
    alpha=-(2*pi)*(X(n)*SMBTo*CMBPo + Y(n)*SMBTo*SMBPo); % Alpha
    AF=AF+ exp(j*alpha)*exp(j*2*pi*(X(n)*(ST.*CP)+Y(n)*(ST.*SP)));
end
AF=abs(AF/(max(max(AF)))));
AF2=AF.*AF.*ST;
D=4*pi/((sum(sum(AF2)))*dtheta*dphi);
DdB=10*log10(D);

% N-Element Array Normalized Space Factor Pattern Display

figure(2)
AFx=AF.*ST.*CP; AFy=AF.*ST.*SP; AFz=AF.*CT; % 3-D Plotting Coords
clf reset;
mesh(AFx,AFy,AFz,AF);
hold on
plot3(xa1,ya1,za1,'k',xa2,ya2,za2,'k',xa3,ya3,za3,'k',xa4,ya4,...
      za4,'k',xa5,ya5,za5,'k',xa6,ya6,za6,'k');

```

```

axis off
view([340,60]);
text(1.6,0,0,'X-Axis');
text(-.1,1.8,0,'Y-Axis');
text(-.2,0,2,'Z-Axis');
title([int2str(N),'-Element Array Space-Factor, D_{dB}=...
      ',num2str(DdB)], 'FontSize',14);
hold off

figure(3)
AFx=AF.*ST.*CP; AFy=AF.*ST.*SP; AFz=AF.*CT; % 3-D Plotting Coords
clf reset;
mesh(AFx,AFy,AFz,AF);
hold on
plot3(xa1,ya1,za1,'k',xa2,ya2,za2,'k',xa3,ya3,za3,'k',xa4,ya4,za4,...
      'k',xa5,ya5,za5,'k',xa6,ya6,za6,'k');
text(1.6,0,0,'X-Axis');
text(-.1,1.6,0,'Y-Axis');
text(-.2,0,1.7,'Z-Axis');
axis off
view([0,90]);
title([int2str(N),'-Element Array Space-Factor, D_{dB}=...
      ',num2str(DdB)], 'FontSize',14);
hold off

% x-y plane cut

AFxd=AFx(1+round(Ntheta/2),1:(Nphi+1));
AFyd=AFy(1+round(Ntheta/2),1:(Nphi+1));
R=(AFxd.^2+AFyd.^2).^5;
BW=.707*ones(size(phi));
figure(4)
polar(phi,R);
title([int2str(N),'-Element Array Pattern (Polar)'], 'FontSize', 14);
figure(5)
plot((phi*(360/(2*pi))),R);
axis([0 360 0 1.05]);
grid
title([int2str(N),'-Element Array Pattern (x-y Plane vs. Phi)']...
      ', 'FontSize', 14);
xlabel('Phi')
ylabel('Normalized Gain')

% N-Element Array Normalized Space Factor - with Offset

n=1; AFdel=0; % Set initial loop conditions
for n=1:N
    alpha=-(2*pi)*(X(n)*SMBTo*CMBPo + Y(n)*SMBTo*SMBPo); % Alpha
    AFdel=AFdel+ exp(j*alpha)*exp(j*2*pi*(Xdel(n)*...
        (ST.*CP)+Ydel(n)*(ST.*SP)));
end
AFdel=abs(AFdel/(max(max(AFdel))));
AF2del=AFdel.*AFdel.*ST;
Ddel=4*pi/((sum(sum(AF2del)))*dtheta*dphi);
DdBdel=10*log10(Ddel);

```

```

% N-Element Array Normalized Space Factor Pattern Display

figure(6)
AFxdel=AFdel.*ST.*CP; AFydel=AFdel.*ST.*SP; AFzdel=AFdel.*CT;
clf reset;
mesh(AFxdel,AFydel,AFzdel,AFdel);
hold on
plot3(xa1,ya1,za1,'k',xa2,ya2,za2,'k',xa3,ya3,za3,'k',xa4,ya4,za4,...
      'k',xa5,ya5,za5,'k',xa6,ya6,za6,'k');

axis off
view([340,60]);
text(1.6,0,0,'X-Axis');
text(-.1,1.8,0,'Y-Axis');
text(-.2,0,2,'Z-Axis');
title([int2str(N),'-Element Array Space-Factor with offset, D_{dB}=...
      ',num2str(DdBdel)], 'FontSize',14);
hold off

figure(7)
AFxdel=AFdel.*ST.*CP; AFydel=AFdel.*ST.*SP; AFzdel=AFdel.*CT;
clf reset;
mesh(AFxdel,AFydel,AFzdel,AFdel);
hold on
plot3(xa1,ya1,za1,'k',xa2,ya2,za2,'k',xa3,ya3,za3,'k',xa4,ya4,za4,...
      'k',xa5,ya5,za5,'k',xa6,ya6,za6,'k');
text(1.6,0,0,'X-Axis');
text(-.1,1.6,0,'Y-Axis');
text(-.2,0,1.7,'Z-Axis');
axis off
view([0,90]);
title([int2str(N),'-Element Array Space-Factor, D_{dB}=...
      ',num2str(DdBdel)], 'FontSize',14);
hold off

% x-y plane cut

AFxddel=AFxdel(1+round(Ntheta/2),1:(Nphi+1));
AFyddel=AFydel(1+round(Ntheta/2),1:(Nphi+1));
Rdel=(AFxddel.^2+AFyddel.^2).^5;
BW=.707*ones(size(phi));
figure(8)
polar(phi,Rdel);
title([int2str(N),'-Element Array Pattern (Polar)'], 'FontSize', 14);
figure(9)
plot((phi*(360/(2*pi))),R,(phi*(360/(2*pi))),Rdel,'g');
axis([0 360 0 1.05]);
grid
title([int2str(N),'-Element Array Pattern (x-y Plane vs. Phi)...
      with offset'], 'FontSize', 14);
xlabel('Phi')
ylabel('Normalized Gain')
legend('Desired Position', 'Offset Position')

```

THIS PAGE INTENTIONALLY LEFT BLANK

APPENDIX J. ONE DIMENSION PERTURB

```
% This is a program that computes the linear cross section in the x-y
% plane of the array factor pattern from a two dimensional array with
% a desired aim point, then modifies element location in one dimension
% while holding alpha (weight factor) constant.
%
% Array makeup to include number and location of elements and desired
% aim point are coded below, but can be modified to handle more complex
% structures. Hard coded is a 5 element array with symmetric positions
% and 10 position increments.
%
% Shows Plots for
%           Array Positions
%           Linear cross-section of normalized Array factor pattern
%           in x-y plane
% Plots after motion are over layed on initial plot to indicate motion.
%
% By W. A. Lintz

% Set up problem space for spherical coordinates

clear all;

Ntheta=90; %input('Enter Number of Theta Segments (default is 90): ');
%if isempty(Ntheta)
%   Ntheta=90;
%end;
dtheta=pi/Ntheta; % Changes to radians
theta=(0:dtheta:pi)'; % Theta vector (0-pi in Ntheta steps)

Nphi=180; %input('Enter Number of Phi Segments (default is 180): ');
%if isempty(Nphi)
%Nphi=180;
%end;
dphi=2*pi/Nphi; % Changes to radians
phi=(0:dphi:2*pi); % Phi vector (0-2pi in Nphi steps)

Theta=theta*ones(1,Nphi+1); % Creates a Theta array Nt x Np
ST=sin(Theta)+eps; % Projection on xy plane
CT=cos(Theta); % Projection on z axis

Phi=ones(Ntheta+1,1)*phi; % Creates a Phi array Nt x Np
SP=sin(Phi); % Projection on y axis
CP=cos(Phi); % Projection on xy plane

% N-Element Array Entry

N=5; %Number of Elements

% Desired main beam pointing direction in degrees
```

```

MBTo=90;           % Theta
MBPo=60;           % Phi

X=[.25 -.25 0 0 0]';
Y=[0 0 0 .25 -.25]';

% Convert to Radians
MBTo=(pi/180)*MBTo;
MBPo=(pi/180)*MBPo;

SMBTo=sin(MBTo); CMBTo=cos(MBTo); % Handy for Alpha
SMBPo=sin(MBPo); CMBPo=cos(MBPo);

% N-element Array Display

figure(1)
clf reset
plot(X,Y,'r*')
axis([-1*max(abs(X))-1 max(abs(X))+1 -1*max(abs(Y))-1 max(abs(Y))+1])
axis('square')
grid
title([int2str(N),'-Element Array Arrangement - Distance in...
      Wavelengths'], 'FontSize', 14);
xlabel('X-Axis')
ylabel('Y-Axis')

% N-Element Array Normalized Space Factor
n=1; AF=0;         % Set initial loop conditions
for n=1:N
    alpha(n)=-(2*pi)*(X(n)*SMBTo*CMBPo + Y(n)*SMBTo*SMBPo); % Alpha
    AF=AF+ exp(j*alpha(n))*exp(j*2*pi*(X(n)*(ST.*CP)+Y(n)*(ST.*SP)));
end
AF=abs(AF/(max(max(AF)))));
AF2=AF.*AF.*ST;
D=4*pi/((sum(sum(AF2)))*dtheta*dphi);
DdB=10*log10(D);

% N-Element Array Normalized Space Factor Pattern Display

AFx=AF.*ST.*CP; AFy=AF.*ST.*SP; AFz=AF.*CT;

% x-y plane cut

AFxd=AFx(1+round(Ntheta/2),1:(Nphi+1));
AFyd=AFy(1+round(Ntheta/2),1:(Nphi+1));
R=(AFxd.^2+AFyd.^2).^5;
BW=.707*ones(size(phi));
figure(2)
plot((phi*(360/(2*pi))),R);
axis([0 360 0 1.05]);
grid
title([int2str(N),'-Element Array Pattern (x-y Plane vs. Phi)']...
      , 'FontSize', 14);

```

```

xlabel('Phi')
ylabel('Normalized Gain')

% Random Position changes - 10 times.

for k=1:10
    X=[.25+k*(round(1-2*rand))*(.001035) ...
        -.25+k*(round(1-2*rand))*(.001035) ...
        0+k*(round(1-2*rand))*(.001035) ...
        0+k*(round(1-2*rand))*(.001035) 0]';
    Y=[0 0 0 .25 -.25]';

    % N-Element Array Normalized Space Factor for movement
    n=1; AF1=0; % Set initial loop conditions
    for n=1:N
        AF1=AF1+ exp(j*alpha(n))*exp(j*2*pi*(X(n)*(ST.*CP)...
            +Y(n)*(ST.*SP)));
    end
    AF1=abs(AF1/(max(max(AF1)))));
    AF21=AF1.*AF1.*ST;
    D1=4*pi/((sum(sum(AF21)))*dtheta*dphi);
    DdB1=10*log10(D1);

    % Post motion N-Element Array Normalized Space Factor Pattern

    AFx1=AF1.*ST.*CP; AFy1=AF1.*ST.*SP; AFz1=AF1.*CT;

    % x-y plane cut

    AFxd1=AFx1(1+round(Ntheta/2),1:(Nphi+1));
    AFyd1=AFy1(1+round(Ntheta/2),1:(Nphi+1));
    R1=(AFxd1.^2+AFyd1.^2).^5;
    BW1=.707*ones(size(phi));
    %figure(4)
    %hold on
    %polar(phi,R1,'g');
    %hold off
    figure(2)
    hold on
    plot((phi*(360/(2*pi))),R1,'g');
    hold off

    figure(1)
    hold on
    plot(X,Y,'r*')
    hold off
end

```

THIS PAGE INTENTIONALLY LEFT BLANK

APPENDIX K. MOTION SMEAR

```
% This is a program that considers the array factor change caused by
% motion over a series of time steps.
%
% Array configuration is random but set for general run. Can be
% modified. Maximum velocity of motion is user defined.
%
% Shows Plots for
%       Initial Array Position
%       Normalized Array Factor pattern
%       Linear cross-section of normalized Array factor
%       pattern in x-y plane in initial positions
%       Linear cross-section of normalized Array factor pattern in
%       x-y plane in after motion vs. initial
%
% By W. A. Lintz

% Set up problem space for spherical coordinates

clear all;

Ntheta=180;          % Number of Theta segments
dtheta=pi/Ntheta;    % Changes to radians
theta=(0:dtheta:pi)'; % Theta vector (0-pi in Ntheta steps)

Nphi=360;            % Number of Phi segments
dphi=2*pi/Nphi;      % Changes to radians
phi=(0:dphi:2*pi);   % Phi vector (0-2pi in Nphi steps)

Theta=theta*ones(1,Nphi+1); % Creates a Theta array Nt x Np
ST=sin(Theta)+eps;        % Projection on x-y plane
CT=cos(Theta);            % Projection on z axis

Phi=ones(Ntheta+1,1)*phi; % Creates a Phi array Nt x Np
SP=sin(Phi);              % Projection on y axis
CP=cos(Phi);              % Projection on x-y plane

% N-Element Array Entry

N=10;                    % Number of elements
for n=1:N
    X(n)=2*rand-1;        % Position of elements around origin x
    Y(n)=2*rand-1;        % Position of elements around origin y
end

% N-element Array Display

figure(1)
clf reset
plot(X,Y,'r*')
axis([-1*max(abs(X))-1 max(abs(X))+1 -1*max(abs(Y))-1 max(abs(Y))+1])
axis('square')
```

```

grid
title([int2str(N),'-Element Array Arrangement - Distance in...
      Wavelengths'], 'FontSize', 14);
xlabel('X-Axis')
ylabel('Y-Axis')

% Set aim point
MBTo=90;
MBPo=60;
MBTo=(pi/180)*MBTo; % Convert to Radians
MBPo=(pi/180)*MBPo;
SMBTo=sin(MBTo); CMBTo=cos(MBTo); % Handy for alpha determinations
SMBPo=sin(MBPo); CMBPo=cos(MBPo);

Vel=input('Enter max velocity for elements (default is 10.35 m/s): ');
if isempty(Vel)
    Vel=10.35;
end;

%%%%%%%%%%%%%%%%%%%%%%%%%%%%%%%%%%%%%%%%%%%%%%%%%%%%%%%%%%%%%%%%%%%%%%%%
% N-Element Array Space Factor - Initial Position
%%%%%%%%%%%%%%%%%%%%%%%%%%%%%%%%%%%%%%%%%%%%%%%%%%%%%%%%%%%%%%%%%%%%%%%%

n=1; AF=0; % Set initial loop conditions
for n=1:N
    alpha=-(2*pi)*(X(n)*SMBTo*CMBPo + Y(n)*SMBTo*SMBPo); % Alpha
    AF=AF+ exp(j*alpha)*exp(j*2*pi*(X(n)*(ST.*CP)+Y(n)*(ST.*SP)));
end

AF2=abs(AF/(max(max(AF))));
AF3=AF2.*AF2.*ST;
D=4*pi/((sum(sum(AF3)))*dtheta*dphi);
Corr=D/N;
DdB=10*log10(D);
AF=abs(AF);
Max=max(max(AF))+.5;

% N-Element Array Normalized Space Factor Pattern Display

xa1=[Max 0 0]; ya1=[0 0 0]; za1=[0 0 0]; % Axis coordinates for plots
xa2=[-Max 0 0]; ya2=[0 0 0]; za2=[0 0 0];
xa3=[0 0 0]; ya3=[Max 0 0]; za3=[0 0 0];
xa4=[0 0 0]; ya4=[-Max 0 0]; za4=[0 0 0];
xa5=[0 0 0]; ya5=[0 0 0]; za5=[Max 0 0];
xa6=[0 0 0]; ya6=[0 0 0]; za6=[-Max 0 0];

figure(2)
AFx=AF.*ST.*CP; AFy=AF.*ST.*SP; AFz=AF.*CT; % 3-D Plotting Coords
clf reset;
mesh(AFx,AFy,AFz,AF);
hold on
plot3(xa1,ya1,za1,'k',xa2,ya2,za2,'k',xa3,ya3,za3,'k',xa4,ya4,za4...
      , 'k',xa5,ya5,za5,'k',xa6,ya6,za6,'k');

```

```

text(Max,0,0,'X-Axis');
text(0,Max,0,'Y-Axis');
text(0,0,Max,'Z-Axis');
axis off
view([0,90]);
title([int2str(N),'-Element Array Space-Factor, D_{dB}=',...
      num2str(DdB)], 'FontSize',14);
hold off

% x-y plane cut

AFxd=AFx(1+round(Ntheta/2),1:(Nphi+1));
AFyd=AFy(1+round(Ntheta/2),1:(Nphi+1));
R=((AFxd.^2+AFyd.^2).^5)*Corr;

%%%%%%%%%%%%%%%%%%%%%%%%%%%%%%%%%%%%%%%%%%%%%%%%%%%%%%%%%%%%%%%%%%%%%%%%%%%%%%
% N-Element Array Normalized Space Factor - w/time steps
%%%%%%%%%%%%%%%%%%%%%%%%%%%%%%%%%%%%%%%%%%%%%%%%%%%%%%%%%%%%%%%%%%%%%%%%%%%%%%

X1=X;
Y1=Y;

for n=1:N;
    Velx(n)=(Vel/(sqrt(2)))*rand;
    Vely(n)=(Vel/(sqrt(2)))*rand;
end

for k=1:10;

    for n=1:N
        X1(n)=X1(n)+Velx(n)*(100e-6);
        Y1(n)=Y1(n)+Vely(n)*(100e-6);
    end

    n=1; AFs=0;           % Set initial loop conditions
    for n=1:N
        alpha=-(2*pi)*(X(n)*SMBTo*CMBPo + Y(n)*SMBTo*SMBPo); % Alpha
        AFs=AFs+ exp(j*alpha)*exp(j*2*pi*(X1(n)*(ST.*CP)+Y1(n)...
            *(ST.*SP)));
    end

    AF2s=abs(AFs/(max(max(AFs))));
    AF3s=AF2s.*AF2s.*ST;
    Ds=4*pi/((sum(sum(AF3s)))*dtheta*dphi);
    DdBs=10*log10(Ds);
    AFs=abs(AFs);
    Max=max(max(AFs))+.5;
    AFxs=AFs.*ST.*CP; AFys=AFs.*ST.*SP; AFzs=AFs.*CT;

    % x-y plane cut

    AFxds=AFxs(1+round(Ntheta/2),1:(Nphi+1));
    AFyds=AFys(1+round(Ntheta/2),1:(Nphi+1));

```

```

Rs=((AFxds.^2+AFyds.^2).^5)*Corr;
Error1=mean(abs(R-Rs));
Error2=R(60)-Rs(60);
Error3=100*Error2/R(60);

figure(k+2)
plot((phi*(360/(2*pi))),R,(phi*(360/(2*pi))),Rs,'g:');
axis([0 360 0 max(Rs)+.5]);
grid
xlabel('Phi')
ylabel('Gain')

end

```

APPENDIX L. AIM POINT GAIN CHANGE

```
% This program refines consideration of motion on arrays by considering
% the gain change on aim point
%
% Array configuration is random but set for run with N=5, but can be
% modified. Maximum velocity of motion is user defined.
%
% Shows Plots for
%           Initial Array Position
%           Normalized Array Factor pattern
%           Linear cross-section of normalized Array factor
%           pattern in x-y plane in initial positions
%           Linear cross-section of normalized Array factor
%           pattern in x-y plane in after motion vs.
%           initial
%
% By W. A. Lintz

% Set up problem space for spherical coordinates

for t=1:10
t
clear all;

Ntheta=180;           % Number of Theta segments
dtheta=pi/Ntheta;     % Changes to radians
theta=(0:dtheta:pi)'; % Theta vector (0-pi in Ntheta steps)

Nphi=360;             % Number of Phi segments
dphi=2*pi/Nphi;       % Changes to radians
phi=(0:dphi:2*pi);    % Phi vector (0-2pi in Nphi steps)

Theta=theta*ones(1,Nphi+1); % Creates a Theta array Nt x Np
ST=sin(Theta)+eps;        % Projection on xy plane
CT=cos(Theta);            % Projection on z axis

Phi=ones(Ntheta+1,1)*phi; % Creates a Phi array Nt x Np
SP=sin(Phi);              % Projection on y axis
CP=cos(Phi);              % Projection on xy plane

% N-Element Array Entry

N=5;                     % Number of elements
for n=1:N
    X(n)=2*rand-1; % Position of elements around origin x
    Y(n)=2*rand-1; % Position of elements around origin y
end

% N-element Array Display

% Set aim point
MBTo=90;
```

```

MBPo=60;
MBTo=(pi/180)*MBTo;      % Convert to Radians
MBPo=(pi/180)*MBPo;
SMBTo=sin(MBTo); CMBTo=cos(MBTo);
SMBPo=sin(MBPo); CMBPo=cos(MBPo);

Vel=60.35;      % Set Velocity

%%%%%%%%%%%%%%%%%%%%%%%%%%%%%%%%%%%%%%%%%%%%%%%%%%%%%%%%%%%%%%%%%%%%%%%%%%%%%%
% N-Element Array Space Factor - Initial Position
%%%%%%%%%%%%%%%%%%%%%%%%%%%%%%%%%%%%%%%%%%%%%%%%%%%%%%%%%%%%%%%%%%%%%%%%%%%%%%

n=1; AF=0; % Set initial loop conditions
for n=1:N
    alpha=-(2*pi)*(X(n)*SMBTo*CMBPo + Y(n)*SMBTo*SMBPo); % Alpha
    AF=AF+ exp(j*alpha)*exp(j*2*pi*(X(n)*(ST.*CP)+Y(n)*(ST.*SP)));
end

AF2=abs(AF/(max(max(AF)))));
AF3=AF2.*AF2.*ST;
D=4*pi/((sum(sum(AF3)))*dtheta*dphi);
Corr=D/N;
DdB=10*log10(D);
AF=abs(AF);
Max=max(max(AF))+.5;

AFx=AF.*ST.*CP; AFy=AF.*ST.*SP; AFz=AF.*CT;

% x-y plane cut

AFxd=AFx(1+round(Ntheta/2),1:(Nphi+1));
AFyd=AFy(1+round(Ntheta/2),1:(Nphi+1));
R=((AFxd.^2+AFyd.^2).^5)*Corr;

%%%%%%%%%%%%%%%%%%%%%%%%%%%%%%%%%%%%%%%%%%%%%%%%%%%%%%%%%%%%%%%%%%%%%%%%%%%%%%
% N-Element Array Normalized Space Factor - w/time steps
%%%%%%%%%%%%%%%%%%%%%%%%%%%%%%%%%%%%%%%%%%%%%%%%%%%%%%%%%%%%%%%%%%%%%%%%%%%%%%

X1=X;
Y1=Y;

for n=1:N;
    Velx(n)=(Vel/(sqrt(2)))*(2*rand-1);
    Vely(n)=(Vel/(sqrt(2)))*(2*rand-1);
end

for k=1:60;

    for n=1:N
        X1(n)=X1(n)+Velx(n)*(100e-6);
        Y1(n)=Y1(n)+Vely(n)*(100e-6);
    end

    n=1; AFs=0; % Set initial loop conditions

```

```

for n=1:N
    alpha=-(2*pi)*(X(n)*SMBTo*CMBPo + Y(n)*SMBTo*SMBPo);
    AFs=AFs+ exp(j*alpha)*exp(j*2*pi*(X1(n)*(ST.*CP)+...
        Y1(n)*(ST.*SP)));
end

AF2s=abs(AFs/(max(max(AFs))));
AF3s=AF2s.*AF2s.*ST;
Ds=4*pi/((sum(sum(AF3s)))*dtheta*dphi);
DdBs=10*log10(Ds);
AFs=abs(AFs);
Max=max(max(AFs))+.5;
AFxs=AFs.*ST.*CP; AFys=AFs.*ST.*SP; AFzs=AFs.*CT;

% x-y plane cut

AFxds=AFxs(1+round(Ntheta/2),1:(Nphi+1));
AFyds=AFys(1+round(Ntheta/2),1:(Nphi+1));
Rs=((AFxds.^2+AFyds.^2).^5)*Corr;
Error2=R(60)-Rs(60);
Error3(k)=100*Error2/R(60);

end

k=1:60;
k=k*(100e-6);

figure(1)
plot(k,Error3)
hold on

end

xlabel('Time')
ylabel('% Decrease in Gain on Target')
text(.1e-3,10,0,'N=5')

```

THIS PAGE INTENTIONALLY LEFT BLANK

APPENDIX M. CHANGE PERCENTAGE FACTOR

```

% This is a program to evaluate the random distribution of the defined
% change percentage factor
%
% Histogram can be built with additional runs as defined within.
% Number of elements is set for N=40 and a velocity of 60.35 mph but
% can be altered.
%
% Shows Plot for
%           Result of G_hat*sum of motion
%
% By W. A. Lintz

% Set up problem space for spherical coordinates

clear all;

Ntheta=180;           % Number of Theta segments
dtheta=pi/Ntheta;     % Changes to radians
theta=(0:dtheta:pi)'; % Theta vector (0-pi in Ntheta steps)
Nphi=360;             % Number of Phi segments
dphi=2*pi/Nphi;       % Changes to radians
phi=(0:dphi:2*pi);    % Phi vector (0-2pi in Nphi steps)

Theta=theta*ones(1,Nphi+1); % Creates a Theta array Nt x Np
ST=sin(Theta)+eps;         % Projection on x-y plane
CT=cos(Theta);             % Projection on z axis
Phi=ones(Ntheta+1,1)*phi;  % Creates a Phi array Nt x Np
SP=sin(Phi);               % Projection on y axis
CP=cos(Phi);               % Projection on xy plane

% Set max vel
Vel=60.35;

% Set time
t=3e-3;

% Set aim point
MBTo=90;
MBPo=60;
MBTo=(pi/180)*MBTo;        % Convert to Radians
MBPo=(pi/180)*MBPo;
SMBTo=sin(MBTo); CMBTo=cos(MBTo);
SMBPo=sin(MBPo); CMBPo=cos(MBPo);

% Repeat

rep=1000;                 % Number of Repetitions
for r=1:rep

    r %Counter

```

```

% N-Element Array Position
N=40; % Number of elements
for n=1:N
    X(n)=2*rand-1; % Position of elements around origin x
    Y(n)=2*rand-1; % Position of elements around origin y
end

% N-Element Velocity
for n=1:N;
    Velx(n)=(Vel/(sqrt(2)))*rand;
    Vely(n)=(Vel/(sqrt(2)))*rand;
end

n=1; AF=0; Num=0; % Set initial loop conditions
for n=1:N
    alpha=-(2*pi)*(X(n)*SMBTo*CMBPo + Y(n)*SMBTo*SMBPo);
    AF=AF+exp(j*alpha)*exp(j*2*pi*(X(n)*(ST.*CP)+Y(n)*...
        (ST.*SP))).*exp(j*2*pi*(Velx(n)*t*(ST.*CP)+...
        Vely(n)*t*(ST.*SP)));
    Num=Num+exp(j*alpha)*exp(j*2*pi*(X(n)*(SMBTo*CMBPo)+Y(n)*...
        (SMBTo*SMBPo))).*exp(j*2*pi*(Velx(n)*t*(SMBTo.*CMBPo)+...
        Vely(n)*t*(SMBTo.*SMBPo)));
end

AF=abs(AF/(max(max(AF))));
AF=AF.*AF.*ST;
D=4*pi/((sum(sum(AF)))*dtheta*dphi);
Result(r)=abs(Num)*D;

end

rep=1:rep;

figure(1)
plot(Result,rep,'*')
xlabel('x')
ylabel('y')
MEAN=mean(Result);
STD=std(Result);
title(['% Difference Distribution, Mean=',int2str(MEAN),', ...
    STD=',int2str(STD)], 'FontSize', 12);

h=hist(Result,100);
bins=1:100;
figure(2)
stem(bins,h)

```

APPENDIX N. RESET ENERGY

```
% This is a program that computes the difference in energy usage
% between using the proposed reset timing method and the
% alternative methods.
%
% Shows Plot Energy usage difference
%
% By W. A. Lintz

clear all;

%%%%%%%%%%%%%%%%%%%%%%%%%%%%%%%%%%%%%%%%%%%%%%%%%%%%%%%%%%%%%%%%%%%%%%%%

% Establish energy used in proposed process
del=1;           % Energy cost for full data and metadata
chi=.1;          % Energy cost for meta-data only
N=8;             % Number of nodes
tau=linspace(501,1000,500); % Number of samples btwn resets

E_p=del*N+((del-chi)*N)*(tau-1);

% Establish energy used in alt process

tau_a=10;        % Number of arbitrary samples btwn resets << tau

% Part 1 - even number
E_a1=floor(tau./tau_a).*(del*N+((del-chi)*N)*(tau_a-1));
% Part 2 - non-even w/ meta
E_a2=(ceil(tau./tau_a)-floor(tau./tau_a))*del*N;
% Part 3 - non-even w/o meta
for i=1:500
    if (tau(i)-(floor(tau(i)/tau_a)*tau_a)-1)>=1
        E_a3(i)=(tau(i)-(floor(tau(i)/tau_a)*tau_a)-1)*...
            ((del-chi)*N);
    else
        E_a3(i)=0;
    end
end

E_a=E_a1+E_a2+E_a3;

Diff_A=abs(E_p-E_a);

% Establish energy used in alt process again with a
% different tau_a

tau_a=12; % Number of arbitrary samples btwn resets << tau

% Part 1 - even number
E_a1=floor(tau./tau_a).*(del*N+((del-chi)*N)*(tau_a-1));
% Part 2 - non-even w/ meta
```

```

E_a2=(ceil(tau./tau_a)-floor(tau./tau_a))*del*N;
% Part 3 - non-even w/o meta
for i=1:500
    if (tau(i)-(floor(tau(i)/tau_a)*tau_a)-1)>=1
        E_a3(i)=(tau(i)-(floor(tau(i)/tau_a)*tau_a)-1)...
            *((del-chi)*N);
    else
        E_a3(i)=0;
    end
end
E_a=E_a1+E_a2+E_a3;

Diff_B=abs(E_p-E_a);

% Establish energy used in alt process again with a different N

tau_a=15;    % Number of arbitrary samples btwn resets << tau

% Part 1 - even number
E_a1=floor(tau./tau_a).*(del*N+((del-chi)*N)*(tau_a-1));
% Part 2 - non-even w/ meta
E_a2=(ceil(tau./tau_a)-floor(tau./tau_a))*del*N;
% Part 3 - non-even w/o meta
for i=1:500
    if (tau(i)-(floor(tau(i)/tau_a)*tau_a)-1)>=1
        E_a3(i)=(tau(i)-(floor(tau(i)/tau_a)*tau_a)-1)*((del-chi)*N);
    else
        E_a3(i)=0;
    end
end
E_a=E_a1+E_a2+E_a3;

Diff_C=abs(E_p-E_a);

% Plot

figure(1)
plot(tau,Diff_A, tau,Diff_B, tau, Diff_C)
xlabel('Tau (samples)')
ylabel('Energy')
legend('tau is diff 10','12','15')

```

APPENDIX O. CHANGE PERCENTAGE EXPECTED VALUE

```
% This is a program that computes the difference in change percentage
% expected value for the proposed reset timing method and the
% alternative methods
%
% By W. A. Lintz

clear all;

%%%%%%%%%%%%%%%%%%%%%%%%%%%%%%%%%%%%%%%%%%%%%%%%%%%%%%%%%%%%%%%%%%%%%%%%

% Change Percentage calculation

% Set up problem space for spherical coordinates

clear all;

Ntheta=180;          % Number of Theta segments
dtheta=pi/Ntheta;    % Changes to radians
theta=(0:dtheta:pi)'; % Theta vector (0-pi in Ntheta steps)

Nphi=360;            % Number of Phi segments
dphi=2*pi/Nphi;      % Changes to radians
phi=(0:dphi:2*pi);   % Phi vector (0-2pi in Nphi steps)

Theta=theta*ones(1,Nphi+1); % Creates a Theta array Nt x Np
ST=sin(Theta)+eps;          % Projection on xy plane
CT=cos(Theta);              % Projection on z axis

Phi=ones(Ntheta+1,1)*phi;   % Creates a Phi array Nt x Np
SP=sin(Phi);                % Projection on y axis
CP=cos(Phi);                % Projection on xy plane

% N-Element Array Entry

N=5;          % Number of elements
for n=1:N
    X(n)=2*rand-1; % Position of elements around origin x
    Y(n)=2*rand-1; % Position of elements around origin y
end

% N-element Array Display

% Set aim point
MBTo=90;
MBPo=60;
MBTo=(pi/180)*MBTo; % Convert to Radians
MBPo=(pi/180)*MBPo;
SMBTo=sin(MBTo); CMBTo=cos(MBTo);
SMBPo=sin(MBPo); CMBPo=cos(MBPo);

Vel=103.5; % Set Velocity
```

```

% Initial gain

n=1; AF=0; % Set initial loop conditions
for n=1:N
    alpha=-(2*pi)*(X(n)*SMBTo*CMBPo + Y(n)*SMBTo*SMBPo);
    AF=AF+ exp(j*alpha)*exp(j*2*pi*(X(n)*(ST.*CP)+Y(n)*(ST.*SP)));
end

AF2=abs(AF/(max(max(AF))));
AF3=AF2.*AF2.*ST;
D=4*pi/((sum(sum(AF3)))*dtheta*dphi);
Corr=D/N;
DdB=10*log10(D);
AF=abs(AF);
Max=max(max(AF))+.5;

% N-Element Array Normalized Space Factor Pattern Display

xa1=[Max 0 0]; ya1=[0 0 0]; za1=[0 0 0];
xa2=[-Max 0 0]; ya2=[0 0 0]; za2=[0 0 0];
xa3=[0 0 0]; ya3=[Max 0 0]; za3=[0 0 0];
xa4=[0 0 0]; ya4=[-Max 0 0]; za4=[0 0 0];
xa5=[0 0 0]; ya5=[0 0 0]; za5=[Max 0 0];
xa6=[0 0 0]; ya6=[0 0 0]; za6=[-Max 0 0];

figure(2)
AFx=AF.*ST.*CP; AFy=AF.*ST.*SP; AFz=AF.*CT;
clf reset;
mesh(AFx,AFy,AFz,AF);
hold on
plot3(xa1,ya1,za1,'k',xa2,ya2,za2,'k',xa3,ya3,za3,'k',xa4,ya4,za4...
    , 'k',xa5,ya5,za5,'k',xa6,ya6,za6,'k');
text(Max,0,0,'X-Axis');
text(0,Max,0,'Y-Axis');
text(0,0,Max,'Z-Axis');
axis off
view([0,90]);
title([int2str(N),'-Element Array Space-Factor, D_{dB}=...
    ',num2str(DdB)], 'FontSize',14);
hold off

% x-y plane cut

AFxd=AFx(1+round(Ntheta/2),1:(Nphi+1));
AFyd=AFy(1+round(Ntheta/2),1:(Nphi+1));
R=((AFxd.^2+AFyd.^2).^5)*Corr;

%%%%%%%%%%%%%%%%%%%%%%%%%%%%%%%%%%%%%%%%%%%%%%%%%%%%%%%%%%%%%%%%%%%%%%%%%%%%%%
% N-Element Array Normalized Space Factor - w/time steps
%%%%%%%%%%%%%%%%%%%%%%%%%%%%%%%%%%%%%%%%%%%%%%%%%%%%%%%%%%%%%%%%%%%%%%%%%%%%%%

for averages=1:500

    X1=X;

```

```

Y1=Y;

for n=1:N;
    Velx(n)=(Vel/(sqrt(2)))*rand;
    Vely(n)=(Vel/(sqrt(2)))*rand;
end

for k=1:50;

    for n=1:N
        X1(n)=X1(n)+Velx(n)*(100e-6);
        Y1(n)=Y1(n)+Vely(n)*(100e-6);
    end

    n=1; AFs=0;           % Set initial loop conditions
    for n=1:N
        alpha=-(2*pi)*(X(n)*SMBTo*CMBPo + Y(n)*SMBTo*SMBPo);
        AFs=AFs+ exp(j*alpha)*exp(j*2*pi*(X1(n)*(ST.*CP)+...
            Y1(n)*(ST.*SP)));
    end

    AF2s=abs(AFs/(max(max(AFs)))));
    AF3s=AF2s.*AF2s.*ST;
    Ds=4*pi/((sum(sum(AF3s)))*dtheta*dphi);
    DdBs=10*log10(Ds);
    AFs=abs(AFs);
    Max=max(max(AFs))+.5;
    AFxs=AFs.*ST.*CP; AFys=AFs.*ST.*SP; AFzs=AFs.*CT;

    % x-y plane cut

    AFxds=AFxs(1+round(Ntheta/2),1:(Nphi+1));
    AFyds=AFys(1+round(Ntheta/2),1:(Nphi+1));
    Rs=((AFxds.^2+AFyds.^2).^5)*Corr;
    Error1=mean(abs(R-Rs));
    Error2=R(61)-Rs(61);
    Error3=100*Error2/R(61);

    if k==30
        C_p(averages)=Error3;
    elseif k==35
        C_a_thirtyfive(averages)=Error3;
    elseif k==40
        C_a_forty(averages)=Error3;
    elseif k==45
        C_a_fortyfive(averages)=Error3;
    elseif k==50
        C_a_fifty(averages)=Error3;
    end

end
averages
end

```

```
Ave_C_p=mean(C_p)
Ave_C_a_thirtyfive=mean(C_a_thirtyfive)
Ave_C_a_forty=mean(C_a_forty)
Ave_C_a_fortyfive=mean(C_a_fortyfive)
Ave_C_a_fifty=mean(C_a_fifty)
```

APPENDIX P. PATTERN PROJECTION AND POLARIZATION

```
% This is a program that considers element pattern projection and
% polarization effects
%
%
% Assumed factors:
%     - Elements are dipoles
%     - Identical polarization
%     - Identical current magnitude
%
% Shows Plot for the effect of pitch angle and roll angle on
% dipole pattern
%
%
% By W. A. Lintz

clear all;

% Pattern projection
El=linspace(0,pi/2,10000);    % Elevation angle.
Th=(pi/2)-El;
PP=(cos((pi/2)*cos(Th))./(sin(Th))).^2;

% Polarization
X=linspace(0,pi/2,10000); % Polarization is top/bottom symmetric
POL=(cos(X)).^2;

figure(1)
plot(rad2deg(El),PP,rad2deg(X),POL)
xlabel('Angle (degrees)')
ylabel('Magnitude')
legend('/O(/pi/2-p)', '/r(/c)')
```

THIS PAGE INTENTIONALLY LEFT BLANK

APPENDIX Q. POTENTIAL ORIENTATION

```
% This is a program that considers potential orientation angles (pitch
% and roll) that may be attributed to signal loss over perfect free
% space
%
% Assumed factors:
%     - Elements are dipoles
%     - Identical polarization
%     - Identical current magnitude
%
% Shows Plot for potential angles associated with percentage drops
%
%
% By W. A. Lintz

%%%%%%%%%%%%%%%%%%%%%%%%%%%%%%%%%%%%%%%%%%%%%%%%%%%%%%%%%%%%%%%%%%%%%%%%

clear all;

% Drop is chosen as .1, .2 and .35 F
% Find associated Psi(Pitch) and Chi(Polarization)

T=[.9,.8,1-.45];
Psi=linspace(0,90,5000);
Chi1=rad2deg(real(acos(sqrt((T(1))./(cos((pi/2)*cos(deg2rad(Psi)))...
    ./sin(deg2rad(Psi))).^2))));
Chi2=rad2deg(real(acos(sqrt((T(2))./(cos((pi/2)*cos(deg2rad(Psi)))...
    ./sin(deg2rad(Psi))).^2))));
Chi3=rad2deg(real(acos(sqrt((T(3))./(cos((pi/2)*cos(deg2rad(Psi)))...
    ./sin(deg2rad(Psi))).^2))));

figure(2)
plot(Psi,Chi1,Psi,Chi2,Psi,Chi3)
xlabel('Psi(degrees)')
ylabel('Xi(degrees)')
legend('10% drop','20% drop', '45% drop')
```

THIS PAGE INTENTIONALLY LEFT BLANK

APPENDIX R. ORIENTATION / POLARIZATION FACTOR

```
% This is a program that the probability of mutual orientation
% polarization factor when each element is assessed a "wobble
% factor" where the user defines the expected standard
% deviation of Theta
%
% Shows Plots for
%     Magnitude of each element to a check positions
%     Instantaneous "wobble" for each element
%     Instantaneous orientation-polarization factor
%     Histogram of orientation-polarization factor
%     Plots showing instantaneous potential angles are hidden
%
% Increased runs provide additional accuracy for histogram.
% Histogram is displayed with a Beta distribution.
%
% By W. A. Lintz

clear all;

for round=1:50000 % Determines number of runs in the
                  % histogram - more runs increases
                  % accuracy.

% Placement of 3 nodes
A=[0 0 0];
B=[1000 500 0];
C=[3000 -100 0];

% Step 1 - Set mags by using a wobble factor of std deviation

    % Enter expected std deviation of Theta in degrees
    STD_T_B=15; % 1 degrees chosen here
    STD_T_C=20; % 1 degrees chosen here

    % Translate to pitch and pol at 45 degrees
    X_B=STD_T_B*sin(deg2rad(45));
    X_C=STD_T_C*sin(deg2rad(45));

    % Translate to expected Pitch and Pol factors
    PP_B=(cos((pi/2)*cos(deg2rad(90-X_B)))...
        ./ (sin(deg2rad(90-X_B)))).^2;
    POL_B=(cos(deg2rad(X_B))).^2;
    STD_F_B=PP_B*POL_B;

    PP_C=(cos((pi/2)*cos(deg2rad(90-X_C)))...
        ./ (sin(deg2rad(90-X_C)))).^2;
    POL_C=(cos(deg2rad(X_C))).^2;
    STD_F_C=PP_C*POL_C;

    % Randomly assign expected magnitude
    mag_AB(round)=1-abs((1-STD_F_B)*(randn));
```

```

        if mag_AB(round)>1
            mag_AB(round)=mag_AB(round)-...
                floor(mag_AB(round));
        end
        mag_AC(round)=1-abs((1-STD_F_C)*(randn));
        if mag_AC(round)>1
            mag_AC(round)=mag_AC(round)-...
                floor(mag_AC(round));
        end

% Step 2 - Get orientation from A to B with a randomly chosen Phi_B

% Rotate B to x axis
K=rad2deg(atan2(B(2),B(1)));

% set Phi as random
Phi_B=2*pi*(rand); % Phi_B_orig=Phi_B;
if Phi_B==0|Phi_B==pi/2|Phi_B==pi|Phi_B==3*.5*pi
    % Slight offset to handle anomaly angles
    Phi_B=Phi_B+eps;
elseif Phi_B==2*pi
    Phi_B==Phi_B-eps;
end

% Find Associated Theta_B

if ((Phi_B>1.5608)&(Phi_B<1.5808))|((Phi_B>4.7024)
    &(Phi_B<4.7224))
    Psi_B=90-eps;
    Chi_B=eps;
else
    % Find potential Psi and Chi range
    Psi_B=linspace(0,90,5000);
    Chi_B=rad2deg(real(acos(sqrt((mag_AB(round))
        ./cos((pi/2)*cos(deg2rad(Psi_B)))
        ./sin(deg2rad(Psi_B)).^2)))));
    Chi_B(1)=0;
    %figure(1)
    %plot(Psi_B,Chi_B)
    %xlabel('Psi(degrees)')
    %ylabel('Chi(degrees)')
    %title('Pitch versus Polarization
        Angles for A to B')

    % Choose Psi and Chi associated with
    % randomly chosen Phi
    temp_B=(Chi_B./(90-Psi_B))-abs(tan(Phi_B));
    index_B=find(abs(temp_B)==min(abs(temp_B)));
    if length(index_B)~=1
        index_B=max(index_B);
    end
    Chi_B=Chi_B(index_B);
    if Chi_B==90;
        Chi_B=Chi_B-eps;
    end
end

```

```

        end
        Psi_B=Psi_B(index_B);
    end

    % Name Theta_B
    Theta_B(round)=Chi_B/(abs(sin(Phi_B)));
    Phi_B=rad2deg(Phi_B);

% Return to original aspect
    % Theta_B does not change
    Phi_B=Phi_B+K;          % Rotates by K
    if Phi_B>=360
        Phi_B=Phi_B-360;
    elseif Phi_B<=(-360)
        Phi_B=Phi_B+360;
    end

% Step 3 - Get orientation from A to C with a randomly choosen Phi_C

    % Rotate C to x axis
    L=rad2deg(atan2(C(2),C(1)));

    % set Phi_C as random
    Phi_C=2*pi*(rand);  Phi_C_orig=Phi_C;
    if Phi_C==0|Phi_C==pi/2|Phi_C==pi|Phi_C==3*.5*pi
        Phi_C=Phi_C+eps;
    elseif Phi_C==2*pi
        Phi_C==Phi_C-eps;
    end

    % Find Associated Theta_C

    if ((Phi_C>1.5608)&(Phi_C<1.5808))|((Phi_C>4.7024)...
        &(Phi_C<4.7224))
        Psi_C=90-eps;
        Chi_C=eps;
    else
        % Find potential Psi and Chi range
        Psi_C=linspace(0,90,5000);
        Chi_C=rad2deg(real(acos(sqrt((mag_AC(round))...
            ./cos((pi/2)*cos(deg2rad(Psi_C)))...
            ./sin(deg2rad(Psi_C)).^2)))));
        Chi_C(1)=0;
        %figure(2)
        %plot(Psi_C,Chi_C)
        %xlabel('Psi(degrees)')
        %ylabel('Chi(degrees)')
        %title('Pitch versus Polarization Angles...
            for A to C')

        % Choose Psi and Chi associated with
        % randomly chosen Phi
        temp_C=(Chi_C./(90-Psi_C))-abs(tan(Phi_C));
        index_C=find(abs(temp_C)==min(abs(temp_C)));

```

```

        if length(index_C)~=1
            index_C=max(index_C);
        end
        Chi_C=Chi_C(index_C);
        if Chi_C==90;
            Chi_C=Chi_C-eps;
        end
        Psi_C=Psi_C(index_C);
    end

    % Name Theta_C
    Theta_C(round)=Chi_C/(abs(sin(Phi_C)));
    Phi_C=rad2deg(Phi_C);

% Return to original aspect
    % Theta_C does not change
    Phi_C=Phi_C+L;           % Rotates by L
    if Phi_C>=360
        Phi_C=Phi_C-360;
    elseif Phi_C<=(-360)
        Phi_C=Phi_C+360;
    end

% Step 4 - B talks to C - Rectify coordinates to place B at center

B_temp=B-B;
C_temp=C-B;

% Step 5 - Get orientation from B to C using info from Steps 1 and 2

    % Rotate B and C to align C on x-axis
    M=rad2deg(atan2(C_temp(2), C_temp(1)));

    % Theta_B does not change

    Phi_B=Phi_B-M;           % Rotate Phi B
    if Phi_B>=360
        Phi_B=Phi_B-360;
    elseif Phi_B<=(-360)
        Phi_B=Phi_B+360;
    end

    % Theta_C does not change

    Phi_C=Phi_C-M;           % Rotate Phi C
    if Phi_C>=360
        Phi_C=Phi_C-360;
    elseif Phi_C<=(-360)
        Phi_C=Phi_C+360;
    end

% Step 6 - Translate Orientation into Pitch and Polarization
% information

```

```

Psi_BC=90-Theta_B(round)*abs(cos(Phi_B)); % Pitch of B towards C
                                         % (note non-additive so
                                         % away vs. towards does
                                         % not matter)

    if Psi_BC<0
        Psi_BC=Psi_BC+180;
    elseif Psi_BC>180
        Psi_BC=Psi_BC-180;
    end
Chi_BC=Theta_B(round)*sin(Phi_B); % Polarization of B WRT x-axis

Psi_CB=90-Theta_C(round)*abs(cos(Phi_C)); % Pitch of C towards B
                                         % (note non-additive so
                                         % away vs. towards does
                                         % not matter)

    if Psi_CB<0
        Psi_CB=Psi_CB+180;
    elseif Psi_CB>180
        Psi_CB=Psi_CB-180;
    end
Chi_CB=Theta_C(round)*sin(Phi_C); % Polarization of C WRT x-axis

% Step 7 - Match them up

Pitch_B=Psi_BC;
Pitch_C=Psi_CB;
Pol_BC=abs(Chi_BC-Chi_CB);

% Step 8 - Find the factor

P=(cos(.5*pi*cos(deg2rad(Pitch_C)))/sin(deg2rad(Pitch_C))).^2;
Pe=(cos(.5*pi*cos(deg2rad(Pitch_B)))/sin(deg2rad(Pitch_B))).^2;
r=(cos(deg2rad(Pol_BC))).^2;

Factor(round)=P*Pe*r;
    if Factor(round)<0
        Pitch_B
        Pe
        Pitch_C
        P
        Pol_BC
        r
        Factor(round)
        break
    end

round

end

Max=max(Factor)
Min=min(Factor)

figure(3)
plot(1:length(mag_AB), mag_AB, round, mag_AC)

```

```

legend('Magnitude A to B','Magnitude A to C')

figure(4)
plot(1:length(Theta_B),Theta_B,1:length(Theta_C),Theta_C)
legend('Theta_B','Theta_C')

figure(5)
axis([1 length(Factor) min(Factor)-.05 1.05])
plot(1:length(Factor),Factor, '.')
title('Factor')
xlabel('run')
ylabel('Magnitude')

figure(6)
bins=linspace(min(Factor),max(Factor),60);
histogram=(hist(Factor,60));

average=(1/(length(Factor)))*sum(Factor);
variance=(1/(length(Factor)))*sum((Factor-average).^2);
alpha=average*((average*(1-average)/variance)-1);
beta=(1-average)*((average*(1-average)/variance)-1);
fx=(gamma(alpha+beta)/(gamma(alpha)*gamma(beta)))*...
    (bins.^(alpha-1)).*((1-bins).^(beta-1));

stem(bins,histogram/max(histogram))
hold on
plot(bins,fx/max(fx),'r')
hold off
xlabel('Transmission Factor Bins')
ylabel('Normalized Magnitude')

```

APPENDIX S. TRANSMISSION STRENGTH CORRECTION

```
% This is a program that applies the predictive beta distribution for
% orientation-polarization to apply a correction of 1/mean(Factor)
% to transmission strength
%
% Shows Plots for
%     SNR with factor under ideal conditions
%     SNR with the correction
%     Corrected histogram
%
% Increased runs provide additional accuracy for histogram. Histogram
% is displayed with a Beta distribution.
%
% This algorithm is dependent on the algorithm in Appendix R
%
% By W. A. Lintz

% Step 1 - Establish a baseline Eb/No and call it SNR

    d_BC=sqrt(((B(1)-C(1))^2)+((B(2)-C(2))^2)+((B(3)-C(3))^2));
    % distance from B to C
    Pt=.001;      % Power Xmitted
    Gt=1.64;      % Dipole gain
    Gr=1.64;      % Dipole gain
    lambda=.01;  % Wavelength
    Rb=100000;    % Bit rate
    T=290;        % Standard temperature
    k=1.38e-23;   % Boltzmann's constant

    SNR=Pt*Gt*Gr/(((4*pi*d_BC/lambda)^2)*Rb*T*k)

% Step 2- Introduce a Beta RV from one of Part 4's runs

    SNR_wFac=SNR*Factor;
    figure(7)
    title('SNR w/ Factor')
    plot(1:length(SNR_wFac), SNR_wFac)
    average_wFac=mean(SNR_wFac)

% Step 3 - Introduce correction

    Cor=1/average;
    SNR_wCor=SNR_wFac*Cor;
    figure(8)
    title('SNR w/ Correction')
    plot(1:length(SNR_wCor), SNR_wCor)
    average_wCor=mean(SNR_wCor)
    figure(9)
    bins2=linspace(min(SNR-SNR_wCor),max...
        (SNR-SNR_wCor),60);
```

```
histogram2=(hist(SNR-SNR_wCor,60));  
stem(bins2,histogram2/max(histogram2))  
title('Histogram of Eb/No before factor - Eb/No...  
      with correction')
```

INITIAL DISTRIBUTION LIST

1. Defense Technical Information Center
Ft. Belvoir, Virginia
2. Dudley Knox Library
Naval Postgraduate School
Monterey, California
3. U.S. Special Operations Command
MacDill Air Force Base
Tampa, Florida
4. Navy Information Operations Command, Suitland
National Maritime Intelligence Center
Suitland, Maryland
5. Office of Naval Research
Arlington, Virginia
6. Prof. John McEachen
Naval Postgraduate School
Monterey, California
7. Prof. Murali Tummala
Naval Postgraduate School
Monterey, California
8. Prof. Roberto Cristi
Naval Postgraduate School
Monterey, California
9. Prof. David Jenn
Naval Postgraduate School
Monterey, California
10. Prof. Christopher Frenzen
Naval Postgraduate School
Monterey, California